



# Development of Improved Methane Drainage Technologies by Stimulating Coal Seams for Major Risks Prevention and Increased Coal Output

## (GasDrain)

A large, abstract graphic occupies the bottom half of the page. It features flowing, wavy lines in shades of blue and white, creating a sense of motion and depth. In the upper left area, there are several circular, translucent shapes in light blue and white, resembling stylized bubbles or drops of water.

**Development of Improved Methane Drainage Technologies by Stimulating Coal Seams for Major Risks Prevention and Increased Coal Output (GasDrain)**

European Commission

Directorate-General for Research and Innovation

Directorate D – Clean Planet

Unit D.3 — Low Emission Future Industries

Contact Andrea Gentili

E-mail [RTD-STEEL-COAL@ec.europa.eu](mailto:RTD-STEEL-COAL@ec.europa.eu)

[RTD-PUBLICATIONS@ec.europa.eu](mailto:RTD-PUBLICATIONS@ec.europa.eu)

European Commission

B-1049 Brussels

Manuscript completed in 2020.

This document has been prepared for the European Commission however it reflects the views only of the authors, and the Commission cannot be held responsible for any use which may be made of the information contained therein.

More information on the European Union is available on the internet (<http://europa.eu>).

Luxembourg: Publications Office of the European Union, 2020

PDF

ISBN 978-92-76-23801-0

ISSN 1831-9424

doi:10.2777/495448

KI-NA-30-413-EN-N

© European Union, 2021.

Reuse is authorised provided the source is acknowledged. The reuse policy of European Commission documents is regulated by Decision 2011/833/EU (OJ L 330, 14.12.2011, p. 39).

For any use or reproduction of photos or other material that is not under the EU copyright, permission must be sought directly from the copyright holders.

All pictures, figures and graphs © Główny Instytut Górnictwa (GIG), RFCR-CT-2014-00004 GasDrain

# Research Fund for Coal and Steel

## ***Development of Improved Methane Drainage Technologies by Stimulating Coal Seams for Major Risks Prevention and Increased Coal Output***

**(GasDrain)**

Janusz Makówka (Coordinator)

Jan Drzewiecki, Józef Kabiesz, Eugeniusz Krause, Jacek Skiba, Bartłomiej Jura  
**Główny Instytut Górnictwa (GIG)**  
Plac Gwarków 1, 40-166 Katowice, Poland

Wiesław Szott, Krzysztof Sowiżdżała, Grzegorz Leśniak, Małgorzata Słota-  
Valim, Paweł Budak

**Instytut Nafty i Gazu – Państwowy Instytut Badawczy (INIG)**  
Lubicz 25A - 31-503 Kraków, Poland

Piotr Bojarski, Jerzy Król, Marian Zmarzły, Tomasz Gabzdyl  
**Jastrzębska Spółka Węglowa (JSW)**  
Aleja Jana Pawła II- 44-330 Jastrzębie-Zdrój, Poland

Sevket Durucan, Anna Korre, Ji-Quan Shi, Zhenggang Nie, Guangyao Si,  
Wenzhuo Cao

**Imperial College Of Science, Technology And Medicine (IMPERIAL)**  
Exhibition Road, South Kensington Campus - SW7 2AZ London, UK

Stephane Lafortune, Regis Farret

**Institut National de l'Environnement et des Risques (INERIS)**  
Parc Technologique Alata - 60550 Verneuil en Halatte, France

Jose Raul González Ruizsanchez  
**Hulleras Del Norte SA (HUNOSA)**  
Avda. de Galicia 44 33005 Oviedo, Spain

Bernhard M. Krooss, Alexandra Amann, Laura Zieger  
**Rheinisch-Westfälische Technische Hochschule Aachen (RWTH)**  
Templergraben 55- 52062 Aachen, Germany

Grant Agreement RFCR-CT-2014-00004

1/07/2014 – 30/06/2018

**Final Report**



## **Table of contents**

1.	Final summary .....	5
1.1.	WP1: Characterisation of Coal Seams and Surrounding Rocks: Field Site Characterisation.....	5
1.2.	WP2: Development of Borehole Stimulation Technologies for Coal and Rock Formations .....	6
1.3.	WP3: Numerical Modelling and Design of Field Scale Stimulated Methane Drainage Processes .....	8
1.4.	WP4: Field Scale Implementation of Improved Methane Drainage Systems at Mine Sites .....	9
1.5.	WP5: Long-term Monitoring and Assessment of Improved Methane Drainage Efficiency.....	11
1.6.	WP6: Conclusions, Recommendations and Dissemination.....	12
2.	Scientific and technical description of the project.....	14
2.1.	Objectives of the project.....	14
2.2.	Description of activities and discussion .....	14
2.2.1.	WP1, Task 1.1: Laboratory experiments to define the baseline reservoir properties of coal and coal measures rocks.....	14
2.2.2.	WP1, task 1.2: Assessment of the prevailing stress state at different mine layouts .....	21
2.2.3.	WP1, Task 1.3: In-situ measurements of coal and surrounding rock properties.....	27
2.2.4.	WP2, Task 2.1: Development of the equipment and tools for the stimulation of coal seams as well as surrounding rocks (GIG) .....	41
2.2.5.	WP2, Task 2.2: Laboratory investigations into stimulation techniques.....	47
2.2.6.	WP2, Task 2.3: Numerical modelling to assess the performance of stimulated wellbores (led by IMPERIAL).....	63
2.2.7.	WP2, Task 2.4: Field testing and development borehole stimulation methods (led by GIG, JSW, HUNOSA, AITEMIN).....	80
2.2.8.	WP3, Task 3.1: Numerical modelling of multi-seam mining layouts and gas flow patterns around longwall faces for enhanced methane drainage at JSW mines (led by INIG).....	85
2.2.9.	WP3, Task 3.2: Numerical modelling of sub-level caving mining layouts and gas flow patterns around development headings and production faces for enhanced methane drainage (led by IMPERIAL) .....	96
2.2.10.	WP4, Task 4.1 In situ testing of the effectiveness and performance range of the newly developed blasting materials and fracturing techniques using explosives (led by GIG, JSW) .	107
2.2.11.	WP4, Task 4.2 Application of large scale stimulated drainage of methane at multi-seam longwall mining layouts at JSW (led by JSW, GIG, IMPERIAL).....	119
2.2.12.	WP4, Task 4.3: Application of large scale stimulated drainage of methane at sub-level caving mining layouts at Hunosa (led by HUNOSA, AITEMIN – until 30.09.2016, GIG, IMPERIAL, INIG).....	135
2.2.13.	WP4, Task 4.4: Risk assessment and mitigation methods (led by INERIS).....	152
2.2.14.	WP5, Task 5.1 Monitoring and assessment of enhanced methane drainage efficiency of pre-drainage and cross measure boreholes at JSW (JSW, GIG, IMPERIAL) .....	159
2.2.15.	WP5, Task 5.2 Monitoring and assessment of enhanced methane drainage efficiency of pre-drainage and long holes at HUNOSA (HUNOSA, GIG, INIG).....	164
2.2.16.	WP5, Task 5.3 Assesment of the factors which may affect the performance of developed technique in different coal fields and geological conditions (INERIS, all partners). ....	173
2.2.17.	WP6: Conclusions, Recommendations and Dissemination .....	178
2.3.	Conclusions .....	180
2.4.	Exploitation and impact of the research results .....	180
3.	List of figures .....	182
4.	List of tables .....	187
5.	Acronyms and abbreviations used in the report.....	188
6.	List of references.....	189



## **1. Final summary**

### **1.1. WP1: Characterisation of Coal Seams and Surrounding Rocks: Field Site Characterisation**

#### **Task 1.1: Laboratory experiments to define the baseline reservoir properties of coal and coal measures rocks**

The laboratory experiments aimed at defining the baseline reservoir properties for numerical simulations of gas outburst and rock burst risks. Petrophysical data comprise permeability and porosity. Physico-chemical data comprise methane sorption isotherms and gas uptake kinetics determined on different particle sizes. The database is complemented by organic petrological information and petrography of the bedrock samples.

**Mercury injection** (MIP) and **He-pycnometry** analyses performed on 61 coal and bedrock blocks sampled from seam 412 in Zofiówka mine revealed that:

- Porosity values of all samples range between 0.6 and 7.1%, with one outlier at 12.5% determined by He-pycnometry.
- Grain density is ranging from 1.3 - 1.9 g/cm<sup>3</sup> for coals and from 2.5-3.0 g/cm<sup>3</sup> for bedrock samples.
- The specific surface area of the coal samples is generally high (up to 40 m<sup>2</sup>/g) and maximum 5.5 m<sup>2</sup>/g for the bedrock samples.

**N<sub>2</sub> permeability** measurements showed, that apparent permeability coefficients for the coal samples collected at Zofiówka mine range between 5.4E-13 and 1.5E-17 m<sup>2</sup>. A specific anisotropy was not detected, nor a clear porosity-permeability trend. Comparison of the fracture porosity (>0.1mm) determined microscopically and permeability reveals a weak positive trend. All samples are sensitive to stress, with the apparent permeability decreasing exponentially with increasing confining pressures.

N<sub>2</sub> permeability measurements have also been performed on 2 samples from seam 8 in Montsacro mine. Permeability coefficients measured on these two samples ranged between 1.0·10-15 and 3.1·10-15 m<sup>2</sup> (1.0 – 3.1 mD). No hysteresis effects were observed and repeated measurements on the same samples yielded almost exactly the same values permeability coefficients.

**High-pressure methane sorption** isotherms have been measured on dry samples from seams 411, 412, 413 in Zofiówka mine and seam 8 in Montsacro mine. Experiments have been run at 45°C. The maximum excess sorption capacity values range between 12 and 20 m<sup>3</sup>/t for the dry Polish samples. Coals from seam 411 coal have the highest sorption capacities (15-20 m<sup>3</sup>/t). Spanish coals have the lowest sorption capacities (10-12m<sup>3</sup>/t). Most isotherms can be fitted with the basic Langmuir equation but no systematic correlation between Langmuir parameters and sample size is observed

#### **Task 1.2: Assessment of the prevailing stress state at different mine layouts**

The main objective of this task was to implement both numerical and empirical methods to define the state and magnitude of stresses around working longwall and sublevel caving coal faces at JSW and HUNOSA to assist the initial design of field experiments in the project.

The field site selected for the underground experimental work at JSW was longwall D-2 exploiting coal seam 412, which is located at ~900 m below the surface. The thickness of the coal seam is reported as ~4.2 m, underlying a relatively strong sandstone roof. The planned dimensions of the longwall panel is 200 m wide and 1,750 m long.

A model domain was constructed to simulate longwall coal extraction at JSW in FLAC3D. The model was developed to be able to capture the effects of different stages of longwall mining on surrounding coal seams. **Model showed that a stress relief zone can clearly be observed below the goaf area of the mined longwall panel, which can enhance gas drainage performance in the underlying coal seam.**

A second model domain was constructed to simulate coal extraction using the sublevel caving method at Hunosa in FLAC3D. Stress evolution in the roof and floor areas of the mined coal seam observed at both hanging- and footwall regions of the coal seam can be evaluated in order to design the drainage stimulation schemes to be tested. **The floor coal experienced a considerable stress increase. Moderate stress abutments can be observed in all the directions, which increase after each excavation stage both in scale and magnitude.**

#### **Task 1.3: In-situ measurements of coal and surrounding rock properties**

Task 1.3 GasDrain aimed at drilling and instrumenting a number of boreholes at selected JSW and HUNOSA sites to carry out field experiments to establish the in situ stress and reservoir properties of the coal seams and surrounding rocks, that are affected by coal production.

Experiments were carried out in Zofiówka mine where further experiments within WP4 and WP5 were planned to be performed. Based on the measurement results and the borehole parameters, the following **principal stress values** were obtained: vertical stress  $S_v = 4.703 \text{ MPa}$ ; major horizontal stress  $S_H = 59.07 \text{ MPa}$ ; minor horizontal stress  $S_h = 16 \text{ MPa}$ . Direction of major principal stress  $S_H$  was determined as corresponding with the tail gate D-2 direction (deflected by  $3^\circ$ ), minor horizontal stress is perpendicular to it.

A **forecast of the absolute methane emission rate** (i.e. methane release along the designed coal panel length) for the coal panel D-2 in seam 412 in Zofiówka mine was elaborated.

**In situ coal permeability measurements** were carried out in Zofiówka mine using water and only one borehole. The following results were obtained:

- Permeability of the wellbore zone (fracture permeability) =  $1.707 \text{ mD}$ .
- Permeability of coal matrix =  $0.128 \text{ mD}$ .
- Skin effect =  $-4.63$

These results have been compared to the "slug test" method that gave similar data.

In situ coal permeability measurements were carried out in Montsacro mine. Here, measurements were done by using water and 3 boreholes (1 for injection in pulse test mode and 2 for observation). Experimental data obtained have been interpreted applying a classical hydrogeological methodology, obtaining a value of  $1.0 \cdot 10^{-8} \text{ m/s} = 1.04 \text{ mD}$  for the hydraulic conductivity.

## 1.2. WP2: Development of Borehole Stimulation Technologies for Coal and Rock Formations

### Task 2.1: Development of the equipment and tools for the stimulation of coal seams as well as surrounding rocks

Task 2.1 aimed at the development and construction of the equipment and tools for the hydraulic/mechanical slotting and stimulation by blasting. Due to specific underground coal mine conditions, the equipment had to be designed and manufactured with the required specifications and certifications.

The following operational criteria were set:

- Size of the equipment must fulfil underground transportation criteria.
- Performance of the fractures, slots should be possible in inclined boreholes with diameters from 65 to 96 mm and up to 100 m length.
- The equipment must have ATEX certificate allowing its utilisation in methane hazard conditions.
- Power and hydraulic supply must be adjusted to the existing coal mine standards.
- Minimum range of performed fractures/slots: 0.5 to 3.0 m.
- Two principal operating modes: 1,000 bars @ 80 l/min or 650 bars @ 115 l/min.

Equipment are the followings:

- The pump unit ZPM HDP 172, which is set to maintain certain water pressure and flow rate.
- The oil supply unit ZZO-2, which supplies oil to the rotation unit of the rods (and extends the cutting heads to create fractures in the blasting boreholes; see after).
- The stabilisation-rotation unit USO-1 which was constructed and manufactured to transmit water from the pumping unit ZPM HDP 172 down to the cutting head and nozzle, and directing its jet.

Together they constitute an **integrated hydraulic system** aimed at creating slots, fractures and cuts in coal seams to improve their permeability for enhanced gas drainage purposes. A schematic diagram of the integrated system is shown in figure 2.

A **tool to initiate fractures** was developed and tested. It creates mechanically the initial cuts/fractures in boreholes which may be necessary to initiate the stimulation effect.

### Task 2.2: Laboratory investigations into stimulation techniques

The objective of laboratory experiments in Task 2.2 was twofold. The first part aimed at characterising the fracture growth, the performance of different frac fluids, proppant behaviour and fracture closure in stimulated coals in the laboratory. The second part of the laboratory experiments aimed at developing new blasting charges using different mixes of materials. Concerning the first subtask, it was decided to use three different proppants in the experiments. These were:

- 35-40 Mesh sand obtained in UK.
- Carbo Prop 20/40: an intermediate density ceramic proppant at 20/40 Mesh size, supplied by CARBO industrial ceramics, Houston, Texas, USA.
- Inter Prop 30/50: an intermediate density ceramic proppant at 30/50 Mesh size, supplied by Saint Gobain Proppants, Fort Smith, Arizona, USA.

The permeability response of propped fractures in coals was tested.

**Results showed that 38mm core coal samples with sand proppant have shown nearly an order of magnitude increase in permeability to N<sub>2</sub>.** The permeability increase being less pronounced under higher confining stresses. A similar, however much less pronounced increase in propped fracture

permeabilities of coal was observed with the smaller size of the two ceramic proppants (CarboProp 20/40). On the other hand, the larger size proppant (InterProp 30/50) had the opposite effect on permeability of the propped fractures that, at high confining pressures, the permeability of the fracture was significantly (nearly two orders of magnitude) reduced. It is believed that, coal being fairly brittle compared to the relatively hard and stiff reservoir rocks, especially **the large particle size synthetic proppants result in further formation damage and clog the fractures by penetrating into the coal matrix.**

Experiment has also been done with 100mm core coal samples and results showed that **proppant use in fractured coal samples increased the permeability of the coal by a factor of 2 to 10** over the range of effective stresses applied.

Subtask 2 aimed at developing new blasting charges using different mixes of materials. To this effect, a number of laboratory experiments were carried out.

First, explosives and deflagration materials were tested in a research chamber. Two permissible explosives, namely Metanit Specjalny E7H and Emunilit PM were assessed in the laboratory. The objective was to define the dynamic parameters of the explosion using these two explosives.

In parallel, additional experiments aiming at producing the explosive material with extended combustion/oxidation time were carried out. Based on the design requirements of the underground environments targeted (100% moisture, high pressure and temperature), and their combustion dynamics, it was necessary to introduce changes to the chemical composition of the explosive materials tested. Results confirmed that tested solid heterogeneous fuels (mixture of several ingredients such as: ammonium chlorate, potassium chlorate, polybutadiene acrylonitrile PBAN, caoutchouc, plasticizer and aluminium) maintain their principal features in water and at higher environmental pressures. But it must be clearly said that **none of the blasting technologies so far have provided a fine grid of extended fractures. In order to achieve this target, each individual blast hole should be adequately "prepared" by creating inside it a set of initial fractures directing propagation of the gases** (as it is proposed with the tool developed in task 2.1).

Another series of tests were performed to confirm on visual assessment the cracks appearing on the coal samples after firing the propellant charge while maintaining conditions as close to the real environment as possible. Thus, coal samples with a drilled-out hole to contain the propellant charge were each placed in a plastic 65-litre-container and covered in concrete which, after solidification, fulfilled the role of stabilizer and prevented complete fragmentation of the coal. In the upper part of the test model a steel pipe was mounted, through which the propellant charge was inserted in the coal and electric wires of the shooting line were led outside. Electrical duct was made using a spark plug set at the top of the pipe. Just below, a perpendicular measuring orifice was performed to which a piezoelectric pressure transducer was screwed in. Four test units have been prepared.

In the first two tests the appearance of distinct, though isolated fractures was observed, stretching from 6.2 cm to 12.7cm and with a spread of no more than 0.45mm. In the third and fourth test shots, many minor fissures of smaller range and spread appeared. Since the test conditions were the same in all the tests and the examined coal material came from only one mine (from the same coal seam), the explanation and substantiation of a different nature of the fractures is difficult to provide as of this day.

### **Task 2.3: Numerical modelling to assess the performance of stimulated wellbores**

The objective of Task 2.3 was to utilise the data generated for different coal and field conditions mainly under WP1 and partly WP2 and implement numerical models to assess the performance of four different borehole stimulation techniques, namely: hydraulic stimulation of coal seams; slotted boreholes in coal seams; cavity completions in coal seams and explosives for fracturing coal seams.

Numerical modelling of hydrofractured drainage wells using FracPro has shown that hydraulic stimulation can generate long and thin fractures primarily confined in the target coal seams, leading to enhanced connectivity of the wellbore to the coal seam. The simulation results also indicate that higher injection rate and longer injection time have a favourable effect on fracture geometry and proppant distribution. To further reveal the mechanical failure process, a coupled fluid-flow formulation was also implemented in a PFC model to simulate hydraulic fracture propagation. The influence of rock properties, injection time and pumping pressure were analysed. The results have shown that the **hydraulic fracture propagates at a large velocity at the initial stage, and slows down after approaching the interfaces between rock and coal formations.** The results also indicated that **large pumping pressures help generation of cracking.**

Using hydraulically created slotting for enhanced stress relief and permeability has shown by modelling that the **failure zone size is very sensitive to the change of slot diameter.** It was found out that, compared with slot thickness, increasing slot diameter is more effective in enlarging the stress relief zone and pushing the stress concentration zone further away from the borehole. **Gas drainage rate in slotted boreholes can be 2 to 3 times higher than the un-slotted boreholes. However, in slotted boreholes, a faster decline of gas flow rate is observed within the first hour of slotting**

**operation.** As expected, the slot diameter and residual cohesion are the two key parameters that affect gas drainage performance after slotting.

Finite element model OHCAV was used to assess the performance of cavitated drainage wells at JSW and HUNOSA conditions. The modelling work has shown that **rapid depressurisation at borehole would generally cause an enlarged shear failure zone and further stress relief, leading to permeability enhancement around the borehole.**

The blasting process was simulated using FLAC3D using its dynamic module and by applying a period of dynamic stress pulse which has the characteristic of a specific explosive tested in the laboratory. Results showed that **a relatively large range of coal along the borehole direction was fractured due to the propagation of shock wave.** Indeed, after the blasting operation, the stimulated zone with enhanced permeability was found to be five times the borehole radius.

#### **Task 2.4: Field testing and development borehole stimulation methods**

Works within task 2.4 were concentrated around tests of equipment developed for the techniques of stimulation described within task 2.1. Different stimulation techniques were also tested in laboratory and in situ conditions.

Initial trials of the hydroslotting tool designed in task 2.1 were performed in experimental mine Barbara (Poland). For this purpose, a pattern of four boreholes was drilled. One borehole was used for slot cutting and the remaining three were used for monitoring the performance of stimulation. A **degradation of the nozzle of the hydroslotting tool** was observed but it was not clear if it was due to its poor construction or because of the conditions in the borehole, where detached coal particles might cause damage to the nozzle.

In order to test the new nozzle construction a series of tests were performed first on concrete blocks and then on coal (see figure 4). Results showed that **increasing the time of slotting does not change significantly the diameter of slot but the width.** Long lasting tests on concrete blocks have been performed to assess degradation of the nozzles with ceramic inlay. It was noticed that the **average efficiency of nozzle is reduced after 60 minutes of operating** in concrete blocks.

Field tests have also been performed in Montsacro mine to run a long period injection test at high pressure, in order to achieve the hydraulic connection between an injection borehole and three observation boreholes. But a number of technical problems appeared with the pump and it was not possible to perform a continuous injection for several days, as it was initially planned. Despite the lack of continuity of the injection, 75 m<sup>3</sup> of water were injected and a clear connection was established between the injection borehole and one of the observation borehole, which is located at a distance of 40 m. No connection has been detected in the two other observation boreholes.

### **1.3. WP3: Numerical Modelling and Design of Field Scale Stimulated Methane Drainage Processes**

#### **Task 3.1: Numerical modelling of multi-seam mining layouts and gas flow patterns around longwall faces for enhanced methane drainage at JSW mines**

This task aimed at numerical modelling of geological formations in the area of JSW Zofiówka Colliery, developing a geomechanical and gas flow model and assessment of the effectiveness of the stimulation techniques developed in WP2.

The task of numerical modelling of geological formations in the area of Zofiówka coal mine was accomplished in order to develop improved methane drainage technologies by coal seam stimulations. Here, the numerical modelling was carried out using the Schlumberger suite of software packages: Petrel (Petrel Release, 2015), Eclipse (Eclipse 300 Release, 2015) and Visage (Visage Release, 2015). This task was realized in several stages:

- Geological modelling: as the first step, the overall data from different sources (borehole, rock samples collected in mine) were integrated within the 3D geological model of the area.
- Geomechanical modelling: in the next stage geomechanical modelling work was undertaken to access overall stress field for the initial conditions prevailing in the area of interest (the multi-seam layout of Zofiówka coal mine). Further geomechanical modelling was performed according to the requirements of various methane drainage scenarios for different stimulation techniques and different configuration within every analysed stimulation technique as suggested by current analyses of dynamical flow simulations.
- Dynamical fluid flow modelling: the dynamical simulations constitute the final and conclusive part of the modelling tasks. The dynamical models obtained were used to simulate drainage processes from the coal seam including all its fundamental mechanisms: methane desorption from the coal matrix, methane diffusion from the matrix to coal cleats, reservoir fluid (methane, water) viscous transport through the cleats and stimulation elements (hydrofractures, jet slots, etc.) to boreholes. Hydrofracturing, jet slotting, blasting stimulation techniques were investigated.

As conclusions of the task, the following remarks have been made:

- Main direction of the maximum horizontal stresses in the area subjected to stimulation treatment implies the **optimal direction of horizontal stimulation boreholes with azimuth perpendicular to direction of maximum horizontal stress**.
- Limited availability of data used for construction of parametric (petrophysical and mechanical parameters) and dynamical (initial conditions) models introduce uncertainty to the obtained results. In particular, the following parameters: diffusion time, pore pressure and water saturation in coal cleats were shown to significantly influence the dynamical simulation results of the methane drainage process. By then the **simulation results are of more qualitative significance and may be used for the relative comparisons rather than absolute value assessment**.
- Under the conditions of the 412 coal seam of Zofiówka mine, the stimulation method of blasting based on the use of explosives is ineffective. The same conclusion refers to the cavitation method. But hydrofracturing and jet slotting can significantly enhance the methane drainage process in the coal seam.
- **Sizes of the effective drainage zones are larger than the geometrical sizes of the directly stimulated zones**.
- The drainage coefficient is the volume fraction of adsorbed methane drained from coal matrix at the end of simulation. **The uniformity of the drainage coefficient depends on the separation between hydrofractures/slots**.
- From the drainage effectiveness standpoint, a **sequential use of jet slotting and hydrofracturing stimulation techniques does not provide advantages over the hydrofracturing alone**.
- **The larger the distance between the individual borehole stimulation zones the larger the methane production volume** (due to the reduction of interference effect) and the lower the average drainage coefficient and larger non-uniformity of the drainage results.

Modelling results showed that **drainage efficiency increases with hydrofracturing when the number of stimulation operations per borehole increase** (rather than increasing the number of boreholes). Concerning slotting, it is better to increase the **number of boreholes rather than the number of slots in each borehole**.

### **Task 3.2: Numerical modelling of sub-level caving mining layouts and gas flow patterns around development headings and production faces for enhanced methane drainage**

This task aimed at building numerical models field sub-level caving layouts from the Sueros Colliery at Hunosa, where the GasDrain field experiments are carried out, to implement coupled flow-geomechanical modelling to evaluate the performance of enhanced pre-drainage and drainage of gas from the panels that are both being developed and in production in Montsacro mine. The results of this task helped the design and implementation of the stimulation techniques at field scale in WP4. Following the work presented in task 2.3, where numerical models were developed to assess the performance of individual stimulated boreholes, a group of drainage boreholes and their stimulation using slot cutting at field scale sub-level caving panels were investigated.

Results showed that, for an individual borehole, hydraulic fracturing is the most effective stimulation method. In addition, hydraulic fracturing can increase the spacing of drainage boreholes and thus reduce the number of drainage boreholes needed. It requires only four multi-level fracturing cross-measure boreholes to reduce the regional gas content by more than 20%.

In the same manner, stimulation performance of hydraulic fracturing (5 mm aperture) and slotting in inseam downholes are compared. It showed that, for an individual downhole, gas production rate and volume by using hydraulic fracturing are as much as twice of that by using slotting stimulation. In addition, hydraulic fracturing can increase the spacing of drainage boreholes so as to reduce the number of inseam downholes. In terms of gas content reduction in the 4<sup>th</sup> caving level, each hydraulic fracturing downhole can reduce ~7.5% gas-in-place, while one slotted downhole can only achieve 2.8% gas content reduction on average.

## **1.4. WP4: Field Scale Implementation of Improved Methane Drainage Systems at Mine Sites**

### **Task 4.1: In situ testing of the effectiveness and performance range of the newly developed blasting materials and fracturing techniques using explosives**

Within this task the field trials of the newly developed blasting materials in SubTask 2.2.2 were conducted at the Experimental Mine Barbara - Central Mining Institute, where appropriate facilities to test the explosives can be found, including blasting bunker and underground research fields .

The field trials aimed at testing the potential for controlled methane release and drainage as a result of fracturing coal by explosives. The tests used explosives with reduced detonation speed and increased gas production. For comparison, tests were carried out using traditional explosives, which were routinely used in mines, and were approved for use under methane hazard conditions. The tests showed a significant increase in rock fracturing around the openings, which could have been a reason to recommend using such explosives to stimulate drainage holes. However, it was also found the presence

of increased amounts of toxic components in the gas which called into the big question possibility of using new explosives in terms of underground workings. One test was carried out using the distributed charge of traditional explosive in the borehole with the slots made, but there was no significant methane recovery from this well observed.

#### **Task 4.2: Application of large scale stimulated drainage of methane at multi-seam longwall mining layouts at JSW**

In this task use the designs developed in WP3 for the pre-drainage and drainage during mining of methane from the coal seams at JSW in the field was planed to test.

In the course of preparation, test drilling was performed, during which difficulties were encountered in patency of the openings of the boreholes, which were either clenched or filled with water flowing from the goafs from the upper seam. As a result of the trials, the method of drilling at the contact between the seam and the roof rock was developed, thanks to which the boreholes unobstructed for several weeks.

Four horizontal boreholes have been drilled using this method, and stimulated. Camera inspections (endoscope) and aeraulic tests have been performed in the boreholes prior and after stimulation. Slotting was made starting 5 m from the bottom of each borehole, and each following slot was made 2 m closer to the gallery. After the stimulation the four boreholes were connected to mine drainage pipeline and the tests begun. Gas pressure, gas volume, methane content, temperature and moisture content were monitored at the outlet of the boreholes. Due to very low depression of coal mine drainage pipeline, volume of collected gas was relatively low. It was thus decided to stop operations as Polish mining regulations prohibit introducing into the collective pipeline gas mixture with methane concentration lower than 20% vol.

#### **Task 4.3: Application of large scale stimulated drainage of methane at sub-level caving mining layouts at Hunosa (led by HUNOSA, AITEMIN, GIG, IMPERIAL, INIG).**

This task's aim was to apply the designs developed in WP4 for the pre-drainage and drainage during mining of methane from the outburst prone seams of HUNOSA mines in the field. The possible procedures for the sub-level caving mining districts was one or two of the following methods:

- Drilling in-seam pre-drainage boreholes downwards from the operating sublevels to the future sub-level caving panels in coal as well as the horizon where the new sublevels will be driven in order to mitigate against outburst risks.
- Drilling horizontally from galleries excavated in rock, to reach the panel and the sublevel headings to be mined.

Extracted methane will be released into the main ventilation flow in a controlled manner. In principle, it was not planned to implement a methane drainage network within the project, but it was considered as an option for the future. All important parameters of the process were controlled by dedicated system RELIA AV - a system developed specifically for gas monitoring and control applications in underground mining.

Between February 2016 and February 2018, a number of boreholes have been drilled perpendicular to monitor the seam 8 in Sueros Colliery (HUNOSA) from a rock gallery located in the footwall to perform hydrofracture tests. The boreholes crossed seam 9. Besause of that it has been necessary to develop a specific procedure to seal the boreholes and guarantee that they are isolated from this seam. It was decided to cement the boreholes in the surrounding rocks.

It was decided to check the effect of water injection on methane drainage by resuming mining operations of seam 8 but HUNOSA didn't get the approval from the Spanish mining authority to do so. Thus, it was decided to check efficiency of stimulation operations by drilling four horizontal boreholes in the front of mining operations in seam 8. The objective was to collect coal samples to assess their gas content. Unfortunately, results were not unequivocal and conclusions on the efficiency of the stimulation operations cannot be drawn.

#### **Task 4.4: Risk assessment and mitigation methods**

For the developed methods of stimulation, a detailed analysis of the risks was performed. It took into account specifically the new elements and technologies with regard the existing methods of firedamp drainage already used in coal mines. These new elements were mainly: hydraulic fracturing and fracturing by explosives, as well as the potential impact of the specific products used during the implementation of new developed techniques (additives for the fracturing, gels for sealing etc.)

The primary objective was to identify information about potential critical events (leakages, explosion, spontaneous combustion, etc.) and to identify their causes, by classifying them in several categories: conception errors, failures of equipment during operation, errors in gas or pressure management, undesired event in the rock or the coal etc. Secondly, the distinction was made between the different units (coal and surrounding rocks, boreholes, holes head equipment, pipelines, pumping equipment...) and between the different stages of the project (drilling phase, tests, operating phase, monitoring phase...)

Within the task a detailed risk analysis to help risk management when designing future firedamp drainage projects has been performed, by identifying several risk scenarios (or chains of events) that begin with a specific hazard (initial cause) and end with the exposure of a stake at risk (an effect). All the scenarios with cause-consequence relationships have been drawn on a chart called an "event tree" to ensure a synthetic vision.

Managing risks also implies to define preventive or corrective barriers to prevent any impact in case a hazard occurs. Those safety barriers have been defined with all the partners during the second annual meeting held by AITEMIN in February 2016. All the barriers have been chosen among solutions already in use in mines, to ensure that they are operational and that their efficiency is proven. They are reported on an updated version of the event tree.

Because identified central events are typical risks in underground operations and because most of the described safety barriers are commonly used in mining environments, it appeared that **workers would not face unusual risks when performing stimulation operations**. Managing risks related to the stimulation of firedamp drainage boreholes did not seem to be particularly challenging. **Protection of workers, environment and equipments should thus be ensured adequately.**

## 1.5. WP5: Long-term Monitoring and Assessment of Improved Methane Drainage Efficiency

### Task 5.1. Monitoring and assessment of enhanced methane drainage efficiency of pre-drainage and cross measure boreholes at JSW

Objective of the task was monitoring of the long term performance of both stimulated methane drainage techniques and the different stimulation methods applied at JSW longwall panels. Intended methods were:

- using monitoring boreholes drilled within the area of influence (predicted through numerical modelling in WP3) of the stimulated boreholes and by recording pressure depletion over the drainage period.
- residual gas content measurements within the area of influence of the stimulated drainage boreholes
- drainage borehole and/or range monitoring for gas pressure, flow rates and concentration
- district ventilation air monitoring for methane concentration and flow/mission rates

before and during coal extraction. The monitoring systems applied will, to an extent, depend on the drainage system and mining layout implemented.

Specification of measurement system to measure all parameters necessary of gas obtained during drainage from stimulated boreholes were elaborated in the task. It appeared necessary to know the following physical parameters: methane concentration, barometric pressure, methane volume flow in given time in galleries adjacent to longwalls and methane drainage pipe-lines. It seemed important to have continuous results of measurements from measuring devices and the measuring series should be made during mining operations in the longwall.

Four ZCO sensors developed by EMAG Institute and designed for measurements of physical properties and gas flow volume in the pipe-lines of the methane drainage system were installed on pipes in Zofiówka mine. The module of the detectors of the integrated methane drainage sensor ZCO consisted of the following components:

- CH<sub>4</sub> concentration sensor for high concentrations (0 to 100 % vol.)
- Internal and external (mounted at the pipe-line) temperature detector (10 to 40°C).
- Absolute pressure sensor (0 to 110 kPa) and differential pressure sensor (0 to 200 Pa).

To prepare test site a new set of boreholes was prepared in district G. At this testing field totally 24 boreholes were performed. Some of them were used for technical trials of new drilling method, two of them were kept for comparison tests, 5 of them were protected from falling down by inserting different diameters' rubber hoses and used for hydroslotting. Whole technique and procedure of test site preparation is described in part concerning actions under the Task 5.1 (Chapter 2.2.14).

Tests in the site consisted of three stages:

**Stage 1.** The boreholes: 7 (G11b/2018), 8(G11a/2018) and 9(G11/2018) were connected with the drainage pipeline. After connecting the vacuum there was a gas flow from borehole G11b with differential pressure of 240 Pa, in the boreholes 8(G11a) and 9(G11) the differential pressure (and actually the flow itself) was almost as small as the measurement mistake (about 5 Pa).

**Stage 2.** Due to above the middle borehole 8(G11a) located between 7(G11) and 9(G11b) boreholes was disconnected and stayed opened. The purpose of this was to enable eventual flow of gas through the system of fractures into the boreholes 9(G11) and 7(G11b).

The required effect was not achieved: the differential pressure in the flange of the borehole 9(G11) stayed unchanged, and in the 7(G11b) borehole slightly increased up to 260 Pa. It did not also changed after closing the 9(G11) borehole.

**Stage 3.** In these circumstances ZCO with all measurement equipment previously connected to the borehole 8(G11a) was moved and connected with 5(G13) borehole. The flow, which was recorded was again very low - as previously: the differential pressure was between 5 and 10 Pa. Methane content stayed at very low level at about 0.2%. The sensor did not react also for the standard mixture.

Undertaken methane drainage in above boreholes confirmed poor permeability of the coal seam resulting in small gas outflows and proved that there are very few chances for measurement of methane concentration when the flow of gas is very small. Due to above it was planned to check of the measurement installation and to modify it, check patency of the boreholes and possibility of gas flow through the slots cut in the rubber hoses of the pipeline. It was also considered additional fracturing of the coal seam by using small blasting materials.

Unfortunately, finishing of the plans appeared impossible. On the 5th of May 2017 a strong seismic tremor (magnitude 3.4, energy  $2 \cdot 10^8$  J) and rockburst occurred in the proximity of the test site, 800m in straight line. It resulted with a collapse of the boreholes. Further tests in the district in that situation were impossible.

#### **Task 5.2. Monitoring and assessment of enhanced methane drainage efficiency of pre-drainage and long holes drilled from rock galleries at HUNOSA (led by HUNOSA, GIG, AITEMIN, IMPERIAL)**

Objective of the task was long term performance monitoring of both stimulated methane drainage techniques and the different stimulation methods applied at HUNOSA sub-level caving panels, during sub level heading development, before and during coal extraction. Due to administrative decision the development and exploitation was impossible.

Regular procedure of coal exploitation in a new panel in the gassy seam 8 was as follows: exploiting a neighboring panel in seam 7 to destress an equivalent panel in seam 8, then develop a heading in seam 8 and proceed with exploitation. As exploitation of thin seam 9 was unprofitable, company's intention was to drain out methane by the boreholes drilled from the ditch to seam 8 to enable developing incline 8a III and then drill downside a set of long boreholes to drain methane from exploitation panel. Unfortunately, for mining authority the results of drainage and methane content from samples obtained from test drilling in seam 8 were unconvincing. In that situation the authority did not give permission to develop the incline 8a. In such situation the main part of research was impossible to perform and drainage by the previous borehole system was continued.

The test duration was subdivided into 14 periods. The test consisted in injecting water into an injection well and monitoring the gas flow on suction pipe which evacuates gas from two drainage wells. The injection pressure and water flow rates were recorded. The objective of this test was to assess the possibility of producing methane by injecting water in a well to displace the gas contained within the coal towards drainage wells. Note that the drainage flow was enhanced using the vacuum pump which was installed at gas evacuation pipe.

The following comments can be made from the results of the test:

- **Water flow causes opening of the system of micropores and microfractures within coal.** Each increase of injection pressure causes microfracturing of coal, leading to an increase of the pore volume accompanied by the increase of flow rate which in turn causes decrease of injection pressure and so on.
- **In a water flooded zone the water can displace only the gas present in micro and macro pores, fractures and crevices.** But the water does not mobilize the gas particles absorbed at the specific surface area of coal matrix. Because the volume of gas absorbed at the coal specific surface is several time greater than volume of micropores, the **water flooding process doesn't seem to be an effective method of enhancing the methane production.**

#### **Task 5.3: Assessment of the factors which may affect the performance of developed techniques in different coal fields and geological conditions**

Task 5.3 aimed at assessing the factors which may affect the performance of stimulation techniques of firedamp drainage boreholes in different coal fields and geological conditions. The objective was to collect all kind of practical information that may appear useful for the developments planned in the project. The analysis was focused on positive as well as negative experiences in order to understand the main factors influencing the efficiency of the coal seam drainage process.

**Recommendations have been proposed in D5.3 to assist the choice of a technique to stimulate firedamp drainage boreholes and improve pre-drainage efficiency.** It summarises all the experience gained in the project through field testing or modelling. In this purpose, a review of all project deliverables (published by project partners before the 1<sup>st</sup> of March 2018) was done in order to highlight factors that have a positive or a negative impact on the performance of a stimulation.

It appeared that **site-specific geology can play a key role in influencing fracture behavior and thus stimulation/drainage efficiency, as well as operator-controlled actions.** Site-specific and method-specific factors were identified from a literature review and from results obtained by project partners.

### **1.6. WP6: Conclusions, Recommendations and Dissemination**

#### **Task 6.1 Dissemination workshop**

On June 25th, 2018, a workshop disseminating the effects of the GasDrain project was organized at the Central Mining Institute. 35 participants, employees of coal companies, mines and scientific institutions took part in it, including those taking part in the project. The workshop run according to the following main points of agenda:

#### Laboratory tests and preparation of in-situ tests

- In situ tests in JSW SA, Poland
- In situ tests in HUNOSA, Spain
- Risk assessment and Lesson learned
- Conclusions and discussion

Press reports from the workshop were published in websites of GIG, but also by Polish Press Agency and by Trybuna Górnica.

#### **Task 6.2 Lessons learned document**

Lesson learned document formulated the following main conclusions:

1. The stimulation method of blasting based on the use of explosives is ineffective. The same conclusion refers to the cavitation method as shown in Task 2.3.
2. The hydrofracturing and jet slotting can significantly enhance the methane drainage process to the degree dependent on detailed parameters of the techniques.
3. The vertical extension of the drainage zone induced by a single borehole, drilled in the mid depth of the seam and stimulated with either hydrofractures or jet slots covers the total thickness of the seam.
4. The horizontal sizes of the effective drainage zone are only slightly larger (ca. 2 m) than the geometrical sizes of the directly stimulated zone.
5. The uniformity of the drainage coefficient\* in the drainage zone around each stimulated drainage borehole depends on separation between hydrofractures/slots. To obtain full uniformity the separation as low as 2 m is required.
6. The average drainage coefficient in the directly stimulated zone may reach the value of 0.85 or more for the hydrofracturing or jet slotting stimulating methods with appropriate separation between hydrofractures/slots.
7. From the drainage effectiveness standpoint a sequential use of jet slotting and hydrofracturing stimulation techniques does not provide advantages over the hydrofracturing alone.

#### **Task 6.3 Scientific journal and conference publications**

As a result of project GasDrain 7 papers were published, 3 patents are filled, 2 another under preparation) and 2 presentations were given.

A full list of publications, conference presentations and patents is presented in chapter 3.4.

## **2. Scientific and technical description of the project**

### **2.1. Objectives of the project**

The primary objective of this project is to investigate and research into borehole stimulation techniques and develop novel and improved methane drainage technologies, which will break the existing technological barriers and help to increase safety and productivity in the coal mines.

The technology options considered in this project include:

- *hydraulic fracturing*, which has been successfully applied in the conventional and unconventional hydrocarbons industry,
- novel stimulation techniques such as *open or cased hole cavitation*, which have been very successful in coalbed methane (CBM) well stimulations,
- *high pressure water jet slotting*, which has been tested and found effective in combatting gas outbursts
- the use of the *explosives* to stimulate coal seams and the surrounding rock strata.

In the case of soft coal seams, further developments and designs of drilling patterns may also be necessary. To achieve these project objectives, it is necessary to develop, design, and construct new equipment; introduce new drilling and blasting patterns; elaborate experimental and numerical techniques, that simulate the *in situ* behaviour of the coal seams and the surrounding strata; and develop specific application procedures for the new drainage solutions. These new techniques must be validated by performing *in situ* experiments at field scale in different mining conditions. During such tests and research, the main parameters characterising the drainage process will be defined and investigated. They will be essential for the numerical modelling of the improved/enhanced drainage process and in designing the new drainage technology.

### **2.2. Description of activities and discussion**

This main section of the report presents the progress made during the project under each Work Package.

#### **2.2.1. WP1, Task 1.1: Laboratory experiments to define the baseline reservoir properties of coal and coal measures rocks**

The laboratory experiments aimed at defining the baseline reservoir properties for numerical simulations of gas outburst and rock burst risks. Petrophysical data comprise permeability and porosity. Physico-chemical data comprise methane sorption isotherms and gas uptake kinetics determined on different particle sizes. The database is complemented by organic petrological information and petrography of the bedrock samples.

Majority of the progress made on characterising the petrophysical and physico-chemical properties of coal and bedrock samples from the JSW SA Borynia-Zofiówka mine in Poland and the HUNOSA Monsacro Colliery in Spain was already reported in detail in the Revised 1st annual Report. The Deliverable D1.1 submitted recently also described all these experiments and the additional work carried out since. Therefore, this report only summarises the most important elements of these experiments.

#### **Petrophysical and geomechanical characterisation of the samples collected**

Samples collected at Zofiówka Colliery included coal and rock cores from exploration wells as well as large coal block samples which were cored and tested by INIG and RWTH. Two sets of coal samples were collected from the Sueros Colliery at Hunosa. As the first coal samples did not yield any cores at RWTH, second coal samples were successfully cored and tested for porosity and permeability at IMPERIAL as a remedial action after the May 2015 TGC1 review. Various coal and rock characterisation data obtained using these samples are summarised in the following sections.

Table 2.2.1.1 presents an overview of the experimental and analytical measurements conducted by the project partners under this task.

**Table 2.2.1.1:** Overview of the experimental and analytical measurements conducted by the project partners.

	RWTH	INIG	Imperial
<b><u>Coal samples</u></b>			
<b>Permeability</b>	ZOFIOWKA 412 (413)	ZOFIOWKA 412	HUNOSA
<b>Porosity</b>			
<b>Adsorption isotherms</b>	ZOFIOWKA 411, 412, 413		
<b>Sorption kinetics</b>			
<b>Organic petrology</b>	HUNOSA		
<b>Proximate analysis</b>			
<b><u>Bedrock samples</u></b>			
<b>Permeability</b>		ZOFIOWKA 412	
<b>Porosity</b>		(ID: 10268-10307)	
<b>Petrography</b>			

Basic sample characterisation work such as proximate analysis, petrography and organic petrology was carried out and reported in detail in Deliverable D1.1 report and will not be repeated here.

Table 2.2.1.2 presents an extract from a comprehensive petrophysical characterisation data obtained from the samples collected at Zofiowka Colliery which were later used in numerical modelling work in Tasks 2.2 and 3.1 by IMPERIAL and INIG respectively.

**Table 2.2.1.2:** Results of petrophysics investigations of samples from G-172 +90° well at Zofiówka Colliery.

Well	Sample ID	Depth [m]	Grain density	Total porosity	Skeletal density	Bulk density	Effective porosity	Average capillary	Surface area	Pores >1 um	Threshold diameter	Hysteresis	Permeability x	Permeability z
			[g/cm³]	[%]	[g/cm³]	[g/cm³]	[%]	[µm]	[m²/g]	[%]	[µm]	[%]	[mD]	[mD]
G-172 + 90°	10268	0.81	2.67	1.28	2.56	2.53	1.16	0.02	0.79	38	0.03	36	0.164	0.005
	10269	1.41	2.75	1.48	2.68	2.65	1.39	0.02	1.16	34	0.05	36		
	10270	3.55	3.04	0.59	2.94	2.92	0.54	1.02	0.01	81	bm	21		
	10271	4.63	2.74	1.84	2.72	2.68	1.80	0.03	0.89	54	0.03	32		
	10272	5.23	2.70	1.88	2.63	2.58	1.75	0.02	1.34	41	0.04	40		
	10273	6.35	2.67	1.84	2.57	2.52	1.67	0.02	1.19	42	0.04	41		
	10274	7.63	2.70	1.32	2.65	2.62	1.26	0.02	1.04	41	0.02	53		
	10275	8.38	2.74	1.77	2.70	2.57	1.71	0.02	1.69	37	0.05	51		
	10276	9.73	2.73	2.08	2.66	2.61	1.95	0.03	0.95	59	0.02	34		<0.009
	10277	10.73	2.66	2.23	2.56	2.51	2.02	0.02	1.27	46	0.03	39		
	10278	11.33	2.72	1.69	2.65	2.60	1.57	0.02	1.48	35	0.03	51		0.254
	10279	12.65	2.51	5.72	2.44	2.31	5.35	0.06	1.48	73	0.20	10		
	10280	14.65	2.78	2.79	2.74	2.67	2.70	0.03	1.50	56	0.04	35		
	10281	16.55	2.74	1.77	2.68	2.64	1.67	0.02	1.58	30	0.02	58		
	10282	18.51	2.80	2.76	2.74	2.67	2.62	0.01	2.71	16	4; 0.03	52	<0.007	<0.006
	10283	18.96	2.77	2.89	2.70	2.63	2.71	0.03	1.36	16	0.02	65		
	10284	19.72	2.66	2.83	2.57	2.50	2.60	0.02	1.78	44	0.04	47		
coal	10300	12.73	3.03	1.90	3.00	2.94	1.85	0.02	1.38	28	0.05	75	0.001	0.001
	10301	13.48	2.78	4.99	2.70	2.58	4.61	0.03	2.20	63	0.05	20		
	<b>10302</b>	<b>14.60</b>	<b>1.43</b>	<b>4.40</b>	<b>1.41</b>	<b>1.35</b>	<b>4.31</b>	<b>0.03</b>	<b>4.01</b>	<b>62</b>	<b>2; 0.05</b>	<b>8</b>		
	<b>10303</b>	<b>15.29</b>	<b>1.35</b>	<b>6.86</b>	<b>1.31</b>	<b>1.22</b>	<b>6.56</b>	<b>0.04</b>	<b>5.56</b>	<b>65</b>	<b>0.10</b>	<b>14</b>		
	<b>10304</b>	<b>16.46</b>	<b>1.31</b>	<b>9.56</b>	<b>1.28</b>	<b>1.16</b>	<b>9.32</b>	<b>0.06</b>	<b>5.50</b>	<b>77</b>	<b>0.06</b>	<b>5</b>		
	10305	17.58	2.68	2.01	2.64	2.59	1.93	0.03	1.02	54	0.03	32	<0.010	<0.012
	10306	18.38	2.70	3.15	2.65	2.57	3.00	0.03	1.38	57	0.40	22		
	10307	18.74	2.72	3.58	2.63	2.54	3.26	0.02	3.20	15	0.50	54	0.001	0.001

### *Strength and Elastic properties*

Figure 2.2.1.1 presents an axial stress-axial strain plot for the one Zofiowka coal sample tested under triaxial conditions up to 20 MPa confinement. The Young's Modulus of the coal sample was determined as 1.05 GPa and 4.85 GPa for the cleat and the matrix respectively.

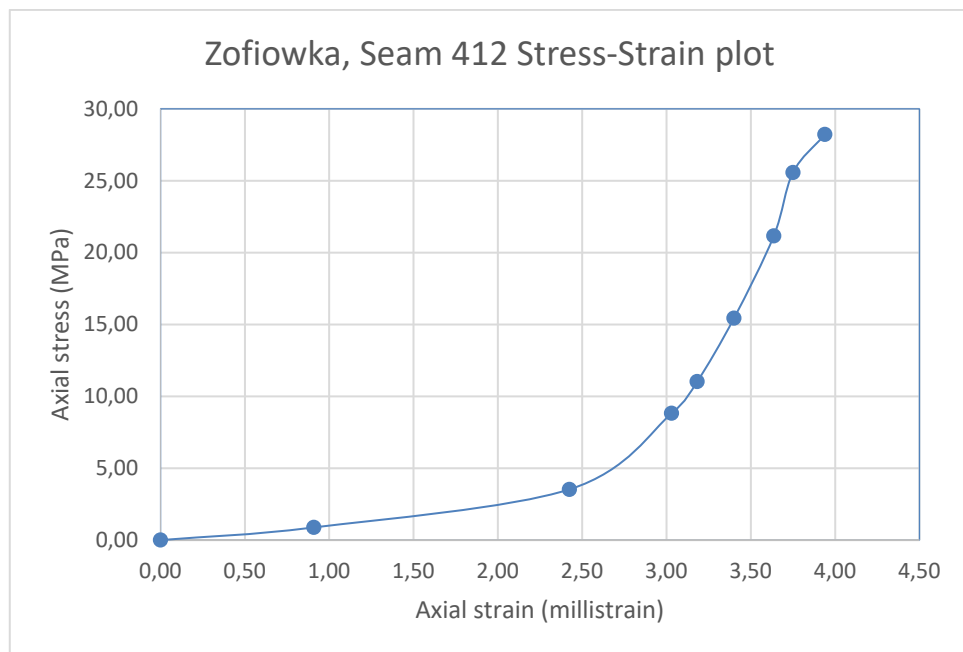


**Figure 2.2.1.1:** Stress-strain plot for the Zofiowka coal sample plug from seam 412 (butt cleat direction). \* Axial load was applied under confined ("isostatic") conditions (confining pressure = axial pressure).

### *Porosity measurements*

A total number of 61 coal block samples from seam #412 at Zofiowka were analysed by mercury injection (MIP, effective porosity) and standard, unconfined He-pycnometry (total porosity). From each block 3 analyses were performed. Porosity values of all samples range between 0.6 and 7.1%, with one outlier at 12.5% determined by He-pycnometry. Table 2.2.1.1 presents these results.

**Table 2.2.1.3:** MIP pore size distribution classes of similarity for coals from ZOFIOWKA (seam 412).

Class	Porosity (%)	Curve type	Threshold diameter	Specific surface area
I	<6	Bimodal	1-4 – 0.01-0.06	<6
II	0 – 14	Monomodal or bimodal	<1	<10
III	5-10	Monomodal	<0.04	>10

### *Permeability measurements*

Gas permeabilities of the collected samples was determined at INIG, RWTH and IMPERIAL depending on the need and specific equipment availability. All measurements were performed with N<sub>2</sub>, low fluid pressures (0.03 and 0.32 MPa) and four confining pressures ranging from 0.27 to 11 MPa to analyse the stress dependence of permeability on lithological stress.

Apparent permeability coefficients for the coal samples collected at Zofiowka ranged in between 5.4x10-13 and 1.5x10-17 m<sup>2</sup>. A specific anisotropy was not detected (Figure 2.2.1.2). Due to the initial difficulties experienced in coring the Sueros Colliery coal samples at Hunosa the second batch of large coal blocks obtained were cored at IMPERIAL and tested for permeability under confinement. An example output from these permeability experiments is given in Figure 2.2.1.3.

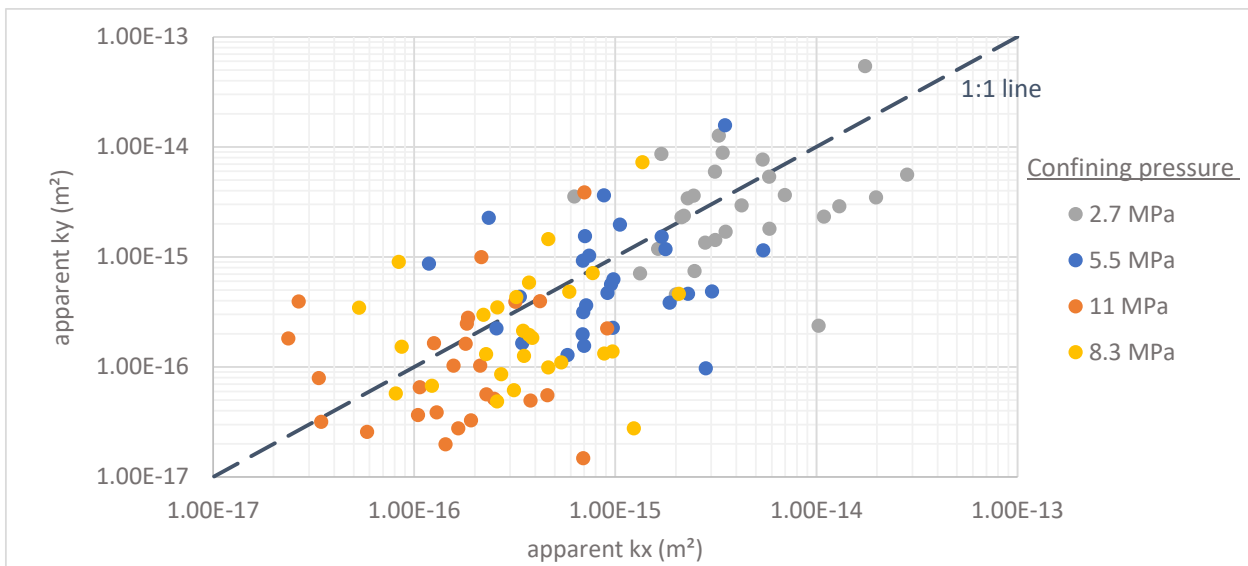


**Figure 2.2.1.2:** Gas (N<sub>2</sub>) permeability coefficients in x- and y-direction (Zofiowka seam #412).

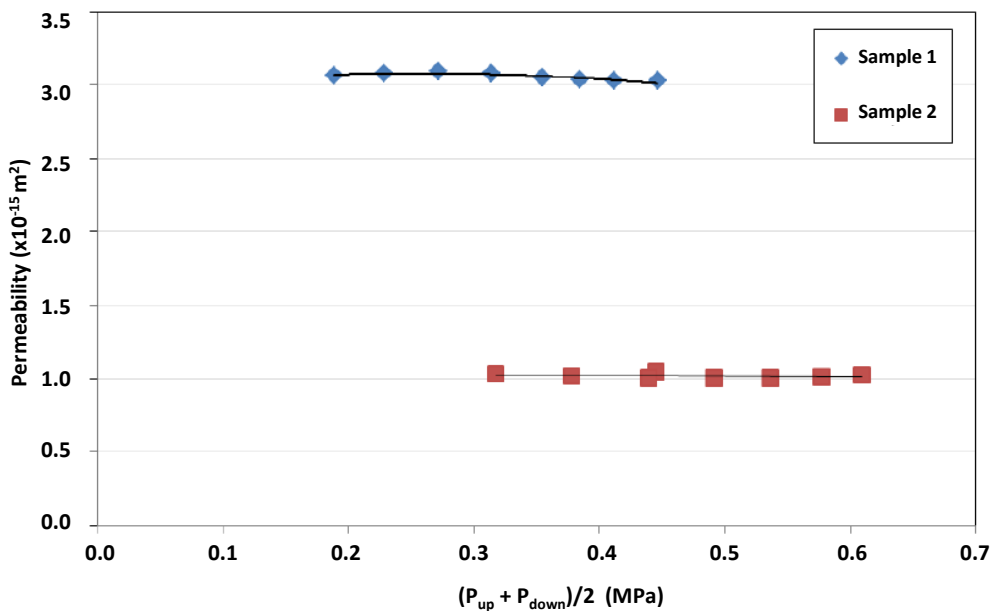


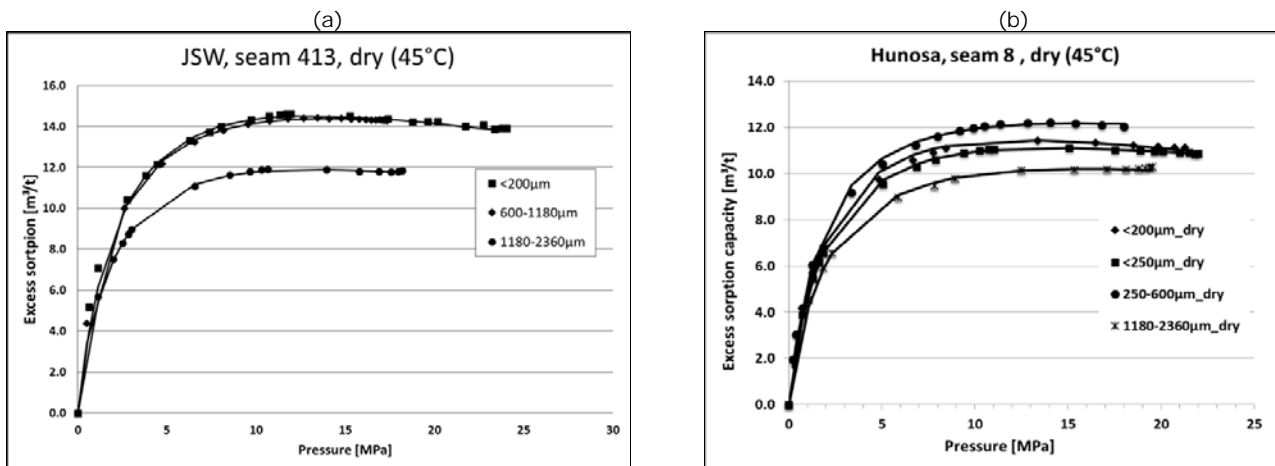
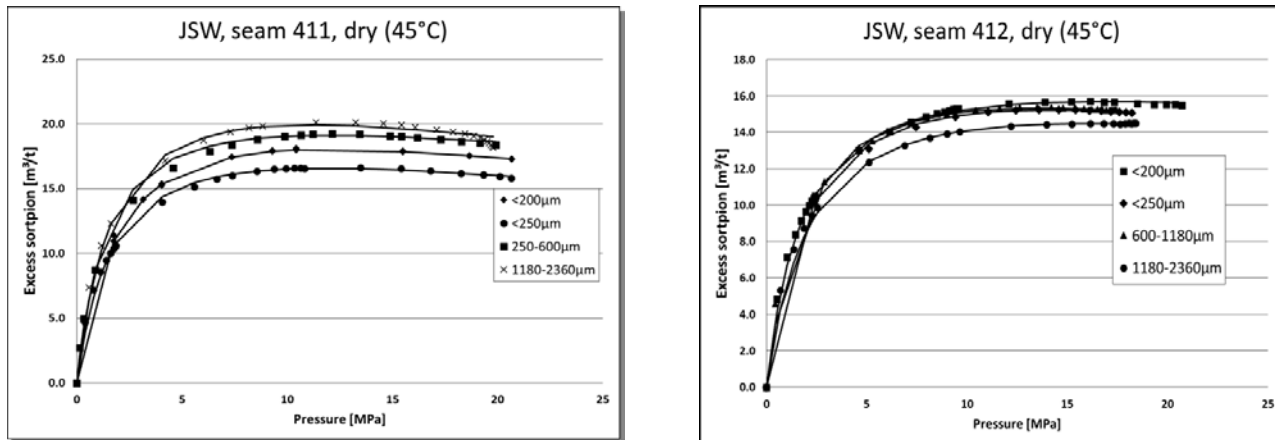
**Figure 2.2.1.3:** Permeability data for two coal samples from the Monsacro/Sueros Colliery Seam#8.

#### High-pressure sorption isotherms

High-pressure methane sorption isotherms were measured on dry samples from Zofiowka Colliery seams #411, #412, #413 and the Monsacro/Sueros #8 seam at 45°C. Example outputs from these measurements are presented in Figure 2.2.1.4.

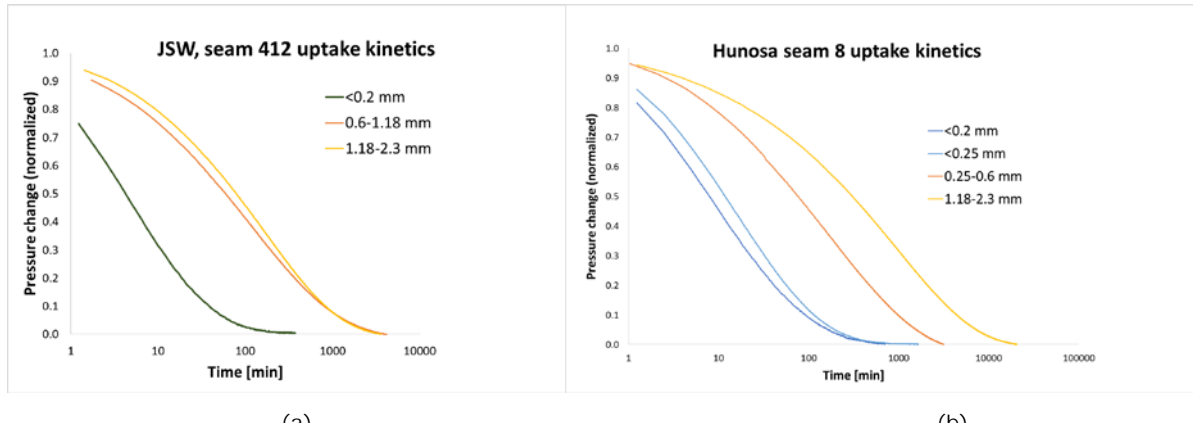
#### Gas uptake kinetics

Figure 2.2.1.5 presents normalised pressure decline curves for different grain fractions of the individual coal samples recorded during the high-pressure sorption experiments. As expected, the methane uptake is fastest for the smallest particle size fraction (<0.25 mm). Usually a significant decrease in uptake rates is observed for all larger grain size fractions.



**Figure 2.2.1.4:** Langmuir 3 parameter fitted high pressure isotherms of (a) seam #411 samples, (b) seam #412, (c) seam #413, and (d) from Monsacro/Sueros. All isotherms were measured in dry conditions and at a temperature of 45°C.





**Figure 2.2.1.5:** (a) Normalised pressure decline curves for gas uptake by different grain sizes of Zofiowka seam #412 coal, (b) normalised pressure decline curves for gas uptake by different grain sizes of Monsacro/Sueros seam #8 coal (semi-logarithmic plots).

## 2.2.2. WP1, task 1.2: Assessment of the prevailing stress state at different mine layouts

The main objective of this task was to implement both numerical and empirical methods to define the state and magnitude of stresses around working longwall and sublevel caving coal faces at JSW and HUNOSA to assist the initial design of field experiments in the project. As the progress in this task was already reported in the 1<sup>st</sup> Annual Report and Deliverable D1.2 in detail before, only a brief summary is included in this report.

### Numerical modelling of stress field affected by longwall mining at JSW

The field site selected for the underground experimental work at JSW is longwall D-2 exploiting coal seam 412, which is located at ~900 m below the surface. The thickness of the coal seam is reported as ~4.2 m, underlying a relatively strong sandstone roof. The planned dimensions of the longwall panel is 200 m wide and 1,750 m long (Figure 2.2.2.1).

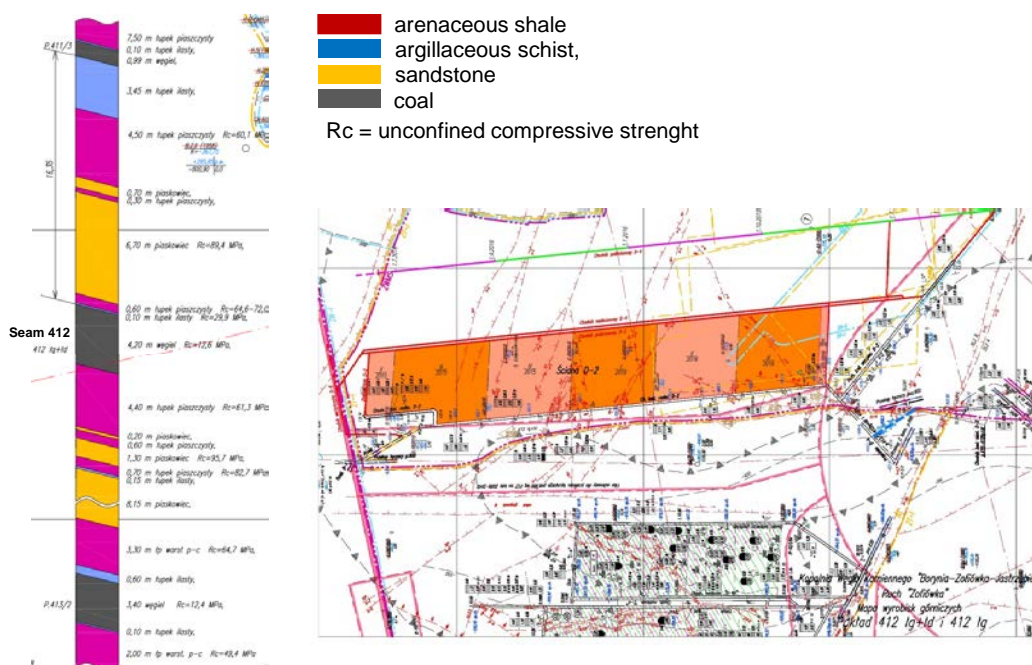


**Figure 2.2.2.1:** The seam section and Longwall D-2 selected as the experimental field site at JSW.

A  $150\text{ m} \times 250\text{ m} \times 61\text{ m}$  (length  $\times$  width  $\times$  height) model domain was constructed to simulate longwall coal extraction at JSW (Figure 2.2.2.2) in FLAC<sup>3D</sup>. A simplified geological setting of the longwall panel is illustrated in Figure 3.2.2.2a.

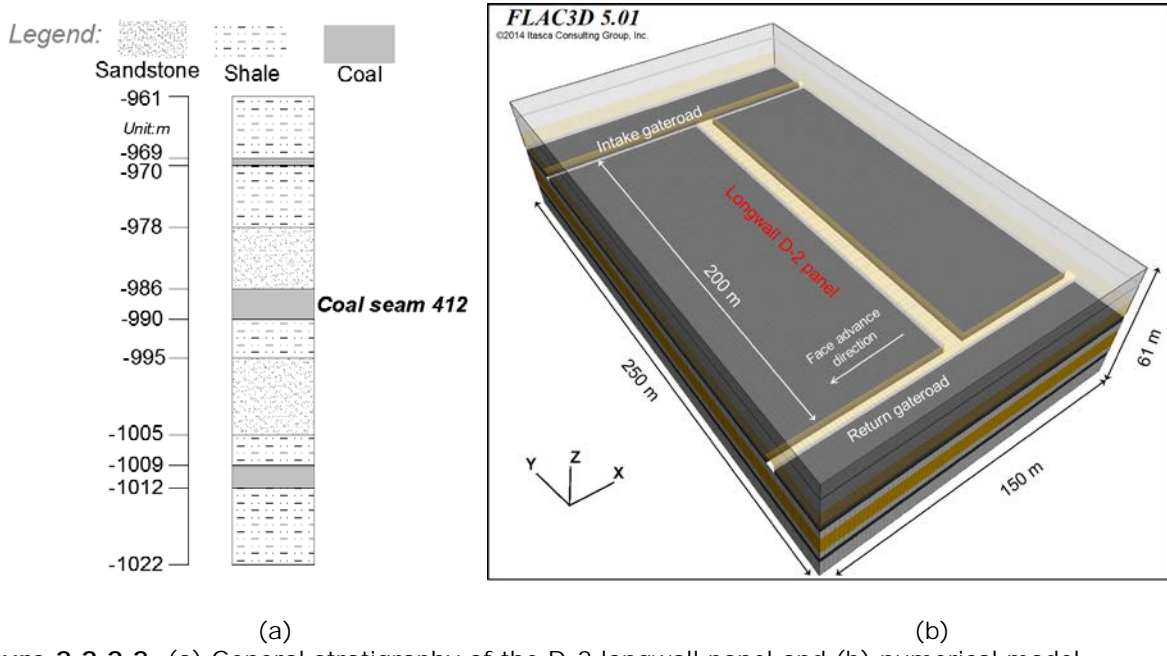


**Figure 2.2.2.2:** (a) General stratigraphy of the D-2 longwall panel and (b) numerical model geometry.

The model was developed to capture the effects of different stages of longwall mining on surrounding coal seams. Five stages of coal extraction at this panel were simulated and the coal produced was replaced with recompacted goaf material during the simulations. The key geomechanical parameters used in this study are summarised in Table 2.2.2.1

**Table 2.2.2.1:** Rock mechanical properties used for JSW longwall model.

	Bulk modulus (GPa)	Shear modulus (GPa)	Cohesion (MPa)	Internal friction angle (°)	Tensile strength (MPa)
<b>Coal seam</b>	1.26	0.60	4.25	22	1.26
<b>Sandstone</b>	8.00	3.70	25.82	30	8.94
<b>Shale</b>	2.90	1.35	19.53	25	6.13
<b>Goaf</b>	2.40	1.11	--	--	--

Longitudinal stress profiles for panel D-2 at different stages of face advance are shown Figure 2.2.2.3. The assessment of the change of stresses around the longwall openings and in the surrounding strata at each stage of face development provides the basis for gas drainage stimulation modelling.

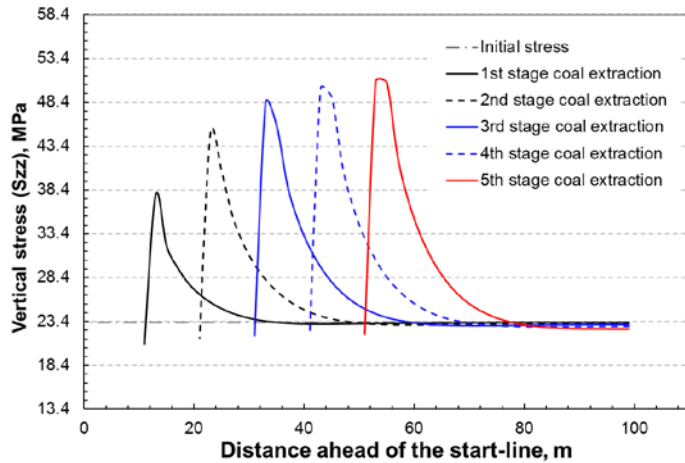


**Figure 2.2.2.3:** Vertical stress profiles over D-2 longwall panel: longitudinal section.

Stress redistribution in the underlying coal seam over five stages of face advance is shown in Figure 2.2.2.4. A stress relief zone can clearly be observed below the goaf area of longwall panel D-2, which can enhance gas drainage performance to a large extent.

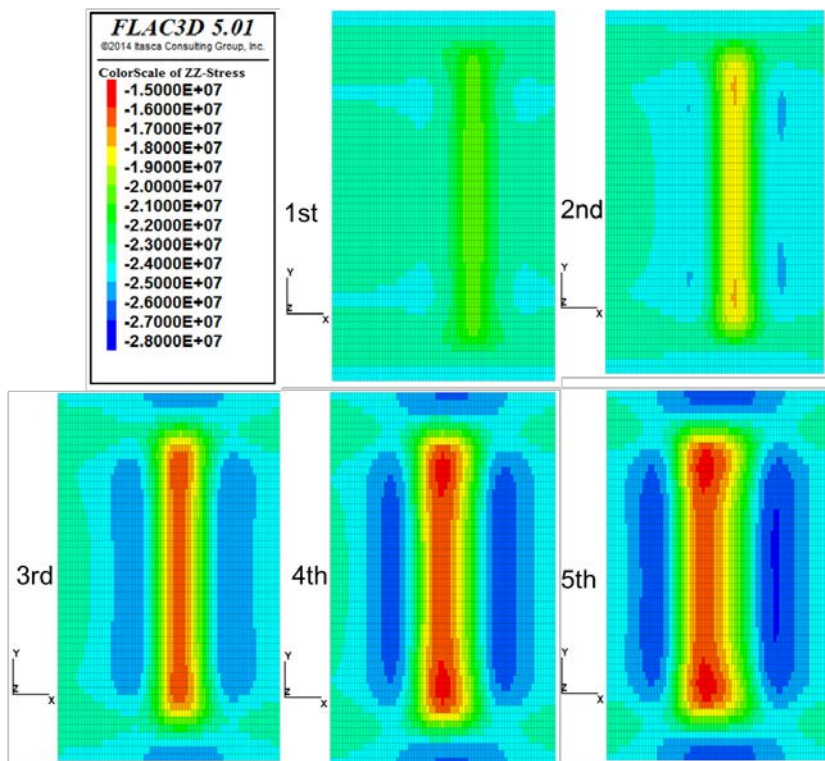


**Figure 2.2.2.4:** Vertical stress evolution at the floor coal seam during the extraction of the D-2 longwall panel (Pa).

#### Numerical modelling of stress field affected by sublevel caving at HUNOSA

The relatively soft coals with high gas content at Hulleras del Norte SA (HUNOSA) are characterised by the steep gradient (over 45 degrees) of most of the seams and gas outburst risk, particularly when driving the cross-cut and in-seam sub-level production headings (Figure 2.2.2.5). In this figure, hazards zones which are prone to coal and gas outbursts in the steep coal seam are marked in red circles.

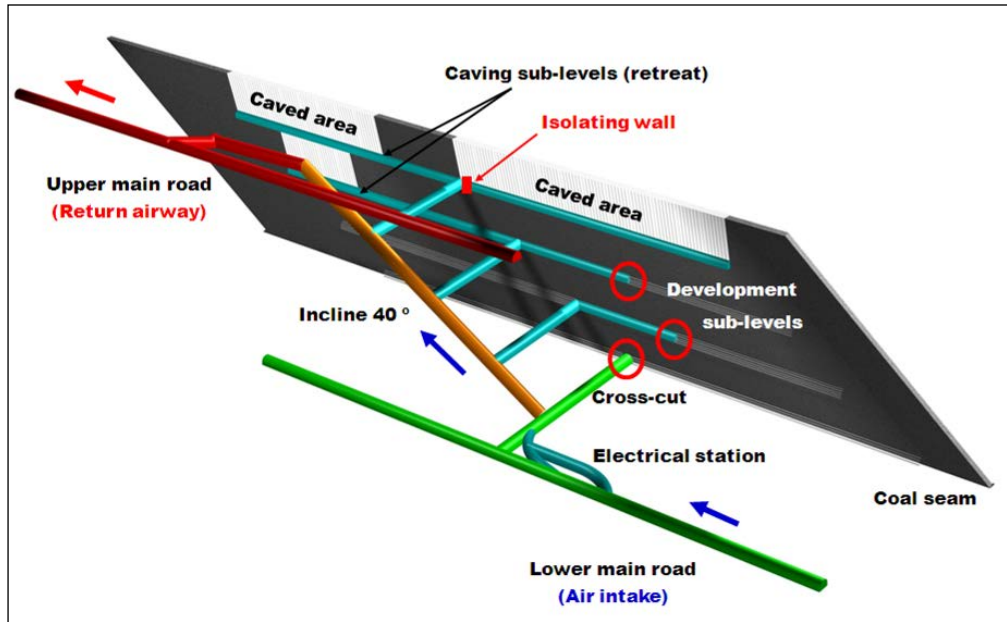
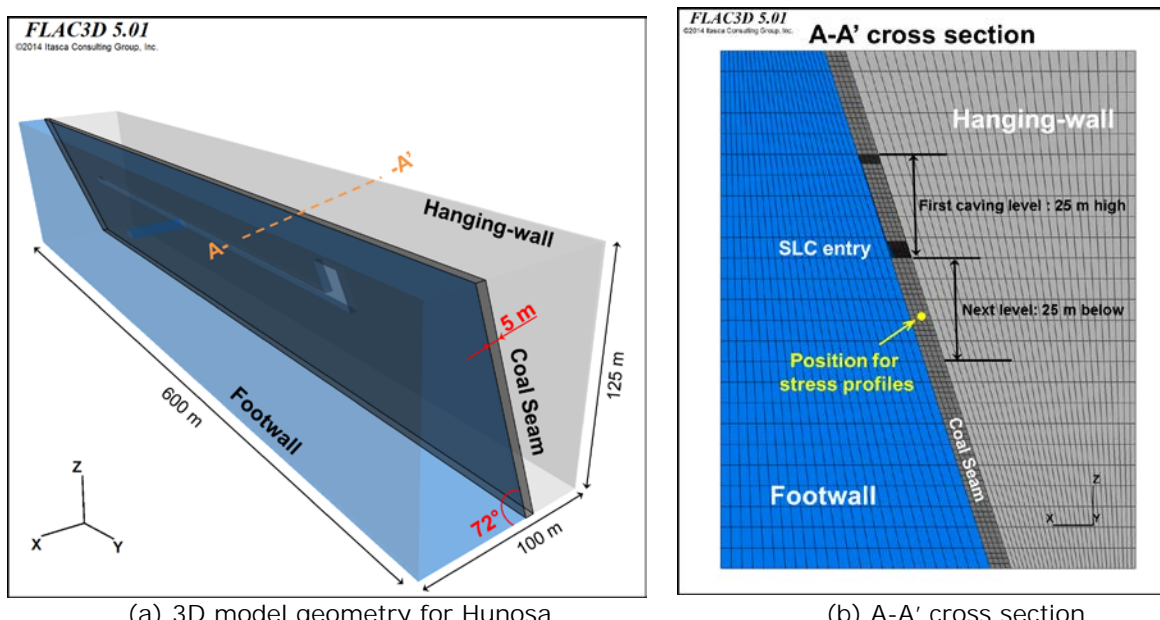


**Figure 2.2.2.5:** The schematic of the sub-level caving (SLC) mining method applied at HUNOSA (not to scale).

situ stress measurements at the Sueros Colliery has shown that, at 500 m depth, the maximum horizontal stress ( $\sigma_1$ ), minimum horizontal stress ( $\sigma_2$ ), and vertical stress ( $\sigma_3$ ) are 24 MPa, 16 MPa, and 11 MPa, respectively. The coal seam study in the study mine is ~4.5 m thick, dipping at an angle of 72°.

At this early stage of geomechanical modelling in the project, the effect of sublevel caving at one level on the stress distribution on coal seam at different elevations was investigated in a generalised SLC layout. A 600 m × 100 m × 125 m (length × width × height) model domain was constructed in FLAC3D. The hanging wall and the footwall were assumed to be sandstone with the same rock properties. The 125 m high model was designed to simulate a section of coal seam from 500 m to 625 m depth (Figure 2.2.2.6).



**(a) 3D model geometry for Hunosa**  
**Figure 2.2.2.6:** Model geometry developed for SLC at HUNOSA.

Six stages of coal extraction at the first level were simulated. At each stage of coal extraction, 20 m (along Y-axis) by 25 m (height) coal blocks are “removed” from the geomechanical model grid; these elements are “reinstated” at the next stage of coal extraction and assigned with the properties of a recompacted goaf material. The key geomechanical parameters used in this early modelling effort are summarised in Table 2.2.2.2.

**Table 2.2.2.2:** Elastic properties used for Hunosa SLC model.

	Bulk modulus (GPa)	Shear modulus (GPa)
<b>Coal seam</b>	1.26	0.60
<b>Sandstone (Hanging wall and footwall)</b>	62.96	12.06
<b>Goaf</b>	0.38	0.18

The initial stress equilibrium was established before any excavation was performed. The modelled *in situ* stresses at a depth of 540 m (1st caving level) were 15.6 MPa, 23.6 MPa, and 12.7 MPa, in the x, y and z axis respectively. The boundary conditions of the model were such that it was laterally confined and fixed at the base.

In total, six stages of coal extraction were simulated to observe the impact of different stages of SLC on stress redistribution in the coal seam. For each stage, vertical stress contours of the coal grids, which are adjacent to the footwall side are plotted in Figure 2.2.2.7. Different zones of stress evolution in the floor areas of the coal seam observed in the footwall regions of the coal seam will later be investigated in detail in Task 3.2 for the purposes of drainage stimulation schemes considered.

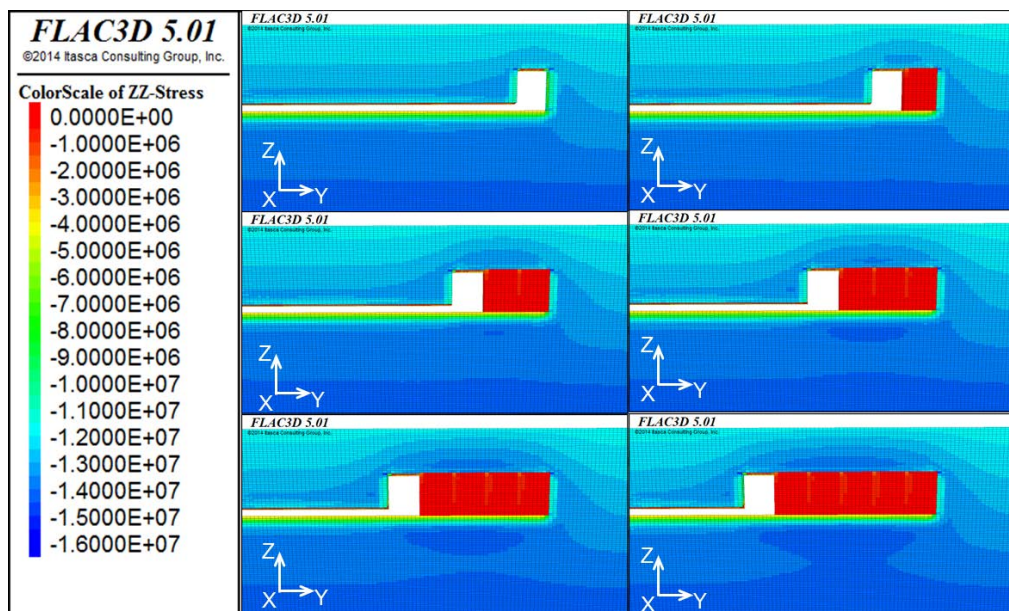


**Figure 2.2.2.7:** Vertical stress contours for the coal directly above the footwall after each stage excavation (viewed from the footwall side).

These initial stress analysis have shown that the floor coal, which is due to be extracted at the next sub-level, has experienced a considerable stress increase. Note that this increase is more significant for the coal directly above the footwall side. Example stress profiles for the coal seam at the next SLC level are shown in Figure 2.2.2.8. These stress profiles were plotted along the strike of the coal seam and at location marked in Figure 2.2.2.6b. Increased stress abutments can be observed in all the directions, which increase after each excavation stage both in scale and magnitude.

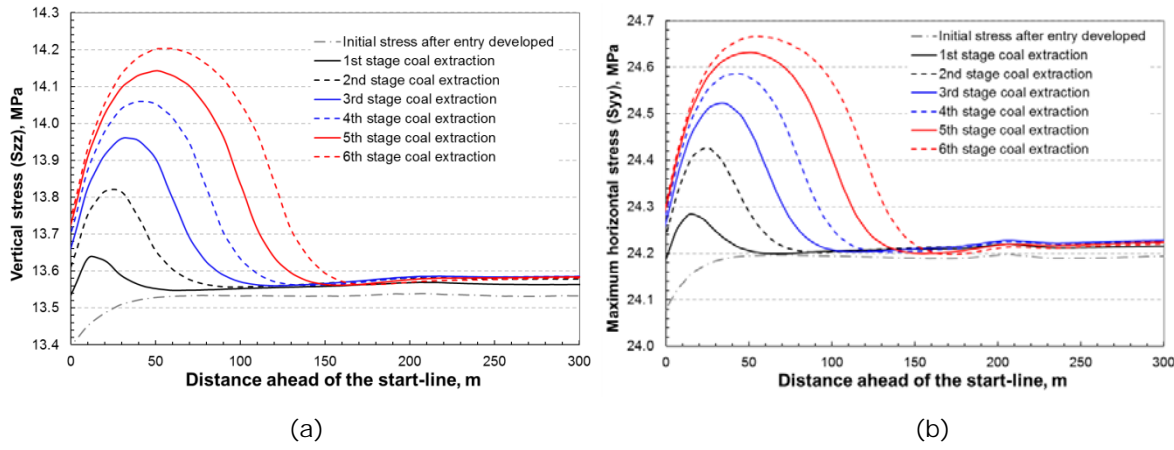


**Figure 2.2.2.8:** (a) Vertical stress profiles, (b) Maximum horizontal stress profiles at the floor coal being affected by SLC in an upper level.

As described under Task 3.2 report, a more detailed stress analysis was later conducted when evaluating the drainage performance of slotted boreholes at Sueros Colliery, Hunosa.

#### Assessment of stress influence due to mining in adjacent levels at JSW Zofiówka Colliery

Coal mine "Zofiówka" is exploiting multi coal seam deposits. In the proximity of coal seam #412, four other seams were exploited. Among them, three seams induce stress changes reaching the longwall panels D-2 and D-4 (Figure 2.2.2.9). Seams #409/3, #409/4 and #410, lie in vertical distances of 97m, 70m and 35m, respectively. To calculate vertical stress distribution in the plane of seam #412, empirical-analytical method developed at GIG (Kabiesz, Makówka 2009) has been used

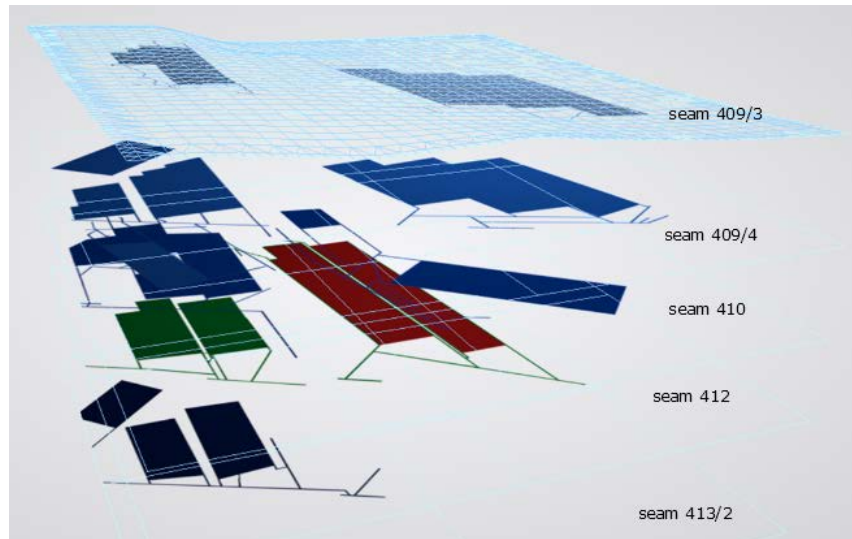


**Figure 2.2.2.9:** Location of extracted panels in seam #412 and surrounding seams.

One example findings of the calculations is presented in Figure 2.2.2.10, which takes into account stress changes due to the presence of workings and local faults. As a follow on study to the work carried out in this task, the Deliverable D1.3 report further expands on the methodology and results obtained by this methodology.

Stress state highly influences methane desorption rate. As described under Task 3.1 report, a more detailed stress analysis was later conducted for the evaluation of drainage performance of stimulated boreholes at the Zofiówka Colliery.

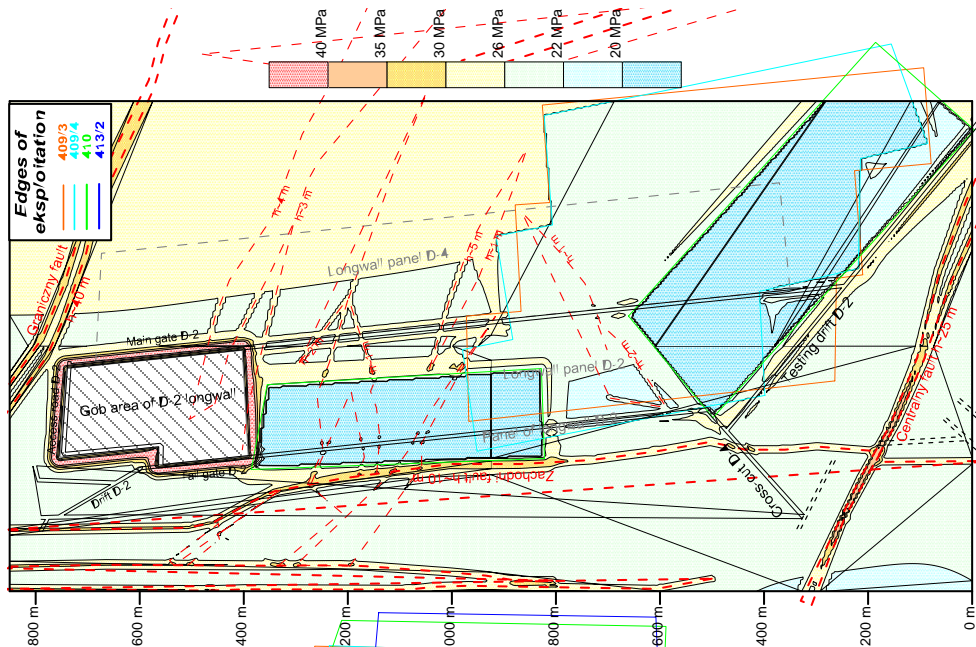


**Figure 2.2.2.10:** Vertical stress distribution in the longwall panel D-2 and neighbourhood in seam 412 in 31 December 2015.

### 2.2.3. WP1, Task 1.3: In-situ measurements of coal and surrounding rock properties

The effectiveness of the stimulation methods depends on the prevailing stress regime, stress and permeability contrasts induced under underground coal mining conditions. The in situ stress state, orientation and magnitude, as well as the mechanical/elastic properties of coal seams and the roof and floor rocks will control fracture propagation in stimulated underground gas drainage.

Task 1.3 in GasDrain involved drilling and instrumenting a number of boreholes at selected JSW and HUNOSA sites to carry out field experiments to establish the in situ stress and reservoir properties of the coal seams and surrounding rocks that are affected by coal production. The Deliverable D1.3 presented a comprehensive description of the work carried out under this task. Therefore, this report presents a brief summary of the results of the experiments carried out by the research partners.

#### 3D in situ stress measurements at JSW

The measurement of in situ 3D state of stresses underground help verify the numerical modelling results. This information is also necessary to design the system of drainage boreholes in longwall panel D-2 at JSW collieries. The in situ stress measurement has been performed using the "directed hydrofracturing" method (N-UHS) as described below (Makówka 2015).

#### Field measurement methodology

The prerequisite for determining triaxial stress state with directed hydrofracturing is to conduct a series of measurements on the closing pressure of fractures induced perpendicularly towards the axes of boreholes of differentiated spatial orientations. In each of the boreholes an initial fracture is created, i.e. a kind of a cut in the plane perpendicular towards the axis of the borehole, as shown in Figure 2.2.3.1. Detailed description of the methodology is described in Deliverable D1.3 Report.

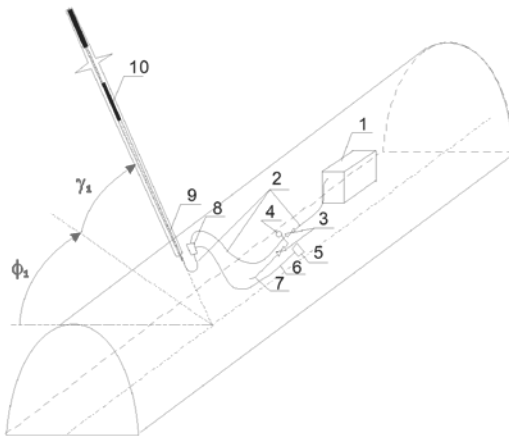


**Figure 2.2.3.1:** Simplified schematics of N-UHS measuring system. 1 – mobile pump, 2 – high-pressure hoses, 3 – valves, 4 – manometer, 5 – recorder, 6 – signal cable, 7 – drain hose, 8 – pressure and flow sensors, 9 – cable/high-pressure hose, 10 – packer.

### Measurement site and results

The measurement site was located in the tail gate D-2 as shown in Figure 2.2.3.2a. This is also the site where further experiments within WP4 and WP5 will be performed. Figure 2.2.3.2b presents the site with 9 boreholes. The number of drilled holes, in excess to the requirements of the method, stems from the need to ensure against the possibility of encountering unforeseen discontinuities in the rock mass or other factors preventing effective hydrofracturing.

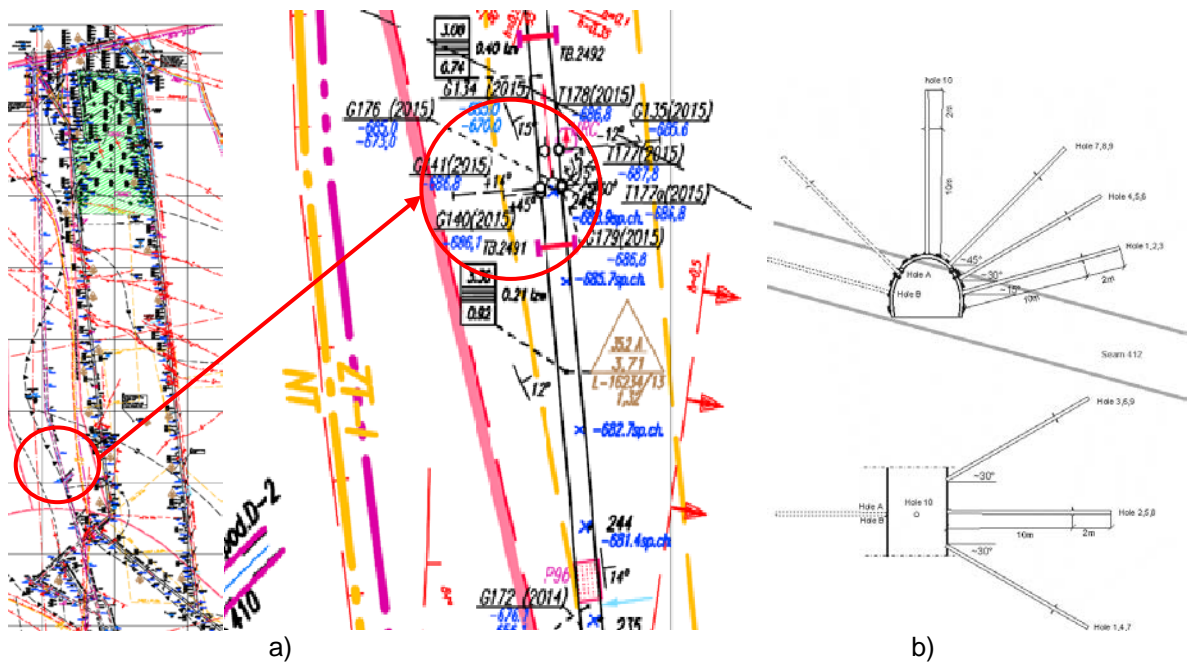


**Figure 2.2.3.2:** Site of the stress measurements (a) and boreholes to measure characteristic hydrofracturing pressures (b).

From each of the boreholes a record of changes in pressure and flow rate of the pumped water were obtained. An example of such a record is shown in Figure 2.2.3.3. When loss of water flow is observed in the same record, the fracture re-closure is determined.

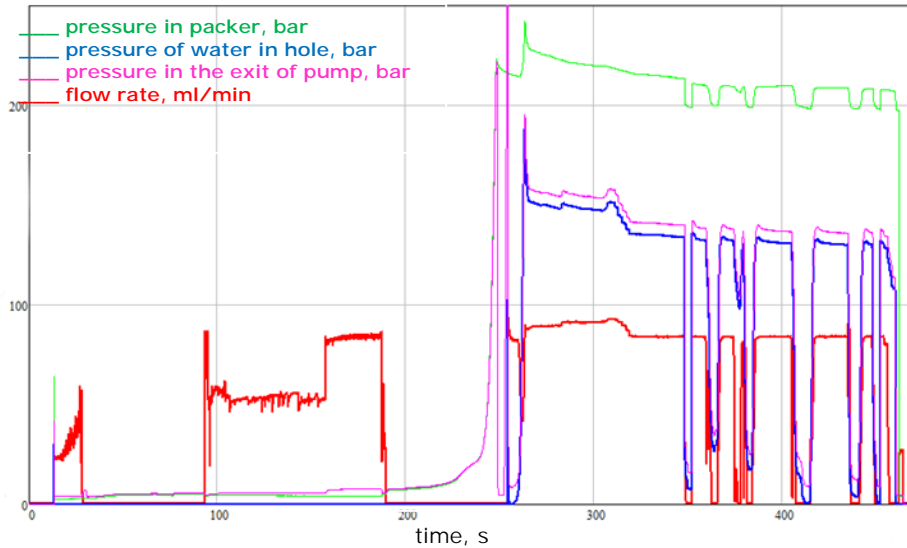


**Figure 2.2.3.3:** Example of pressure and flow rate record measured in one of the boreholes.

Table 2.2.3.1 lists parameters of holes and re-closing pressure in the holes, which gave the best results of hydrofracturing.

**Table 2.2.3.1:** Borehole angles and re-closing pressures.

Borehole No.	Elevation angle $\gamma$ , deg	Direction angle $\varphi$ , deg	Reopening pressure $P_s'$ , MPa
1	14	55	4.74
5	30	94	11.5
6	26	124	12.03
7	48	55	4.77

On the basis of the measurement results and the borehole parameters principal stress values were obtained as follows:

- vertical stress  $S_v = 4.703$  MPa
- major horizontal stress  $S_H = 59.07$  MPa
- minor horizontal stress  $S_h = 16$  MPa

Direction of major principal stress  $S_H$  was determined as corresponding with the tail gate D-2 direction (deflected by  $3^\circ$ ), minor horizontal stress is perpendicular to it.

Further details of the methodology and the analysis of individual measurement results are available in Deliverable D1.3 report.

### 3D stress distribution in the rock mass surrounding longwall panel D-2

Complicated geological and mining conditions in longwall panel D-2 and its surroundings implied the need for knowledge of stress distribution in the seam 412 and also in its neighbourhood where potential sources of stress disturbance and methane are located. It was therefore necessary to analyse a large volume of rock mass in proximity of longwall panel D-2. For this purpose an empirical-analytical method, originally developed in GIG and recently improved, was employed.

### Results of stress distribution analysis

The next figures present the results of modelling of stress distribution in the panel of longwall D-2 in seam 412, being influenced by a complex system of edges produced by earlier mining conducted in 3 neighbouring seams and in seam 412. An example of such representations is presented in Figure

2.2.3.4, which shows the layout of many edges marking, in many seams, many panels of completed mining.

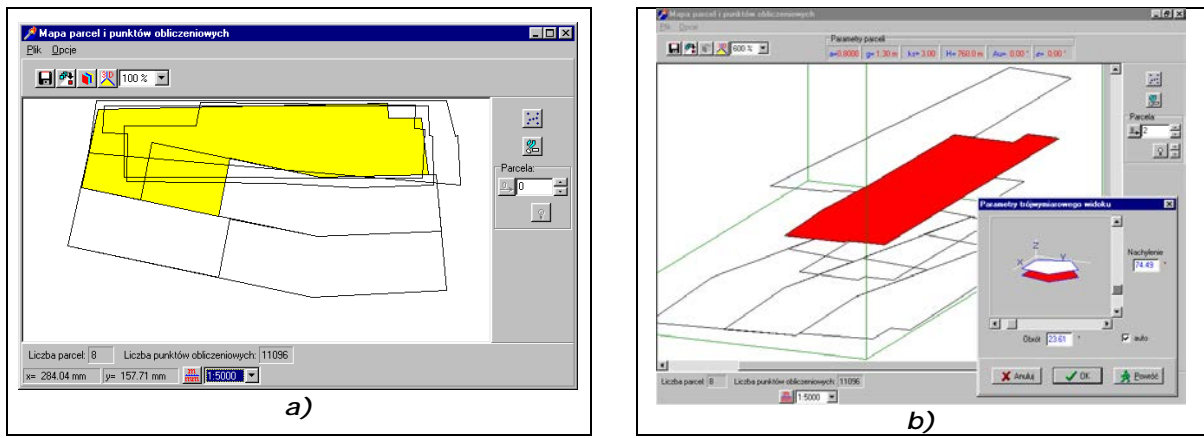


**Figure 2.2.3.4:** Layout showing many mining plots (edges) in the bundle of seams, a) projection on a plane of analysed seam, b) spatial view.

Longwall panel D-2 is located in coal seam 412. Stress distribution in the area is shaped by:

- the depth of the seam: between 950 and 1000 m; it gives natural stress from overburden of 25 MPa;
- local tectonic faults,
- gob areas of mined longwall panels in the seams above:
  - in seam 409/3 located 88 to 130 m above seam 412,
  - in seam 409/4 located 70-90 m above and
  - in seam 410 located 35-50 m above.

In the middle part of panel D-2 stress distribution is affected by exploitation conducted in seam 410 by longwall D-4 above. The longwall was finished in December 2015 and the extended range of destressing effect of the gob area to seam 412 was evident as described in detail in Deliverable D1.3 report.

Longwall exploitation also alters stress distribution around produced goaf areas in vertical direction. It strongly influences methane inflow. To analyse that in the proximity of longwall D-2 in seam 412 a series of calculations for different planes parallel to seam 412 has been made. The results are integrated to 3D representations. One of the visualisations of the results is presented in Figure 2.2.3.5.

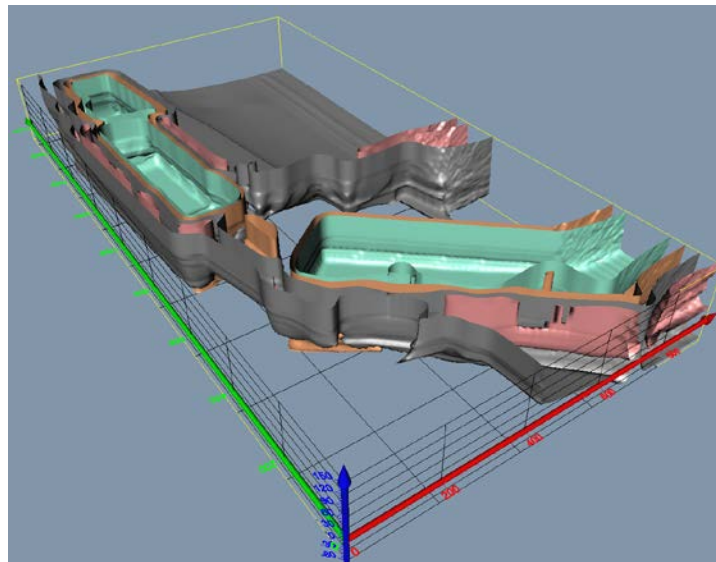


**Figure 2.2.3.5:** Vertical stress distribution around longwall panel D-2 isosurfaces of 15 MPa (green), 20 MPa (orange), 25 MPa (grey) and 30 MPa (red).

The images give information about how strongly the stress state is disturbed by the exploitation of seams 409/3, 409/4, 410 and 412 itself. Destressed zones cause increased release of methane from neighbouring seams and it can migrate to the free spaces and active mine workings.

The results served as input to calculate long term forecast of absolute methane emission rate for the coal panel D-2.

#### **Methane content distribution and emission rates in longwall panel D-2**

Forecast of the absolute methane emission rate for the coal panel D-2 in the coal seam 412 was evaluated based on the Central Mining Institute Instruction #14 entitled "Dynamic forecast of absolute methane-bearing capacity of the coal panels (technical guide)". Above method was used to determine volume of released methane in the environment of coal panel D-2 subject to the progress of coal exploitation.

Forecast of absolute methane emission rate, i.e. methane release along the designed coal panel length also takes into account the following sources of methane:

- methane release from the exploited coal seam,
- methane release from the underlying and overlying coal seams,
- methane release from the longwall goafs after decay of direct drainage,
- possible methane inflow into the exploitation district.

#### *Characteristics of mining and geological conditions and development of methane content*

D-2 coal panel is exploited in the coal seam 412 - in the developed part of the bed at the depth from 958.3 m down to 1,037.6 m. Coal thickness of the coal seam varies there from 4.06 m up to 4.89 m.

The parameters of D-2 coal panel in the coal seam 412 are as follows:

- total length of the panel: 1230 m;
- height of the exploitation gate: 4.1 m;
- width of the panel: 165 (length 0-180 m), 205 m (length 180-1230 m),
- system of exploitation: along the strike with caving.

Inclination of the coal panel: crosswise +12° – -10°, lengthwise 0 – 19° (locally 24-30° in the neighbourhood of incline drift D-2).

The value of methane content in the coal seam to be exploited was identified based on the results of methane content laboratory tests conducted during roadway development, surrounding plot of the designed panel. In the coal seams strongly saturated with gas - above  $4.5 \text{ m}^3 \text{CH}_4/\text{Mg}_{\text{daf}}$  and endangered by gas and rock outburst, the methane content tests are conducted during roadway development works - every 50 meters.

Figure 2.2.3.6 shows the coal seam methane contents in the roadways surrounding coal panel D-2 and their determined isolines in the panel designed for exploitation. Marked isolines with the values of 5, 6, 7 and 8  $\text{m}^3 \text{CH}_4/\text{Mg}_{\text{daf}}$  indicate changes of methane content in the individual sections designed for coal exploitation by D-2 coal panel.

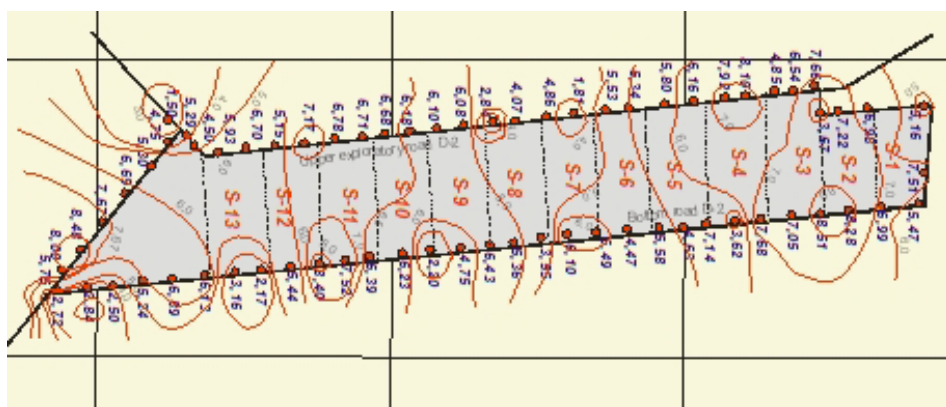


**Figure 2.2.3.6: Distribution of methane content in D-2 coal panel**

The D-2 coal panel was divided into 13 smaller sections at 100 m lengths from S1 up to S13 in accordance with the direction of coal exploitation.

The average methane content in the individual sections can be calculated as an arithmetic mean from the division of the coal panel length - every 50 m. For each cross-section from 13 exploitation sections average methane content was calculated giving methane content distribution shown in Figure 2.2.3.7.

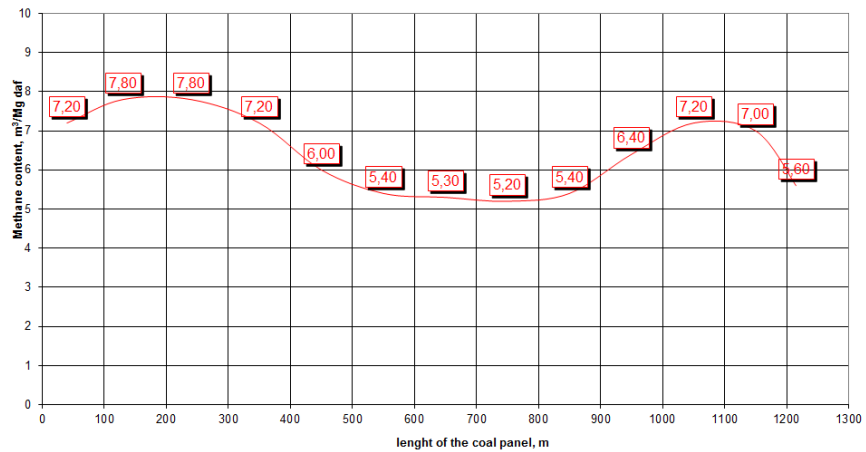


**Figure 2.2.3.7:** Average methane content along the length of the D-2 coal panel

During the calculations impact of bed relaxation and degassing of the coal seams (including coal seam 412, as a result of the exploitation already carried out in seams 409/2, 409/3 and 410) were considered. Further details of these studies are available in Deliverable D1.3 report.

#### Determination of the desorption zone and rate of degasifying the underlying and overlying seams

Rate of degasifying the roof and floor layers in the neighbourhood of the designed coal panel is being calculated using trigonometric interrelations and its graphical interpretation is shown on Figure 2.2.3.8.

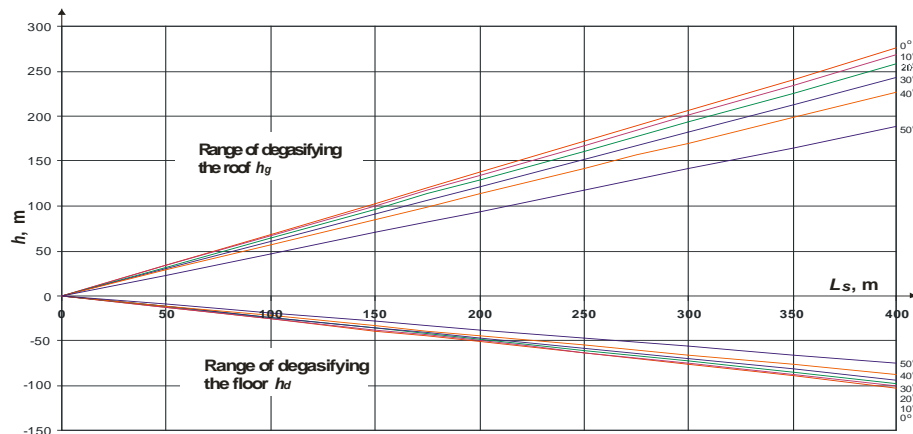


**Figure 2.2.3.8:** Rate of degassing the underlying and overlying layers subject to the length and inclination of the coal panel.

#### Dynamic forecast of absolute methane emission rate for the coal panel D-2

Forecast of absolute methane emission rate of D-2 coal panel enables determination of methane hazard, relating the volume of methane emissions to the location of the coal face along its length and to the determined gassy conditions in the specific location. For the individual cross-sections: S1-S13, relating the results to the daily progress of the coal face between 1 - 10 m/d, following forecasted parameters were calculated.

Estimation of methane release to the environment of the longwall from individual sources allows for adjusting the parameters and method of ventilation the longwall, drainage technology to be applied and selecting methane hazard prophylactics.

Based on daily progress of the longwall, collective register of the forecasted volumes of released methane for the cross-sections S1-S13 was prepared. Further details of emission predictions for the panel are reported in Deliverable D1.3 report. The predicted methane emission rates in D-2 coal panel along the cross-sections S1-S13 are also shown graphically in Figure 2.2.3.9.

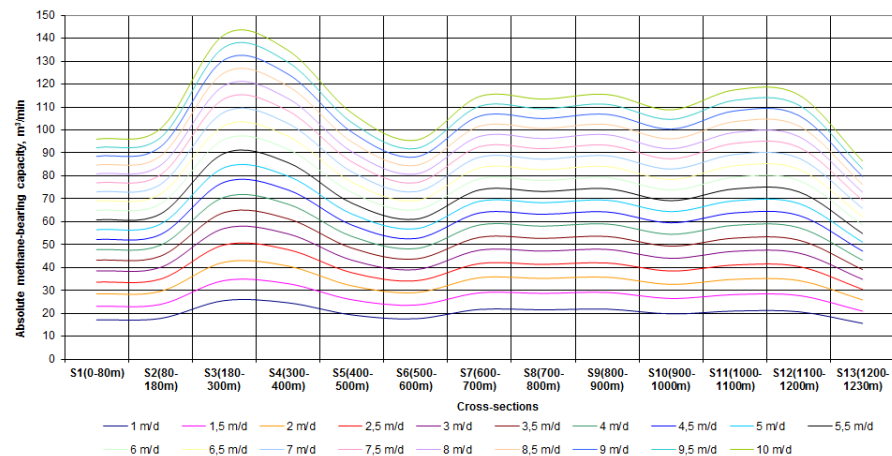


**Figure 2.2.3.9:** Forecasted absolute methane emission rate along the length of the coal panel D-2.

#### In situ gas content of coal seam 412

At the start of GasDrain project D-2 bottom gateroad was being driven, following the completion of the exploratory D-2 tail gate and D-2 raise at the end of 2014. In situ gas contents of the coal seam around the D-2 coal panel which will be studied at the field test site was determined during the development of this heading.

Gas content measurements were conducted in 4 locations at the length of D-2 bottom gateroad, starting from D-2 ventilation-exploratory incline (at 208, 504, 700 and 750 m).

Figure 2.2.3.10 shows the locations and dates of collecting the coal samples in order to perform the gas content measurements. At locations 208 and 750 m along the length of the D-2 bottom roadway, 3 samples were collected at each place in the cross-section of the coal seam 412 as:

- from the top part, close to the roof of the seam,
- from the middle part of the seam,
- from the bottom part of the seam.

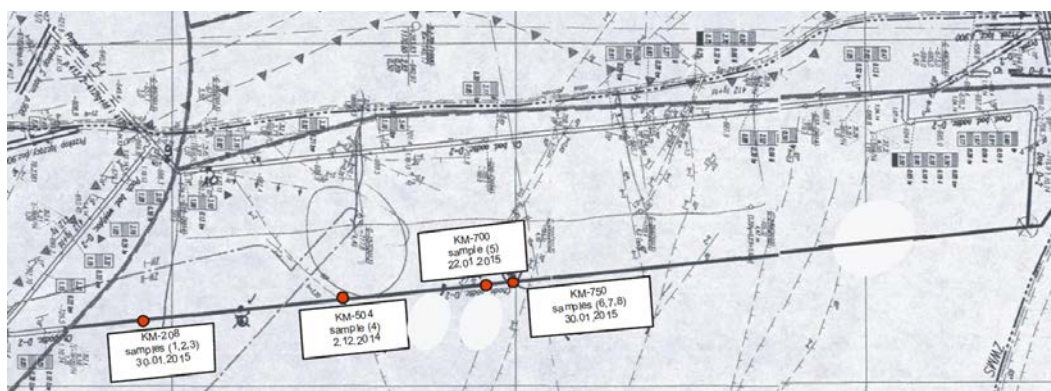


**Figure 2.2.3.10:** Locations and dates of collecting the coal samples in order to perform in situ gas content measurements.

In situ gas contents of the coal seam are presented in Table 2.2.3.2. The last column of this table presents the average methane contents in the sections of the panel length, where the gas content measurements were conducted.

**Table 2.2.3.2:** In situ gas content measurement data for the coal seam 412.

Length of the D-2 bottom road Date of collection	Collected sample	Gas content, $a$	Gas content in clean coal, $a_{\text{daf}}$	Ash content $P$	Average methane content in sections of the panel
		$\text{m}^3/\text{tonne}$	$\text{m}^3/\text{tonne}_{\text{daf}}$	%	$\text{m}^3 \text{CH}_4/\text{Mg}_{\text{daf}}$
1 KM-208 30.01.2015	2 Top part of the seam	3 5.500	4 5.659	6 2.82	7 S-13 5.6
KM-208 30.01.2015	Middle part of the seam	5.494	6.384	13.94	S-13 5.6
	Floor part of the seam	5.227	5.655	7.57	
	KM-504 2.12.2014	Middle part of the seam	3.882	4.429	12.35 S-10 6.40
KM-700 22.01.2015	Middle part of the seam	5.022	5.120	1.92	S-9 5.4
KM-750 30.01.2015	Top part of the seam	4.381	4.590	4.54	S-8 5.2
	Middle part of the seam	5.005	5.113	2.10	
	Floor part of the seam	5.867	6.175	4.98	

#### **In situ measurements of coal permeability at JSW**

The in situ coal permeability measurements were carried out in a vertical borehole drilled from the 930 m level down to 967.0 m from the ground surface. The borehole length was 37.0 meters. The 5 inch casing was set and cemented at 961.0 m leaving open the coal seam between 961.0 to 967.0 m. The coal seam thickness was about 6 m. Next, the borehole was left for pressure stabilisation.

After some days, the water table in the well stabilised to some centimetres below the surface. No outflow of water was observed which means that the reservoir pressure in coal seam around the well corresponds to the hydrostatic pressure of water column i.e. 0.37 MPa.

Next, the pressure gauge was run to the mid-point of coalbed (i.e. 964 m) and some water was blown out of well using the compressed air. This caused the water table to drop 3 m below the stabilised level. The Figure 2.2.3.11 shows the diagram of the coal permeability measurements.

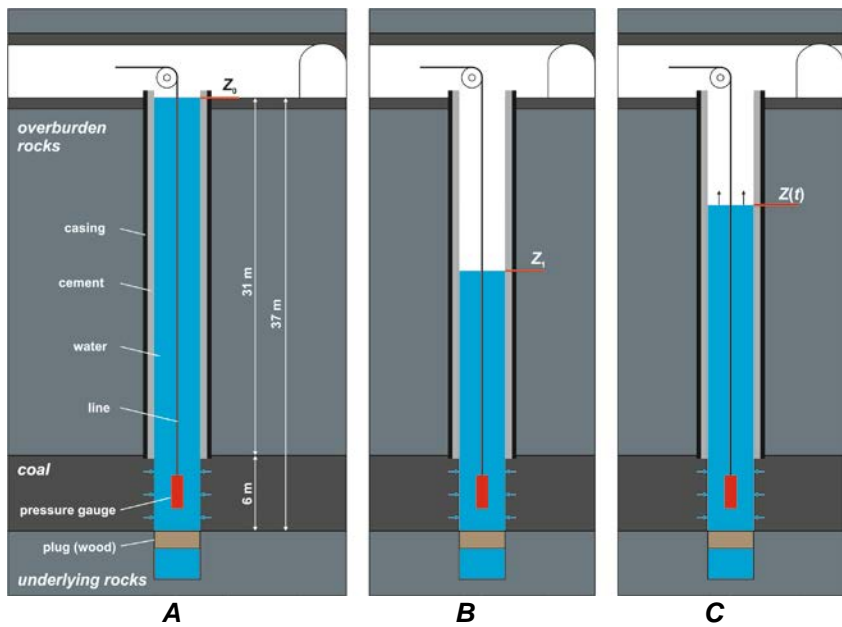


**Figure 2.2.3.11:** Diagram of the coal permeability measurement A).Hydrostatic pressure balance the reservoir pressure in coal, B) Removal of some fluid volume from the well, C) Monitoring the fluid table behaviour.

Measurement of water table behaviour was carried out using the INiG-PIB pressure gauge developed specially for that purpose. This new equipment (Figure 2.2.3.12) meets the restrictive safety regulations which are obligatory for methane coal mine like Zofiówka (JSW).

Measurements of the water table level are based on the relation between length of water column and pressure. Major parts of pressure gauge are: measuring system, DAQ modulus and battery.



**Figure 2.2.3.12:** Pressure gauge developed by INiG-PIB

The measuring segment is a piezo-resistive silicon cell protected from water contact with special membrane. The gauge amplifier is protected from overloading by special overvoltage protection system. The signal emitted by the measuring system is changed to digital form and transferred to microprocessor used for control the measuring signal, correcting temperature errors, performing signal linearization and so on. The results of measurements are recorded in gauge memory. The pressure gauge is a stainless steel cylinder with outer casing which protect the measuring system from mechanical impacts. The gauge is run into hole using the nylon line.

#### *Results of permeability measurements*

Time of measurements was around 1,400 min. The pressure vs. time relation recorded while the well returns to stabilisation is shown in Figure 2.2.3.13.

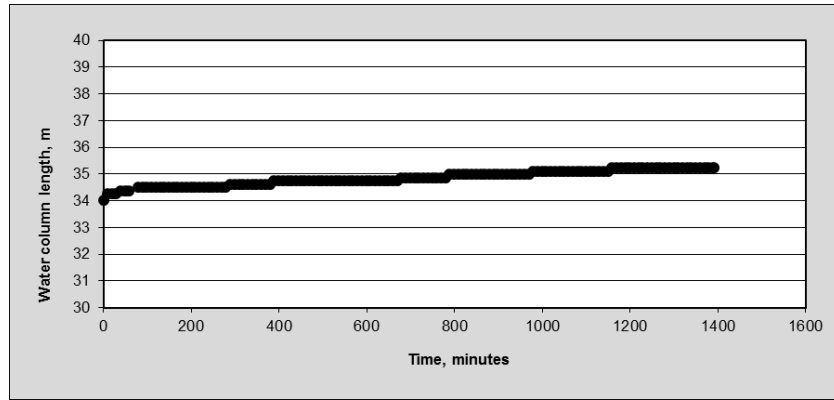


**Figure 2.2.3.13:** Pressure vs. Time curve.

The recorded data was interpreted using INiG-PIB and slug test methods. The input data were as follows:

- Well depth – 37.0 m
- Stabilised water level - 37.0 m
- Water level after some water is removed from the well – 34.0 m
- Coal porosity – 4 %
- Well radius – 0.065 m
- Casing inner radius – 0.06 m
- Water viscosity – 1 mPas
- Thickness of coalbed – 6 m
- Water density – 1000 kg/m<sup>3</sup>
- Total compressibility – 0.00306 1/MPa

#### *Results of test interpretation – INiG-PIB method*

The log pD vs.t relation is shown in Figure 2.2.3.14.

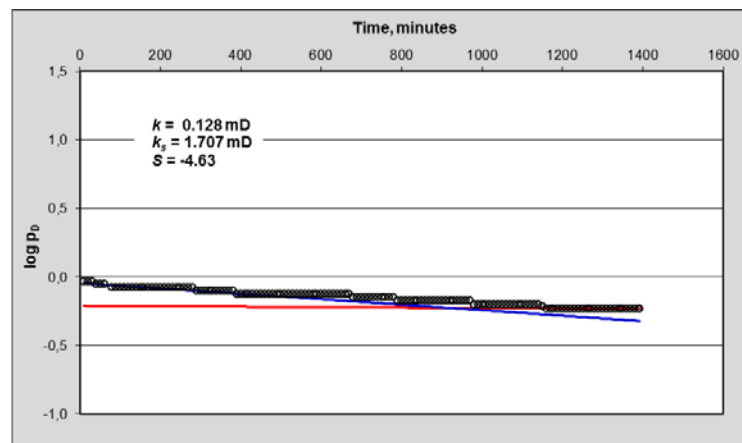


**Figure 2.2.3.14:** log pD vs. time curve.

The short time data indicate a fracture permeability (permeability of the wellbore zone) whereas the late time data indicate the coal matrix permeability. The following results were obtained:

- Permeability of the wellbore zone (fracture permeability) – 1.707 mD.
- Permeability of coal matrix – 0.128 mD.
- Skin effect – -4.63

It should be noted that if a coal pressure is greater than that assumed then the calculated permeability would be lower.

#### *Results of test interpretation – Slug Test method*

The “slug test” method consists in fitting the curve (constructed using the recorded data) to one of curves among the family of theoretical curves.

Results of test interpretation using the “slug test” method are given below in Table 2.2.3.3.

**Table 2.2.3.3:** Results of slug test method interpretation.

Match of real curve to theoretical curves	Permeability [mD]	Skin effect	Parameter of theoretical curve
Parameter of theoretical curve	0.1771	-5.2394	2
Initial portion of curve	0.1778	-5.2394	2
Final portion of curve	0.1826	-5.2394	2

As shown, both methods (INiG-PIB and “slug test” method) yielded similar results.

In the near future, it is planned to run the several short time water injection tests in horizontal gas drainage wells using specially developed equipment. The test results will be interpreted using novel methods developed in INiG-PIB.

#### **In situ measurements of coal permeability at HUNOSA**

The objective of Task 1.3 at HUNOSA was to carry out a series of in-situ measurements to determine the values of the coal seam parameters which have an influence in the hydraulic stimulation processes that is planned for enhanced methane drainage. Work has been focused in the investigation of the hydraulic permeability of the #8 coal seam on Sueros Colliery (HUNOSA).

To achieve this objective, a number of boreholes have been drilled perpendicular to the seam, from a rock gallery located in the footwall, at about 65 m from the seam.

These boreholes cross seam #9, which is not an objective of the project, so it has been necessary to develop a specific procedure to seal the boreholes and guarantee that they are isolated from this seam. Different alternatives have been tested to solve this problem. In total, 10 boreholes were drilled to tests different methods. This caused some delay in the execution of this task, but finally an adequate solution was found, and a total of three boreholes could be drilled and adequately equipped.

A series of water injection pulse tests have been carried out in the #8 seam from one of these boreholes, using the other two, plus another in-seam borehole drilled from the gallery heading, as observation boreholes. The objective of these tests was to characterise the seam from the hydraulic conductivity point of view.

#### **Hydraulic characterisation of the 8th coal seam at Sueros Colliery**

##### *Seam layout at the test area*

The target of the project is seam #8, which in the area selected for the test has an inclination of about 70° and a thickness of about 4 m (see Figure 2.2.3.15). This seam has a high methane content and is prone to gas outbursts. The seam #9, which is located at the footwall of #8, is of poor quality but has been traditionally mined as a shield seam to release stresses in #8, in order to prevent gas outbursts risks when mining the latest. One of the main objectives of this project is to investigate the possibility of not mining seam #9. It is expected that the planned hydraulic stimulation, in combination with enhanced gas drainage, will enable to achieve a sufficient degree of stress release in #8, providing similar safety conditions at much lower cost.

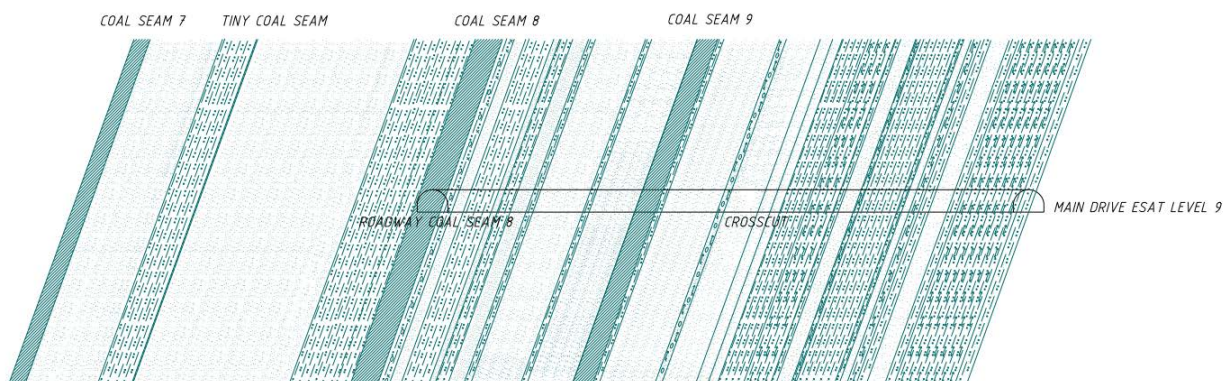


**Figure 2.2.3.15:** Stratigraphy at the mine test area in Sueros Colliery.

### Borehole configuration

The borehole drilling pattern for the hydraulic characterisation is shown in Figure 2.2.3.16 (plan view) and Figure 2.2.3.17 (vertical cross section). Four boreholes (S11 to S14) were drilled from the access gallery to the panel 8<sup>a</sup>-III at Level 9, all them starting from the same point. The boreholes have an upwards inclination of 4° and cross seam #9 at about 31 m, and seam #8 at about 64 m.

An in-seam borehole (S21) was also drilled from the gallery heading, parallel to the seam (Figure 2.2.3.16).

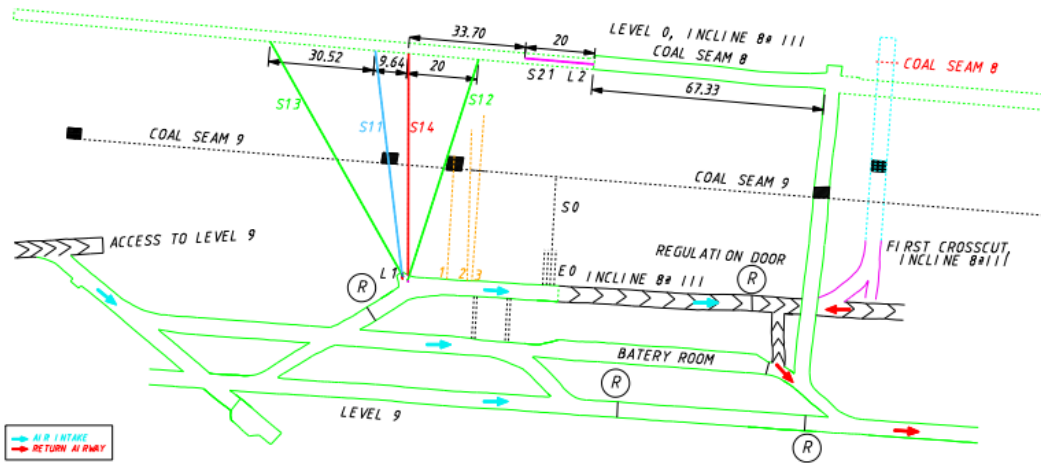


Figure 2.2.3.16: Borehole layout at the Sueros Colliery test site (plan view).

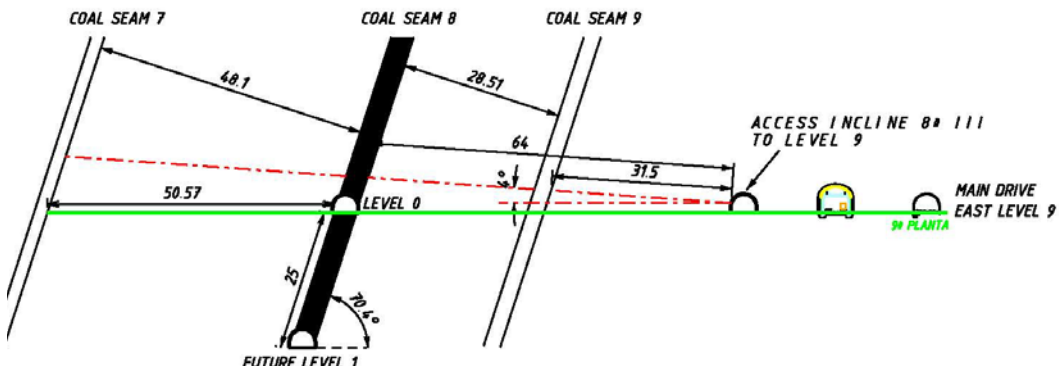


Figure 2.2.3.17: Borehole layout at the test site (vertical cross section at S14).

### Borehole completion

A high pressure steel pipe, used in the past for testing CO<sub>2</sub> blasting in this area (DACP system), was selected as injection tubing, as the injection pump can reach a pressure of up to 280 bar. The DACAP tube has an internal diameter of 12.5 mm and 25.00 mm external, and can withstand up to 840 bar. Centering devices were built to keep the tube in the borehole axis. Figure 2.2.3.18 shows different phases of these tests.



**Figure 2.2.3.18:** Preliminary cement injection tests.

The boreholes were not cased, as the idea was to cement the annulus between the injection pipe and the borehole to avoid fluid circulation along the borehole. In particular, sealing of the crossing of the #9 seam was critical.

A series of preliminary tests were carried out in a different group of boreholes drilled entirely in rock between two parallel galleries, to adjust the parameters of the cement grout, and to test and refine the grouting process. After solving a series of practical problems, finally a good cementing could be obtained. Further details of the measurements and analysis are presented in Deliverable D1.3 report.

### Hydraulic characterisation tests

The permeability of the coal seam is the basic parameter to design the hydraulic stimulation system, and in particular aspects such as the optimal borehole spacing and injection pressure. Laboratory tests can hardly provide data about permeability at macro scale, as #8 coal seam is of a very heterogeneous nature, being actually composed by a series of thin coal strata with some dirt bands, and in consequence it is impossible to get a representative sample at lab scale. The aim of the mine tests was therefore to try to characterize the #8 coal seam from the hydraulic conductivity point of view at macro scale.

#### Test procedure

A test protocol was agreed with the Imperial College team, which is summarised in the following points:

- The test should be carried out by applying short water injection pulses in borehole S14 (injection borehole), using S12, S13 and S21 as observation boreholes.
- Each pulse should have a duration of about 5 minutes, after which the injection pump should be stopped and the pressure drop recorded. It is the pressure recovery curve what is mainly used for interpretation.
- Injection pulses should start at 20 bar, increasing 20 bar more on each step. The tests should stop at 120 bar, as this pressure is in the range of the estimated minimum stress in the area, and could cause hydraulic fracturing.

- In case that a pressure variation is observed in any of the observation boreholes, the pressure increment between steps should be reduced to 10 bar.

#### *Test layout*

The final test layout is shown in Figure 2.2.3.19. The water injection pump is applied to the injection borehole S14, whereas boreholes S13 and S14, as well as the in-seam borehole S21 were used as observation boreholes.

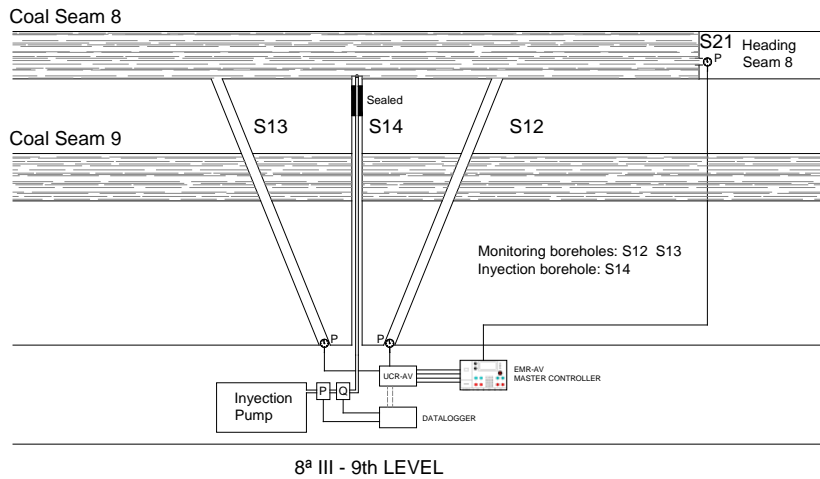


**Figure 2.2.3.19:** Test layout.

Monitored parameters were: pressure at the pump output, water flow at pump output, pressure at borehole S12, pressure at borehole S13, pressure at borehole S21, methane content at heading, methane content at the pump location, pump current and pump input pressure.

#### *Pulse tests*

Water injection tests have been carried out according to the protocol described in deliverable N° 1.3, in pulses of about 5 minutes duration at pressure steps of 20, 40, 60, 80, and 120 bar.

It is also interesting to see that the water flow is very irregular (as expected), but is larger at lower pressures than at higher ones, confirming that permeability is lower at higher pressure, possibly due to the closing of flow paths and the swelling of the clayish dirt bands in the seam. Figure 2.2.3.20 shows the total amounts of water injected on each pulse test.

**Volume of water injected according to injection pressure**

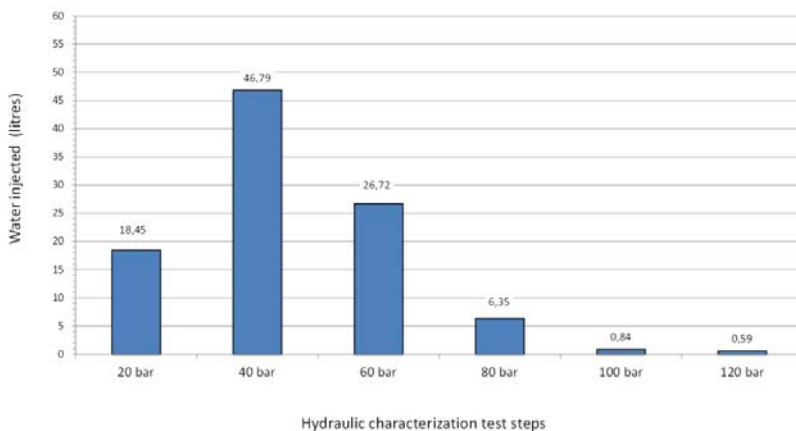


**Figure 2.2.3.20:** Total amount of water injected on each pulse test.

#### *Interpretation*

The pressure drop curves have been interpreted from a classical hydrogeological approach. This work was carried out by the Hydrogeology Department of AITEMIN, which has analysed the pulse tests at 20, 40 and 60 bar, as the pulses at higher pressure show some anomalies in the curve shape.

The obtained results are shown in Table 2.2.3.4, where:

- T = Hydraulic Transmissivity
- K = Hydraulic Conductivity
- S = Storage Coefficient

**Table 2.2.3.4:** Results from the hydrogeological interpretation

<b>Test</b>	<b>Cooper &amp; Jacob</b>		<b>Barker</b>		
	<b>T (m<sup>2</sup>/s)</b>	<b>K (m/s)</b>	<b>T (m<sup>2</sup>/s)</b>	<b>K (m/s)</b>	<b>S</b>
<b>20 bar</b>	$3.8 \times 10^{-8}$	$9.4 \times 10^{-9}$	$2.0 \times 10^{-8}$	$5.0 \times 10^{-9}$	$1.4 \times 10^{+1}$
<b>40 bar</b>	$5.7 \times 10^{-8}$	$1.4 \times 10^{-8}$	$5.7 \times 10^{-8}$	$1.4 \times 10^{-8}$	$4.3 \times 10^{-1}$
<b>60 bar</b>	$4.0 \times 10^{-8}$	$9.9 \times 10^{-9}$	$3.2 \times 10^{-8}$	$8.0 \times 10^{-9}$	$3.1 \times 10^{-3}$

According to these results, the hydraulic conductivity may be estimated in around  $1.0 \times 10^{-8}$  m/s. The value of the storage coefficient is not considered reliable, as it can only be estimated at a check point.

### Conclusions

A complex set-up has been prepared at the Sueros Colliery, including three boreholes quasi-perpendicular to seam #8, a parallel, in-seam borehole, a water injection pump, and a monitoring and control system that enables the remote operation of the system and the automatic acquisition of data provided by the installed instruments.

This set-up has been used to perform pulse injection tests for determining the hydraulic conductivity of the #8 seam at a macro scale, and will also be used to carry out long duration injection tests in Task 2.4 "Field Testing of borehole stimulation methods".

The information obtained from the pulse injection tests has been interpreted applying a classical hydrogeological methodology, obtaining a value of  $1.0 \times 10^{-8}$  m/s for the hydraulic conductivity.

This value is considered as reasonable. However some anomalies have been detected in the pulses over 80 bar, possibly caused by a malfunction of the pressure regulating valve at the pump output. It is therefore planned to carry out additional characterisation tests at borehole S14 once this valve is repaired.

### 2.2.4. WP2, Task 2.1: Development of the equipment and tools for the stimulation of coal seams as well as surrounding rocks (GIG)

Permeability enhancement in hard coal deposits should be performed before the commencement of coal production and must be the result of technical measures performed in the rock mass. This can be achieved by different means of stimulating the coal seams. The planned stimulation applications require specialist instruments to deliver the necessary fluids at controlled pressures. Adaptation and further development of blasting techniques may also be required. Task 2.1 aimed at the development and construction of these equipment.

In order to develop the stimulation techniques required by the underground conditions in the hard coal mines the following assumptions were made:

- stimulation of the strata will cover part meant for exploitation and (at least initially) developed by mine workings,
- stimulation will be conducted using boreholes drilled for gas drainage purposes,
- boreholes will be modified by using them to perform so called initial fractures,
- initial fractures can be created by a mechanical or hydraulic means,
- stimulation of the strata can be performed using either hydro-fracturing or blasting techniques.

The assumptions mentioned above determined the type and extent of the equipment, installations and other elements of technical accessories necessary to be utilised. Due to specific conditions where the subject technique will be used, the equipment had to be designed and manufactured based on the original conception and design, which included the following:

### **Initial efficiency tests of cutting rocks with water jet**

Following the initial discussions on the methodology and extent of stimulation required by the coal seams the very first cutting tests of a coal sample/concrete composite with water jet was carried out in the laboratory. As described in detail in Deliverable D2.1 report, a hard coal sample cast in concrete was cut by water jet at two different water pressures (800 and 2,400 bars) and hydraulic head nozzle diameters (1.8 mm and 1.0 mm) respectively as shown in Figures 3.2.4.1 a and b. Water jet cutting performance was recorded for perforation and slots/cuts achieved for the nozzle diameter and distance from the nozzle outlet during these experiments.



(a)



(b)

**Figure 2.2.4.1:** (a) Water jet cutting of the coal sample, (b) Cuts in coal after water jet treatment

### **Design, manufacture and assemble of the water jet cutting tool**

Positive results of the water jet cutting tests led to the construction of a set of equipment which would be used to cut slots and/or create fractures to improve the hydraulic properties (using boreholes) of coal seams. In constructing the said equipment, parts available on the market were purchased, others that are not available were designed and manufactured in house. All the designs and assembling work were performed by TECH-TRADING Ltd Company.

In manufacturing and assembling the equipment, the following operational criteria were set:

- size of the equipment must fulfil underground transportation criteria,
- performance of the fractures, slots should be possible in inclined boreholes with diameters from 65 to 96 mm and up to 100 m length,
- the equipment must have ATEX certificate allowing its utilisation in methane hazard conditions,
- power and hydraulic supply must be adjusted to the existing coal mine standards,
- minimum range of performed fractures/slots: 0.5 to 3.0 m,
- two principal operating modes:
  - pressure: 1,000 bars and flow rate: 80 l/min,
  - pressure: 650 bars and flow rate: 115 l/min,
- typical basic hydraulic and electrical equipment.

The following equipment, for which the main specifications are presented in detail in Deliverable D2.1 report, forms the main components of the tools developed for this purpose:

- The pump unit ZPM HDP 172 with a high pressure pump HDP 177 and the electrical engine dSg315M4B-EP (Figures 3.2.4.2 a and b)
- Oil supply unit ZZO-2 with a flow rate of 22 l/min and maximum pressure of 200 bars, and electric motor dSKg160MB-EP at 7.5 kW power rating (Figure 2.2.4.3a)
- The stabilisation-rotation unit USO-1 to transfer water from the pumping unit ZPM HDP 172 down to the cutting head and nozzle, and directing its jet (Figure 2.2.4.3b)

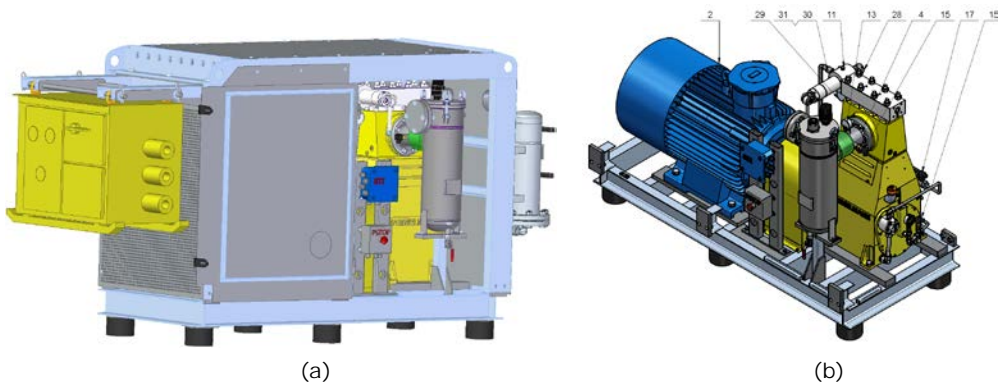


**Figure 2.2.4.2:** (a) Pump unit ZPM HDP 172, (b) Hydraulic pump HDP 172, its drive, filter and control system.

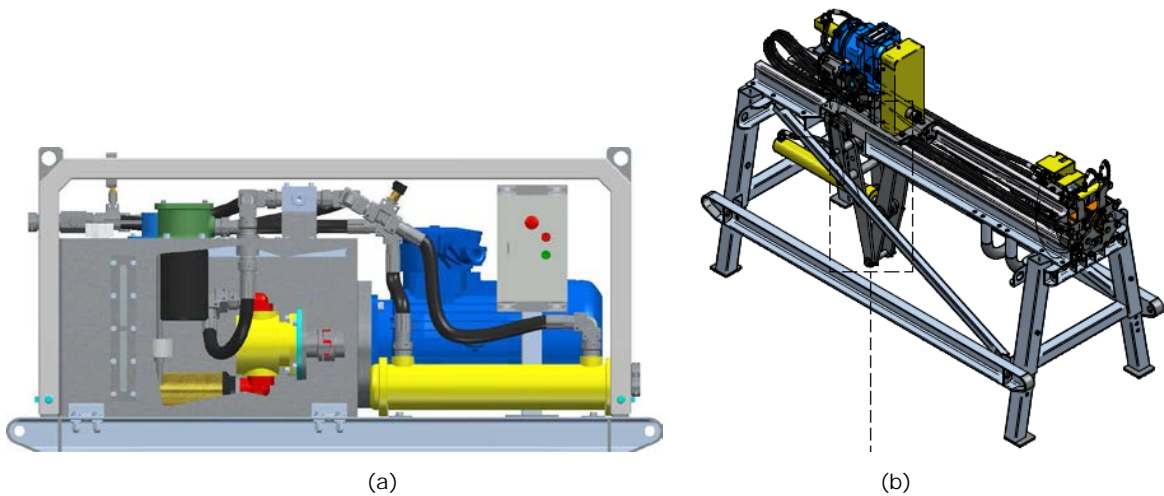


**Figure 2.2.4.3:** (a) Oil supply unit ZZO-2, (b) Stabilisation-rotation unit USO-1.

Together with the individual parts such as high pressure hydraulic hoses, power cables, set of 100 pieces of rods, hydraulic heads with nozzles, borehole packers, valves, switches, joints, rotating joint-heads, transportation boxes etc., the equipment constructed forms an integrated hydraulic system aimed at creating slots, fractures and cuts in coal seams dedicated to improve their permeability for enhanced gas drainage purposes. A schematic diagram of the integrated system is shown in Figure 2.2.4.4.

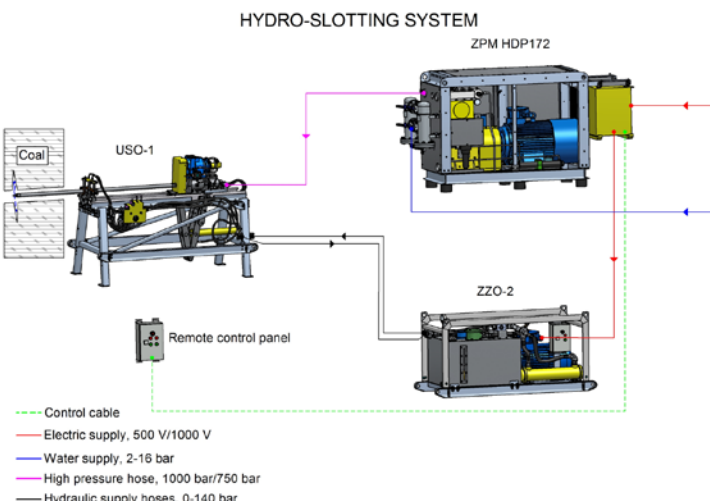


**Figure 2.2.4.4:** A schematic diagram of integrated parts assembled for hydro-fracturing/cutting of coal seams.

After completing all units, their technical approval, basic training of the staff and other organisational issues, the very first underground operational experiments were performed, including the very first cuts in the coal seam from the boreholes which is shown on Figure 2.2.4.5.



**Figure 2.2.4.5:** (a) The pumping unit ZPM HDP 172 in underground gallery of the hard coal mine, (b) Initial fracture in borehole

#### Borehole probe for cutting the fractures/slots

The necessary modifications for the tool to create the initial fractures were also performed and tested. This also included the testing of slot cutting by mechanical means. In order to adopt it to the coal mine methane drainage requirements the modification of the mechanical construction of the head to perform the initial fractures was carried out to cut the fractures at desired length of the borehole. The result of the above modifications is the tool shown in Figure 2.2.4.6.

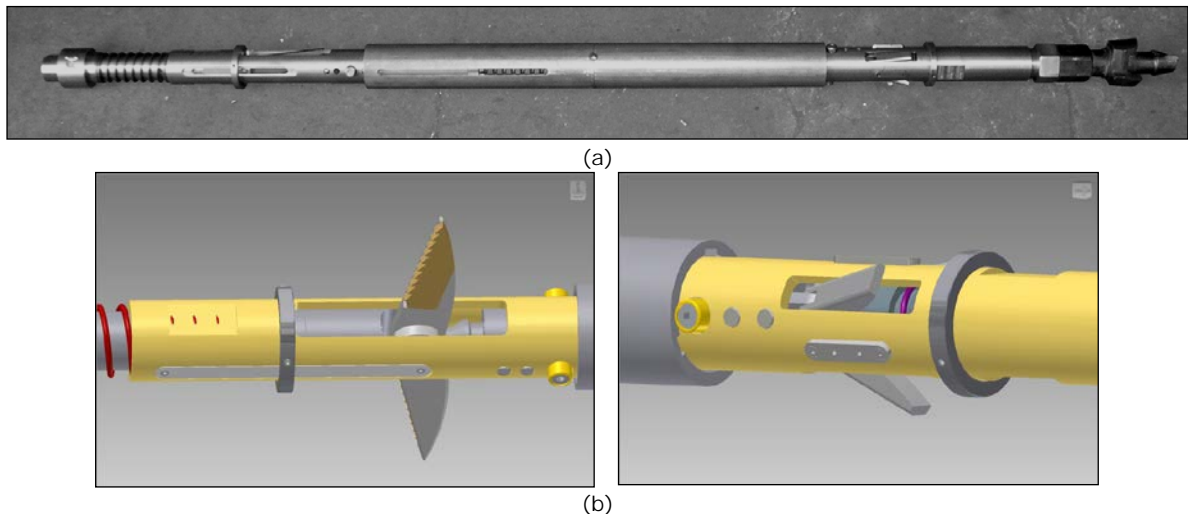


**Figure 2.2.4.6:** (a) Mechanical head aimed at cutting the initial fractures, (b) Cutting and anchoring module of the head.

#### Blasthole designs and the construction of the charges

Impact of the explosives for the surrounding strata has a local range. In case of its utilisation in the rocks its range depends on the density and elastic properties of rock i.e. on its mechanical strength. One can identify five zones of charge impact, which is the joint characteristic of size, type of the charge and properties of the rock (Figure 2.2.4.7)

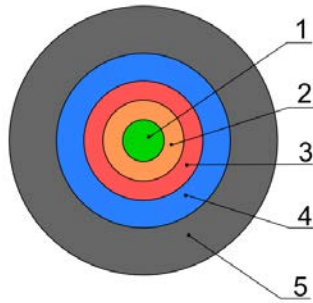


**Figure 2.2.4.7:** Impact zones of the explosive charge

1- charge, 2 - mastication zone, 3 - crushing zone, 4 - cracks zone, 5 - zone of vibrations.

*Mastication zone* is the zone adjacent to the charge, which causes the largest pulverisation of the environment.

*Crushing zone* is where separation between the particles and parts of the bed is taking place, the further from the centre of explosion the smaller separated parts are.

*Cracks zone* is the zone around the borehole, where the diminishing gas pressure is causing only fractures and cracks, which are becoming smaller with the increasing distance from the source of the explosion.

*Zone of vibrations* is the zone where no permanent effect of the explosion occurs. The vibrations are becoming smaller with the increasing distance from the source of the explosion until they completely disappear. When firing larger number of charges, zones of vibrations overlap and have impact on the scale of mastication, crushing and cracks.

The result of the explosives' firing in the heavy gassy coal seam should not be destruction of the coalbed but only establishing in it a fine grid of fractures and dividing it into smaller fractions. Therefore, application of this method in coal seams requires the design and development of new charges, which lead to a minimum mastication zone and a maximum crushing and cracks zones. Furthermore, in the hazardous and gassy conditions of mining, the boreholes need to be prepared by cutting/creating a number of fractures (so called initial fractures) to direct the post-explosion gases. The smaller the distance between these initial fractures the bigger effect of their effect will be. Currently, GIG uses one tool to create such fractures in sandstones. Further modifications to this tool to enable fracture cutting and explosive charging of the blast holes in coal has also been undertaken. The tools and designs developed include:

**Column charge design (extended charge)** – where the explosive charge is placed in the borehole. Due to the shape of the borehole, the tool has cylindrical and elongated shape (Figure 2.2.4.8).

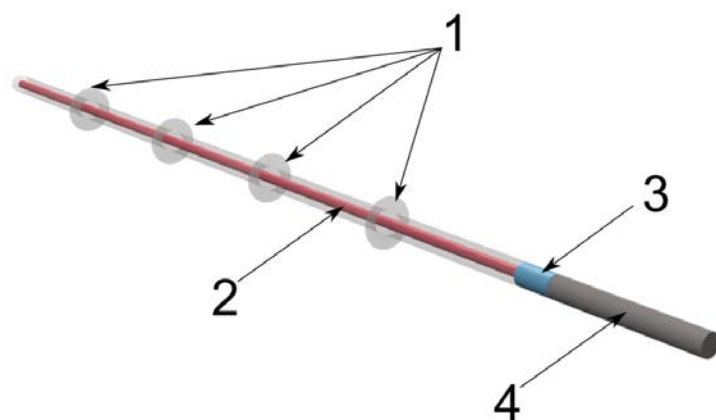


**Figure 2.2.4.8:** Column charge (extended charge)

1 - initial fractures, 2 – explosives, 3 - initial charge, 4 – stemming.

**Distributed charge design** (Figure 2.2.4.9) several charges are placed in a single borehole, being separated with stemmings or with air.

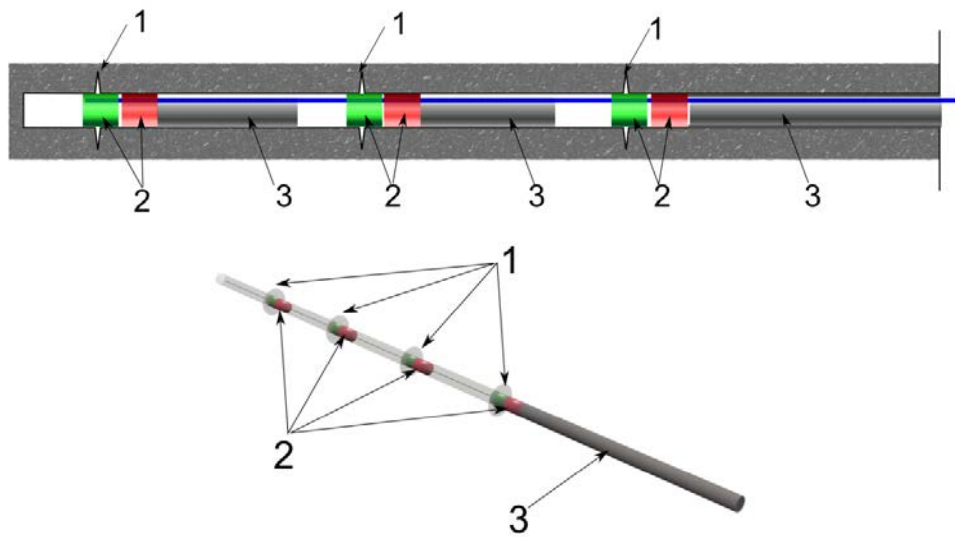


**Figure 2.2.4.9:** Distributed charge

1 – initial fractures, 2 – explosives, 3 – stemming.

**Short column charge design** – single explosive charge or heterogenic material placed in the blast hole. The borehole may be filled in with water until the initial slot cut. These type of charges have cylindrical and elongated shape (Figure 2.2.4.10).

One essential element in initiating methane desorption from the coal seam is the development and application of the hammer charge or initiating combustion of the heterogenic solid fuel, deflagrating material. In the first case, a typical charge with electric detonators are used. In the second case, the charge should have a construction providing resistance against moisture and water in the long term. It must be emphasised that the ignition mass and ignition head utilised in such charges are not moisture resistant, therefore, they were equipped with a special cover to protect against moisture and, they must be particularly tight in the vicinity of the initiating combustion unit (Figure 2.2.4.11).

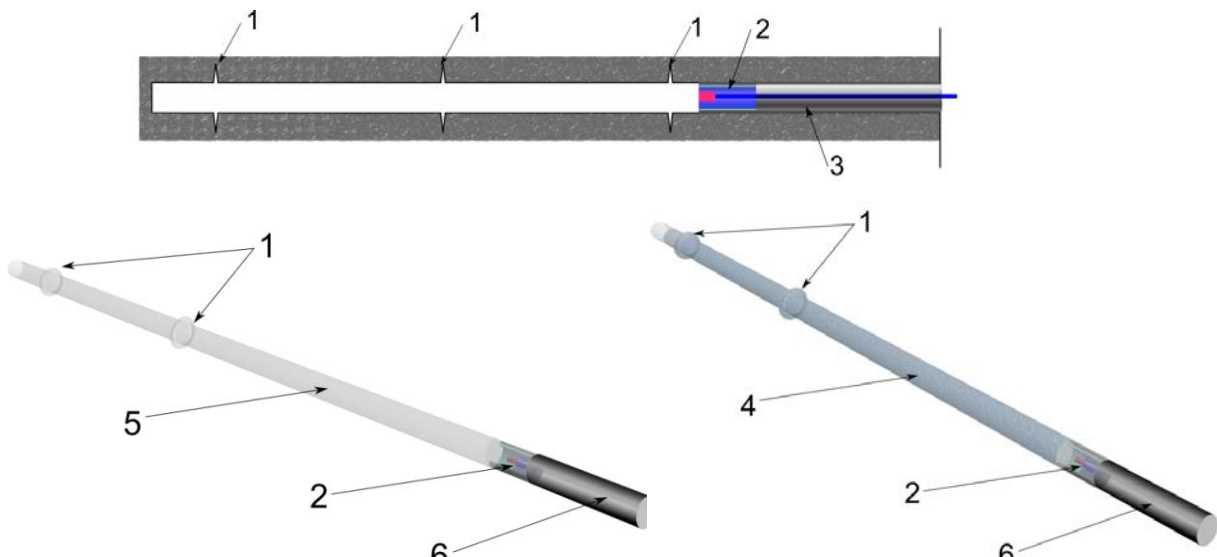


**Figure 2.2.4.10:** Short column charge design

1 initial fractures, 2 – explosives, 3 -stemming, 4 - air, 5 – water.

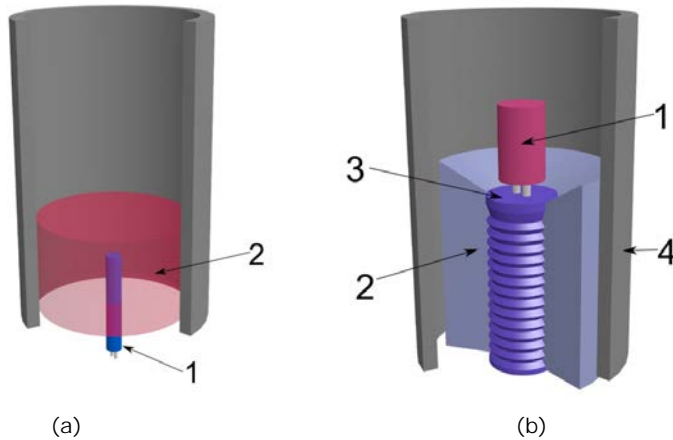


**Figure 2.2.4.11:** Examples of initiating charges, (a) hammer cartridge 1 – detonator, 2 – explosives; (b) cartridge initiating combustion of heterogenic fuel: 1 – detonator unit, 2 – heterogenic fuel.

Proposed designs aim at achieving hammer phenomena of the compressed post combustion gases or steam-water mixture in the space of initial fractures. It is assumed that permitted explosives will be used to perform the blasting operations in methane hazard conditions i.e. column charge, distributed or the short column charge. The designs for blasting include cutting several initial slots in the boreholes, therefore, it is planned to use 80 mm diameter boreholes drilled with 86 mm bits. The following design parameters are proposed:

- Diameter of the borehole – 80mm
- Length of the blast hole between 10m to 40m
- Charge according to the construction and length of the borehole: about 1kg of explosive per 1 running meter for the column charge; from 125g to 300g for the distributed charge; and from 1kg to 4kg of explosive for the short column charge.
- Dynamics of the pressure increase from  $6.4 \times 10^{11}$ Pa/second up to  $9 \times 10^{11}$ Pa/second
- Maximum pressure - 9GPa
- Time of total combustion of 1 kg charge 4-10 seconds.

Charges will be initiated with sharp electric immediate detonator. Due to the presence of very high toxic gases in the applications of heterogenic materials, the use of these materials is not foreseen in GasDrain.

## 2.2.5. WP2, Task 2.2: Laboratory investigations into stimulation techniques

The objective of laboratory experiments in Task 2.2 is twofold. The first part aims at characterising the fracture growth, the performance of different frac fluids, proppant behaviour and fracture closure in stimulated coals in the laboratory. The second part of the laboratory experiments aim at developing new blasting charges using different mixes of materials.

### **SubTask 2.2.1 Laboratory experiments to characterise fracture growth, frac fluid and proppant behaviour in coal seams (IMPERIAL).**

The objective of laboratory experiments in this SubTask is to characterise the fracture growth, the performance of different frac fluids, proppant behaviour and fracture closure in stimulated coals in the laboratory. Also investigated are fracture fluid leakoff and potential for permeability enhancement and/or impairment through formation damage by these interventions.

Large blocks of coal samples (~ 600 x 600 x400 mm) from the Seam #412 underground at Zofiowka Colliery were jointly collected (Figure 2.2.5.1 a and b) by JSW and GIG and shipped to IMPERIAL for coring and testing for fracture growth, proppant and frac fluid behaviour using 38 mm solid cores and 100 mm hollow cylinder core samples (Figure 2.2.5.1 b and c).

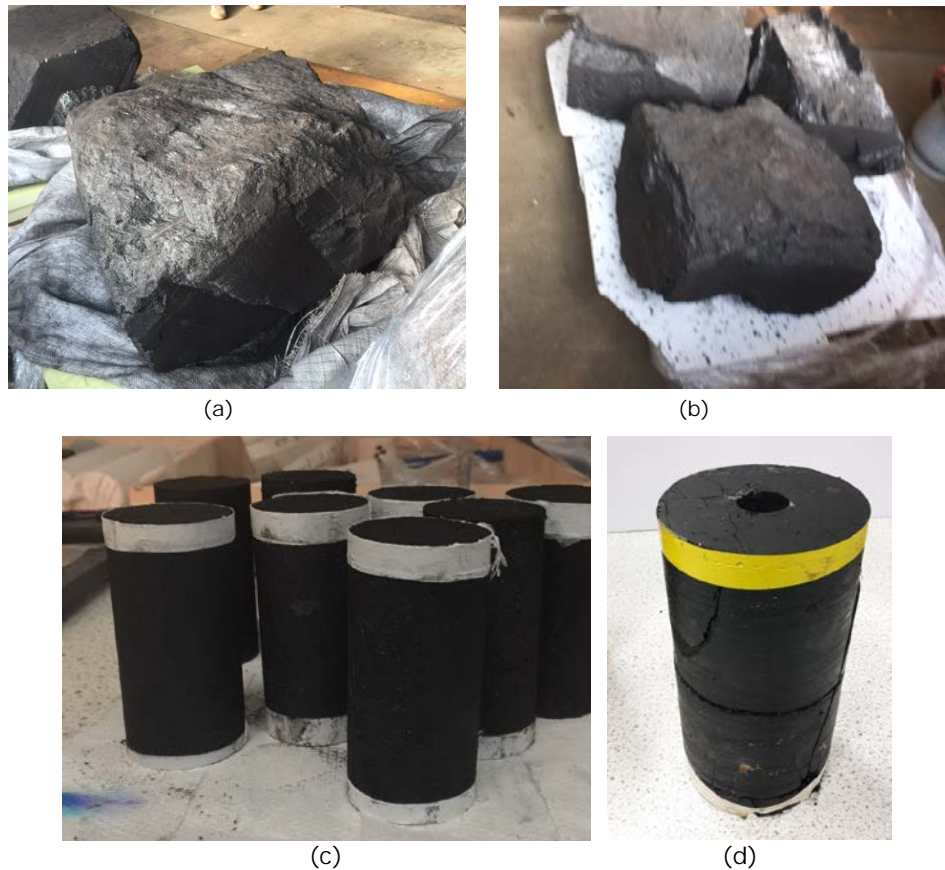


**Figure 2.2.5.1:** (a), (b) Large blocks of coal samples from JSW Zofiowka Seam #412 received at IMPERIAL, (c) 38 mm solid cores, (d) 100 mm hollow cylinder cores.

#### Stress-permeability characterisation of coal

The first stage stress permeability characterisation of the Zofiowka coal samples was carried out at 2.4 MPa confining pressure and at pore pressures of up to 0.6 MPa in a Hassler cell, using the 38mm solid core samples cored from the large blocks shown in Figure 2.2.5.2.

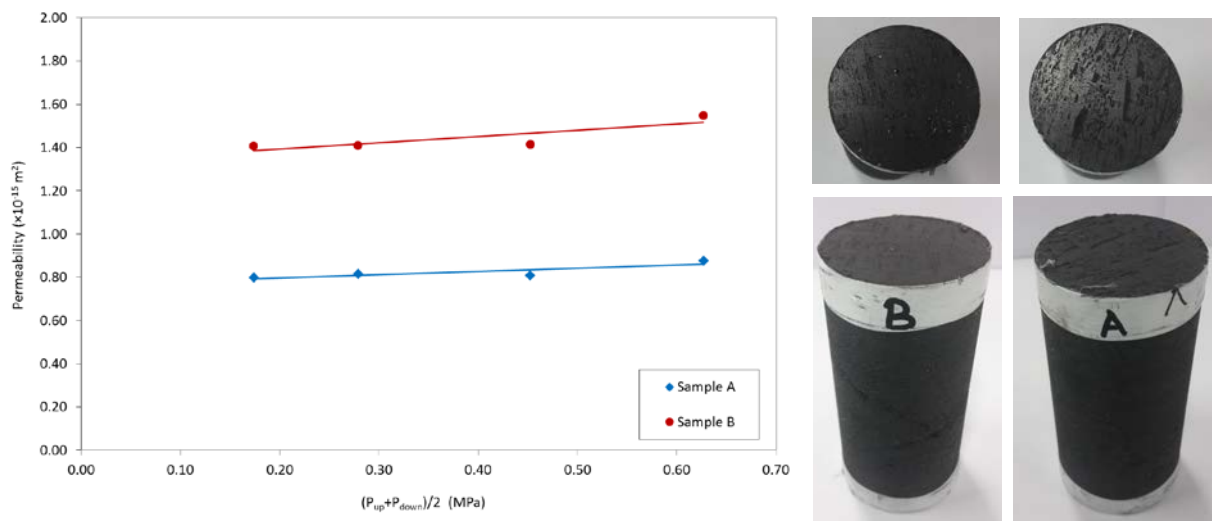


**Figure 2.2.5.2:** Permeability behaviour of Zofiowka coal samples at 2.4 MPa confining pressure.

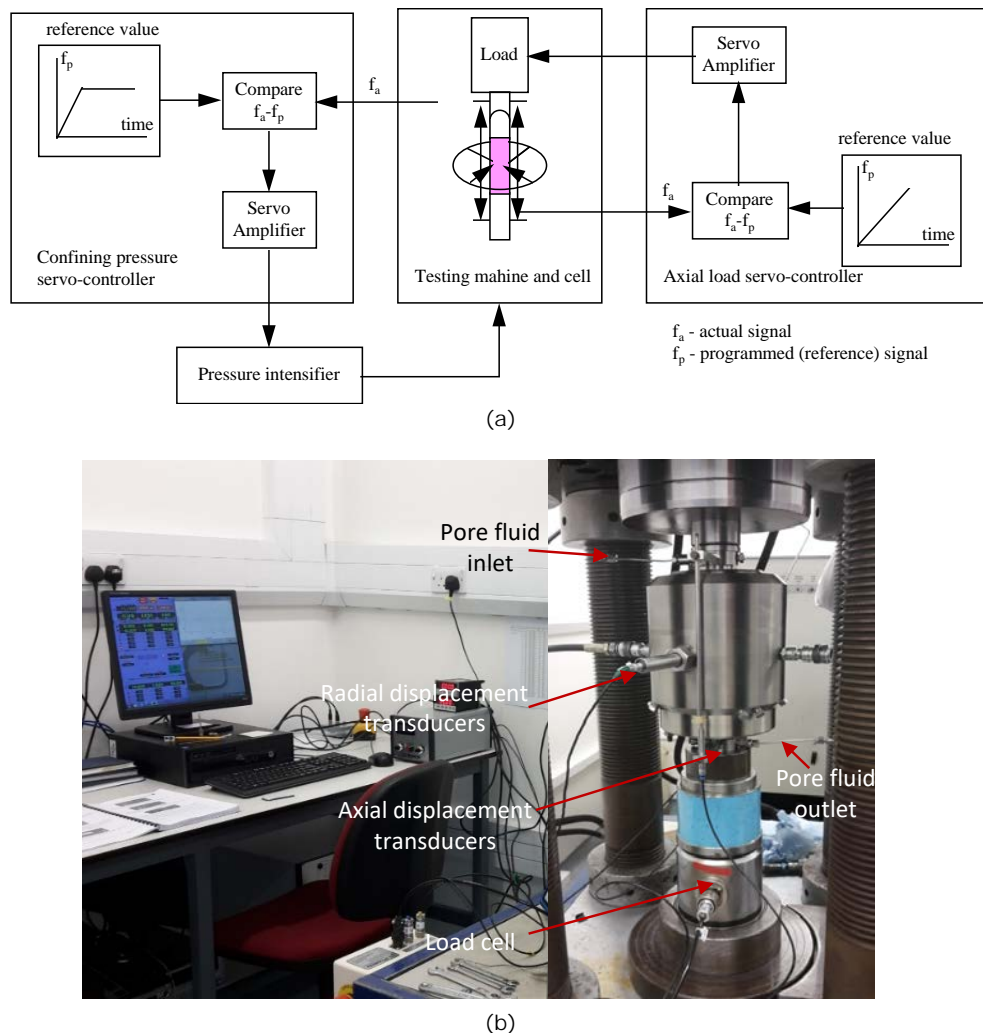


**Figure 2.2.5.3:** (a) Schematic of the triaxial testing system configuration, (b) 28 mm core triaxial cell and stress-permeability testing components.

As the second stage in stress-permeability characterisation of the coal samples multistage triaxial testing of 38 mm core samples is being carried out, which also yields the elastic properties (Young's modulus and Poisson's ratio) for the coals tested. The multistage triaxial tests are carried out using a four column 2,000 kN capacity rock testing system (ESH Testing Limited, Brierley, UK) at IMPERIAL (Figure 2.2.5.3). The hydrostatic and deviatoric loads are controlled independently using servo-controlled systems while the upstream and downstream pore pressures are applied using manually controlled pressure regulators. The flow rate is measured using a flow meter. Coal permeability is measured by applying a differential pressure of gas between the upper and lower platens. The components of the testing system and the triaxial cell used for 38 mm diameter stress-permeability testing is illustrated in Figure 3.2.5.3 (a) and (b).

#### Coal fracture and proppant behaviour characterisation

In order to characterise the performance of different proppants and the permeability response of propped fractures in coal in the laboratory IMPERIAL held some discussions with INIG and it was decided to use three different proppants in these experiments. These are:

- 35-40 Mesh sand obtained locally
- Carbo Prop 20/40. An intermediate density ceramic proppant at 20/40 Mesh size, supplied by CARBO industrial ceramics, Houston, Texas, USA.
- Inter Prop 30/50. An intermediate density ceramic proppant at 30/50 Mesh size, supplied by Saint Gobain Proppants, Fort Smith, Arizona, USA.

The permeability specifications of the two commercial ceramic proppants kindly provided to IMPERIAL by INIG are shown in Figures 3.2.5.4 and 3.2.5.5.

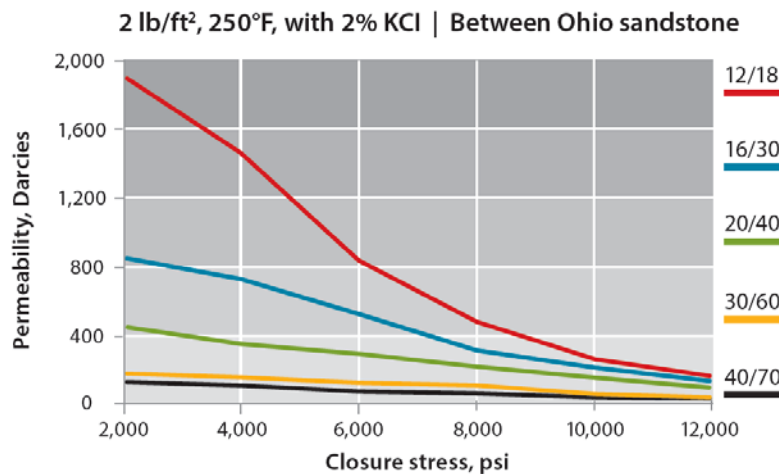


**Figure 2.2.5.4:** Permeability characteristics of CarboProp ceramic proppants (CarboProp, 2015).

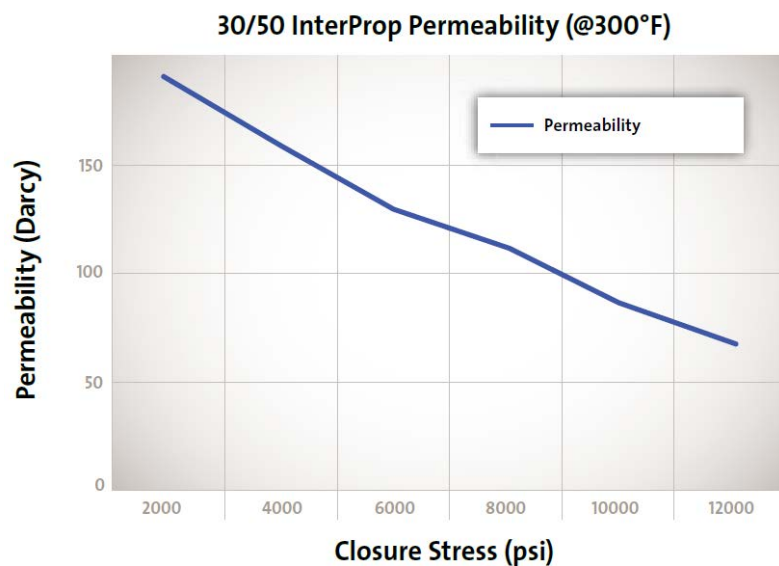


**Figure 2.2.5.5:** Permeability characteristics of InterProp 30/50 ceramic proppant (InterProp, 2015).

The permeability response of propped fractures in coals was first tested using 38 mm diameter core samples. The stress-strain-permeability behaviour of the coal samples was first characterised through a multistage triaxial testing as described in the previous section. The Young's modulus and Poisson's ratio of the samples, as well as the permeability under different confining stresses determined. The sample is finally brought to failure to obtain a shear fracture which can then be tested for proppant behaviour. Figure 2.2.5.6 presents one such example of a multistage triaxial test results for a coal sample which was then tested for proppant characterisation as discussed in this section.

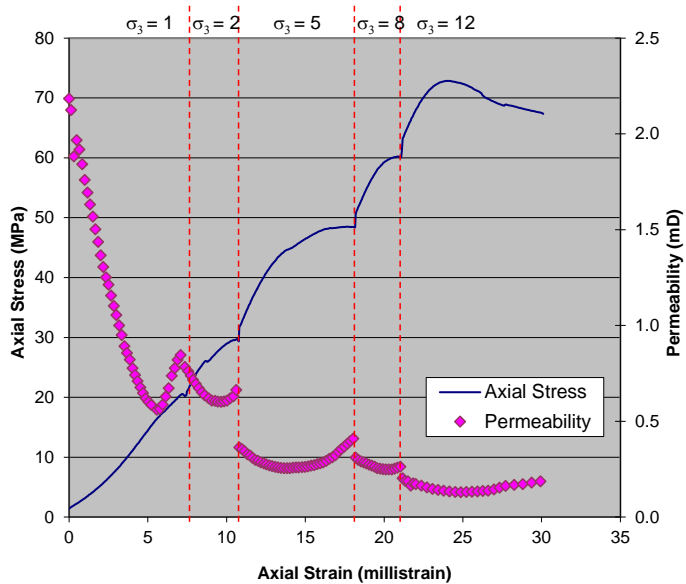


**Figure 2.2.5.6:** Axial stress-strain-permeability behaviour coal determined through multi-stage triaxial testing (Young's modulus,  $E = 3.5 \text{ GPa}$ ; Poisson's Ratio,  $\nu = 0.26$ ).

Figure 2.2.5.7 shows a fractured coal sample prepared for proppant characterisation experiments using different proppants obtained for the project. Figure 2.2.5.8 shows the fractured coal samples treated with sand (35-40 Mesh) and ceramic (InterProp 30/50) proppants before permeability testing under confining stress.



**Figure 2.2.5.7:** Fractured coal sample prepared (through multistage triaxial testing) for proppant characterisation experiments.



**Figure 2.2.5.8:** Fractured coal samples treated with 34-40 Mesh sand proppant (left) and InterProp 30/50 ceramic proppant (right).

A number of fractured coal samples treated with the three proppants were tested for their permeability behaviour under four different confining stresses (1.4, 2.0, 2.8 and 3.5 MPa) in the laboratory and the results obtained compared with their baseline (without proppant) permeabilities to N<sub>2</sub>. Figures 3.2.5.8, 3.2.5.9 and 3.2.5.10 present results of these experiments for 35-40 Mesh sand, CarboProp 20/30 and InterProp 30/50 respectively.

As Figure 3.2.5.8 illustrates, depending on the confining stress, samples with sand as the proppant have shown nearly an order of magnitude increase in permeability of the samples tested. The permeability increase being less pronounced under high confining stresses.

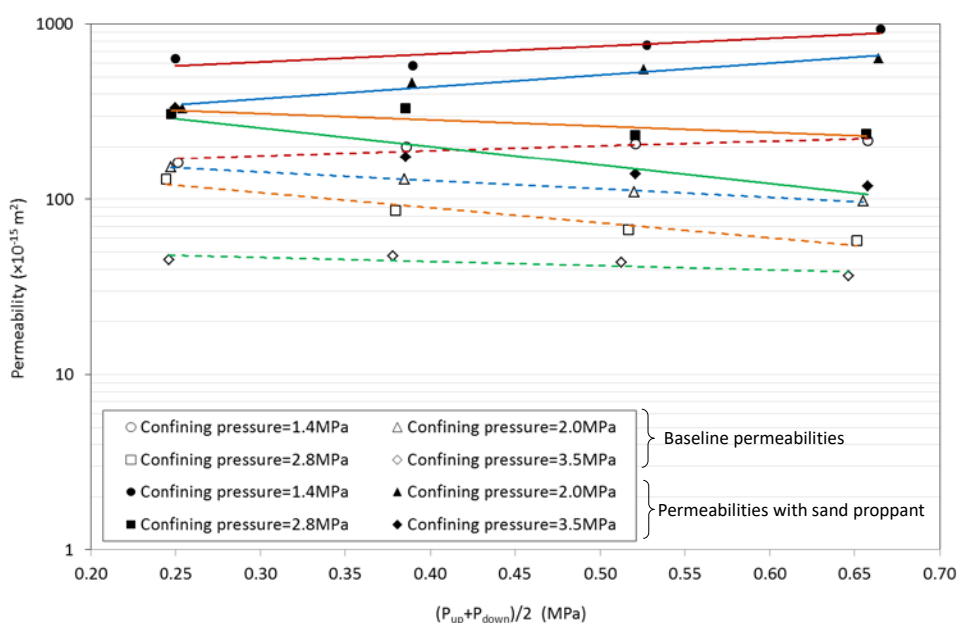


**Figure 2.2.5.9:** Permeability behaviour of a sand propped fracture in coal comparing baseline (un-propped) and propped N<sub>2</sub> permeabilities.

As Figure 2.2.5.9 illustrates, a similar, however much less pronounced increase in propped fracture permeabilities of coal was observed with the smaller size of the two ceramic proppants (CarboProp 20/30). On the other hand, the larger size proppant (InterProp 30/50) had the opposite effect on permeability of the propped fractures that, at high confining pressures, the permeability of the fracture was significantly (nearly two orders of magnitude) reduced. It is believed that, coal being fairly brittle compared to the relatively hard and stiff reservoir rocks, especially the large particle size synthetic proppants result in further formation damage and clog the fractures by digging in to the coal matrix. The use of sand as a proppant in almost all coalbed methane wells by the industry may also explain this behaviour.

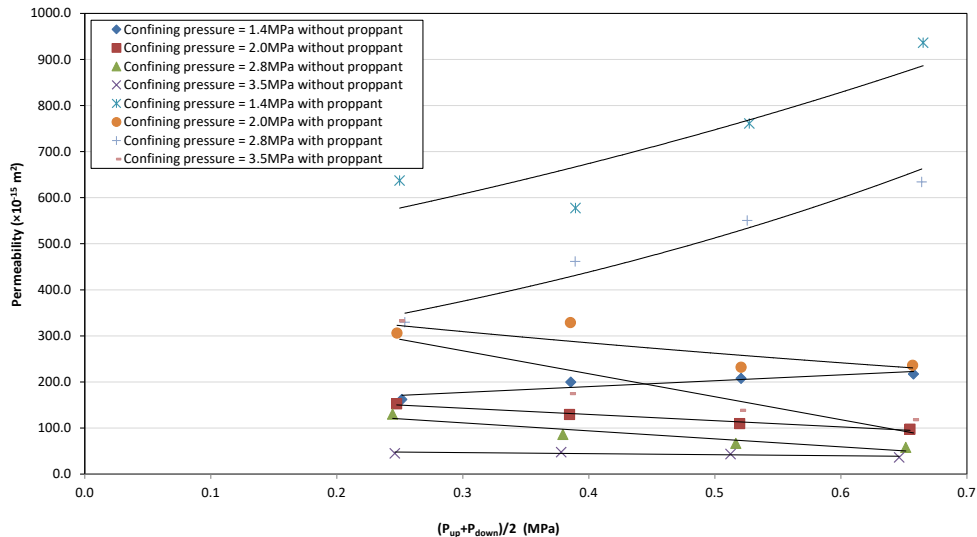


**Figure 2.2.5.10:** Permeability behaviour of a CarboProp 20/30 propped fracture in coal comparing baseline (un-propped) and propped N2 permeabilities.

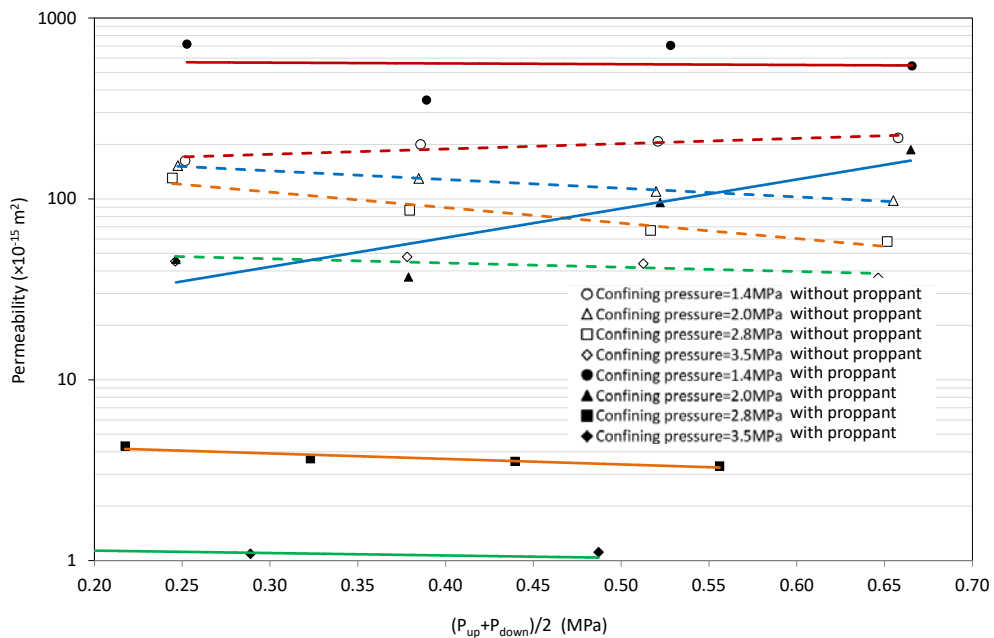


**Figure 2.2.5.11:** Permeability behaviour of an InterProp 30/50 propped fracture in coal comparing baseline (un-propped) and propped N2 permeabilities.

Currently, attempts are being made to test the same proppants under triaxial state of stresses duplicating the permeability behaviour presented (for an un-propped coal sample) in Figure 2.2.5.6 above. Achieving a workable shear fracture, preserving and re-using of the same sample for (and with) different proppants in a triaxial cell proved to be a challenging and time consuming task which is taking longer time than originally anticipated to accomplish.

#### **Construction and testing of the large triaxial cell for hollow cylinder testing**

The objective of the large diameter (100mm) hollow cylinder testing in this project is to simulate, in the laboratory, hydrofracturing and (if possible) cavitation of coal samples under in situ stress and pore pressure conditions and test proppant and frac fluid behaviour. These experiments require much larger coal samples (both as coal blocks to core and cores to simulate the wellbore and reservoir) to achieve the objectives of the experiments.

For this purpose, the construction and pressure testing of a new, large diameter triaxial cell was recently completed (Figures 3.2.5.12 and 3.2.5.13). The new cell enables application of axial and radial load,

both radial and wellbore pore pressure application/measurement, hydrofracturing of the coal under in situ stress conditions, frac-fluid and proppant injection through the wellbore while measuring stress-strain and permeability.

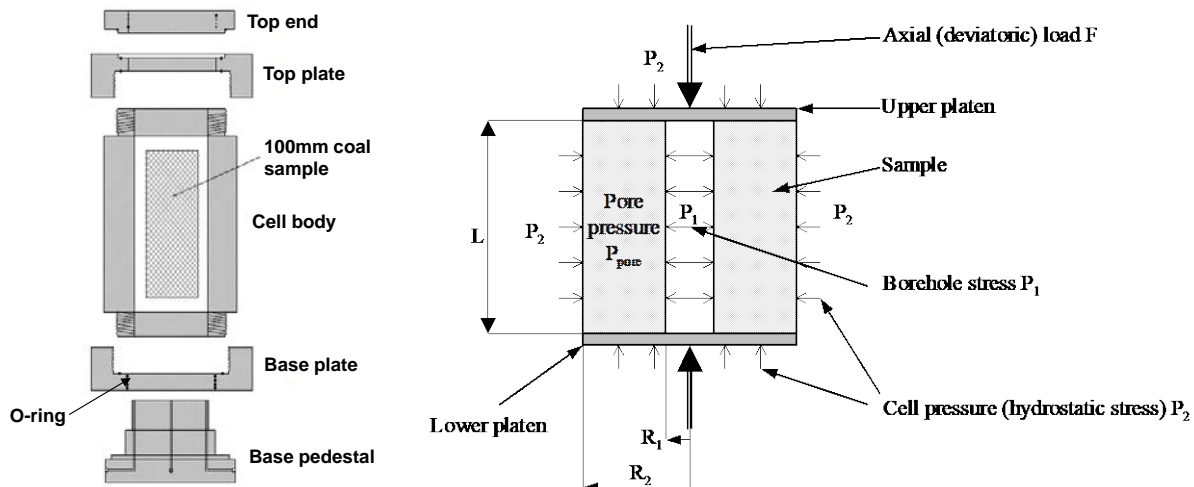


**Figure 2.2.5.12:** Schematic drawings of the newly constructed 100mm hollow cylinder triaxial cell and coal sample, mechanical stress and pore pressure application principles.

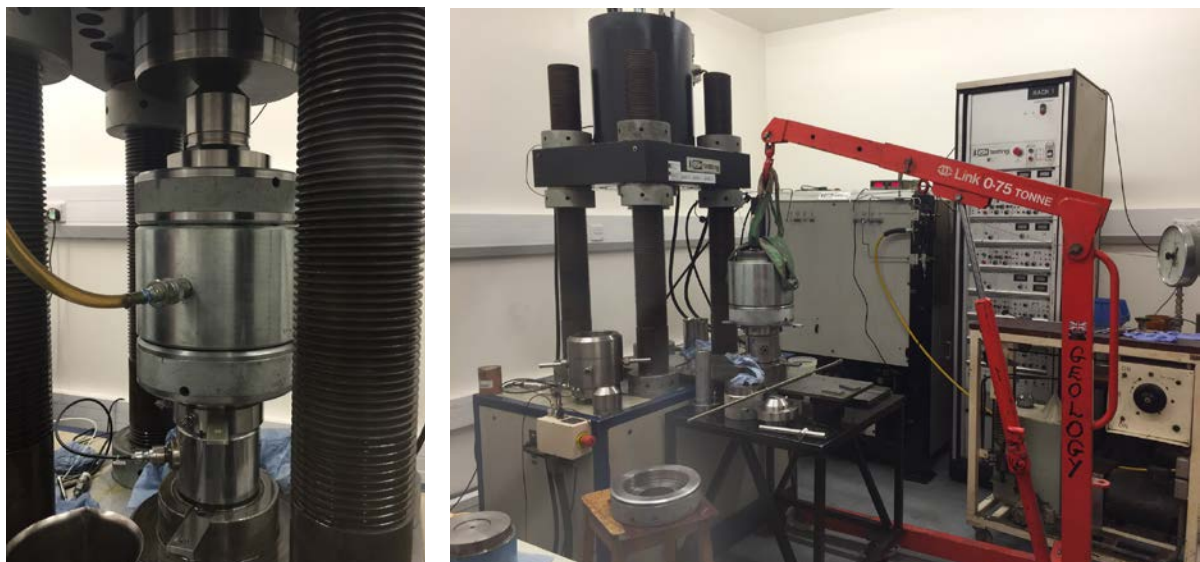


**Figure 2.2.5.13:** The newly constructed 100mm hollow cylinder testing triaxial cell during pressure testing. Large cell size and weight requires lifting and stabilising tools.

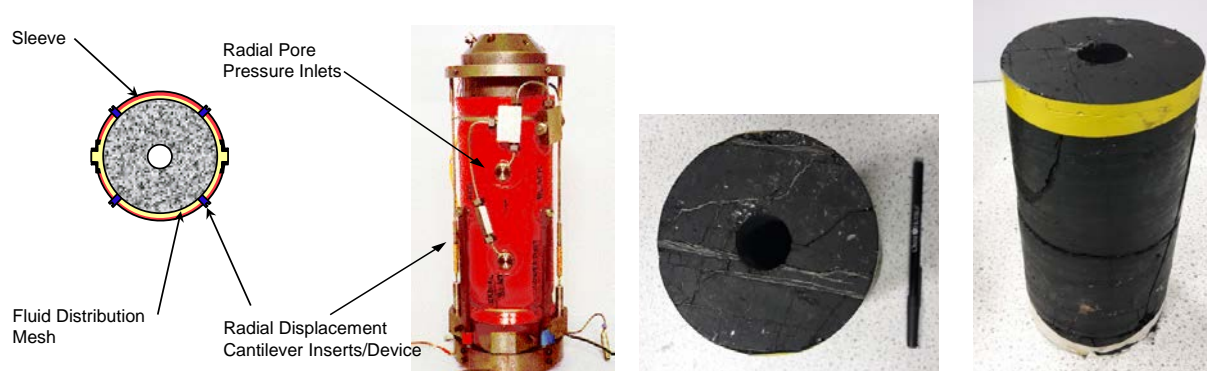


**Figure 2.2.5.14:** The newly constructed 100mm hollow cylinder testing triaxial cell during pressure testing. Large cell size and weight requires lifting and stabilising tools.

Besides the completion of the new triaxial cell, a number of 100mm core samples are prepared (Figure 2.2.5.14) for stimulation testing and frac fluid and proppant injection ready to start the experiments. However, this process have taken longer than anticipated at the proposal stage. Therefore, a further 3 months extension to Task 2.2 is requested to complete the planned testing and data analysis.

### **SubTask 2.2.2 Laboratory experiments to develop new blasting techniques for fracturing coal and rock masses**

The laboratory experiments under this SubTask aim at developing new blasting charges using different mixes of materials. To this effect, a number of laboratory experiments were carried out, the results of which are reported in the following pages.

The energy of the gases released during the blasting (deflagration) of the explosives can be used in order to initiate the fractures in the vicinity of the drainage boreholes and to fracture the coal seam. For this purpose, it is proposed to use explosives with a slow combustion speed and increased pressure, which are different from classic mining explosives. Therefore, it is necessary to determine some characteristic parameters for these types of explosives. This requires a special experimental set up, which was designed and manufactured as:

- test chamber,
- manual hydraulic pump,
- recording set, and
- electrical equipment.

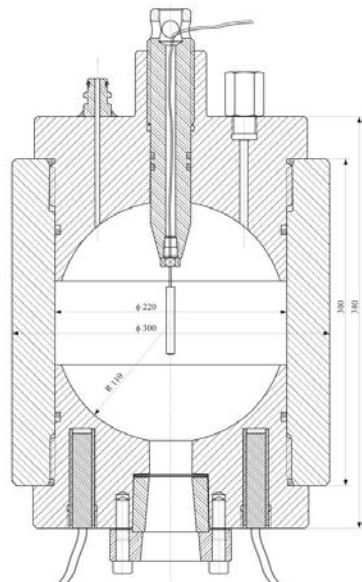


**Figure 2.2.5.15:** Test chamber for determining the explosive characteristics.

This set up enables conducting the combustion tests of the explosives in the environment of increased temperatures and external pressures comparable with their charge. Cross-section of the testing chamber developed is shown in Figure 2.2.5.15.

#### **Explosives and deflagration materials tested in the research chamber**

The use of explosives can create a fine grid of fractures in the coal seam and initiate migration of methane from the seam into the drainage boreholes. However, the use of explosives in boreholes drilled along the coal seam only is not very effective and, an effective drainage can only be achieved by the use of a fine grid of blast holes. By creating initial fractures inside the boreholes and using specially constructed explosives one can reduce the number of such boreholes required. Such explosives should have limited ability to break the rock, however, they should provide effective fracturing. In order to test these features two permissible explosives, namely Metanit Specjalny E7H and Emunilit PM were assessed in the laboratory.

Testing of explosion dynamics were performed in the blasting bunker at Experimental Mine „Barbara” with the 10g charges. Individual charges were blasted in the closed space filled with water with volume of 5 litters for the assumed water pressures – detour pressures. Graphically, the results of the tests are shown in Figure 2.2.5.16 and Figure 2.2.5.17.

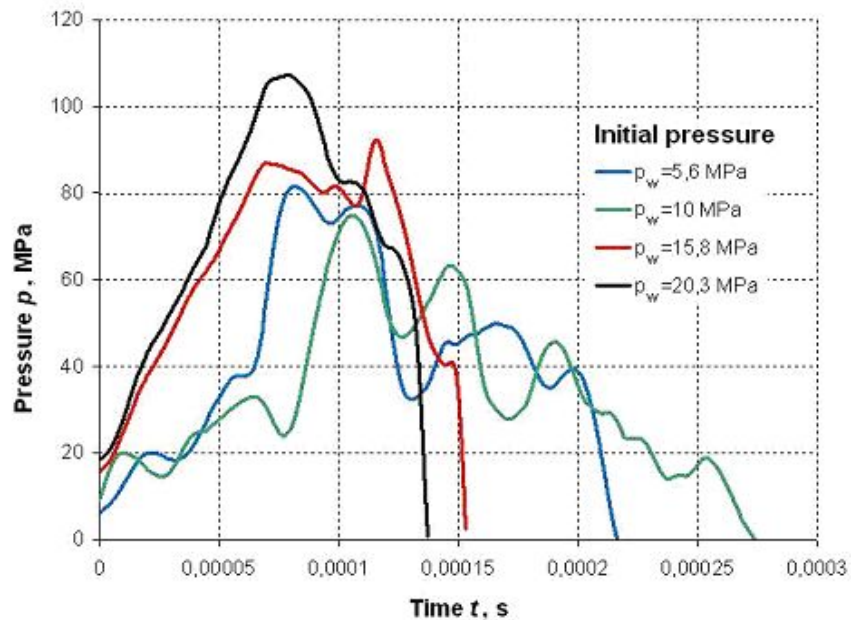


**Figure 2.2.5.16:** Characteristics of the pressure changes during explosion of the 10 g EMULINIT PM charge for different values of initial pressure.

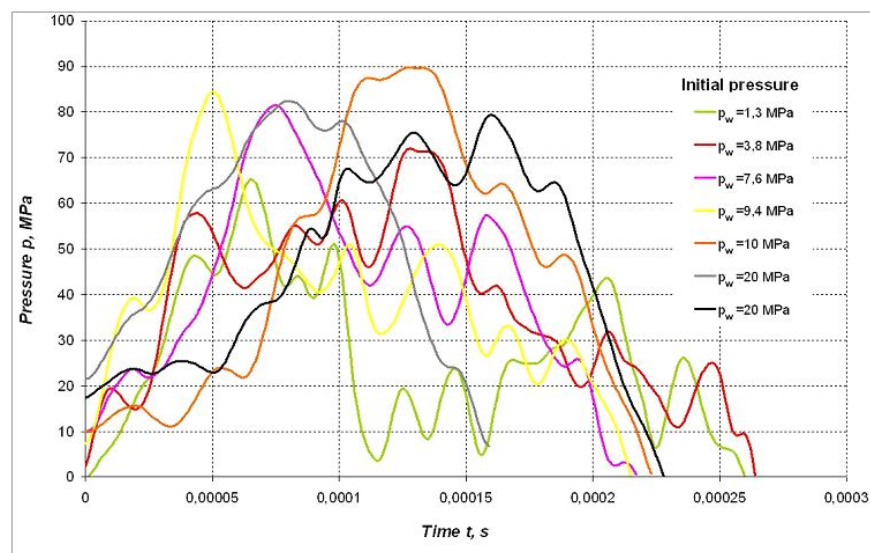


**Figure 2.2.5.17:** Characteristics of the pressure changes during explosion of the 10 g METANIT SPECJALNY E7H charge (Initial pressure = 1.3 MPa).

In Polish conditions high methane content coal seams occur below the depth of 1,000m. Drainage boreholes are normally used at these conditions, therefore, for the explosion experiments to be credible they must be carried out under representative conditions. Furthermore, as these explosive properties will be used in numerical modelling of stimulated boreholes, representative graphs of graphs of explosion dynamics were developed for Metanit Specjalny E7H (Figure 2.2.5.18) and Emulinit PM (Figure 2.2.5.19).

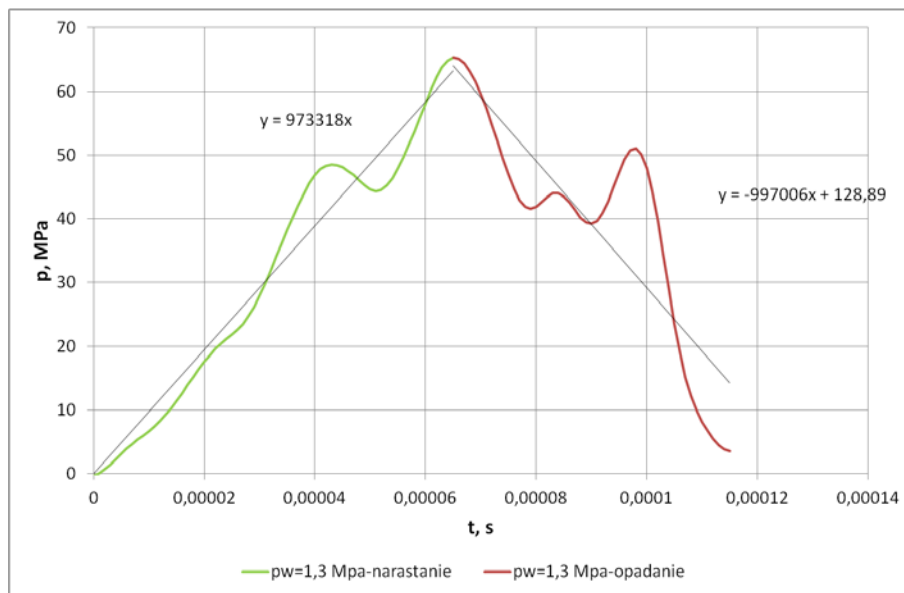


**Figure 2.2.5.18:** Characteristics of the pressure changes during explosion of the 10 g METANIT SPECJALNY E7H charge (Initial pressure = 1.3 MPa).

For the METANIT SPECJALNY E7H charge, a linear approximation of the rate of pressure increase and decrease was made and the average speed of increase and decrease were calculated:

$$v_{\text{increase}} = 9.7 \cdot 10^5 \text{ MPa/s}$$

$$v_{\text{decrease}} = 9.9 \cdot 10^5 \text{ MPa/s}$$

The period analysed was: **115  $\mu$ s** (including: **66  $\mu$ s increase, 49  $\mu$ s decrease**).

Maximum pressure values were:

- Course with filtration: 65.1 MPa,
- Course without filtration: 70.9 MPa.

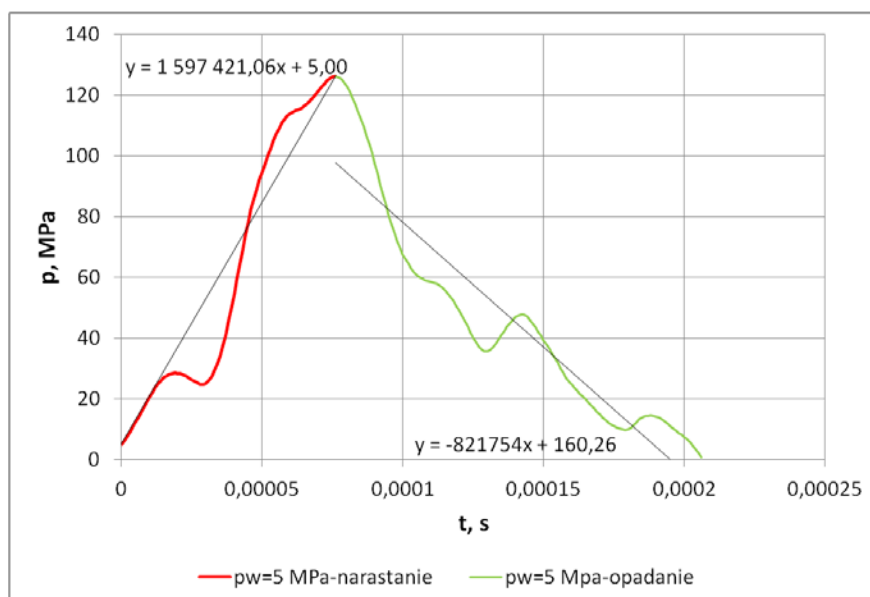


**Figure 2.2.5.19:** Characteristics of the pressure changes during explosion of the 10 g EMULINIT PM charge (initial pressure = 5 MPa).

For the EMULINIT PM charge, a linear approximation of the rate of pressure increase and decrease was made and the average speed of increase and decrease were calculated:

$$v_{increase} = 1.58 \cdot 10^6 \text{ MPa/s}$$

$$v_{decrease} = 8.2 \cdot 10^5 \text{ MPa/s}$$

The period analysed was: **206 µs** (including: **76 µs increase, 130 µs decrease**).

Maximum pressure values were:

- Course with filtration: 126.2 MPa,
- Course without filtration: 127.8 MPa.

In order to define dynamic parameters of the explosion, the important parameters to define are the initial changes of pressure (increase) during the explosion of the explosive charge. For this period of time (i.e. until reaching maximum value) the pressure development function was determined. Although this is representative in the laboratory conditions, it allows for the approximation of such process for the in situ conditions assuming that the balance between the explosive charge and the volume of water (10grams charge in 5,000 cm<sup>3</sup> H<sub>2</sub>O) at which the experiment is carried out is maintained. It must be emphasised that in each case elaboration of new technology of coal seam destruction „the water factor” as no-compressible-one will be recognised as a penetrating-destructive medium, the impulse however of such a process will be dynamic change of its pressure.

### Deflagration materials

In parallel with the dynamic tests of the explosive materials described above, additional experiments aiming at producing the explosive material with extended combustion/oxidation time were carried out. It must be emphasised that eventual future constructions of the explosive charges with deflagrative combustion characteristics, e.g. solid heterogeneous fuels can be used in high pressure and temperature environments, i.e. in the conditions characteristic for deep mining. Furthermore, these types of explosives with extended combustion time compared with conventional mining explosives have one principal advantage. Their energy of explosion does not aim at destructing the coal structure, rather, it is aimed at penetration of the gases or compressing the liquid in the borehole. The very first experiments in this domain were performed using rocket fuels. Their results confirmed the suitability of the test chamber for this type of experiments, the method of initiation for these materials, and how to prepare the charges for the experiments in the presence of water.

It must be also be pointed out that these type of explosives are not initiated by fuses and the detonators used are not waterproof. Prepared materials were tested in the Department of High Energy Materials, which is part of the Institute of Organic Industry in Warsaw. In the current series of experiments the explosive materials, their composition and recipe were adjusted according to the GIG specialists' requirements i.e. the combustion time. The solid heterogeneous fuels tested were the mixture of several ingredients based on required combustion dynamics. The materials used in these mixes were as follows:

- Ammonium chlorate or potassium chlorate
- Poli(butadien-co-acid acrylic-co-acrylonitril) PBAN + hardener
- Caoutchouc + hardener
- Plasticizer
- Aluminium

The charges of solid heterogeneous fuel were characterised by the following physical parameters:

- Weight: about 20g,
- Diameter: 30 mm,
- Density: 1.61 g/cm<sup>3</sup>

Based on the design requirements of the underground environments targeted, and their combustion dynamics, it was necessary to introduce changes to the chemical composition of the explosive materials tested.

Before performing the main experiments in the research chamber, the explosive charges were tested under normal conditions, i.e. at 20°C and atmospheric pressure, using exploder units adjusted to electrical fuses (class 0.2 A). These tests proved that electrical impulse initiated the charges, which in these conditions needed about 20 seconds for the combustion. It must be noted that the combustion time of this type of materials decrease proportionally with the increase of the pressure in its neighbourhood, which was also researched.

### Preparation of the material/ solid heterogeneous fuel to be tested

The usable matrix of the explosive material was prepared by filling and thermal processing. It was cut into pieces and adjusted to the required size. 0.5 g of the ignition mass was inserted inside the cartridge, then the ignition head used for initiation of the combustion process was placed. The following charges were prepared:

- charges without the inhibitor Figure 2.2.5.20a,
- charges with the inhibitor Figure 2.2.5.20b.

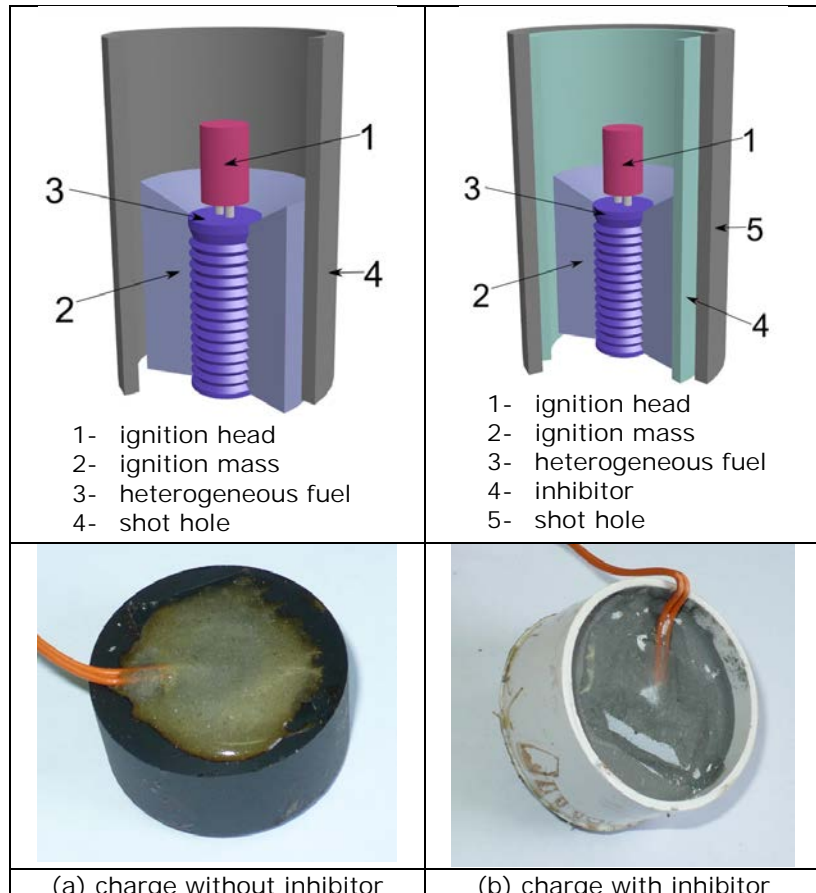


**Figure 2.2.5.20:** Examples of the fuel.

### Results of the experiments

Based on the designed experimental methodology, individual charges were initiated in the sealed testing/research chamber at different water pressures. The results of the experiments carried out for different heterogeneous fuels indicate how the dynamics of their combustion processes changes. These experiments also helped decide how the explosive mixture should be modified to control its combustion dynamics.

Current methods of determining the speed of combustion of the heterogeneous fuel in the ballistic chamber (micro engine) do not allow the simulation of the conditions represented by a borehole drilled in rock/coal in order to verify its fracturing properties. Above methods do not consider variable conditions of pressure surrounding of the heterogeneous fuel and, in fact, that tightness of the environment is partially lost in the moment of breaking the rock (in the case of test chamber the properties of the strata can be simulated by setting the hydraulic valve which is an integral element of the test chamber). This type of information is necessary to determine critical values of combustion dynamics and their utilisation for fracturing the strata (including the coal seams) characterised by various mechanical parameters.

### Fuel without an inhibitor

In the experiments shown in Figure 2.2.5.21, when the initial pressures  $p_w$  were about: 5 MPa, 8.6 MPa, 13.9 MPa and 20.9 MPa, the overflow valve was set at 39.1 MPa. During the experiments with the initial pressure of 21.9 MPa, the overflow valve was blocked.

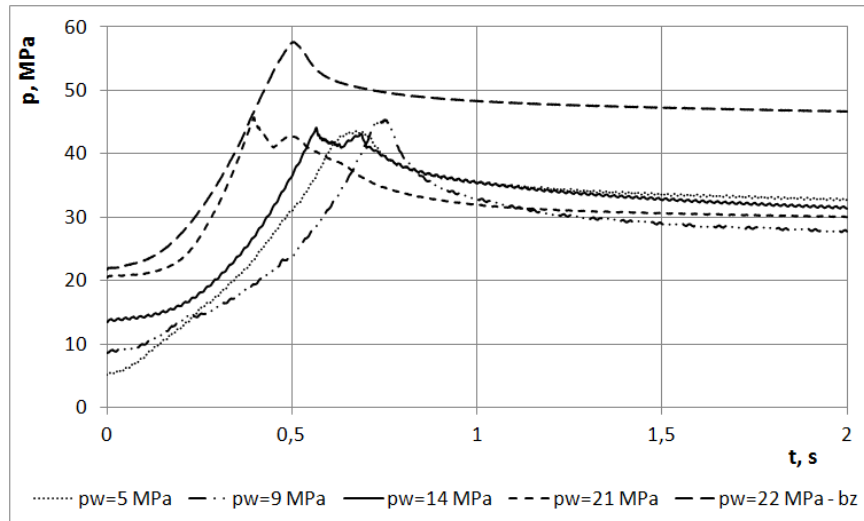


**Figure 2.2.5.21:** Pressure path for the charge tested without an inhibitor.

For the experiment at an initial pressure  $p_w$  of 21.9 MPa, the full course of fuel combustion was determined which reached a maximum pressure of 58 MPa. For the remaining experiments, when the overflow valve was used, the sudden drop of pressure was observed, even though the combustion was continued. The above graphs show the fracturing conditions of the rocks with the hypothetical compression strength of 39 MPa, and opening of the valve can be recognised as fracturing of the rocks. Maximum time of combustion for different explosives tested was not higher than 0.75 s.

#### Fuel with an inhibitor

During the experiments with an inhibitor, the opening of the valve was not observed for the samples fired at the initial pressure of 7 MPa and 10 MPa, which was confirmed by the recording made with high speed camera. The maximum time of combustion was 1.54 s, which is almost twice as high as combustion of the fuel without an inhibitor.

Considering these results, the dynamics of the pressure increase in the test chamber can be interesting from the assessment of the new methane prophylactics techniques point of view when using charges with solid heterogeneous fuels. The above process can be characterised by the interrelation between the speed of combustion and time of pressure increase for certain initial pressures. Variability of the fuel combustion speed can be defined for selected period of time when the process is taking place i.e. since its initiation.

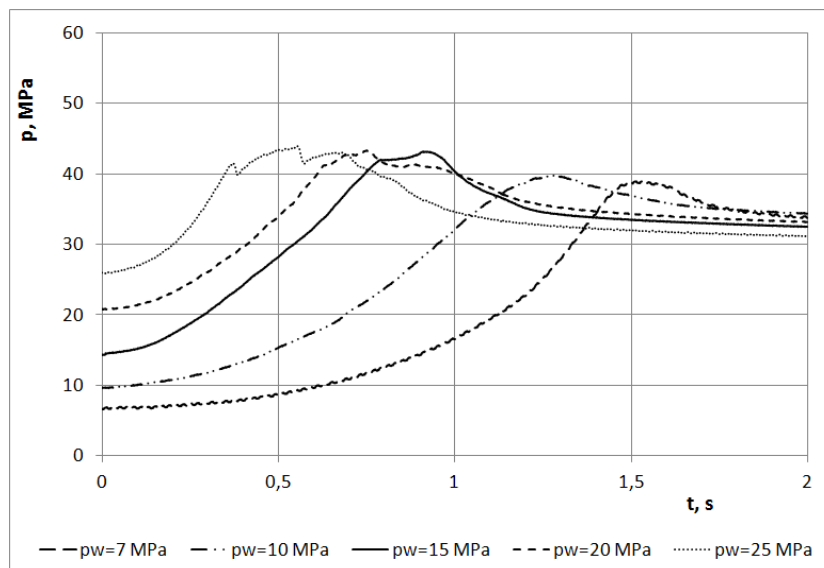


**Figure 2.2.5.22:** Pressure path changes for the samples tested without an inhibitor.

The results of pressure paths changes for the explosive charges tested have certain maximum values depending on the time of opening the safety valve (Figure 2.2.5.21 and Figure 2.2.5.22). Their analysis indicate different explosion dynamics for individual values of initial pressures. Considering the above, and to compare, further analyses assumed 50% of the pressure increase – combustion half-time starting from initial pressure till the pressure of opening the safety valve. Above assumption is based on the analysis where the combustion speed for the analysed samples was assumed as 50% of pressure increase time (Szymczak, 2009), and it was explained by the impact on the fuel being a function of initial temperature and pressure. It is noted that this time is becoming shorter with an increase in initial pressure. For such defined moment in the combustion process, the combustion speed and time period when it reaches 50% of the value is shown in Table 2.2.5.1. The relationship between the combustion speed and initial pressure is shown in Figure 2.2.5.23 and Figure 2.2.5.24 shows the relationship between the initial pressure and the time of pressure increase.

**Table 2.2.5.1:** Principal data registered for 50% time of the samples' combustion.

Type of fuel	Initial Pressure $P_w$ , MPa	Speed of fuel combustion at 50% time of pressure increase MPa/s	Pressure increase time, $T$ , s
without inhibitor	5.16	59.9	0.673
without inhibitor	8.53	40.4	0.753
without inhibitor	13.43	61.3	0.688
without inhibitor	20.52	89.3	0.505
without inhibitor	21.70	81.7	0.502
with inhibitor	6.67	15.8	1.535
with inhibitor	9.60	24.6	1.283
with inhibitor	14.39	38.1	0.916
with inhibitor	20.68	35.7	0.751
with inhibitor	25.97	87.5	0.681

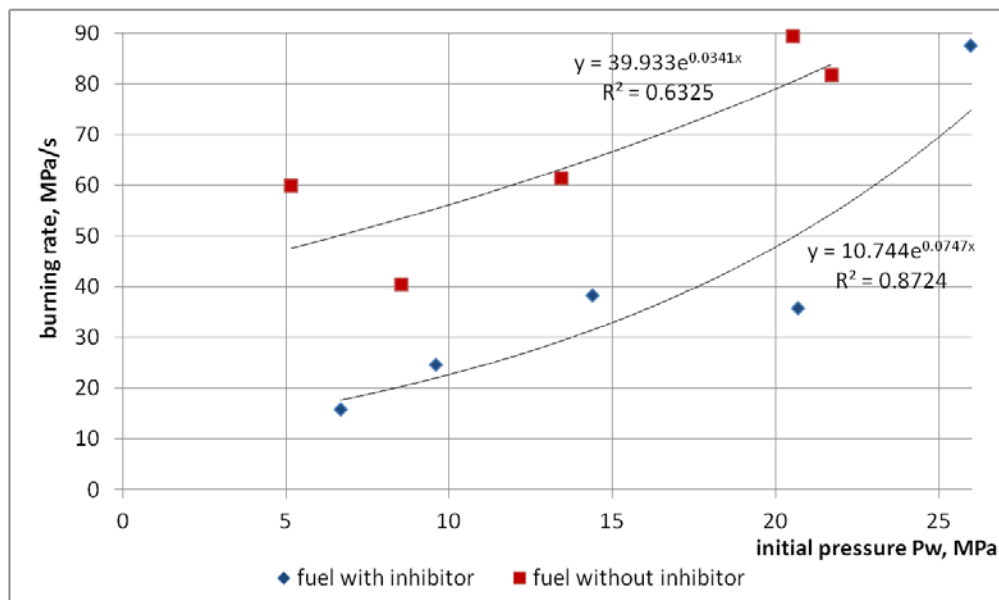


**Figure 2.2.5.23:** Relationship between combustion rate in the intermediate period of the course, and initial pressure for 50% time of pressure increase.

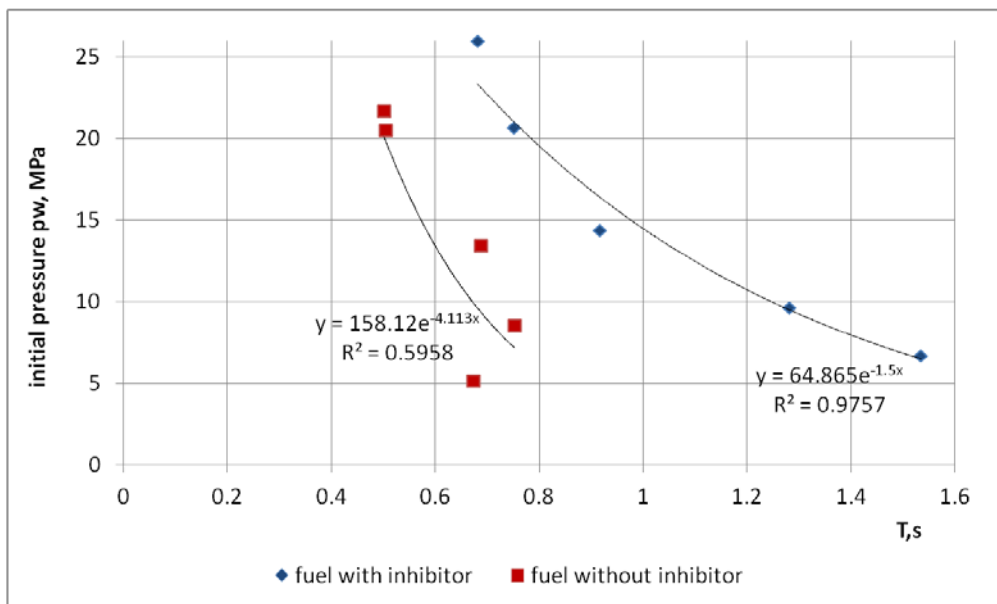


**Figure 2.2.5.24:** Relationship between initial pressure and period of pressure increase.

When analysing both courses in Figure 2.2.5.23 and Figure 2.2.5.24 it must be mentioned that together with the increase of initial pressure the combustion speed is growing (at the same time pressure increase time is decreasing) and the combustion speed for the fuel without inhibitor is higher. Individually, when increasing initial pressure in the surroundings of the sample with inhibitor, higher dynamics of the combustion time shortening and higher combustion speeds were registered. This confirms smaller impact of the environmental pressures on the combustion process without an inhibitor, which results from the construction of the charge (smaller effective surfaces).

Having concluded this part of the initial research aiming at determining the impact of environmental pressure on the combustion dynamics of selected materials with deflagration combustion characteristics it must be emphasised that this type of materials, often utilised as solid heterogeneous fuel, can be more extensively utilised by the mining industry in the near future. The use of above mentioned materials in underground mining will be possible only when their chemical content and construction for use underground is approved and permitted. The environment where they are planned to be used very often has 100% moisture, high pressure and temperature.

The current results also confirm that the fuels maintain their principal features in water and at higher environmental pressures. The problems experienced with initiation of some of the samples tested (connected with proper protection against hydrostatic pressure) were due to the necessity of using the ignition mass with the ignition head. Commonly used method of initiation is the electric detonator with the lead fuse, which was not used due to the small size of the test samples and not a very large combustion chamber.

It was concluded that the dynamics of pressure increase depends on the initial temperature and pressure as well as on the initial environmental pressure of the surroundings. It is assumed that estimation of the above mentioned dynamics for the new generation of materials will allow to judge if they will fulfil the necessary conditions for the development of the mining technologies – both for production and methane control purposes. It must be emphasized, however, that new technologies using explosives require application of the materials which would be able to break structure of the rocks and provide penetration of the strata by limiting their destruction. At the same time, it must be clearly said that none of the blasting technologies so far have provided a fine grid of extended fractures. In order to achieve this target each individual blast hole should be adequately „prepared” (Myszkowski, 1996) by creating inside it a set of initial fractures directing propagation of the gases. Considering the above, Central Mining Institute is conducting intensive research aiming at developing of new drilling equipment as described in Deliverable D2.1.

## 2.2.6. WP2, Task 2.3: Numerical modelling to assess the performance of stimulated wellbores (led by IMPERIAL).

The objective of Task 2.3 in WP2 is to utilise the data generated for different coal and field conditions mainly under WP1 and partly WP2 and implement numerical models to assess the performance of four different borehole stimulation techniques, namely:

- hydraulic stimulation of coal seams,
- slotted boreholes in coal seams,
- cavity completions in coal seams,
- explosives for fracturing coal seams.

It is not necessary or appropriate that all four methods will be applicable to both the coking and steam coal types mined by partner industries. Furthermore, depending on the mining layout, and the drainage objective the stimulation methods modelled and trialled in the field will vary.

The Deliverable D2.3 report submitted presents a detailed account of numerical modelling work carried out for all four stimulation methods by IMPERIAL. This section in the MidTerm report presents a summary of the work described in D2.3.

### **SubTask 2.3.1 Numerical modelling of hydraulic stimulation (IMPERIAL)**

At IMPERIAL two different software applications were used and appraised for modelling hydraulic stimulation of drainage boreholes in coal seams, namely FRACPRO by CARBO Ceramics Inc. (2016) and Particle Flow Code (PFC) by Itasca (2016).

#### **Numerical modelling of hydraulic stimulation using FRACPRO**

##### *Modelling procedure*

Field and laboratory data obtained from WPs 1 and 2 for different types of coals and coal measures rocks were used as input parameters to the models, and prevailing stress and fracture conditions at mining sites were also considered. Stimulation performances such as fracture growth and geometry, propped dimension and proppant concentration were evaluated, which can provide data and guidance to the design of field scale stimulation practices later in the project. Modelling was firstly performed using the field data obtained at HUNOSA, which followed the following 6 steps stimulation practices later in the project. Modelling was firstly performed using the field data obtained at HUNOSA, which followed the following 6 steps, described in detail in Deliverable D2.3 report:

- (1) Fracture model selection: 3D shear-decoupled model was applied in the simulation analysis.
- (2) Wellbore configuration: A 50 m-long horizontal borehole with a diameter of 60 mm drilled through coal seam from the intake entry.
- (3) Reservoir parameters: The height of the model was 650 m, and the coal seam is located at a depth of 550 m with thickness 5 m. The reservoir parameters used are presented in Table 2.2.6.1.
- (4) Fluid and proppant selection was automatic by FracPro with some user control
- (5) Treatment selection: Maximum bottomhole pressure at, maximum injection rate of 15.90 m<sup>3</sup>/min and required fracture length, 0.05 m<sup>3</sup>/min.
- (6) Treatment schedule: As shown in Table 2.2.6.2.

**Table 2.2.6.1:** Reservoir parameters representative of Hunosa field.

Layer	Pore Fluid Permeability (mD)	leak off Coefficient (m/min <sup>½</sup> )	Closure Stress Grad (MPa/m)	E (GPa)	$\mu$	Fracture Toughness (MPa)	Composite Layering Effect
Coal	3	$3.35 \times 10^{-4}$	0.017	1.55	0.29	0.77	1
Sandstone	10	$3.36 \times 10^{-4}$	0.014	34.0	0.41	1.10	25

In the case of JSW , most settings were the same as that for Hunosa, specifically as:

- (1) Wellbore configuration: the geological setting for the panel used only three types of lithology, i.e., coal, shale and sandstone, with the target coal seam being 4 m thick. A 50 m-long borehole with a diameter of 100 mm is drilled into the panel for hydraulic fracturing.

**Table 2.2.6.2:** Design treatment schedule for hydraulic fracture stimulation at Hunosa.

Stage #	Stage Type	Elapsed Time min:sec	Fluid Type	Clean Volume (m <sup>3</sup> )	Prop Conc (kg/m <sup>3</sup> )	Stage Prop. (tonnes)	Slurry Rate (m <sup>3</sup> /min)	Proppant Type
Wellbore Fluid								
1	Main frac pad	10:00	WG1853cP65C	0.500	0	0.0	0.05	CarboLite 8/12
2	Main frac slurry	20:00	WG1853cP65C	0.435	240	0.1	0.05	CarboLite 8/12
3	Main frac slurry	30:00	WG1853cP65C	0.385	480	0.2	0.05	CarboLite 8/12
4	Main frac slurry	40:00	WG1853cP65C	0.346	720	0.2	0.05	CarboLite 8/12
5	Main frac slurry	50:00	WG1853cP65C	0.313	960	0.3	0.05	CarboLite 8/12
6	Main frac slurry	60:00	WG1853cP65C	0.287	1,200	0.3	0.05	CarboLite 8/12
7	Shut-in	80:00	SHUT-IN	0.000	0	0.0	0.00	

- (2) Reservoir parameters: The reservoir pore pressure was 3.0 MPa, and pore fluid compressibility was 0.33 MPa<sup>-1</sup>. The average pressure in fracture was 20.35 MPa in the simulation. Other reservoir parameters are summarised in Table 2.2.6.3.

**Table 2.2.6.3:** Reservoir parameters representative of the conditions at JSW.

Layer	Pore Fluid Permeability (mD)	leak off Coefficient (m/min <sup>1/2</sup> )	Closure Stress Grad (MPa/m)	E (GPa)	$\mu$	Fracture Toughness (MPa)	Composite Layering Effect
Sandstone	10	4.27×10 <sup>-4</sup>	0.014	9.61	0.30	1.10	25
Coal	0.1	3.65×10 <sup>-4</sup>	0.017	1.55	0.29	0.77	1
Shale	0.001	6.97×10 <sup>-5</sup>	0.016	3.50	0.30	2.20	25

The same fluid and proppant were selected for the treatment. It is noted that the injection rate at JSW cannot exceed 115 litre/min, so an injection rate of 0.05 m<sup>3</sup>/min was also adopted in this simulation. In addition, the same design treatment schedule was used in order to yield comparable results with the Hunosa conditions.

It was found that the fractures propagate along with the orientation of the maximum principal stresses at both Hunosa and JSW conditions. The treatment summaries for both cases are tabulated in Tables 3.2.6.4 and 3.2.6.5. Similar sizes of fracture length and height are induced at the two coalfield conditions, but fracture width at JSW is about twice that at Hunosa.

**Table 2.2.6.4:** Fracture treatment summaries at Hunosa conditions.

(a) Fracture geometry summary				(b) Operation summary				
Fracture Half-Length (m)	26	Total Clean Fluid Pumped (m <sup>3</sup> )	2.89					
Total Fracture Height (m)	11	Total Slurry Pumped (m <sup>3</sup> )	3.03					
Fracture Slurry Efficiency	0.27	Pad Volume (m <sup>3</sup> )	0.50					
Propped Half-Length (m)	13	Primary Fluid Type	WG1853cP65C					
Total Propped Height (m)	5	Total Proppant Pumped (tonnes)	1.20					
Max. Fracture Width (cm)	0.08	Total Proppant in Fracture (tonnes)	0.20					
Avg. Fracture Width (cm)	0.06	Avg. Btm. Slurry Rate (m <sup>3</sup> /min)	0.05					
Avg. Proppant Concentration	0.74	Primary Proppant Type	CarboLite 8/12					
(c) Hydraulic fracture growth history*								
End of Stage #	Stage Type	Time (mm:ss)	Fracture Half-Length (m)	Fracture Height (m)	Fracture Width at Well (cm)	Avg. Fracture Width (cm)	Model Net Pressure (MPa)	Slurry Efficiency
1	Main frac pad	10:00	19	5	0.219	0.138	0.42	0.44
2	Main frac slurry	20:00	23	7	0.276	0.129	0.36	0.34
3	Main frac slurry	30:00	25	8	0.306	0.137	0.33	0.30
4	Main frac slurry	40:00	26	10	0.325	0.146	0.32	0.28
5	Main frac slurry	50:00	27	11	0.341	0.155	0.31	0.27

End of Stage #	Stage Type	Time (mm:ss)	Fracture Half-Length (m)	Fracture Height (m)	Fracture Width at Well (cm)	Avg. Fracture Width (cm)	Model Net Pressure (MPa)	Slurry Efficiency
6	Main frac slurry	60:00	27	11	0.365	0.169	0.33	0.27
7	Main frac slurry	80:00	26	11	0.081	0.056	-0.19	0.06

\* All values reported are for the entire fracture system and at the end of each stage

**Table 2.2.6.5:** Fracture treatment summaries at JSW conditions

(a) Fracture geometry summary			(b) Operation summary					
Fracture Half-Length (m)	28		Total Clean Fluid Pumped (m <sup>3</sup> )				3.04	
Total Fracture Height (m)	8		Total Slurry Pumped (m <sup>3</sup> )				3.04	
Fracture Slurry Efficiency	0.31		Pad Volume (m <sup>3</sup> )				0	
Propped Half-Length (m)	0		Primary Fluid Type				WG1853cP65C	
Total Propped Height (m)	0		Total Proppant Pumped (tonnes)				1.6	
Max. Fracture Width (cm)	0.18		Total Proppant in Fracture (tonnes)				0	
Avg. Fracture Width (cm)	0.10		Avg. Btm. Slurry Rate (m <sup>3</sup> /min)				0.05	
Avg. Proppant Concentration	0		Primary Proppant Type				CarboLite 8/12	
(c) Hydraulic fracture growth history*								
End of Stage #	Stage Type	Time (mm:ss)	Fracture Half-Length (m)	Fracture Height (m)	Fracture Width at Well (cm)	Avg. Fracture Width (cm)	Model Net Pressure (MPa)	Slurry Efficiency
1	Main frac pad	10:00	19	5	0.238	0.152	0.42	0.41
2	Main frac slurry	20:00	23	6	0.303	0.185	0.39	0.36
3	Main frac slurry	30:00	25	6	0.354	0.212	0.37	0.34
4	Main frac slurry	40:00	27	7	0.390	0.232	0.34	0.32
5	Main frac slurry	50:00	28	7	0.424	0.251	0.34	0.31
6	Main frac slurry	60:00	28	8	0.447	0.267	0.32	0.31
7	Main frac slurry	80:00	28	8	0.179	0.096	-1.02	0.10

\* All values reported are for the entire fracture system and at the end of each stage

A parametric study was also carried out to investigate the effect of injection rates and injection time at both Hunosa and JSW conditions. It was seen that larger fracture dimensions, propped dimensions as well as fracture slurry efficiency are induced at higher injection rates. It was noted the lowest injection rate to promote propped dimension growth is 0.04 m<sup>3</sup>/min at Hunosa but 0.2 m<sup>3</sup>/min at JSW. Results have shown that injection time had a positive impact on fracture and proppant dimensions but a detrimental effect on fracture slurry efficiency. For Hunosa, slurry injection for 10 min is ideal to generate sufficient fracture dimensions without excessive growth, but better proppant performances can be expected with longer injection time.

### Numerical modelling of hydraulic stimulation using PFC

#### *Modelling procedure*

The theory behind modelling in PFC is described in detail in Deliverable D2.3. A 10 m × 10 m model was designed to simulate a section of Hunosa coal seam at 550 m depth with 7,216 particles. At JSW, an 8 m × 8 m model comprising 4,614 particles was developed to simulate the coal panel at 990 m depth. Three layers were identified, with sandstone in the hanging wall and shale in the footwall (Figure 2.2.6.1).

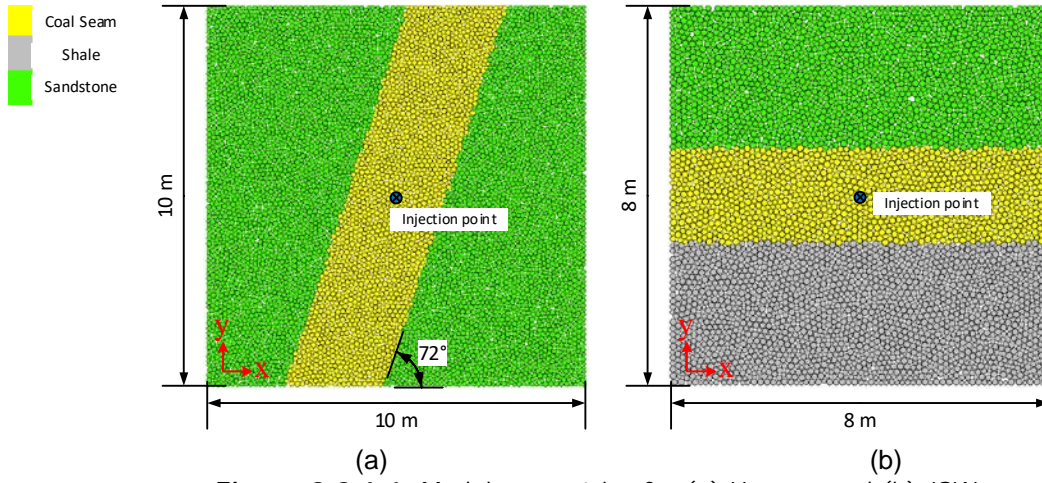


**Figure 2.2.6.1:** Model geometries for (a) Hunosa and (b) JSW.

Tables 3.2.6.6 and 3.2.6.8 list the rock mechanical properties used for calibration and calibrated macro properties from numerical experiments as well. Tables 3.2.6.7 and 3.2.6.9 tabulate the microscopic parameters for Hunosa and JSW models, respectively.

**Table 2.2.6.6:** Rock mechanical properties used for Hunosa model.

Layer	Value	E (GPa)	$\mu$	c (MPa)	$\Phi$ ( $^{\circ}$ )	$\sigma$ (MPa)	T (MPa)
Coal	Measured value	1.55	0.29	2.81	22	8.32	0.40
	Calibrated value	1.55	0.30	--	--	8.40	0.39
	Errors ( $\pm\%$ )	0	3.40	--	--	1.00	2.50
Sandstone	Measured value	34.0	0.41	10.0	25	31.40	--
	Calibrated value	34.1	0.39	--	--	32.50	3.11
	Errors ( $\pm\%$ )	0.3	4.90	--	--	3.50	--

**Table 2.2.6.7:** Microscopic parameters used for Hunosa model.

	Flat joint bond parameters	Coal	Sandstone
Contact properties	Elasticity modulus E (GPa)	2.0	58.4
	Stiffness ratio ( $k_n/k_s$ )	3.4	7.2
	Tensile strength T (MPa)	0.6	5.6
Bond properties	Cohesion c (MPa)	4.5	14.0
	Internal friction coefficient f ( $^{\circ}$ )	22.0	25.0
Friction properties	Friction coefficient $\phi$	0.577	0.577

**Table 2.2.6.8:** Rock mechanical properties used for JSW model.

Layer	Value	E (GPa)	$\mu$	c (MPa)	$\Phi$ ( $^{\circ}$ )	$\sigma$ (MPa)	T (MPa)
Coal	Measured value	1.55	0.29	4.25	22	12.6	1.26
	Calibrated value	1.55	0.28	--	--	13.0	1.27
	Errors ( $\pm\%$ )	0	3.40	--	--	3.2	0.80
Sandstone	Measured value	9.61	0.30	25.82	30	89.4	8.94
	Calibrated value	9.57	0.30	--	--	90.0	8.98
	Errors ( $\pm\%$ )	0.40	0	--	--	0.7	0.40
Shale	Measured value	3.50	0.30	19.53	25	61.3	6.13
	Calibrated value	3.50	0.30	--	--	61.7	6.13
	Errors ( $\pm\%$ )	0	0	--	--	0.7	0

**Table 2.2.6.9:** Microscopic parameters used for JSW model.

	Flat joint bond parameters	Coal	Sandstone	Shale
Contact properties	Elasticity modulus E (GPa)	1.7	10.4	3.8
	Stiffness ratio ( $k_n/k_s$ )	3.4	3.4	3.4
	Tensile strength T (MPa)	1.9	14.2	9.7
Bond properties	Cohesion c (MPa)	5.6	37.5	25.7
	Internal friction coefficient $\phi$ (°)	22.0	30.0	25.0
Friction properties	Friction coefficient f	0.577	0.577	0.577

Pore pressure and crack distribution was determined for the models after hydraulic fracturing. In both Hunosa and JSW cases, both tensile and shear cracks were generated. It was observed that the cracks change the contact network geometry and create new fluid flow paths. Pore pressure propagates simultaneously with crack growth. Figure 2.2.6.2 illustrate the pore pressure and crack distribution for the Hunosa case at different stages of hydrofracturing. The effect of pumping pressure on crack growth was also investigated as summarised in Figure 2.2.6.3 for the JSW case.

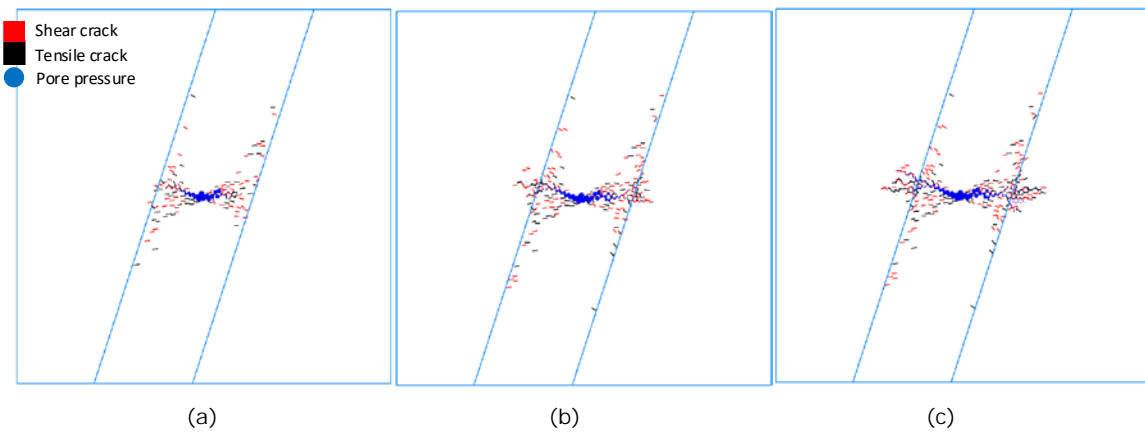


**Figure 2.2.6.2:** Pore pressure and crack evolution in Hunosa model at (a) 1,000 steps, (b) 3,000 steps and (c) 6,000 steps

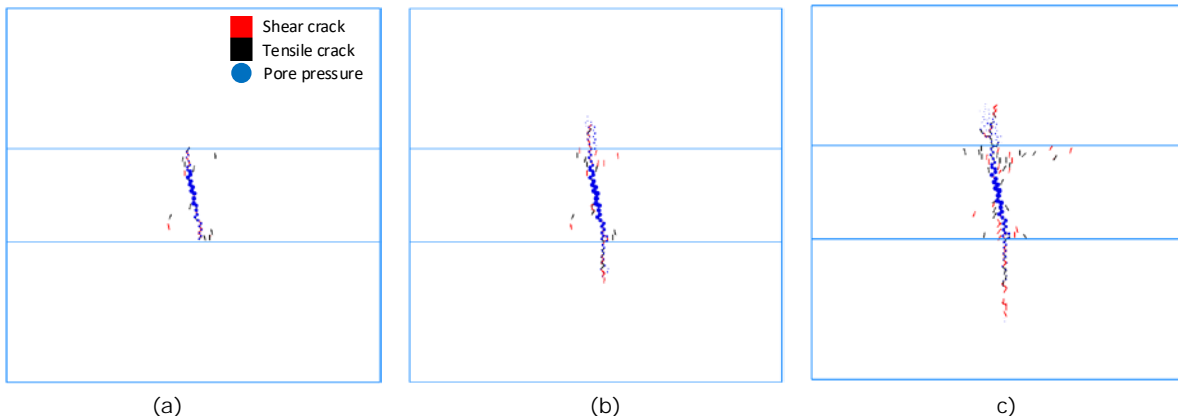


**Figure 2.2.6.3:** Pore pressure and crack distribution in JSW model at pumping pressure of (a) 20 MPa, (b) 30 MPa, and (c) 50 MPa.

#### **SubTask 2.3.2 Numerical modelling of stress relief and fracturing induced around slotted wellbores (IMPERIAL)**

In this subtask the researchers at IMPERIAL assessed the slotting technique for its performance in stimulating the long horizontal in-seam pre-drainage boreholes in the soft coking coals of JSW and the sublevel in-seam predrainage down-holes in the soft coals of HUNOSA. The extent of stress relief and fracturing around the borehole depends on slotting geometry, coal mechanical/elastic properties,

permeability and borehole stability, which have been all considered in the numerical modelling work as described in detail in Deliverable D2.3 report. Numerical modelling assessed the performance of different configurations of slots implemented in the field using FLAC<sup>3D</sup>. A coupled geomechanics and fluid flow modelling approach was developed to capture the key physics of slot cutting and its effects on permeability enhancement around boreholes.

### Numerical modelling of slotting techniques at JSW

#### Geomechanical modelling

The field site selected for the underground experimental work at JSW was the longwall D-2 in coal seam #412, at a depth of ~900 m. As shown in Figure 2.2.6.4, the physical dimensions of the model are 10×6×10m (length×width×height) and a cylindrical zone at the centre of the model is refined to accommodate the simulated borehole and slots. The thickness of the coal seam is reported as ~4.2 m, underlying a relatively strong sandstone roof and overlying a shale floor. The entire model domain was assumed to be ranging from the mudstone floor to sandstone roof at the depth from -984 to -994 m. Only a small section of the 100mm diameter borehole (6 m long) within the coal seam was simulated considering a single slot being created mechanically or by water-jet slotting. Table 2.2.6.10 presents the rock mechanical and strength properties of the coal seam #412 at JSW.

After borehole drilling, a slot (diameter D=0.50 m, thickness w=0.03 m) was created at the centre of the refined area. Using a Strain Softening (SS) constitutive model, different thickness and diameter of the slot plane in JSW was analysed and compared.

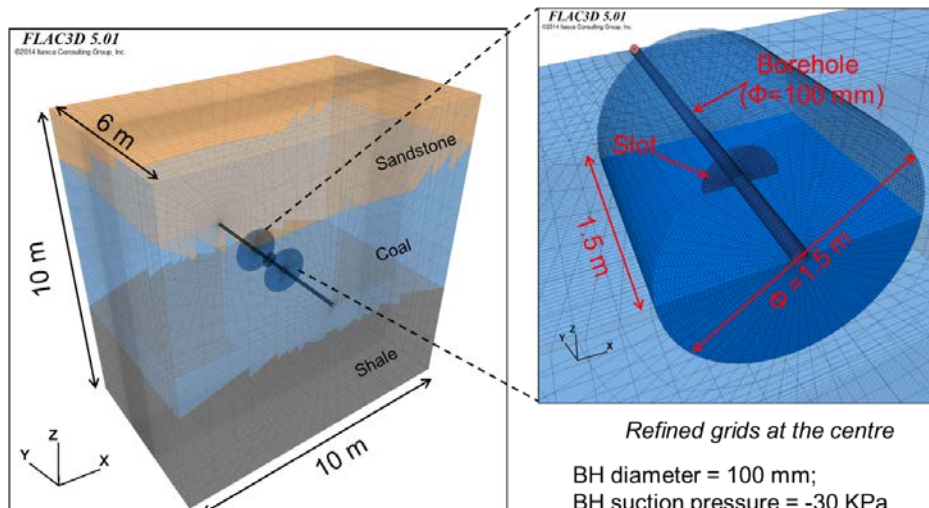


**Figure 2.2.6.4:** Model geometry and the centre refined area for JSW.

**Table 2.2.6.10:** Rock mechanical and strength properties of coal in JSW.

Model	K (GPa)	G (GPa)	$\varphi$ (°)	C (MPa)	$C_t$ (MPa)	$\varepsilon_p$	t (MPa)
MC	1.26	0.60	22	4.25	-	-	-1.26
SS	1.26	0.60	22	4.25	1	1e-4	-1.26

The failure zone size and vertical stress distributions at the horizontal cross-cut plane for the different slot thickness and diameters were determined (Figure 2.2.6.5 and Figure 2.2.6.6). These stress contours confirm that compared with slot thickness, increasing slot diameter is more effective in enlarging the stress relief zone and pushing the stress concentration zone further away from the borehole.

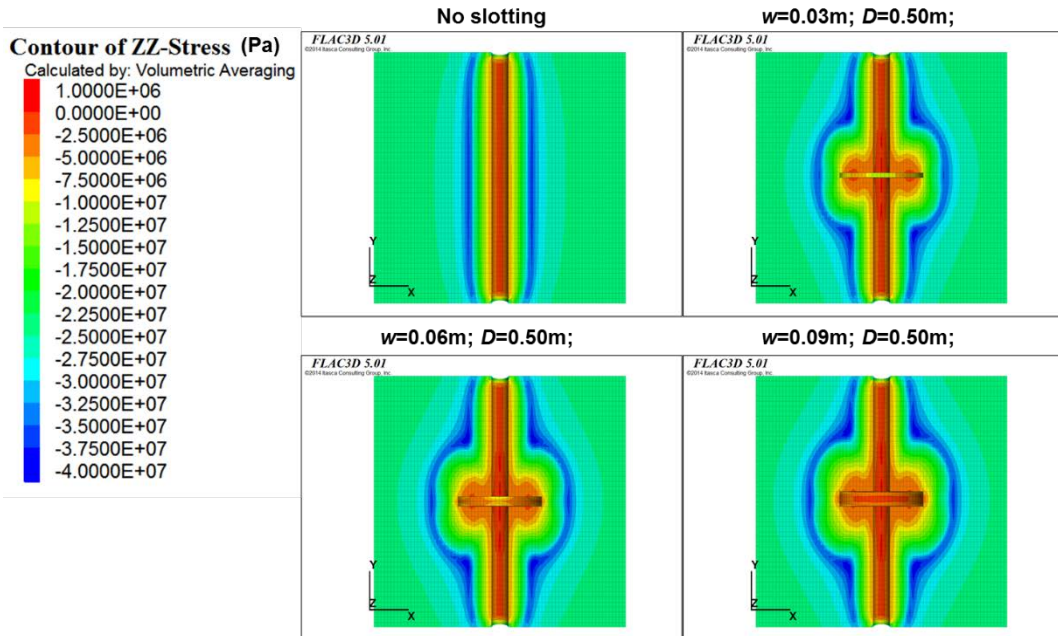


**Figure 2.2.6.5:** Vertical stress distribution with different slot thicknesses.

#### *Gas drainage modelling in stimulated boreholes*

Based on the geomechanical modelling results, numerical models to simulate gas drainage in stimulated boreholes were developed in ECLIPSE300. After each slotting operation, the stress distributions generated by FLAC<sup>3D</sup> were used to calculate the permeability field around boreholes for different slot thicknesses and diameters using the stress-dependent permeability relationships developed earlier at IMPERIAL.

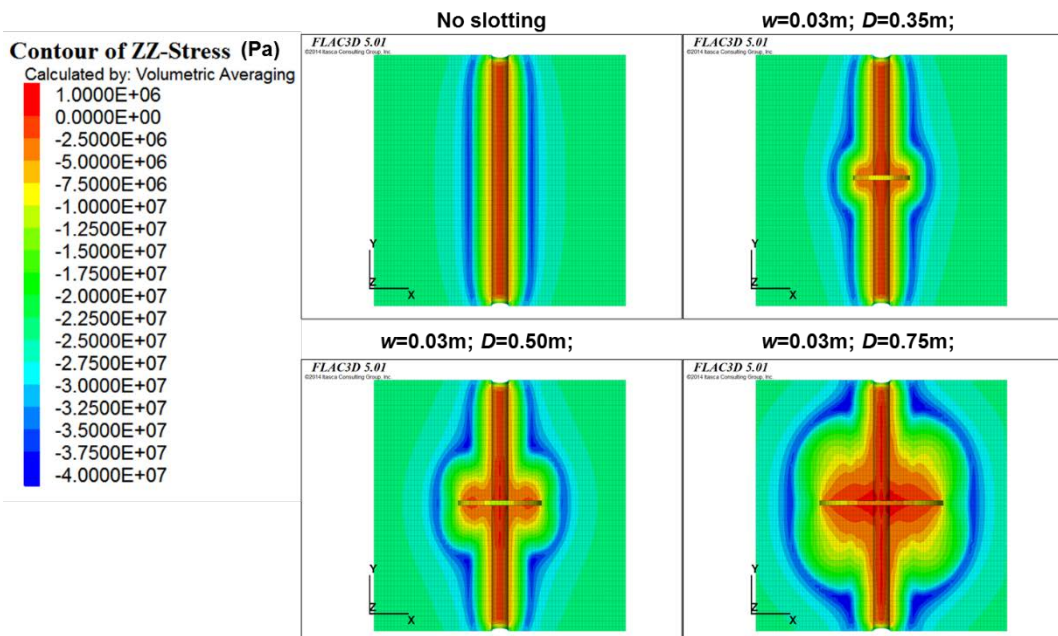


**Figure 2.2.6.6:** Vertical stress distribution with different slot diameter.

For each slot thickness and diameter, gas drainage performance was simulated for 4 hours. As a result of permeability enhancement within the failure zone, a dramatic pressure relief was observed. Larger slot diameter have created larger pressure relief shadows along the two sides of the slot. Analysing the

gas flow rate and cumulative volume of captured gas it was found out that, as expected, larger diameter slots outperformed its counterparts in terms of both gas flow rate and total volume of captured gas (Figures 3.2.6.7 and 3.2.6.8) which should be the primary consideration when designing slotted boreholes.

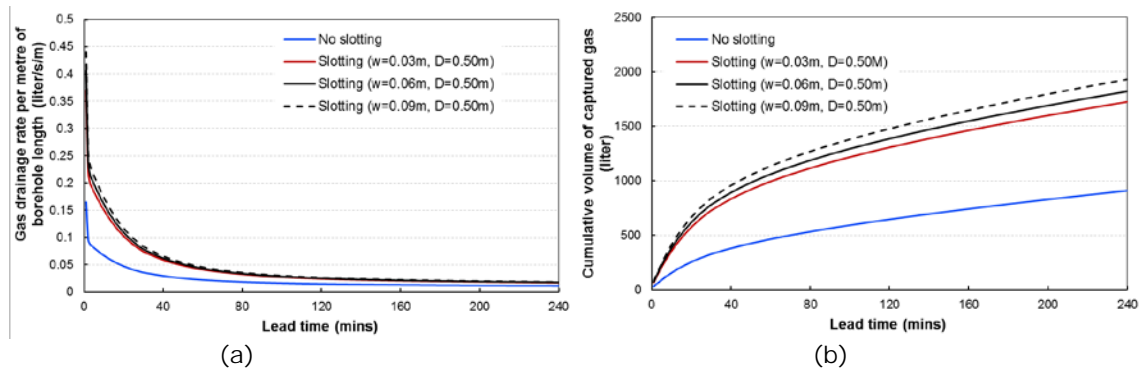


**Figure 2.2.6.7:** Gas drainage performance with varying slot thicknesses: (a) gas drainage rate per metre of borehole length, and (b) cumulative volume of captured gas.

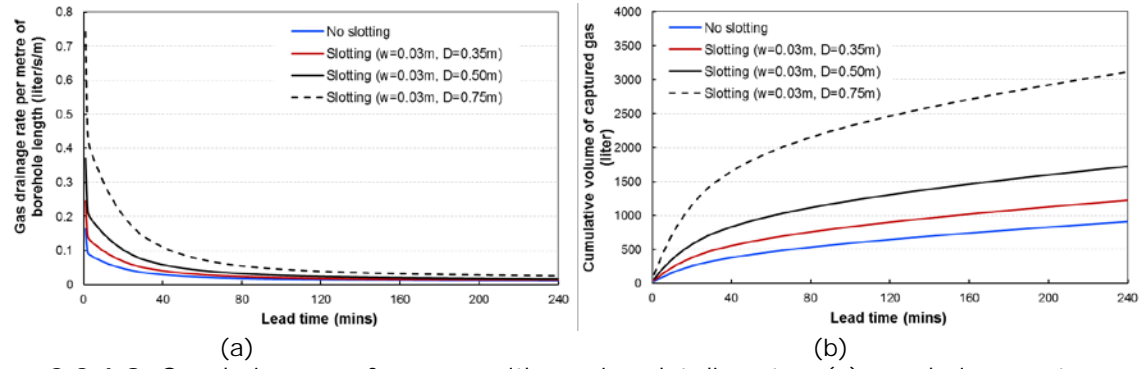
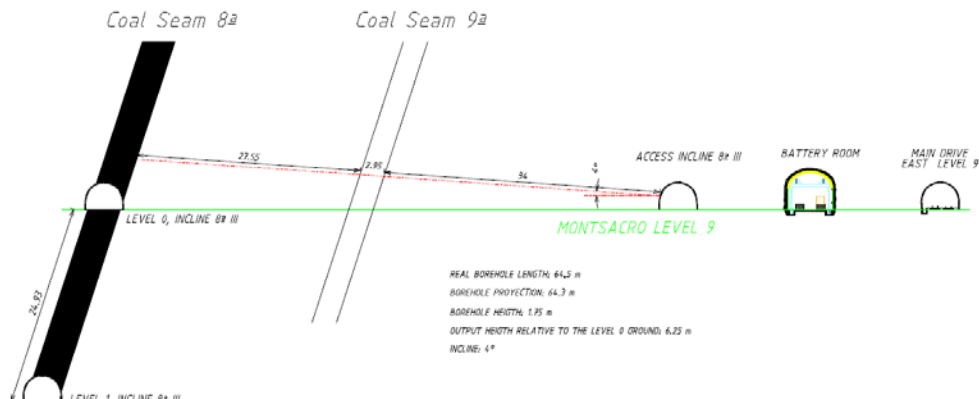


**Figure 2.2.6.8:** Gas drainage performance with varying slot diameter: (a) gas drainage rate per metre of borehole length, and (b) cumulative volume of captured gas.

### Numerical modelling of slotting techniques at Hunosa

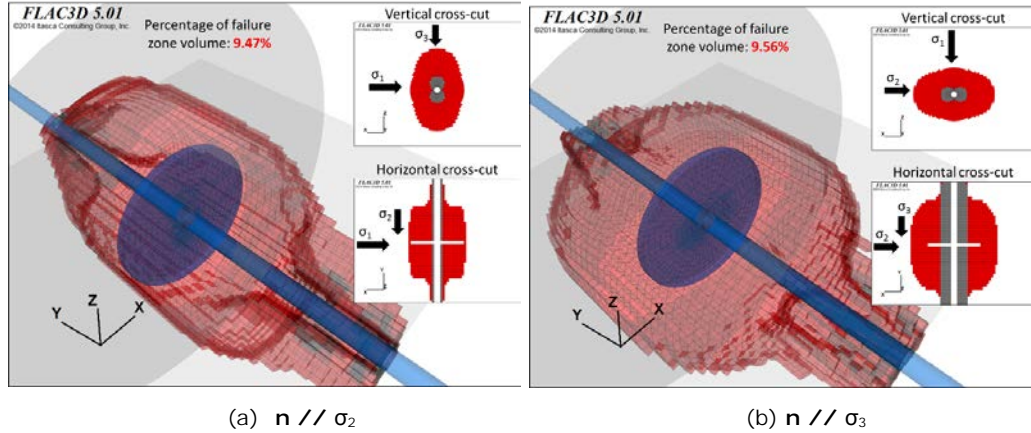
#### Geomechanical modelling

Figure 2.2.6.9 illustrates the drilling plan of the stimulation boreholes at Hunosa. Boreholes were designed to be drilled from the gallery at the foot wall. The length of these boreholes are around 60 to 70 m long and their diameter is ~60 mm.



**Figure 2.2.6.9:** Borehole drilling plan at Hunosa.

A similar model geometry to that used for JSW shown in Figure 2.2.6.4 was used for Hunosa. However, this time the entire model domain was assumed to be within the #8 coal seam at a depth from -500 to -510 m. The diameter of the borehole was modelled as 60 mm. The maximum principal stress, intermediate principal stress, and minimum principal stress are taken as 24 MPa, 16 MPa, and 11 MPa, respectively.



**Figure 2.2.6.10:** The effect of varying dip direction and dip angle on failure zone geometry.

As in the case for JSW, Strain Softening model was used and parametric studies were carried out to determine the effect of slot width, radius, shape and slot plane orientation on the performance of slotting. This helped optimise the slotting process for the Hunosa case (Figure 3.2.6.10).

#### *Gas drainage modelling in stimulated boreholes*

The coupling methodology between geomechanical and fluid flow simulators followed the same procedure used for JSW. After each slotting operation, the stress distributions generated by FLAC<sup>3D</sup> were used to calculate the permeability field around boreholes based on the stress-dependent permeability relationship developed at IMPERIAL (Figure 2.2.6.11).

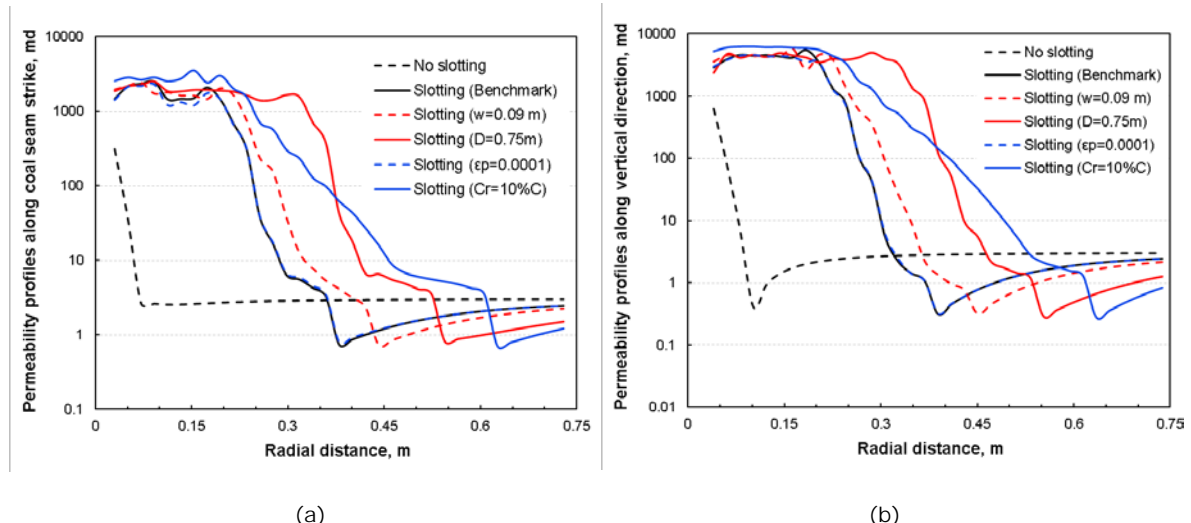


**Figure 2.2.6.11:** Permeability profiles along the (a) coal seam strike and (b) vertical direction.

As seen in Figure 2.2.6.11, slotting can stimulate the permeability around the borehole: the enhanced permeability zone ( $k > k_0$ ) in the benchmark scenario is more than ten times of the borehole diameter. The enhanced permeability zone size is very sensitive to the residual cohesion  $C_r$ .

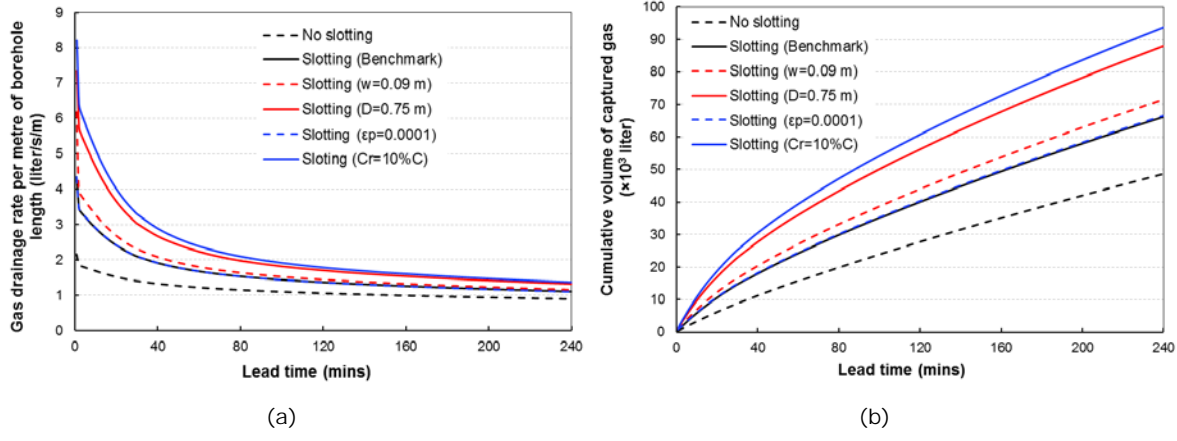


**Figure 2.2.6.12:** Gas drainage performance after borehole stimulation: (a) gas drainage rate per metre of borehole length, and (b) cumulative volume of captured gas.

Figure 2.2.6.12 compares the gas drainage performance between un-slotted and slotted boreholes at Hunosa. Gas drainage rate in slotted boreholes can be 2 to 3 times higher than the un-slotted boreholes. However, in slotted boreholes, a faster decline of gas flow rate is observed within the first hour of slotting operation. It was concluded that, in order to maximise the performance of slotting operation, one needs to aim at achieving as large as possible of slot diameter ( $D$ ), while increase slot width ( $w$ ) can be only considered as an additional measure which can only slightly enlarge the stimulated zone

### SubTask 2.3.3 Numerical simulation of cavity completions (IMPERIAL)

Inspired by the success of cavity completions in the Fairway zone of the San Juan Basin coalbed methane wells, this SubTask investigated the potential for cavitation of methane drainage wells at JSW and Hunosa. The modelling work was carried out using IMPERIAL's in house cavity completion model OHCAV, which is able to assess the development of tensile and shear failure zones, and the cavity size around wellbores in different coal seams and layouts. A detailed description of the model and its implementation at JSW and HUNOSA are presented in the Deliverable D2.3 report. A summary of the main findings is presented here.

### Cavity completion modelling of Hunosa conditions

As presented in Figure 3.2.6.9 above, the drilling pattern at Hunosa would follow the sub-level caving layout and mining progress. In that respect, two potential predrainage borehole configurations were considered (Figure 2.2.6.13).

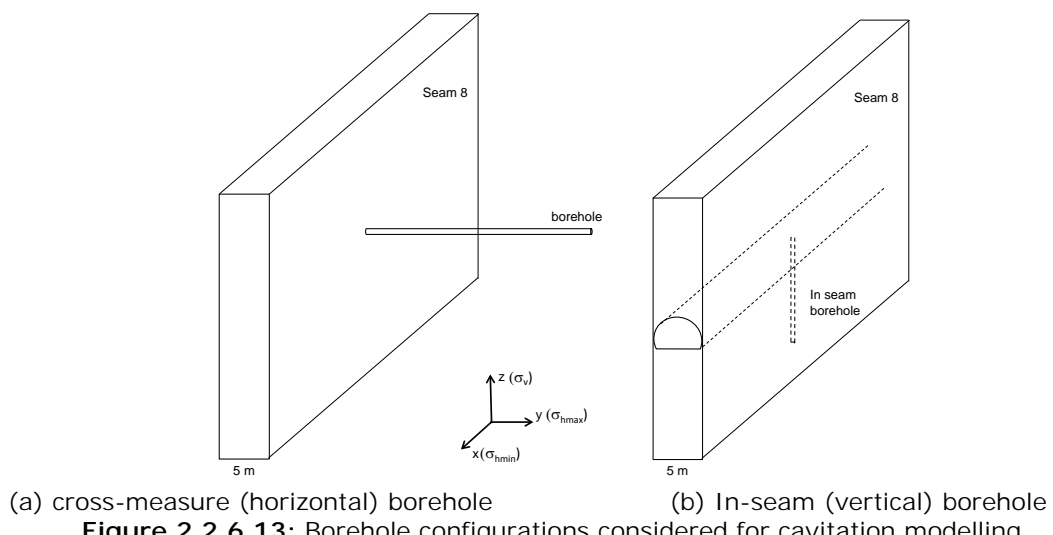


**Figure 2.2.6.13:** Borehole configurations considered for cavitation modelling.

### Model domain and boundary conditions

Cavitation modelling is carried out in a plane perpendicular to the borehole under plane-strain conditions. Figure 2.2.6.14 presents the plane-strain model domains used and associated boundary

conditions for the two borehole configurations. Only half of the domain ( $45\text{m} \times 45\text{m}$ ) needs to be considered due to symmetry. The borehole has a diameter of  $0.06\text{ m}$ . Unlike the horizontal cross-measure borehole where the whole domain is within the coal seam Figure 2.2.6.14a), the model domain for the in-seam borehole extends beyond the  $5\text{-m}$  thick seam (Figure 2.2.6.14b).

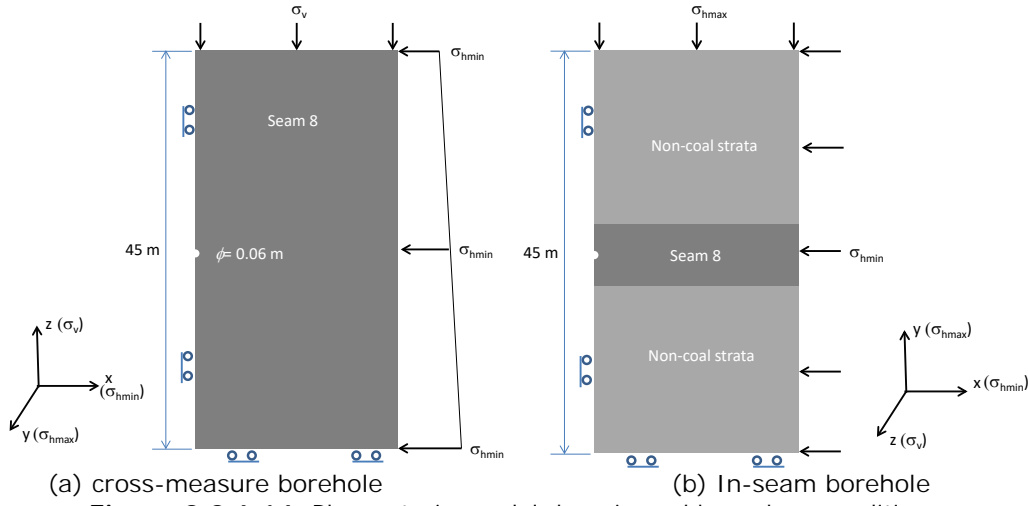


**Figure 2.2.6.14:** Plane-strain model domain and boundary conditions.

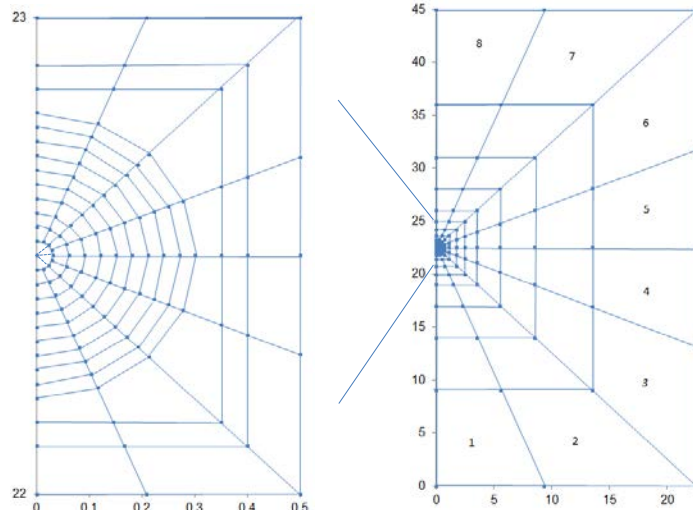


**Figure 2.2.6.15:** Model mesh (right) and close-up around the borehole (left).

The finite element mesh used is presented in Figure 2.2.6.15. It gets progressively coarser away from the borehole. A close-up of the region around the borehole ( $1\text{m} \times 0.5\text{ m}$ ) is also shown. For ease of presenting the modelling results, the domain is divided into 8 sub-sections. The mechanical and elastic properties of the coal used was same as those used for the Hunosa coal in the slotting study.

#### *Model results at Hunosa conditions*

Cavitation modelling consists of two stages: 1) borehole drilling; and 2) rapid depressurisation of the borehole pressure. The geomechanical and sorption properties of the Hunosa coals determined by the project partners were used in the simulations.

First the cross-measure (horizontal) borehole scenario illustrated in Figures 3.2.6.13a and 3.2.6.14a was simulated, starting with the analysis of stress and permeability distributions around the borehole after drilling. Analyses have shown that the permeability would be greatly enhanced due to stress relief in the vicinity of the borehole. Next, the cavitation process is simulated by reducing the borehole pressure at a rate of  $0.2\text{ MPa/s}$  to  $0.1\text{ MPa}$  from the initial pressure of  $2\text{ MPa}$ . It was seen that rapid depressurisation has further enlarged the shear failure zone beyond that reached during the drilling stage. The performance of cavitation in terms of permeability enhancement was then evaluated and, as

illustrated in Figure 2.2.6.16, the permeability within a region of 0.9 m radius around the borehole was increased by over one-order of magnitude.

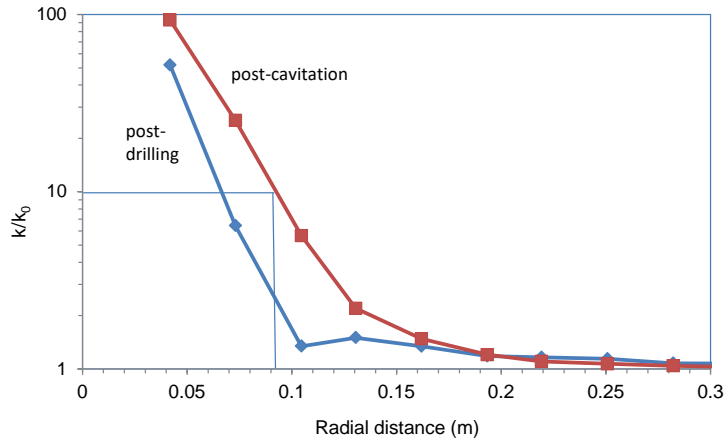


**Figure 2.2.6.16:** Performance of cavitation in terms of permeability enhancement around the borehole.

A parametric study was carried out to determine the influence of coal seam permeability, strength and in situ gas pressure. It was found that the first two parameters have no significant impact on cavitation performance. On the other hand, the simulated stress redistributions for a higher seam pressure (3 MPa) has shown a notable improvement in the post-cavitation permeability enhancement is observed as compared to lower in situ pressure (Figure 2.2.6.16).

Next the in seam (vertical) borehole scenario illustrated in Figures 3.2.6.13b and Figure 2.2.6.14 were evaluated. The resulting stress and corresponding permeability profiles have shown that permeability within a region of 0.7 m radius around the borehole has increased by over one-order of magnitude.

### Cavity completion modelling at JSW

#### *Model domain and boundary conditions*

Here only in-seam horizontal borehole configuration is considered. Cavitation modelling is carried out in a plane perpendicular to the borehole under plane-strain conditions. Figure 2.2.6.17 presents the plane-strain model domains used and associated boundary conditions for the two borehole configurations. As before only half of the domain (45m x 45m) needs to be considered due to symmetry. The borehole has a diameter of 0.1 m. The in situ (total) stress state considered in the modelling is as follows:

- Vertical stress  $\sigma_v = 23$  MPa
- Horizontal stress  $\sigma_x = \sigma_y = 0.7\sigma_v = 16.1$  MPa

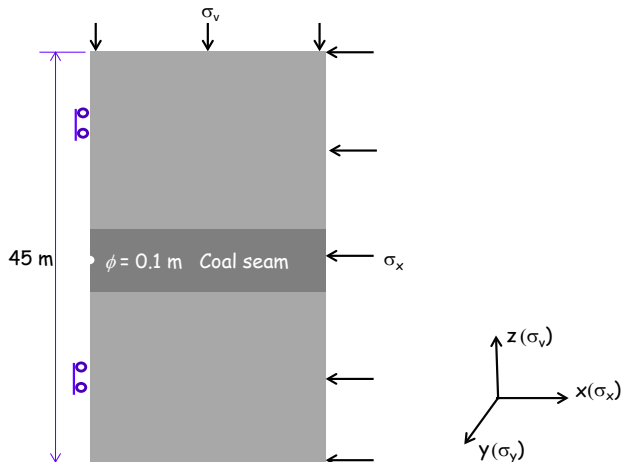


**Figure 2.2.6.17:** Plane-strain model domain and boundary conditions.

The mechanical and elastic properties of the coal used was same as those used for JSW coal in the slotting study.

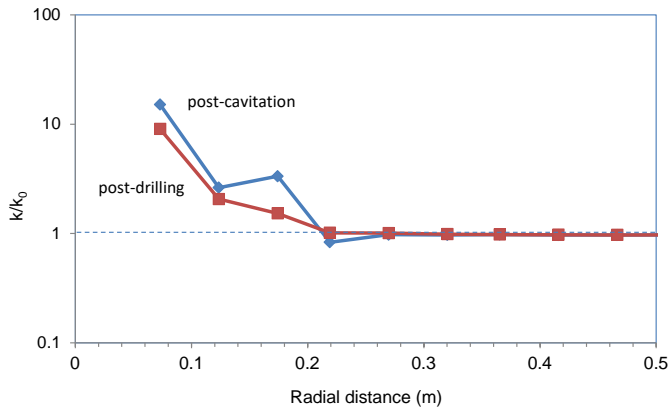


**Figure 2.2.6.18:** Performance of cavitation in terms of permeability enhancement around the borehole at JSW conditions.

#### *Model results at JSW conditions*

Drilling simulations, which enhanced the permeability of the coal seam around the borehole to some extent was followed by the cavitation modelling which assumed that the borehole pressure is reduced at a rate of 0.3 MPa/s to 0.1 MPa from the initial in situ gas pressure of 3 MPa. The modelling results show that rapid depressurisation has resulted in only a marginal enlargement of the shear failure zone over that which was formed by the drilling stage and associated stress redistribution. As illustrated in Figure 2.2.6.18, cavitation has failed to lead to any noticeable improvement in seam permeability in this case.

When compared for the two partner mines' conditions, the cavitation modelling work has shown that rapid depressurisation at borehole would generally cause an enlarged shear failure zone and further stress relief, leading to permeability enhancement around the borehole. However, the modelling results suggest that best performance is likely to be achieved with the horizontal borehole configuration at Hunosa.

#### **SubTask 2.3.4 Numerical simulation of the use of explosives for fracturing coal seams and coal measures rocks (IMPERIAL)**

This SubTask aimed at modelling blasting induced stress wave propagation and the response of coal and rock structures to the induced stresses to define the fracture zones generated. The stress permeability relationships developed in the project, as well as the library of relationships at Imperial College were used to define the resulting fracture permeabilities. A detailed description of the modelling procedure used and results obtained was presented in the Deliverable D2.3 report submitted. Therefore a summary of the research findings is presented here.

#### **Model Set-up and results**

Numerical models to assess stress relief and fracturing induced around blasted boreholes were developed with the dynamic module in FLAC<sup>3D</sup>. As shown Figure 2.2.6.19, the physical dimensions of the model are 10×6×10m (length×width×height) and a cylindrical zone ( $\Phi=1.5$  m) at the centre of the model is refined to accommodate the simulated borehole and blasting zone. Three layers, including the roof sandstone, floor mudstone, and 4 m thick coal seam were assumed in this model, which represents the simplified strata at JSW.

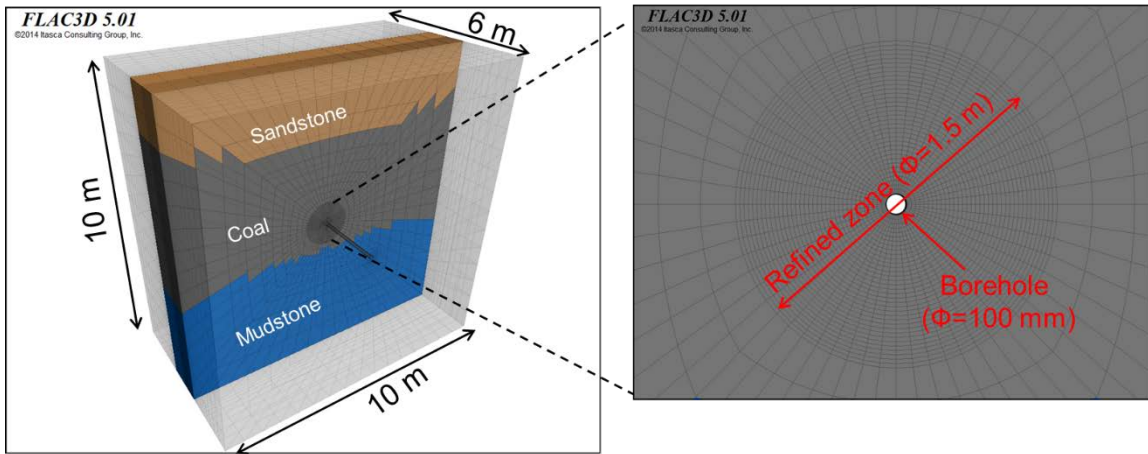


**Figure 2.2.6.19:** Model geometry and the centre refined area.

The preliminary modelling work was carried out under the hydrostatic stress field conditions of 10 MPa. The boundary conditions of the model were such that it is laterally confined and the model base is fixed. Quiet boundaries were used to simulate wave propagation in an infinite field domain. No additional damping was assumed thus all wave attenuation would be caused by plastic deformation of rock/coal.

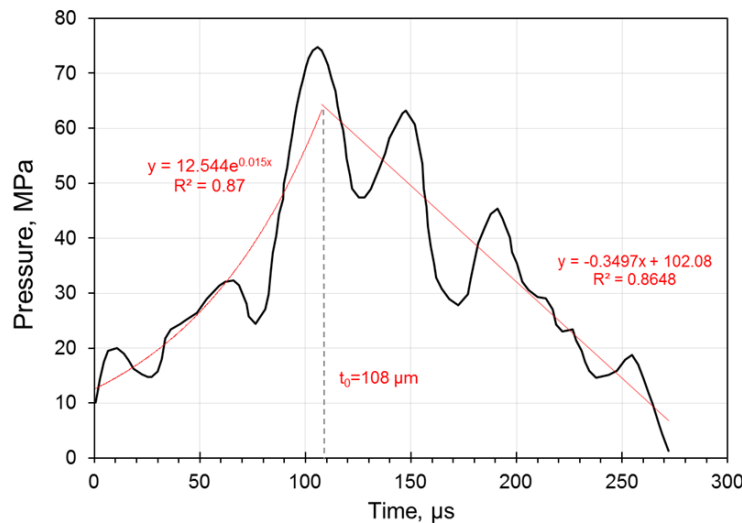


**Figure 2.2.6.20:** Dynamic loading of the stress wave pulse induced by 10g EMULINIT PM blasting experiment at 10 MPa confining pressure from Task 2.2 (data provided by GIG).

In the model, only part of a borehole (6 m long) within the coal seam was simulated, and its diameter is taken as 100 mm. In order to avoid interference between multiple explosives and understand the effect of single charge blasting, the single-explosive model was carried out first to investigate the de-stressed failure zone and stress wave propagation around each blasting point. The blasting process was simulated by applying a period of dynamic stress pulse which has the characteristic of 10 g EMULINIT PM at 10 MP confining pressure (Figure 2.2.6.20). Rock mechanical properties used were the same as those used in the previous SubTasks. The constitutive model used in the initial modelling study was the Mohr-Coulomb model, which provides the lower bound limit for the failure zone size around the borehole. A number of monitoring points around the borehole were organised to evaluate the results (Figure 2.2.6.21).

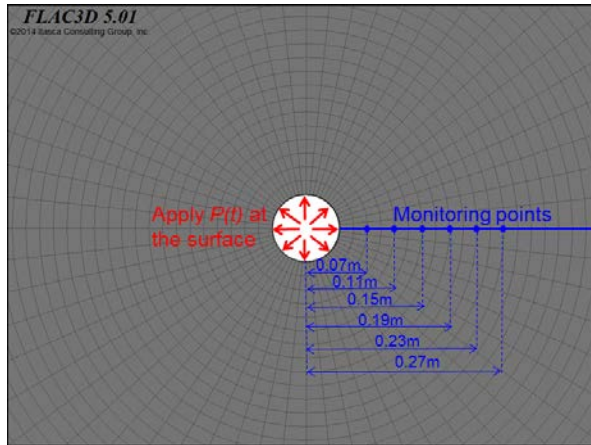


**Figure 2.2.6.21:** Monitoring point locations near the borehole.

Figure 2.2.6.22 shows the velocity response to the applied stress wave pulse created by the explosive. Velocities along the radial direction changed from positive to negative. The peaks of the velocity curves reduce as the monitoring points move further away from the borehole. The surface grids at the wellbore reached the maximum velocity at around 100  $\mu$ s, which is consistent with the peak pressure at  $t_0=108 \mu$ s. At 200  $\mu$ s, grids adjacent to the boreholes started converging inwards while rear grids still propagate outwards, which indicated the oscillation of the velocity field. After 400  $\mu$ s, the velocity vectors decayed significantly and the model developed into the static state.

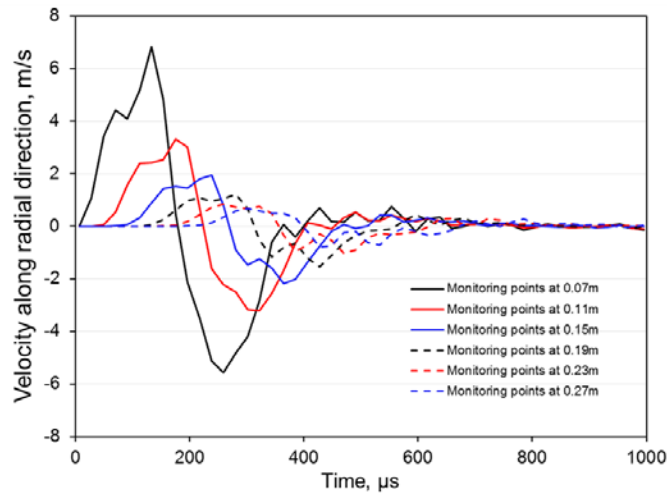


**Figure 2.2.6.22:** Velocity response to the applied stress wave pulse.

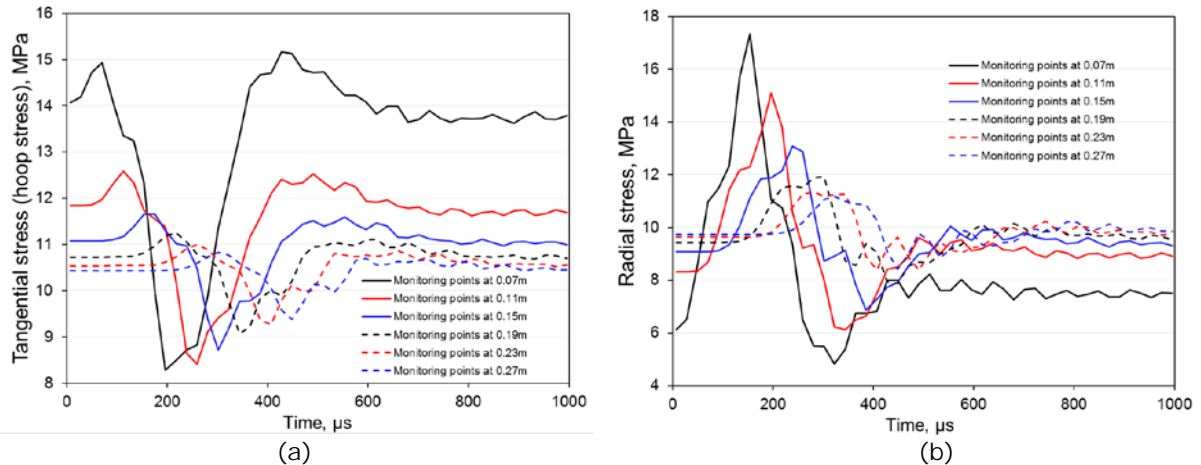


**Figure 2.2.6.23:** Stress respond to the applied stress wave pulse: (a) tangential stress and (b) radial stress.

As the main indication of material failure, tangential and radial stresses at all monitoring points were also plotted (Figure 2.2.6.23). Stress wave propagation can be observed from the regular shifting of peak time in different monitoring points. As suggested by the decreasing magnitude of stress peaks, stress wave also attenuated along the direction of wave propagation.

Figure 2.2.6.24 shows the propagation of tangential stress waves within a 2D cross-section of the blasting point. The propagation and attenuation of these waves can be clearly observed from the evolution of peak stress. For example, during the explosion process, the dark blue circle (at 150 µs) indicated high stress concentration gradually moving away from the borehole and, at the meantime, it enlarged and decayed into a light green circle (400 µs) with much lower stress.

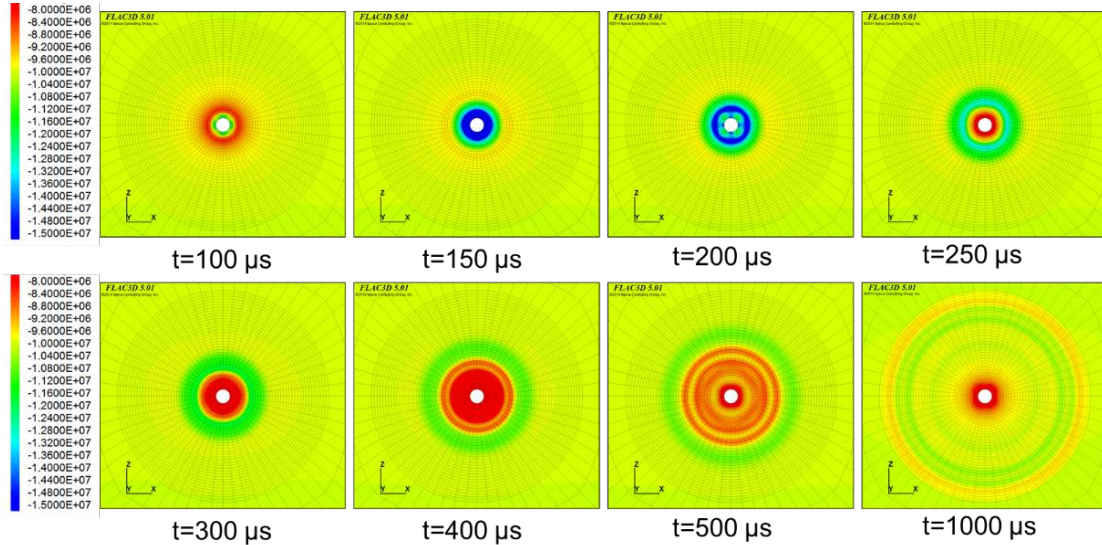
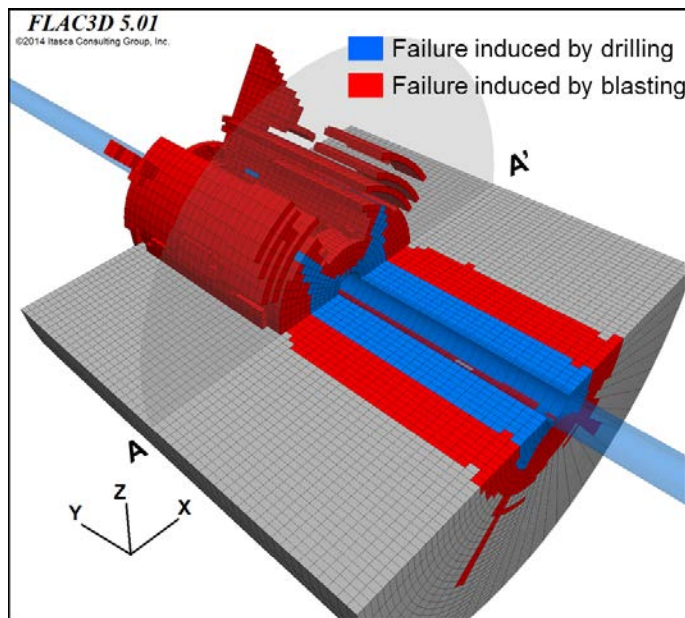


**Figure 2.2.6.24:** Contours showing tangential stress wave propagation during the blast loading period (unit: Pa).

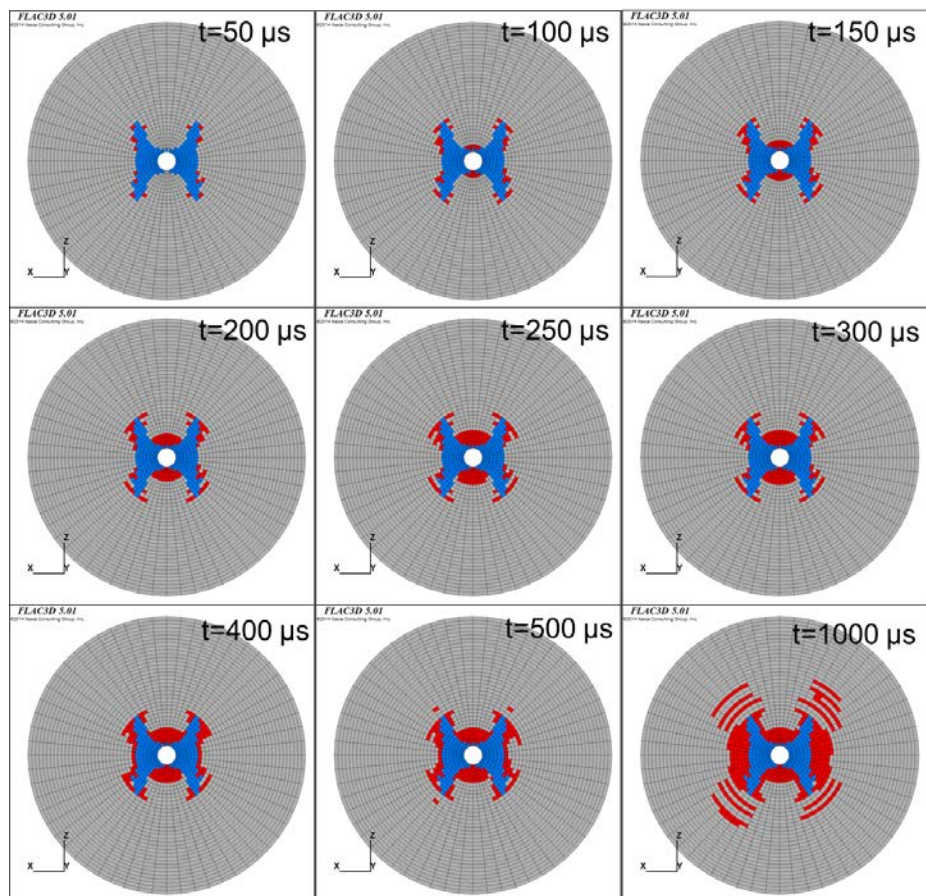
Encouraged by these early modelling results the model was updated to be more closely representing to the field settings. Furthermore, instead of the Mohr-Coulomb (MC) model, the strain softening (SS) model was applied to the coal seam, which can consider the strength weakening with respect to inelastic strain. In addition to the change of constitutive model, the initial stress field was also updated from the hydrostatic stress of 10 MPa to the *in-situ* stress condition of the coal at 990 m depth at JSW.

Figure 2.2.6.25 shows the 3D failure zone distribution 1,000 µs after blasting ignition. The volume percentage of failed coal within the centre refined area was increased from 3.78% after drilling to 13.52% after blasting. Although the blasting ignition only limited to a 0.06 m long section of the borehole, a relatively large range of coal along the borehole direction was fractured due to the propagation of shock wave.

A more clear view showing the propagation of blasting induced failure can be seen in Figure 2.2.6.26, which plots the failure zone at A-A' cross-section (ignition point) during the entire blasting operation. The crushing zone can be observed at the centre of the model and radial failure induced by wave propagation appears further away from the borehole.



**Figure 2.2.6.25:** 3D failure zone distribution 1,000  $\mu\text{s}$  after blasting ignition.



**Figure 2.2.6.26:** Failure zone propagation during the blasting operation.

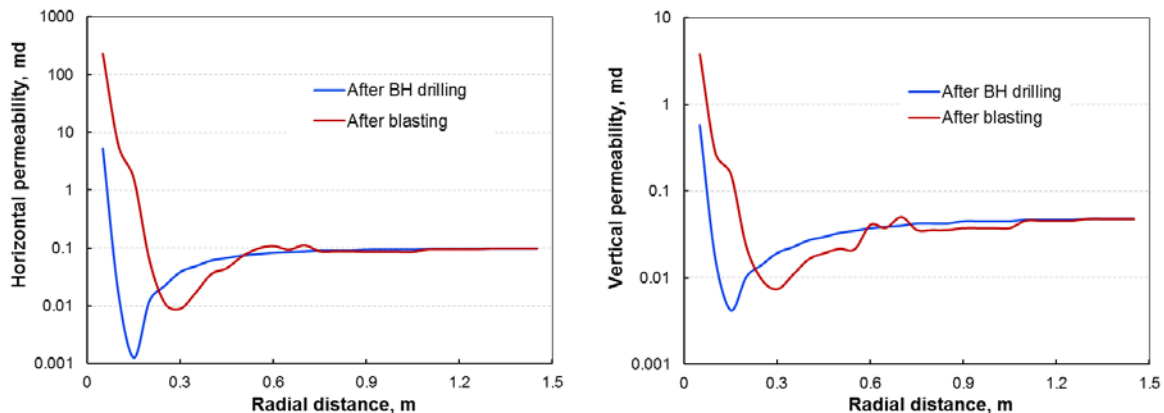


**Figure 2.2.6.27:** Permeability profiles before and after blasting operation.

Using IMPERIAL's stress-permeability relationships, the stress distributions generated by FLAC<sup>3D</sup> were used to calculate the permeability field around boreholes. Since the bedding planes are well-developed along the strike of the coal seam, the initial permeability was assumed to be anisotropic, which is much lower in the direction perpendicular to the coal seam (along z-axis). Thus, the initial permeability was assumed to be 0.1 md in horizontal direction and 0.05 md in the vertical direction. The resulting permeability profiles along the monitoring line are shown in Figure 2.2.6.27. After the blasting operation, the stimulated zone with enhanced permeability ( $k > k_0$ ) is around 0.25 m away from the borehole centre, which is five times the borehole radius.

## 2.2.7. WP2, Task 2.4: Field testing and development borehole stimulation methods (led by GIG, JSW, HUNOSA, AITEMIN)

### Field testing of equipment for hydro slotting and hydrofracturing at JSW

Field tests of the equipment developed for hydro slotting and hydrofracturing under Task 2.1 by GIG is in progress. The main part of the research will be conducted during 2016. So far, after completion of the tool development for hydrofracturing (see Figure 2.2.4.4) initial trials of the equipment were performed together with the constructing company Tech-Trading who have delivered the equipment.

To assure proper and safe performance of further test using high-pressure equipment some training of personnel who will conduct the relevant tests underground has been provided by qualified staff of Tech-Trading as shown in Figures 3.2.7.1 and 3.2.7.2.



**Figure 2.2.7.1:** Training of the use of pumping unit ZPM HDP 172.



**Figure 2.2.7.2:** Training of the use of stabilization-turning unit USO-1.

As part of the field implementation of the tools developed, a slot cutting trial in coal seam was carried out in an underground gallery in Experimental Mine "Barbara" to check the characteristics of the resulting slot and its range (cutting distance). For this purpose, a pattern of boreholes as shown in Figure 2.2.7.3 were prepared. One of these boreholes was used for slot cutting and the remaining three used for monitoring the performance of slot cutting. The nozzle connected with a high-pressure hose and a rotatable head to the pump, which directions the hydraulic fluid inside the borehole was inserted at 5m depth with the help of a rod.

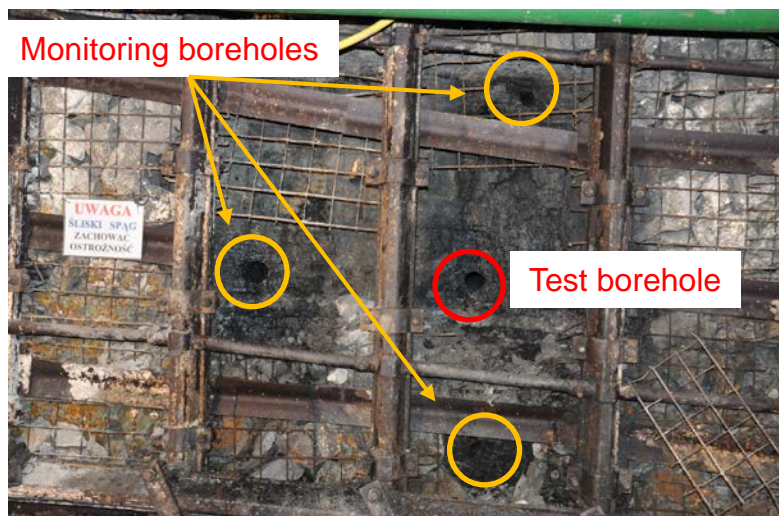


**Figure 2.2.7.3:** Test boreholes used to investigate hydro cutting and hydro slotting technique.

After 3 min 30 sec of slot cutting in the test borehole, the monitoring borehole 0.6 m to the left of the test hole has shown flow of water and steam, the same as observed in test borehole during performing a cut (Figure 2.2.7.4). The steam was produced as a result of heating of the pumped water by friction under high pressure through the nozzle. Thereby, the first confirmation of the range of the hydro slotting achievable using this technique was obtained.

During these underground test some technical problems have also been faced. The most important are:

- 1) uncertainty of range of hydro cutting and
- 2) degradation of nozzle.

To solve both of these problems a new set of nozzles has been ordered and additional tests were performed.



**Figure 2.2.7.4:** Confirmation of hydro slotting range: water and steam flow from the monitoring borehole.

#### **Field testing of borehole stimulation methods at Sueros Colliery**

After conducting the hydraulic characterisation tests described in Task 2.2, the same experimental set-up has been used for carrying out long period injection test, in order to analyse the effect of the hydraulic stimulation method in the seam #8. This task is not yet completed, as it was necessary to stop the water injection after a few days because of a technical problem in the injection pump. The field experiments will be resumed when the pump is repaired. Nevertheless, the experience with these first tests are described in the following sections.

#### ***Hydraulic fracturing tests***

The objective of these tests was to perform a long period injection test at high pressure, in order to achieve the hydraulic connection between the injection borehole S14, and the observation boreholes (S12, S13, or S21), by hydraulic fracturing. The plan was to reach the maximum capacity of the pump (280 bar). However, a number of technical problems appeared with the pump and it was not possible to perform a continuous injection for several days, as it was initially planned. Finally the tests were conducted in three different phases.

In the first test the water pressure was applied in increasing steps (see Figure 2.2.7.5). As water pressure of approximately 120 bar was reached, the pressure dropped suddenly and a peak of water inflow was observed. The pressure then recovered, and the test was continued until 150 bar pressure is reached. At this moment the pump was stopped to observe the pressure drop curve. The test was then continued for about 100 minutes more, and during this time a number of water inflow peaks were also observed. Along this first test, no relevant pressure increase was detected at any of the observation boreholes.

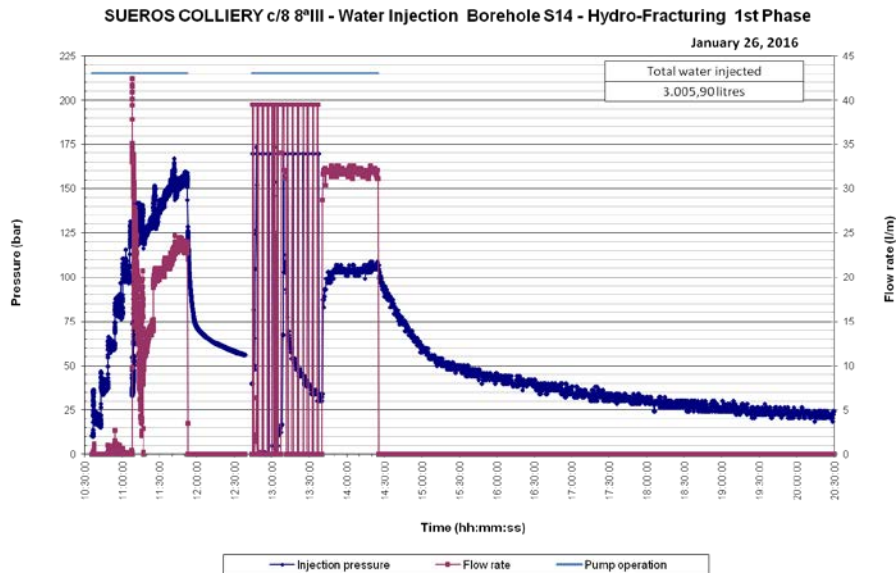


**Figure 2.2.7.5:** Hydrofracturing phase 1.

The second test was carried out several days later, operating the pump from the surface, and starting at a 120 bar pressure (see Figure 2.2.7.6). In this case the duration of the injection phase was about 35 hours, the maximum pressure applied being 177 bar. During this test, an increase in the pressure of borehole S13 was detected, reaching a peak value of 22.8 bar. It is worth to note that S13 cuts the seam at about 40 m away from the injection borehole, whereas no pressure increase was detected in S12, which is located at half the distance (20m, see Figure 3.2.3.16). Therefore, the preferential path for the water flow appears to be in the direction of the virgin area of the panel.

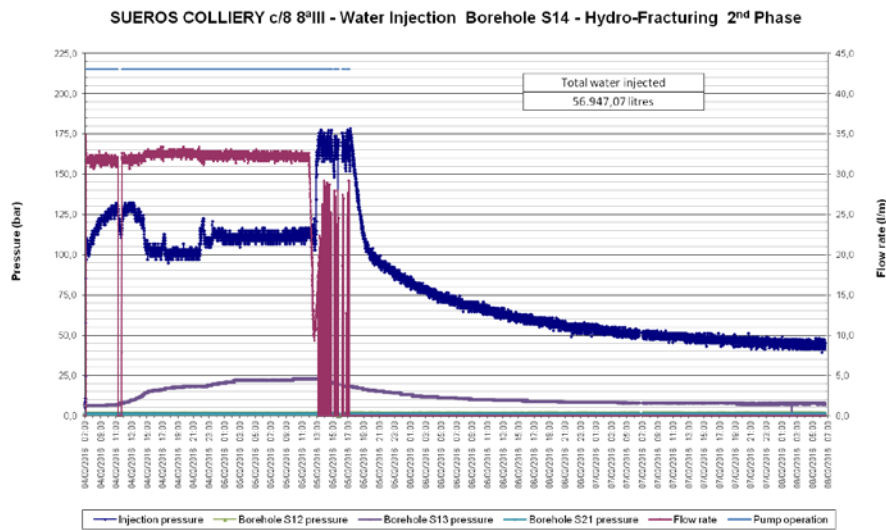


**Figure 2.2.7.6:** Hydrofracturing phase 2.

Phase 3 of the hydrofracturing tests, suffered a number of interruptions due to the above mentioned technical problem with the pump, and also to a shortage in the mains water supply. For this reason the graphics of this phase show a high number of discontinuities. However, the pressure at the observation borehole S13 remained between 7 and 10 bar. Again, no pressure change was observed in the other observation boreholes S12 and S21.

Figure 2.2.7.7 summarises the main results obtained in the hydraulic stimulation tests, as well as the total amount of water injected at these initial field tests at Sueros Colliery. Despite the lack of continuity of the injection, a clear connection was established between the injection borehole S14 and the

observation borehole S13, which is located at a distance of 40 m. On the contrary, no pressure variation has been observed in observation boreholes S12 or S21.

The total amount of water injected during the hydraulic stimulation tests has been 68.2 m<sup>3</sup>, the largest part (57 m<sup>3</sup>) corresponding to the second phase, that is also when the pressure at the observation borehole S13 reached its peak pressure.

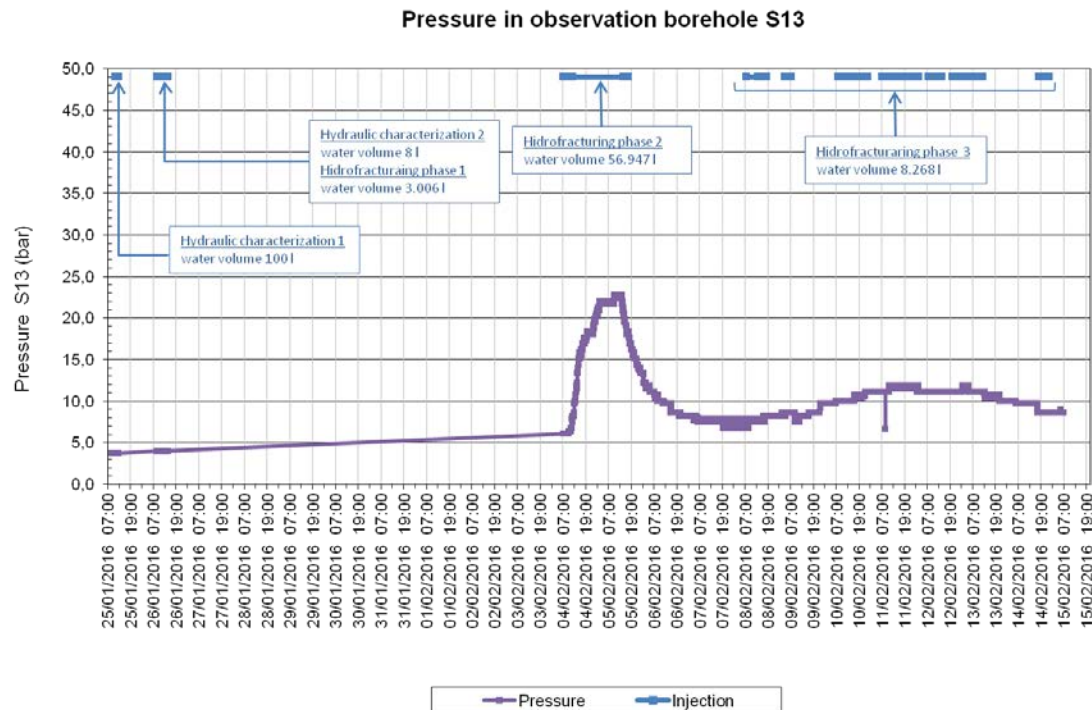


**Figure 2.2.7.7:** Pressure at borehole S13

#### **Conclusions and next steps at Hunosa**

The first series of long period hydraulic stimulation tests have enabled to fine tune the installation, by detecting a number of difficulties that needed to be resolved. Nevertheless, and despite the lack of continuity in the injection, it was possible to initiate the hydraulic connection between the injection borehole and one of the observation boreholes, which intersects the Seam #8 at a distance of 40 m. Surprisingly, no pressure increment has been detected in the other observation borehole which is located at 20 m away. It is too early to make a conclusion from this, however, the preferential flow path for the water appears to be in the direction of the virgin part of the sub-level caving panel.

One of the potential reasons and an explanation for this is the stress abutment formed ahead of the panel face as reported in Deliverable D1.2 report and under Task 3.2 further in this report. The redistribution of the stresses ahead of the production face appear to push the flow of the hydraulic fluid more towards the virgin part of the coal seam. These early observations need to be further investigated and correlate with the numerical modelling data in the next stage of the experiments.

Therefore, the problem detected in regulating valve in the pump is being repaired and it is planned to carry out a test which combines hydraulic stimulation and methane drainage. The plan is to continue with the water injection at S14, and extract methane from the boreholes S12 and S13.

Furthermore, and in order to determine the influence that the hydraulic stimulation method has on the efficiency of the methane drainage process, it will be also necessary to obtain data about the efficiency of the conventional methane drainage in this area (without stimulation). It is therefore planned to conduct a drainage test in another part of the seam, not affected by the current hydraulic stimulation tests, so as to have a baseline for comparison. The location of these new boreholes, identified as S31, S32 and S33, is shown in Figure 2.2.7.8. These boreholes will be located in the deeper in virgin section of the panel, and their relative distance to each other will be the same as S12-S13-S14, in order to make the comparison of the results realistic.

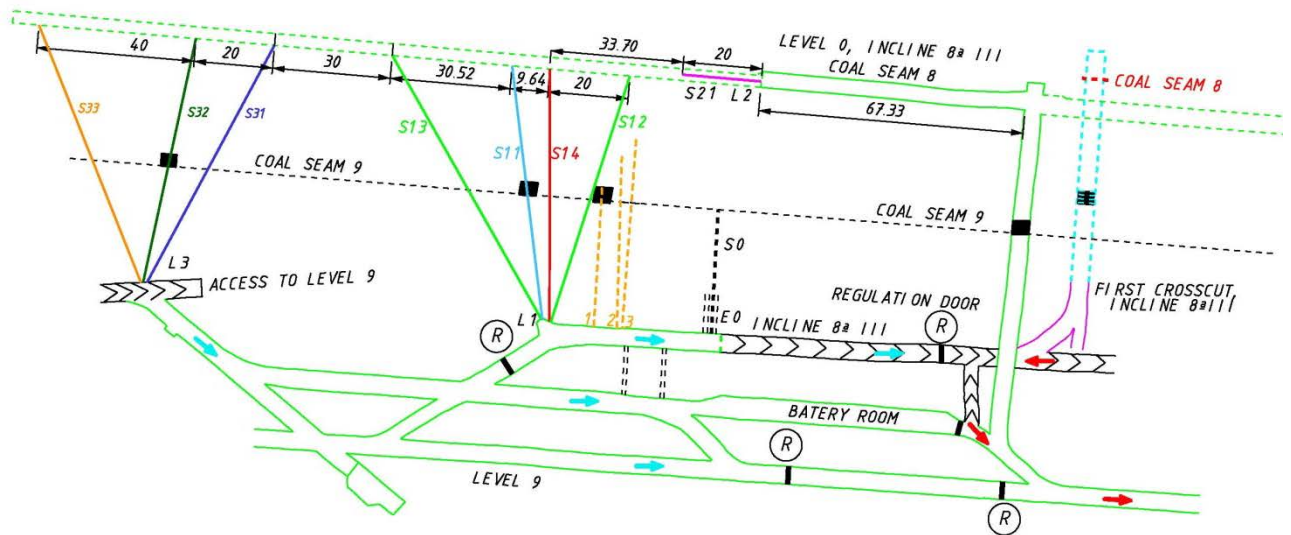


**Figure 2.2.7.8:** Location of the new boreholes S31-S32-S33 planned for the next field tests.

## 2.2.8. WP3, Task 3.1: Numerical modelling of multi-seam mining layouts and gas flow patterns around longwall faces for enhanced methane drainage at JSW mines (led by INIG)

In this task, numerical modelling of geological formations in the area of JSW Zofiówka Colliery was carried out in order to develop improved methane drainage technologies by borehole stimulation. This was achieved in several stages. As a first step, the overall data from different sources (boreholes, rock samples collected in mine) are integrated within a 3D geological model of the area. In the next stage geomechanical modelling work was undertaken to determine stress fields for the initial and disturbed conditions generated by coal production operations. The aim of the final stage of Task 3.1 is to perform dynamic simulations of fluid flow to the boreholes during methane drainage processes.

Several modelling scales are used as the model development proceeds started from a regional model (covering the whole area of Zofiówka coal mine) through to the scale of the selected coal seam being subjected to drainage, and down to the local scale models including stimulated drainage wells.

The numerical modelling tasks were carried out using Schlumberger suite of software packages Petrel, Eclipse and Visage.

### 3D geological model of the Zofiówka Colliery

Geological model of the Zofiówka Colliery was constructed in two modelling scales: a large scale (global) model that covers an entire area of Zofiówka coal mine, while the second - local model - represents only a section of a former one and was constructed for the #412 coal seam within an area where methane drainage is designed. Both models consist of a structural element which defines coal seams and surrounding rocks geometry, as well as 3D distributions of a set of petrophysical properties of coal and rock formations.

The data used in geological model construction included: coal seam maps, well data - lithological profiles of 6 wells, geophysical borehole logging of 2 wells and laboratory measurement results carried out for coal samples collected from an operating longwall within the #412 coal seam. Figure 2.2.8.1 presents data sources used for the development of structural part of the 3D geological model.

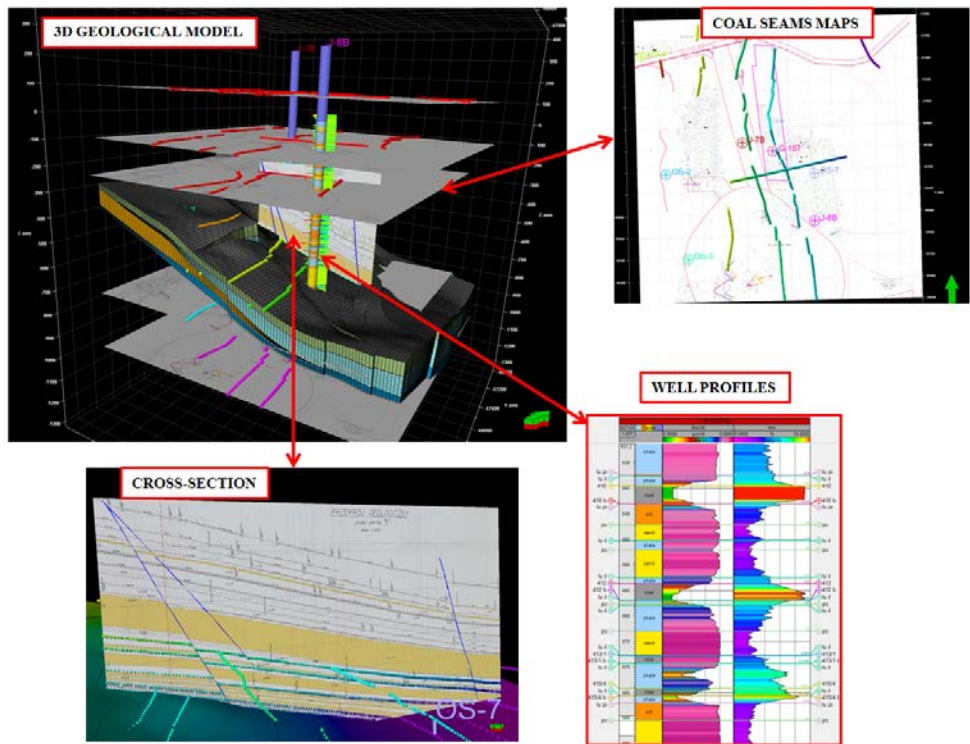


**Figure 2.2.8.1:** Data availability and the development of a structural framework for a 3D geological model of the Zofiówka Colliery.

The geological model for the entire area of Zofiówka coal mine was developed with a grid of lower horizontal resolution equal to  $25 \times 25$  m. Figure 2.2.8.2 show the model developed for the interval between #409/3 - #413/2 coal seams. Most of the property modelling activities were carried out only for the #412 coal seam which is the target for stimulated methane drainage processes, therefore, appropriate reproduction of its geometry was of particular interest for the modelling team (Figure 2.2.8.3).

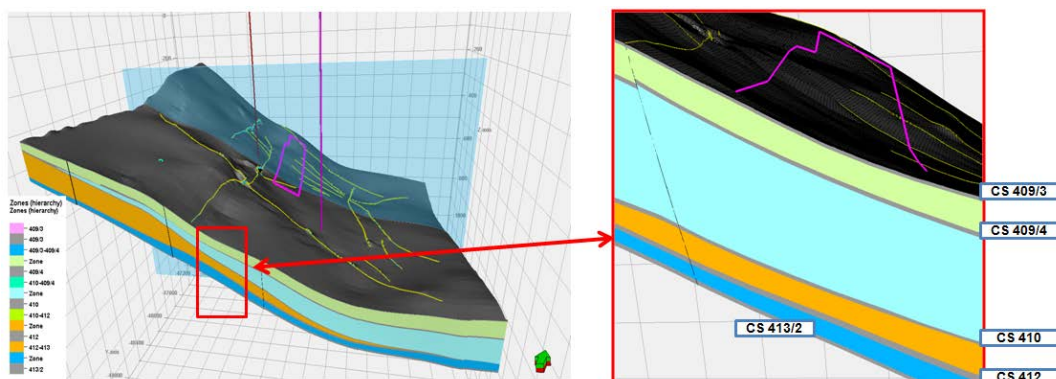


**Figure 2.2.8.2:** Structural model of the interval between #409/3 and #413/2 coal seams

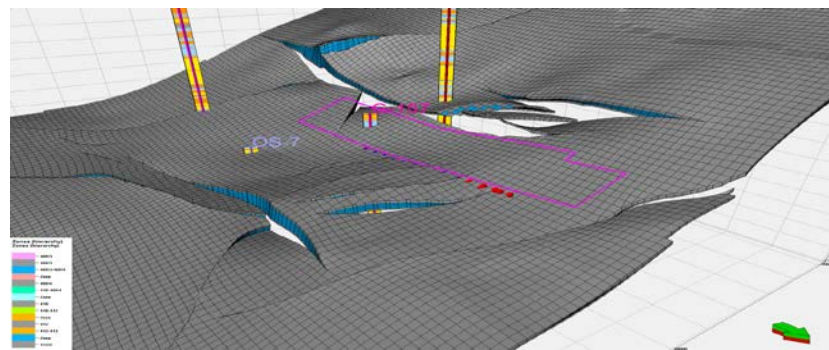


**Figure 2.2.8.3:** Structure of the #412 coal seam with polygon of planned methane drainage activity.

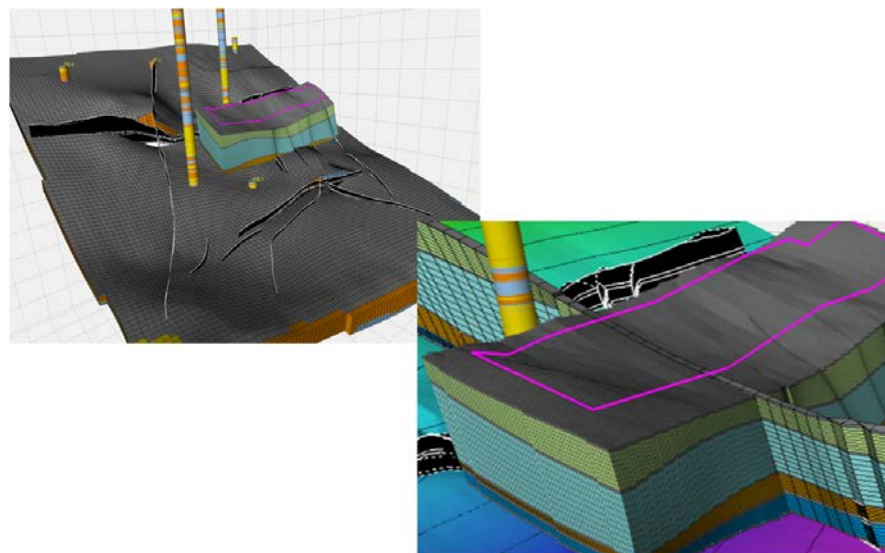


**Figure 2.2.8.4:** Local model of the methane drainage area compared to the extent of the global model.

In order to account for the geomechanical modelling task two additional zones which represent overburden and underburden formations were also added. These were divided into 50 (top) and 20 (bottom) layers. Furthermore, for modelling of the petrophysical properties of the #412 coal seam in a district of the coal mine which will be subjected to methane drainage, a section of detailed structural model was cut out and a horizontal resolution was increased from 25m to 5 m (Figure 2.2.8.4).

#### Petrophysical properties modelling

Petrophysical property modelling was carried out in two different scales: a model covering the geological profile up to the ground level constructed with a horizontal resolution of 25 x 25 m was populated with lithofacies, total porosity and rock density values. For the characterisation of the #412 coal seam within an area of planned methane drainage activity a model with 5 x 5 m horizontal resolution was populated with total and effective porosity values, as well as horizontal and vertical permeability of coal. Figure 2.2.8.5 presents data availability for the petrophysical properties modelling task.

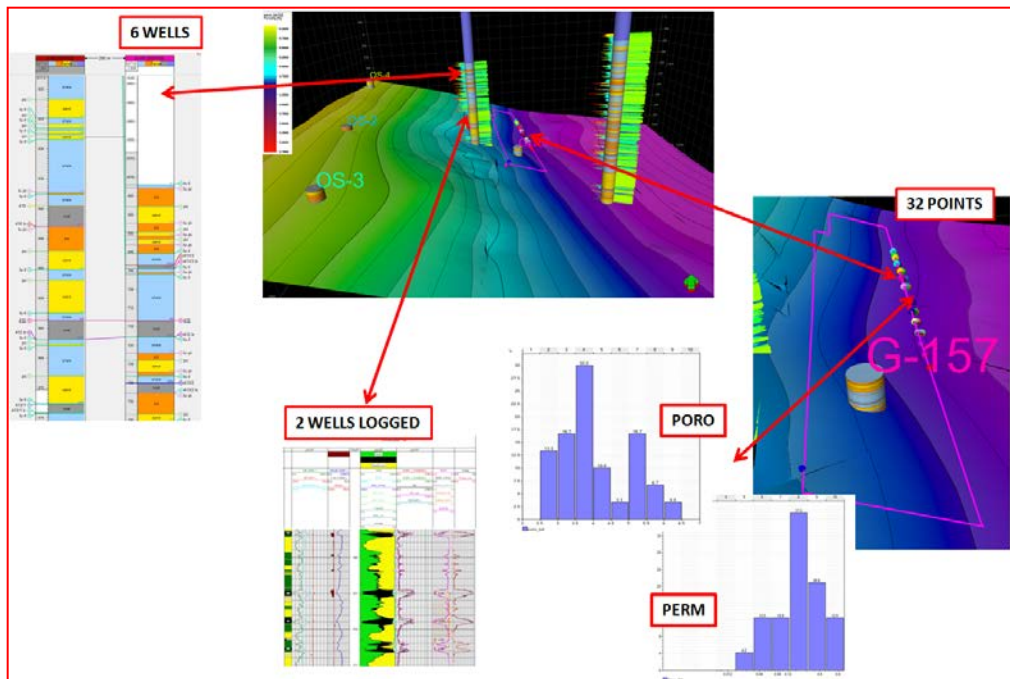


**Figure 2.2.8.5:** Data sets used for the petrophysical modelling.

### Lithofacies model

The 3D distribution of lithofacies was modeled in two steps due to varying availability of well data within interval between CS409/3 - #413/2 for which profiles of 6 wells were present and for overlying formations for which only two wells with lithological profiles were available. The intervals of coal seams: #409/3, 409/4; #410; #412; #413/2 were assigned with coal lithology. Lithological profiles along boreholes were upscaled within the 3D grid and analysed with geostatistical tools in order to define facies proportions and anisotropy for each interval.

### Density and porosity models

The reason for constructing 3D models of rock density and total porosity for entire geological profile was the same as for lithofacies model, i.e.: its usefulness for geomechanical model development. Interpreted borehole profiles of density and porosity, evaluated on the basis of geophysical well logging data (J-7B and J-8B wells), were used as a data source. The same approach as for lithofacies was used for 3D density and porosity modelling.

### Petrophysical models for the #412 coal seam

3D distributions of petrophysical properties within the #412 coal seam were developed on the basis of laboratory measurements of porosity and permeability carried out for coal samples collected from the #412 coal seam in the area where enhanced methane drainage is designed. Point data were upscaled into the 3D grid, analysed with geostatistical tools to define parameters of computation processes leading to 3D distribution of petrophysical properties of the 412 coal seam. For 3D modelling a stochastic algorithm was used which allows to generate multiple equally probable realisations of a property being modeled.

In order to deal with the uncertainty due to limited data, arithmetic average of 25 realisations of porosity was calculated and the results were used in a subsequent stages of the workflow. The results of laboratory measurements of permeability were used to build the permeability models (horizontal and vertical) following the same methodology described for porosity. Figure 2.2.8.6 presents the results of the permeability modelling.

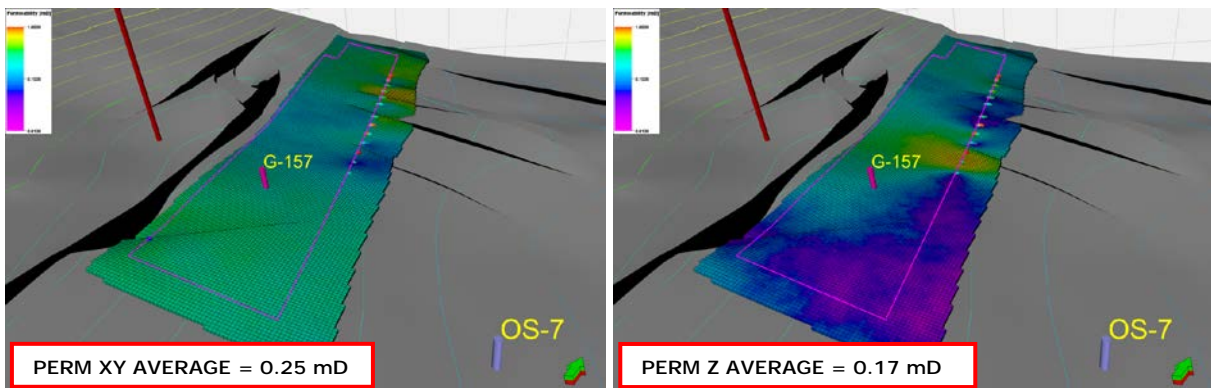


**Figure 2.2.8.6:** The 3D models of permeability (horizontal - above, vertical - below) for the #412 coal seam

#### Gas content

To access the total amount of saturated methane in the coal seam to be produced with stimulated drainage techniques, volumetric calculations were carried out. Following formulae were used (Dallegge and Barker, 2000):

$$GIP = CM_{\text{coal mass}} \times G_{\text{as content}}$$

$$CM_{\text{coal mass}} = Z_{\text{coal zone thickness}} \times A_{\text{rea}} \times D_{\text{ensity}}$$

where GIP is the gas in place, CM is the coal mass and G<sub>as</sub> content is the amount of gas per unit of coal mass. For gas content calculation Langmuir sorption model was applied using laboratory results obtained in WP1:

$$n_{ads} = n_L \frac{p}{P_L + p}$$

where n<sub>ads</sub> is the adsorbed volume of gas, n<sub>L</sub> is the Langmuir volume, P<sub>L</sub> is the Langmuir pressure and p is the reservoir pressure. After correcting the for ash and moisture content, the 3D distribution of methane content for each model grid cell was determined for coal seam #412 (Figure 2.2.8.7).

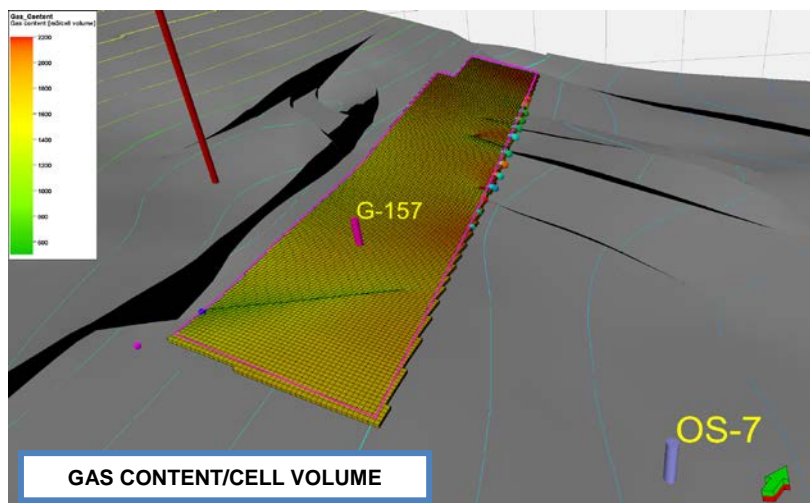


**Figure 2.2.8.7:** Distribution of gas in place calculated for a section of the #412 coal seam.

#### Geomechanical modelling

In the presented study, geomechanical modelling was performed with the use of Petrel Reservoir Geomechanics (RG) platform (Schlumberger) where:

- static model of the reservoir was constructed and
- geomechanical modelling was performed with the use of Petrel RG module with built in **Visage** geomechanical simulator.

Modelling of stresses and mechanical properties of the rock requires information regarding spatial variability of many physical properties of rock formation like petrophysical properties (porosity and density), elastic properties (Young's modulus (E) and Poisson's ratio (PR)) and mechanical properties (Unconfined Compressive Strength (UCS), friction angle (FA), Biot constant, dilation angle (DA)).

The model construction was carried out following a standard workflow and, for the purposes of the borehole stimulation study in the relevant part of the longwall in coal seam #412, a model in the Southern part of the D-2 longwall and extending few meters beyond the D-2 longwall and roadways was extracted from the larger scale geomechanical model developed. Geometry of the models is presented in Figure 2.2.8.8.

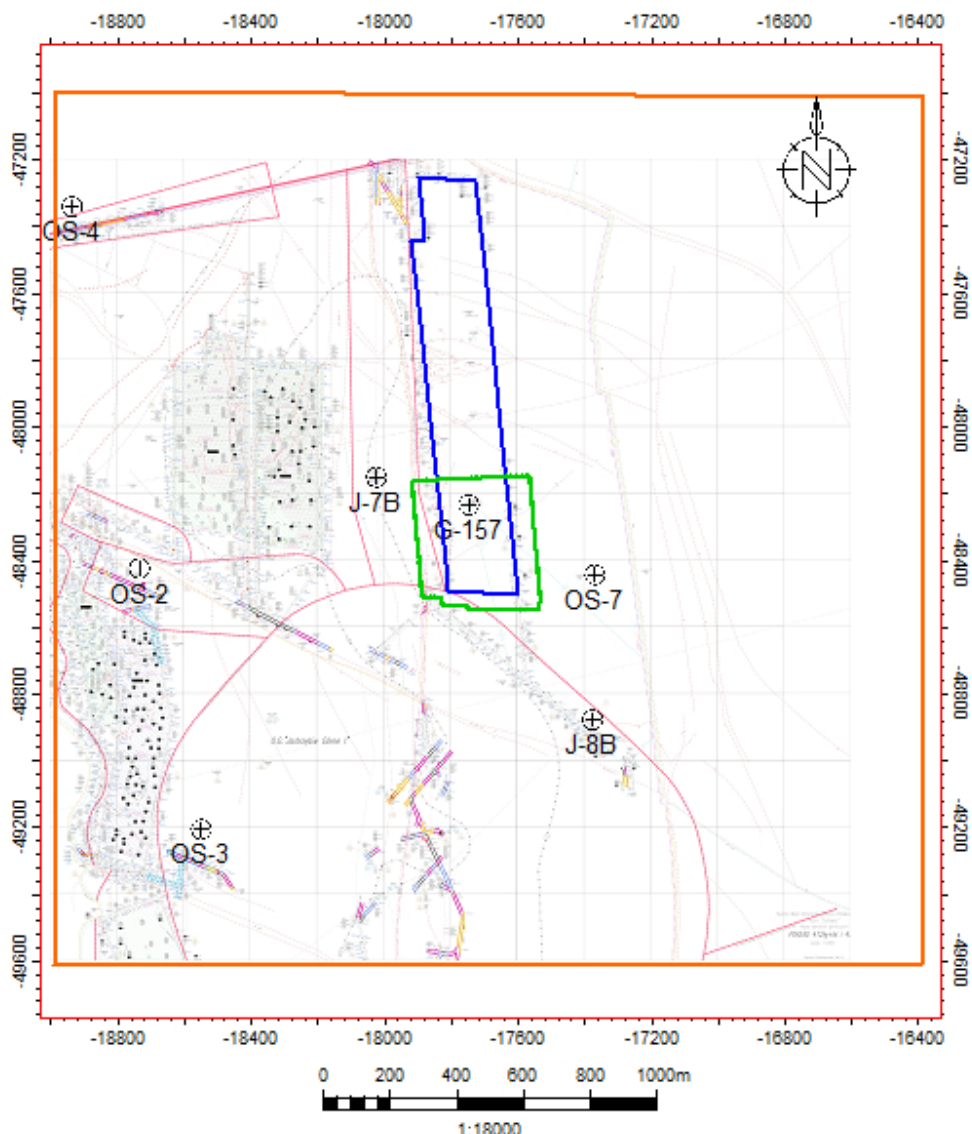


**Figure 2.2.8.8:** Structural map of the bottom of the #412 coal seam presenting the modelling object: the model of reservoir scale (orange boundary), model capturing part of D-2 longwall (green boundary) and the D-2 longwall (blue boundary) subjected to coal seam stimulation treatment.

Horizontal resolution of the model developed varied from 3 m to 0.005 m in the vicinity of the fracture and wellbore. Vertical resolution of the model representing Southern part of D-2 longwall also varied from tens of meters in the overburden part to 0.005 m in the #412 coal seam, where high resolution was required to build detailed elements like stimulated horizontal borehole or further effects of stimulation treatment (fractures, cavities, etc.).

Based on the geological documentation, well logs and point datasets were created with lithotype log, bulk density, porosity, Young's modulus (E) and Unconfined Compressive Strength (UCS) log. Other

properties crucial for geomechanical modelling such as: Poisson's ratio, friction angle and dilatation angle were assumed based on the available literature (Wang et al., 2007; Jienan et al., 2013; Si et al., 2015).

Parametric models representing 3D distributions of elastic and mechanical parameters were driven by evaluated facies (lithotypes) model (see section about lithofacies model). Due to data limitation, values of Poisson's ratio and friction angle were taken from the literature (Si et al., 2015) and Imperial College partners' advice (Table 2.2.8.1). Young's modulus and Unconfined Compressive Strength were evaluated from 54 and 159 laboratory measurements carried out on samples of different lithology and location in Zofiówka Colliery respectively. Other mechanical properties required for geomechanical modelling were assumed according to the literature and are presented in tables below (Table 2.2.8.2).

**Table 2.2.8.1:** The set of parameters of the rock materials occurring in the Zofiówka Colliery necessary in further simulation workflow assigned from available or assumed data.

Parameter [unit] (range of value)	Layer of the model	Coal	Sandstone	Cleyey shale	Sandy shale	Goaf
Poisson's ratio (v) (0-1.0)		0.27	0.11	0.34	0.31	0.27
Young modulus (E) [GPa]	3D model	3D model	3D model	3D model	3D model	3D model
Friction angle ( $\phi$ ) [ $^{\circ}$ ]	22	30	25	26	30	
Dilatation Angle [ $^{\circ}$ ]	0	0	0	0	0	
Bulk density [g/cm <sup>3</sup> ]	3D model	3D model	3D model	3D model	3D model	1.3
Unconfined Compressive Strength (UCS) [MPa]	3D model	3D model	3D model	3D model	3D model	3D model
Porosity [%]	3D model	3D model	3D model	3D model	3D model	30
Biot constant (0-1.0)	1	1	1	1	1	1

Note: 3D model – the model is based on laboratory data and well log interpretation.

**Table 2.2.8.2:** The set of parameters of rock materials representing the Zofiówka Colliery necessary in further simulation workflow assigned from available or assumed data.

Parameter [unit] (range of value)	Layer of the model	Overburden (clay, silts, gravels)	Sideburden (sandstone)	Underburden (sandy shales)
Poisson's ratio (v) (0-1.0)	3D model	0.11	0.34	
Young modulus (E) [GPa]	3D model	20	3.5	
Friction angle ( $\phi$ ) [ $^{\circ}$ ]	3D model	30	25	
Dilatation Angle [ $^{\circ}$ ]	0	0	0	
Bulk density [g/cm <sup>3</sup> ]	3D model	2.7	2.65	
Unconfined Compressive Strength (UCS) [MPa]	3D model	90	40	
Porosity [%]	3D model	12	11	
Biot constant (0-1.0)	1	1	1	

Note: 3D model – the model is based on laboratory data and well log interpretation.

#### Pore pressure and boundary conditions

To obtain the distribution of effective stresses acting on rocks in the Zofiówka Colliery, the pore pressure ( $P_p$ ) populated in the grid from the  $P_p$  gradient was used in the geomechanical modelling. The distribution of pore pressure was calculated from assumed gradient (0.012 MPa/m), the common gradient determined in many coal mines in Great Britain and Germany (Mark and Gadde, 2008). For modelling of stimulation treatment in the #412 coal seam, distribution of pore pressure from the model of reservoir scale was used and the pore pressure property upscaled into the local model of smaller grid.

The model assumed for the simulation purposes corresponds to the normal stress regime. In such state of stresses, which is the most common tectonic regime occurring in the real geological media, among three principal stresses, the lithostatic stress ( $\sigma_v$ ) is dominant and perpendicular to the orientation of the maximum ( $\sigma_H$ ) and minimum ( $\sigma_H$ ) horizontal stresses. The maximum horizontal stress ( $\sigma_H$ ) gradient was determined based on literature to be 0.018 MPa/m (Mark and Gadde, 2008), while the ratio between the maximum and minimum horizontal stresses was set to unity to reflect the simple conditions with

horizontal isotropy. Parameters describing boundary conditions of the model are presented in Table 2.2.8.3.

**Table 2.2.8.3:** Parameters describing initial stress conditions in the model.

Gradient $\sigma_H$	0.018 [MPa/m]
$\sigma_H / \sigma_h$ ratio	1
Azimuth $\sigma_H [^\circ]$	20

Due to long computational times, geomechanical modelling was carried out assuming linear elastic behaviour, and not taking into account plastic (non-linear) behaviour of the modeled rock.

#### Simulation results

As a result of geomechanical modelling, distribution of principal total and effective stresses, together with strains of the rock material being modeled were calculated. Apart from the mentioned parameters, failure mode indicating areas, where rock strength was exceeded and failure occurred were obtained. According to the determined conditions in the area of the study in the reservoir scale, a compressive stress regime (where  $\sigma_v > \sigma_H \geq \sigma_h$ ) can be observed. In this particular case, the isotropy between both maximum and minimum horizontal stresses were assumed, therefore the relation between principal stresses follows:  $\sigma_v > \sigma_H = \sigma_h$ .

On the top surface of the #412 coal seam, in the shallower part, the direction of maximum horizontal stress changes from NE-SW in the northern part to NW-SE in the southern part, while in the part of deeper-laying coal in the #412 coal seam the maximum horizontal stress exhibits longitudinal direction. In the centre of the modeled object, where the stimulation treatment is planned within the D-2 longwall, the maximum horizontal stress assumes NNE-SSW orientation while in the southern part it rotates towards N-S (Figure 2.2.8.9). Direction of maximum horizontal stress should be considered during design of horizontal stimulation boreholes trajectories. Optimal orientation of stimulated horizontal boreholes is perpendicular to the direction of maximum horizontal stress.

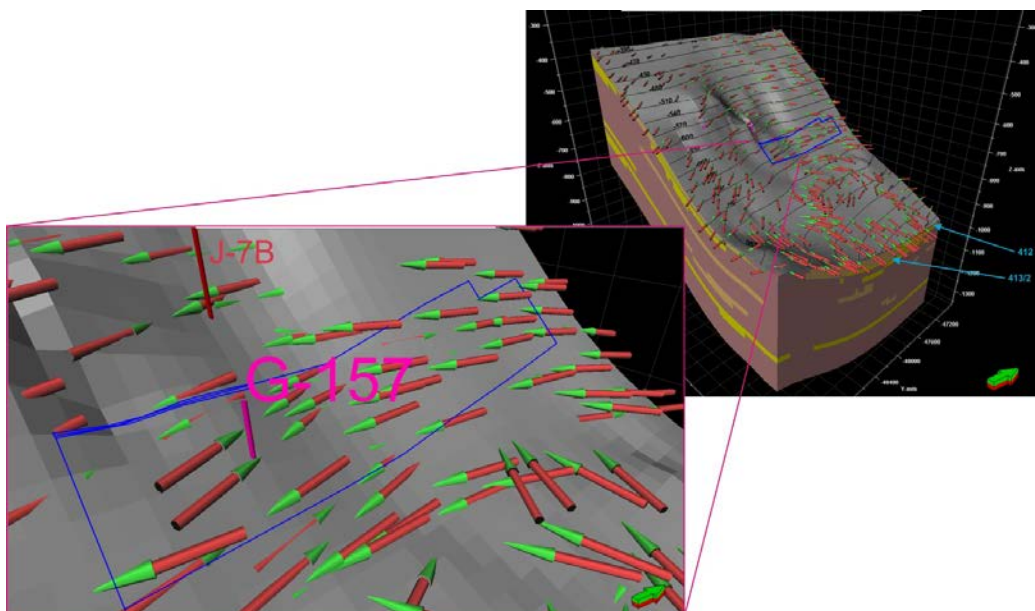


**Figure 2.2.8.9:** Distribution of the effective maximum horizontal stresses ( $\sigma_H$ ) acting on the #412 coal seam in Zofiówka Colliery. The polygon coloured in blue marks the boundary of the D-2 longwall.

The effective vertical stress around the roadways and the stimulated borehole wall were approximately 25 MPa and 33 MPa respectively. The magnitude of effective vertical stress on #412 coal seam within the D-2 longwall was around 8-9 MPa with a local decrease to 7.5 MPa in the South-eastern zone of D-2 longwall, due to coal excavation in the neighbouring #410 coal seam above the #412 coal seam (Figure 2.2.8.10).

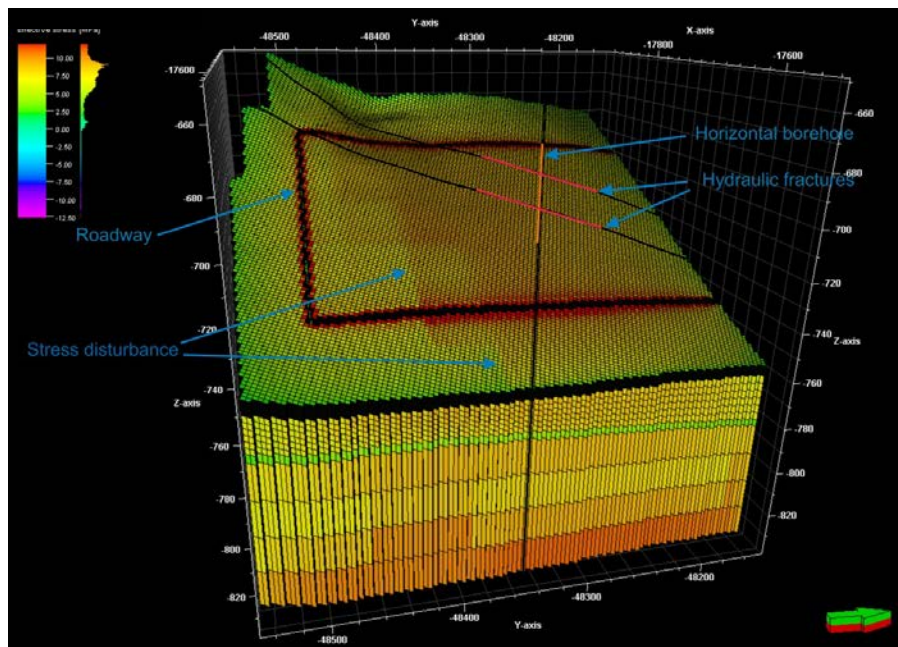


**Figure 2.2.8.10:** 3D distribution of effective vertical stress in the model representing part of the D-2 longwall showing the location of the stimulated horizontal borehole and planes of 2 hydraulic fractures.

### Dynamic modelling

The ultimate purpose of the numerical modelling of coal seams performed in the reported studies is to simulate the enhanced methane drainage processes by various well stimulation techniques. To this aim, the dynamic models of the methane release and flow from the coal matrix to the stimulated zone and further to the boreholes are constructed and the relevant processes are simulated using the models.

This section of the report presents the preliminary stage of the dynamic modelling carried out under the specific conditions of Zofiówka Colliery. The workflow used for this purpose is as follows:

1. Construction of high resolution geological and geomechanical models of the selected coal seam drained with the boreholes stimulated using various techniques (hydraulic fractures, water jet slots, etc.).
2. Simulation of the geomechanical effects of the stimulation processes to obtain the local redistribution of geomechanical stresses and strain.
3. Estimation of the changes in transport properties of the coal seam due to geomechanical effects of the stimulation processes.
4. Performance of the dynamic simulation of the methane desorption and flow into stimulated boreholes.
5. Comparison of drainage process effectiveness for various stimulation techniques and the assessment of the additional factors (proximity of longwall and presence of roadways) that may influence the drainage processes.

The following transport property changes due to the redistribution of geomechanical parameters are taken into account: (1) coal effective permeability, (2) diffusion time for methane desorbed from the coal matrix and diffused to the cleat system.

Two distinct zones of geomechanical effects are considered: (1) intact coal zone with continuous changes of stress and strain redistribution, (2) coal failure zone identified by the failure index resulting from geomechanical modelling.

In the intact coal zone the permeability modifications are calculated according to the Kozeny Carman model (manual of Petrel Reservoir Geomechanics, 2014.1) as a function of the volumetric strain variations due to the presence of the borehole and stimulation regions:

$$\phi = \phi_0 + \Delta\phi$$

$$\Delta\phi = \alpha\Delta\epsilon_v$$

$$K_i = K_{0i} \frac{\phi_0^3 / (1 - \phi_0)^2}{\phi^3 / (1 - \phi)^2}$$

where:

$K_i$  = modified permeability in  $i^{th}$  main direction

$K_{0i}$  = initial permeability in  $i^{th}$  main direction

$\phi$  = modified porosity

$\phi_0$  = initial porosity

$\Delta\phi$  = change in porosity

$\Delta\epsilon_v$  = change in volumetric strain

$\alpha$  = Biot's coefficient

In the failure zone the permeability modifications were calculated according to the Shi and Durucan model (Shi and Durucan, 2005) as a function of the diagonal stress components:

$$K_i = K_{0i} e^{-c \sum_{j=1}^3 \Delta\sigma_j (1 - \delta_{ij})}$$

where:

$K_i$  = modified permeability in  $i^{th}$  main direction

$K_{0i}$  = initial permeability in  $i^{th}$  main direction

$c$  = permeability compressibility

$\Delta\sigma_j$  = change in effective stress in  $j^{th}$  main direction

$\delta_{ij}$  = Kronecker delta

The preliminary modelling was carried out using two vertical hydro-fractures of 5 mm thickness, 50 m half-length, from a 100 long horizontal borehole with a diameter of 150 mm. Both propped and unpropped hydrofractures were modelled. The propped fractures assumed zero strain boundary conditions while unpropped fractures assumed zero stress boundary conditions. Figure 2.2.8.11 presents the permeability distributions calculated using the above relationships for a hydro-fractured wellbore.

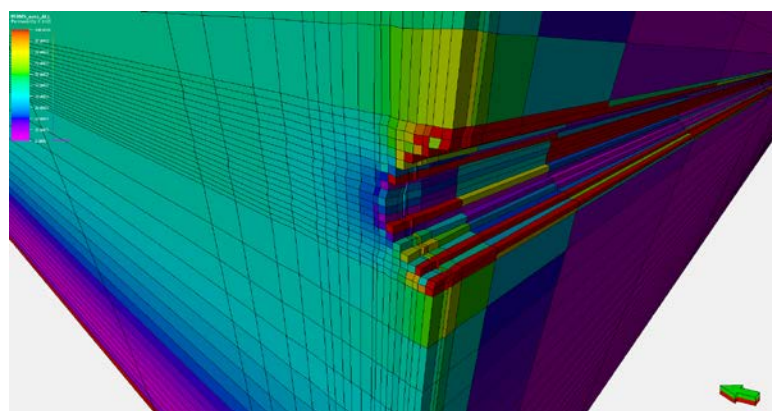


**Figure 2.2.8.11:** Permeability distribution along a wellbore and in the vicinity of a hydro-fracture – detailed vertical cross section of high resolution model.

The results of methane production rates from an unstimulated and stimulated wellbore with two hydro-fractures are presented in Figure 2.2.8.12.

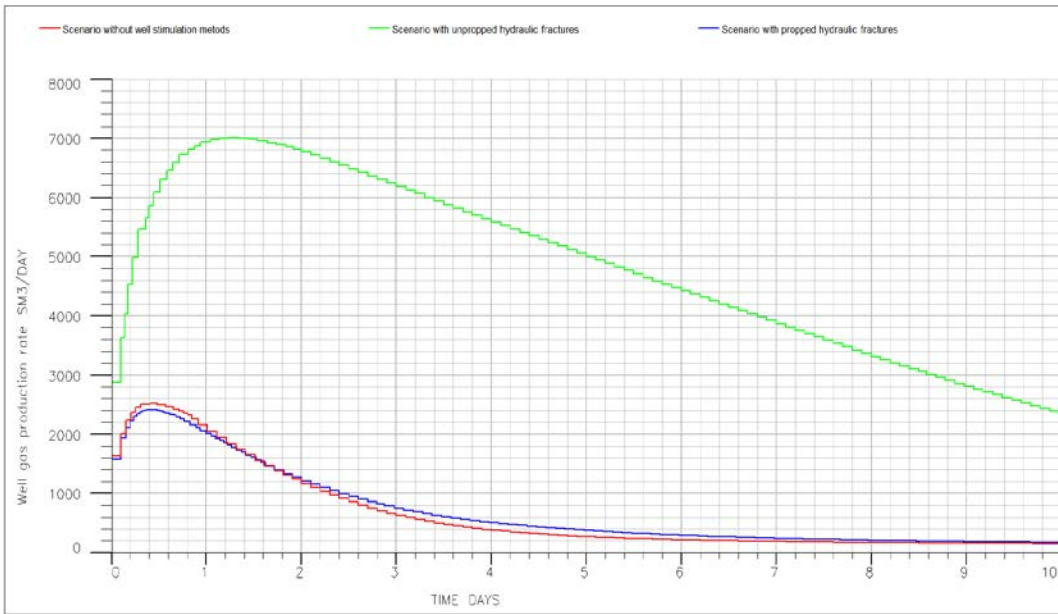


**Figure 2.2.8.12:** Variation of methane production rate with time in stimulated and unstimulated wellbores.

As can be seen from these preliminary modelling results, the effect of borehole stimulation by hydro-fracturing depends strongly on the type of the fractures and the boundary conditions set. In the case of the unpropped fractures (zero stress boundary condition) a significant enhancement of methane drainage is obtained as opposed to the propped fracture case with a zero strain boundary condition.

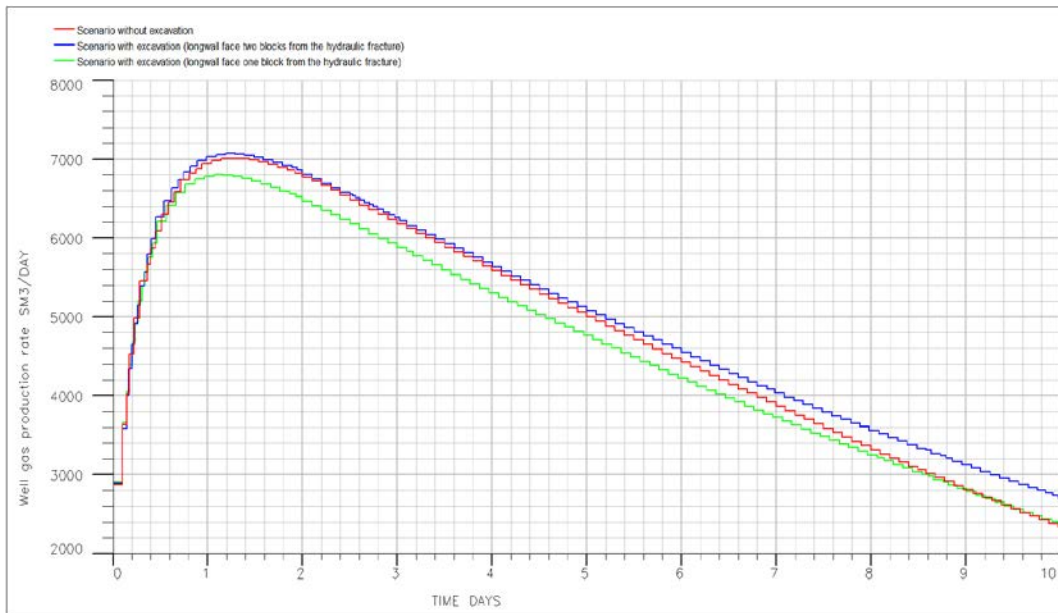


**Figure 2.2.8.13:** Variation of methane production rate with time: effects of longwall face proximity.

The effects of longwall face distance on methane drainage efficiency by a stimulated borehole were also investigated studied for various locations of the longwall with respect to the drainage borehole stimulated with two hydro-fractures. Three cases of the longwall locations were considered: (1) distant location, (2) two blocks (6 m) from the nearest point of the hydro-fracture, (3) one block (3 m) from the nearest point of the hydro-fracture. The simulation results of the methane drainage rate for the above three cases are shown in Figure 2.2.8.13. A relatively limited influence of the longwall proximity on the drainage rate was observed in this study.

## 2.2.9. WP3, Task 3.2: Numerical modelling of sub-level caving mining layouts and gas flow patterns around development headings and production faces for enhanced methane drainage (led by IMPERIAL)

This task aimed at applying field sub-level caving layouts from the Sueros Colliery at Hunosa, where the GasDrain field experiments are carried out, and built numerical models to implement coupled flow-geomechanical modelling to evaluate the performance of enhanced pre-drainage and drainage of gas from the panels that are both being developed and in production. The results of this task will help the design and implementation of the stimulation techniques at field scale in WP4. Following the work presented in Task 2.3, where numerical models were developed to assess the performance of individual stimulated boreholes, a group of drainage boreholes and their stimulation using slot cutting at field scale sub-level caving panels were investigated.

### Geomechanical modelling of sub-level caving layouts at Sueros Colliery

Gas flow patterns and gas drainage behaviour during sub-level caving operations is largely controlled by coal permeability, which is very sensitive to stress changes due to coal extraction. In order to assess drainage performance before and after stimulation, the influence of mining operations in the upper levels, and how the stress field responds to these in the lower levels, need to be considered.

Therefore, first a numerical model to assess stress redistribution induced by sublevel caving at the Sueros Colliery was developed in FLAC<sup>3D</sup>. As shown in Figure 2.2.9.1, the physical dimensions of the model are 132.5×100×100 m (length×width×height), which includes both #8 and #9 coal seams at Sueros Colliery. The thickness of the #8 and #9 coal seams were assumed to be 5 m and 3 m respectively, and both of these seams are dipping at 72°.

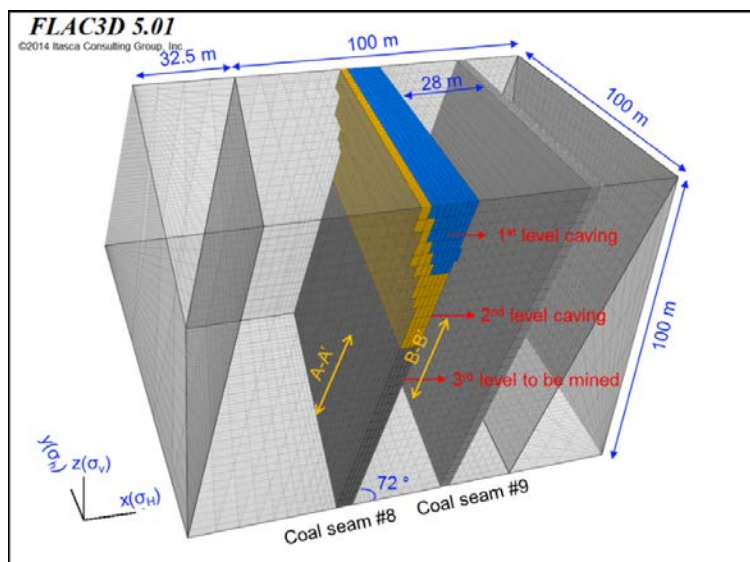


**Figure 2.2.9.1:** Model geometry for geomechanical simulations (after the 2<sup>nd</sup> level caving).

The model domain was assumed to be at a depth from 500 to 600 m. It has been determined that, at around 500 m, the maximum principal stress, intermediate principal stress, and minimum principal stress are 22.4 MPa, 14.4 MPa, and 11.9 MPa, respectively. The minimum principal stress is believed to be in the vertical direction. Considering the geological origin of the steeply dipping coal seams at Hunosa, the maximum principal stress was assumed to be along the x-axis, which is in the horizontal plane, and perpendicular to the strike of the coal seam. The boundary conditions of the model were such that it is laterally confined and the model base is fixed.

**Table 2.2.9.1:** Rock mechanical and strength properties of coal at Sueros Colliery, Hunosa.

Layer	Model	K (GPa)	G (GPa)	φ (°)	C (MPa)	C <sub>r</sub> (MPa)	ε <sub>b</sub>	t (MPa)
Coal	SS	1.26	0.60	22	2.80	0.84	0.001	-0.40
Rock	Elastic	62.9	12.1	--	--	--	--	--
Goaf	Elastic	0.38	0.18	--	--	--	--	--

As stated in Task 2.3, coal at Hunosa was found to be extremely brittle, which has very low strength and has proved to be difficult to core and test in the laboratory. Therefore, the strain softening (SS) model was applied, which can consider the strength weakening with respect to inelastic strain. Rock

mechanical properties used in the geomechanical modelling are summarised in Table 2.2.9.1. In the SS model assumed here, cohesion ( $C$ ) would be reduced to residual cohesion ( $C_r=0.3C$ ) when the plastic shear strain exceeds  $\epsilon_p$ .

### Stress response of sub-level layouts to caving

As shown in Figure 2.2.9.1, the sub-level caving operation extends downwards from the 1st to the 3rd mining level (later to the subsequent levels as mining continues over the years), and the height of each level is 20 m, including a 5 m high inseam development heading. After initial stress equilibrium, roadway development at the 1st mining level was first simulated. Based on this stress field, coal caving at the 1st level was modelled by removing the coal blocks from the model grid, together with the hanging wall rock which would collapse naturally after coal caving. This was followed by backfilling the empty volume with blocks that are assigned with the properties of a recompacted goaf material. The same procedure was repeated for the 2nd level sub-level caving.

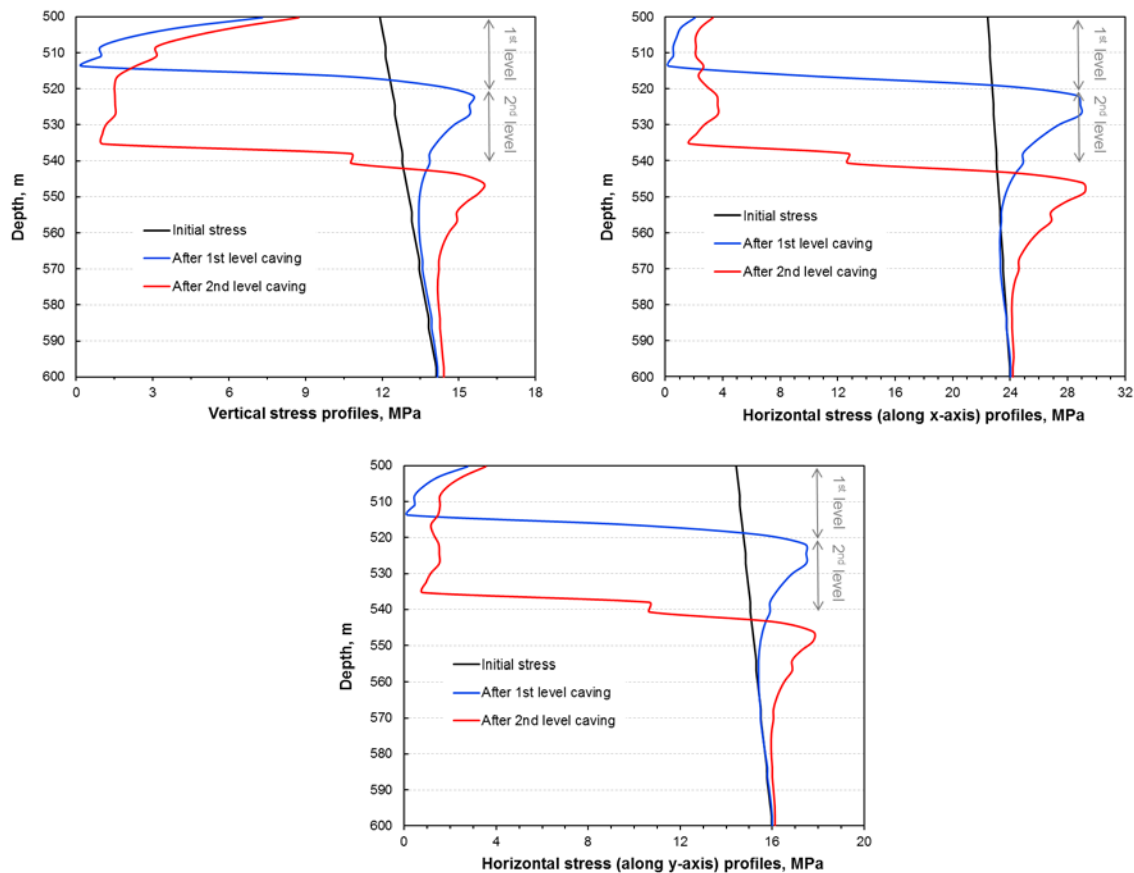


**Figure 2.2.9.2:** Stress changes in #8 coal seam during sub-level caving.

Stress profiles in #8 coal seam along the A-A' direction (as marked in Figure 3.2.9.1) are plotted in Figure 2.2.9.2. As can be seen, coal extraction activities at the current mining level can result in a notable stress abutment in the next level and, among all three principal stresses, the maximum principal stress shows the largest increase in response to the upper level's coal extraction. It is believed that the increased stress may effectively hinder gas migrating from lower levels into the mining level, and it may not favour of gas drainage performance if there is any borehole targeting at capturing gas from the lower levels.

Stress profiles in #9 coal seam along B-B' direction (as marked in Figure 2.2.9.1) are plotted in Figure 2.2.9.3. Unlike the #8 coal seam, which mainly experienced stress concentration, stress response at #9 coal seam to the sub-level caving of #8 coal seam was dominated by dramatic stress relief. This stress relief zone developed up to 30~40 m deeper than the current mining horizon at #8 coal seam. Gas drainage boreholes deployed in this stress relief zone would be largely enhanced to capture the gas at #9 coal seam, prior to the start of mining activities in there should this seam be mined as well.

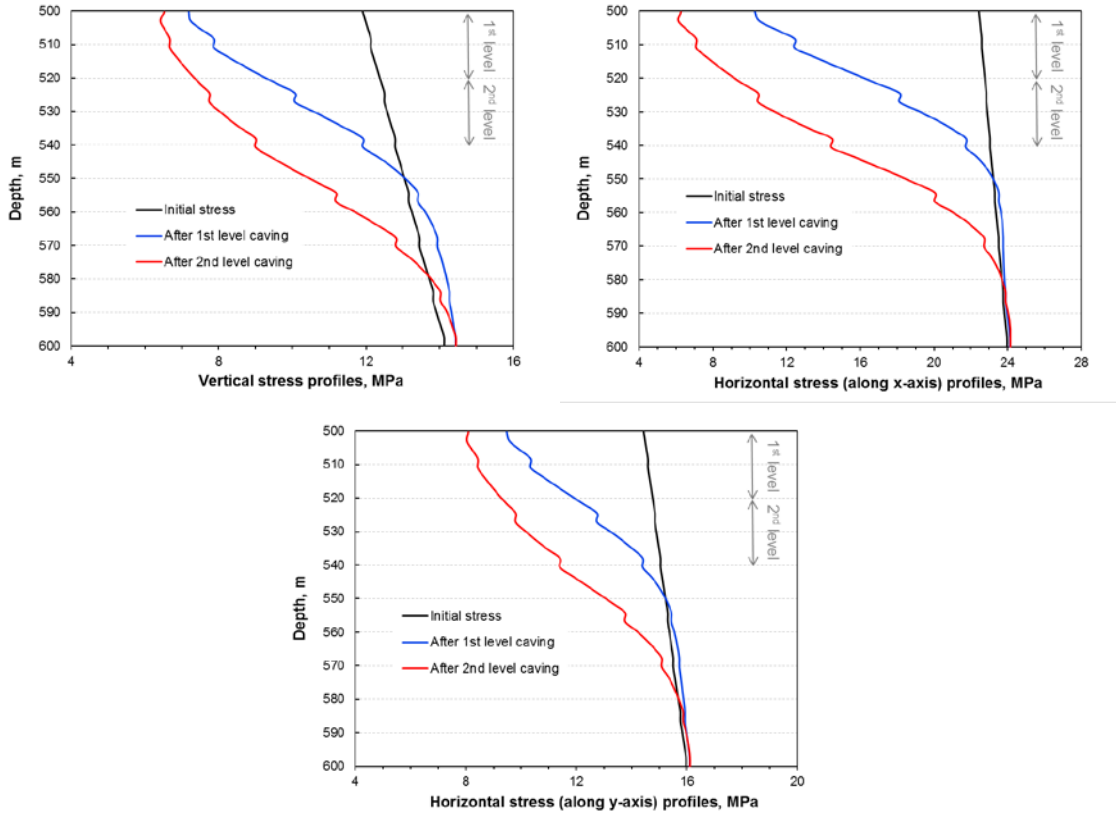


**Figure 2.2.9.3:** Stress changes in #9 coal seam during coal extraction at #8 coal seam.

#### Coupled flow-geomechanical modelling for gas drainage at Hunosa

Based on the geomechanical modelling results presented in the previous section, numerical models to simulate gas drainage during sub-level caving of #8 coal seam at Hunosa were developed in ECLIPSE 300. The build-in coalbed methane module can mimic gas ad/desorption behaviour and multiphase fluid transport in dual-porosity media.

The coupling workflow between the geomechanical and fluid flow simulators is achieved as follows: the stress field after coal extraction are computed from FLAC<sup>3D</sup> and then passed to Matlab to calculate the permeability based on a well-established stress-permeability relationship at IMPERIAL. The derived permeability field is then sent to ECLIPSE 300 as the input to generate the pressure field and assess gas drainage performance after coal extraction.

In order to freely exchange data between simulators, the flow model developed in ECLIPSE has the same geometry with the geomechanical model developed earlier. After caving at each level, the stress distributions generated by FLAC<sup>3D</sup> were used to calculate the permeability field in the model domain based on the stress-dependent permeability relationship (Equation 3.2.9.1). In this relationship, it was assumed that the permeability at  $i$  direction ( $k_i$ ) can change exponentially with the variation of the confining stress ( $\Delta\sigma_j$  and  $\Delta\sigma_k$ ) at the other two directions. The calculated permeability was then used as the input for the reservoir simulator ECLIPSE to assess the gas drainage performance during sub-level caving.

$$k_i = k_{i0} \cdot e^{-C \sum_{j=1}^3 \Delta\sigma_j \cdot (1 - \delta_{ij})} \quad (3.2.9.1)$$

where  $k_{i0}$  is the initial permeability,  $c$  is the permeability compressibility factor for intact coal and  $\delta_{ij}$  is the Kronecker Delta. Since the bedding planes are well-developed along the strike of the coal seam, the initial permeability was assumed to be anisotropic, which is much lower in the direction perpendicular to the coal seam.

The other reservoir properties used in the flow model were taken from laboratory experiments conducted in WP1. Table 2.2.9.2 summaries the input reservoir parameters for ECLIPSE. A dual porosity model was used to simulate the unique coal structure, whereby coal matrix was assumed to be saturated with gas while the gas saturation in the cleat was 90%. The relative permeability relationships measured by Durucan et al. (2014) were adopted as appropriate. It was also assumed that the coal is at depth between 500 and 540 m at #8 coal seam had been extracted and replaced with the goaf rock properties.

Gas adsorption isotherms for Hunosa #8 coal seam indicate that the in situ gas content at 2 MPa seam pressure ranges from 10 to 13 m<sup>3</sup>/t.

**Table 2.2.9.2:** Reservoir properties used for gas drainage simulation at Sueros Colliery, Hunosa.

Layer	$k_{xx}$	$k_{yy}$	$k_{zz}$	$\phi$	$P_L$ (MPa)	$V_L$ (m <sup>3</sup> /t)	$D$ (m <sup>2</sup> /day)	$P$ (MPa)
Coal	0.1	3	3	0.1	0.87	18.5	100	2.0
Rock	0.1	0.1	0.1	0.05	--	--	--	2.0
Goaf	1000	1000	1000	0.2	--	--	--	2.0

#### Gas drainage stimulation using slotted cross-measure boreholes in #8 coal seam

The first gas drainage method considered at Sueros Colliery was using cross-measure boreholes (see Figure 2.2.9.4). These boreholes were designed to start from the rock gallery at the foot wall, penetrate #9 coal seam, and be completed in #8 coal seam. Note that, due to the borehole stability issue during penetrating #9 coal seam, cemented seal was used for the entire borehole length before reaching the #8 coal seam, which stops gas inflow from #9 coal seam. The length of these boreholes are around 60 to 70 m long and their diameter is ~60 mm. Numerical models developed in this section will use this field drainage plan as reference.

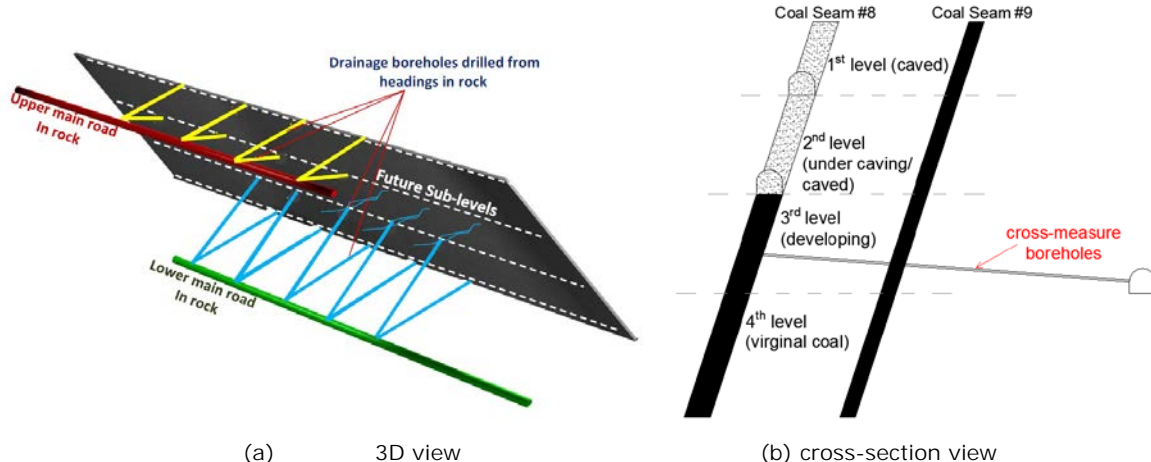


**Figure 2.2.9.4:** Gas drainage using cross-measure boreholes at Sueros Colliery, #8 coal seam.

As shown in Figure 2.2.9.5, following the drilling plan at the mine, a group of 9 cross-measure boreholes with 10 m spacing were first modelled at a depth of 550 m. Each gas drainage borehole was simulated by a horizontal well with a diameter of 60 mm and at a bottomhole pressure of 70 kPa. Given the borehole sealing condition at the mine, only the borehole section within the #8 coal seam was set as open flow section while the rest was kept shut, which suggests no gas flow into the borehole from #9 coal seam.

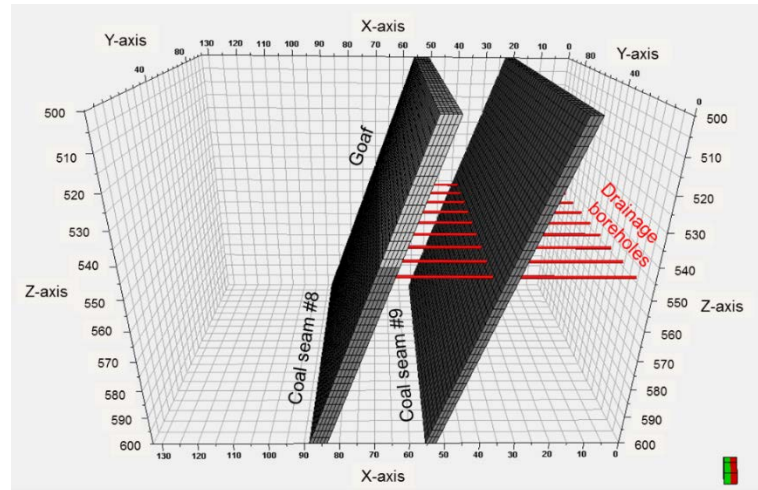


**Figure 2.2.9.5:** Gas drainage model at Sueros Colliery sub-level caving layout developed in ECLIPSE.

The importance of considering the permeability changes induced by the mining of previous levels can be found in Figure 2.2.9.6, which compares the gas drainage performance in both coupled and uncoupled models. In the uncoupled model, permeability was set as the constant value of the initial permeability listed in Table 2.2.9.2, while in the coupled model, coal permeability was determined based on the stress field after the sub-level caving of first two levels. Figure 2.2.9.7 shows the permeability changes in #8 coal seam after the first and second level coal extraction. At the depth of planned boreholes (550 m), nearly one order of permeability reduction was observed after caving in the 2nd level. As can be seen, since the uncoupled model did not include the permeability reduction induced by sub-level caving, gas drainage rate was significantly overestimated.

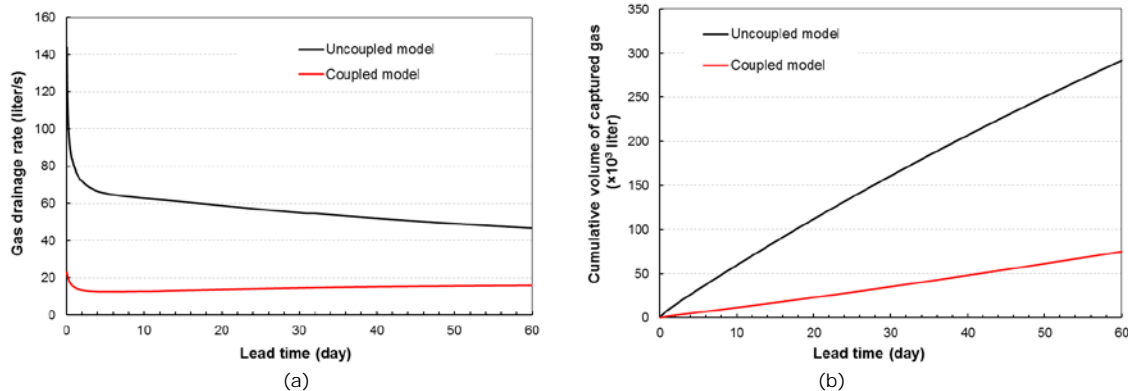


**Figure 2.2.9.6:** Comparison of gas drainage performance between coupled and uncoupled models:  
(a) gas drainage rate, and (b) cumulative volume of captured gas.

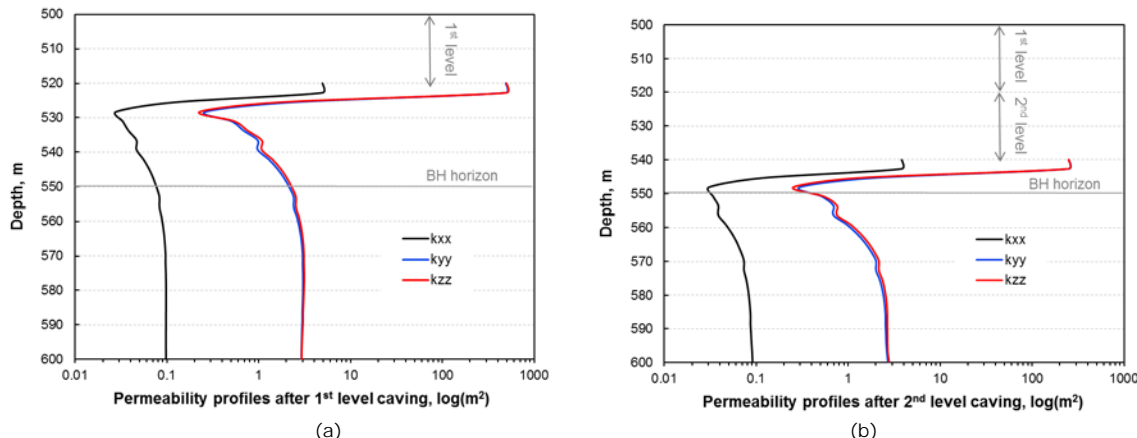


**Figure 2.2.9.7:** Permeability response of # 8 coal seam after (a) 1<sup>st</sup> level caving and (b) 2<sup>nd</sup> level caving.

In Task 2.3, the stimulation effect for individual boreholes was numerically assessed. Utilising the observations from this work, it was decided to test first the performance of slot cutting in the first set of stimulation models at Hunosa. In the benchmark slotting scenario developed for Hunosa in Task 2.3, the radius of the permeability enhanced zone around a slot stimulated borehole was found to be approximately 10 times of the borehole radius. In the preliminary field scale model developed, the stimulated high permeability zone was represented by an enlarged borehole diameters as the first level approximation of the impact of slot cutting which also saved significant computing time. To model stimulation in the large-scale model, the borehole diameter for stimulated boreholes was assumed to be 600 mm instead of 60 mm for un-stimulated boreholes. This helped seamless modelling of multiple slots in a set of boreholes, although this may have led to an overestimate of the performance of the stimulated boreholes. Currently, further refinement of this model is being carried out using realistic slot separation distances in collaboration with GIG in Task 2.4.

Figure 2.2.9.8 compares the gas drainage performance between the stimulated borehole group and an un-stimulated borehole group. Pressure contours of #8 coal seam after 60 days of degasification are shown in Figure 2.2.9.9. Compared with un-stimulated boreholes, gas drainage rate as well as the cumulative volume of captured gas almost doubled in the stimulated boreholes. This results in a much more significant pressure relief in the #8 coal seam as can be seen from Figure 3.2.9.11.

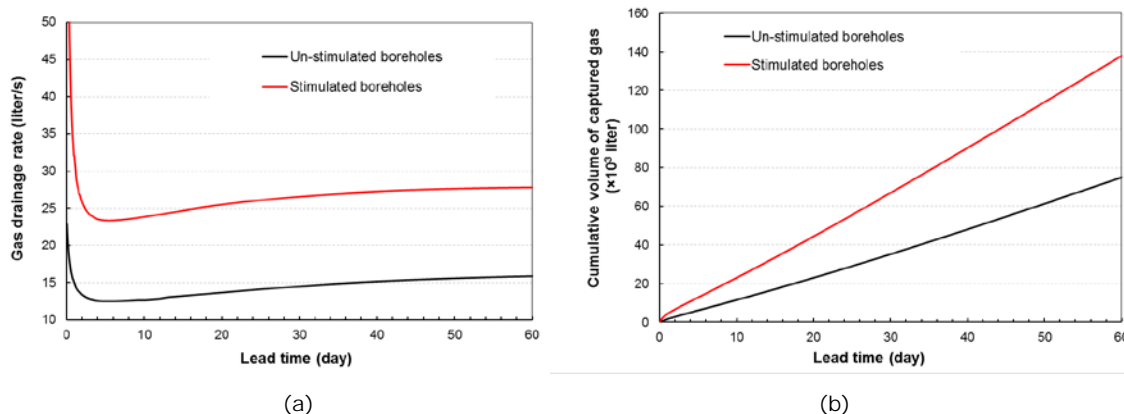


**Figure 2.2.9.8:** Comparison of gas drainage performance between un-stimulated and slot stimulated boreholes at # 8 coal seam: (a) gas drainage rate, and (b) cumulative volume of captured gas.

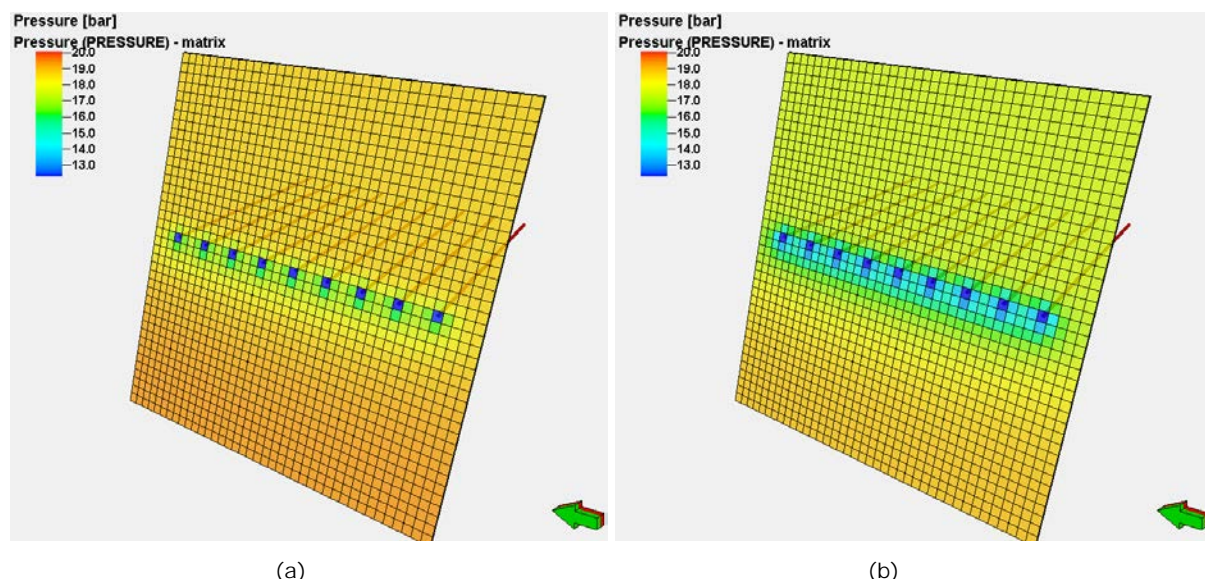


**Figure 2.2.9.9:** Pressure contours at # 8 coal seam after two months of gas drainage with: (a) un-stimulated cross-measure boreholes, and (b) slot stimulated cross-measure boreholes.

During the two months of gas drainage modelling, the in-situ gas content in the 3rd caving level (from 540 to 560 m deep) at #8 coal seam was continuously monitored. Although stimulation techniques can effectively increase gas drainage performance, due to permeability reduction induced by mining abutment stress, gas drainage using cross-measure boreholes has not significantly reduced the in situ gas content at the next mining level. After two months, less than 10% of gas was captured by the stimulated boreholes (Figure 2.2.9.10), which is not that effective considering the high gas content of #8 seam coal. Therefore, an alternative drainage plan needs to be considered.

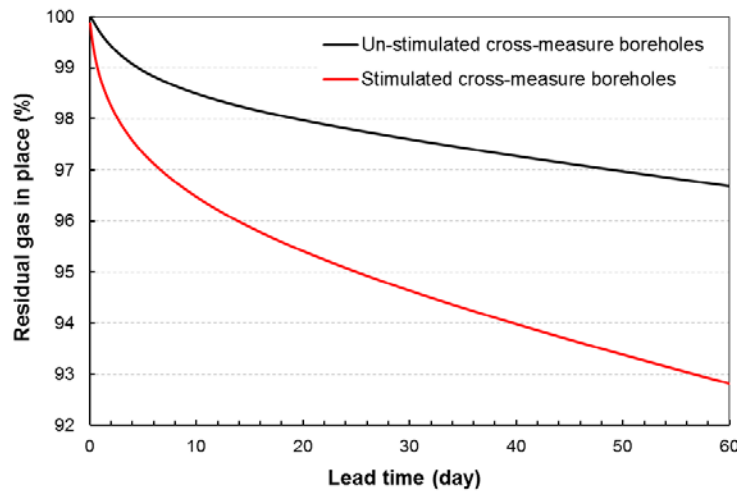


**Figure 2.2.9.10:** The residual gas content within the 3rd caving level at # 8 coal seam using cross-measure boreholes.

#### Gas drainage stimulation using slotted inseam downholes in #8 coal seam

In order to improve gas drainage behaviour in the #8 coal seam, inseam downholes drilled from the development headings downwards to the lower levels are proposed. As shown in Figure 2.2.9.11, this gas drainage method aims at reducing gas content in the successive sublevels.

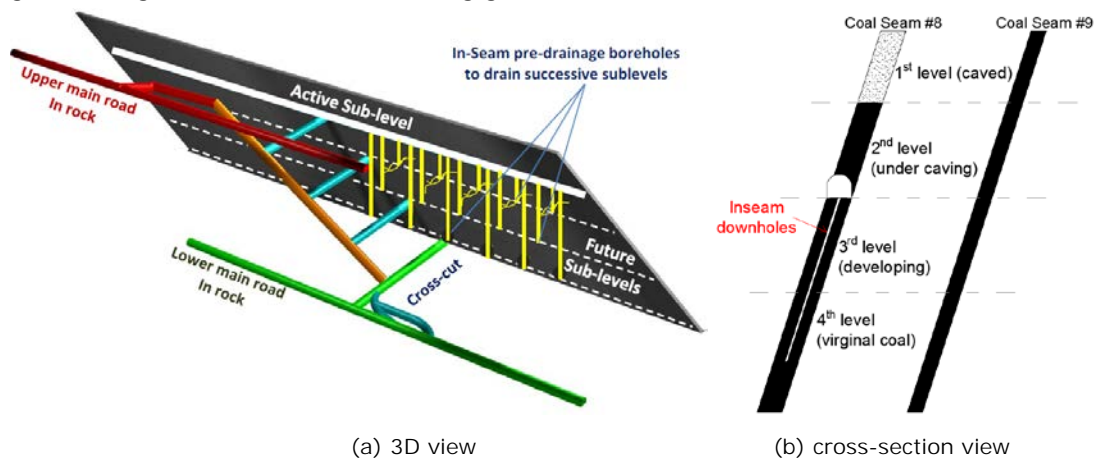


**Figure 2.2.9.11:** Gas drainage using inseam downholes at Sueros Colliery, #8 coal seam.

Accordingly, in numerical models, inseam downholes drilled from the 2nd mining level roadways (540 m) towards the floor coal to drain #8 coal seam gas were simulated. In this practice, the model simulated a period of 60 days pre-drainage after roadway development but before the coal recovery at the 2nd mining level. Therefore, the permeability field implemented in this model was based on that after 1st level caving (Figure 2.2.9.11a) but also considered the development of the 2nd level roadway. Figure 2.2.9.12 shows the permeability input for gas drainage from inseam downholes drilled at the 2nd level roadway.

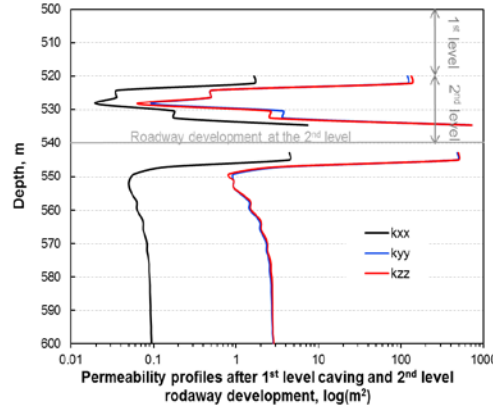


**Figure 2.2.9.12:** Permeability response of #8 coal seam after 1st level caving and 2nd level roadway development.

As shown in Figure 2.2.9.13, a group of 9 inclined boreholes with 10 m spacing were modelled. Each borehole is 40 m long with 20 m standpipe. Referring to the above permeability profiles, the open flow sections of these boreholes (ranging from 560 to 580 m) are away from the stress disturbance zone, and thus they are mostly in coal which has the in-situ permeability. The proposed downholes are expected to reduce the gas content in the second next (4th) mining level.

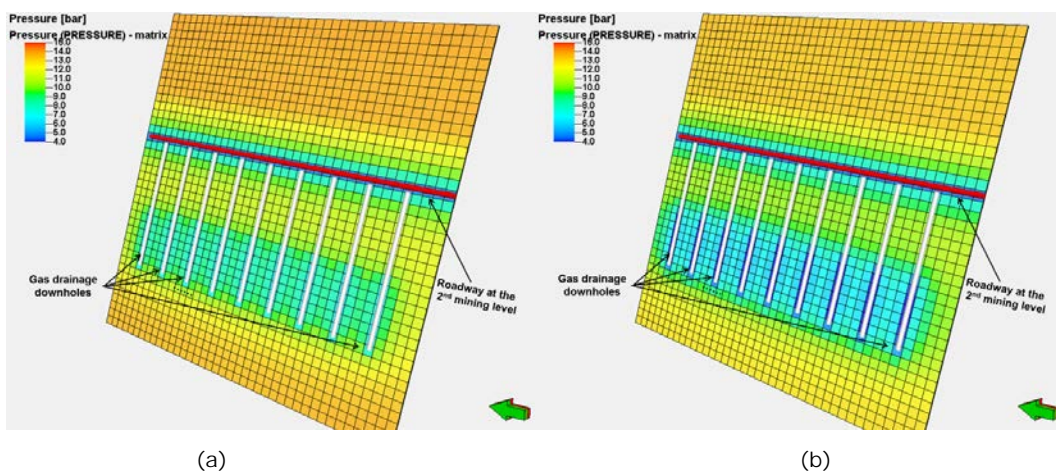


**Figure 2.2.9.13:** Pressure contours of #8 coal seam after two months of gas drainage with: (a) un-stimulated inseam downholes, and (b) slot stimulated inseam downholes.

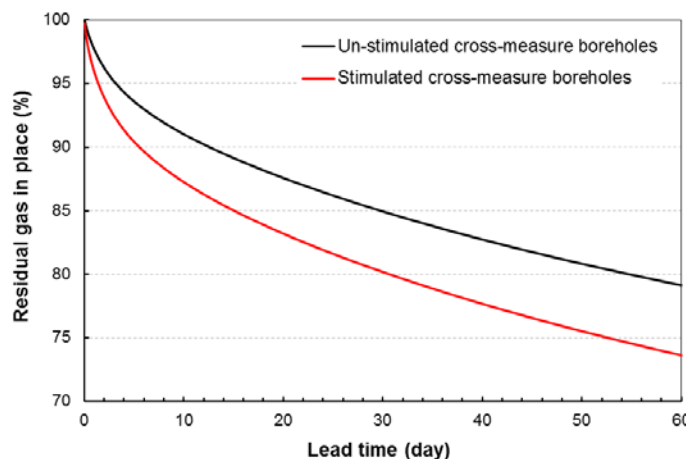


**Figure 2.2.9.14:** The residual gas content within the 4th caving level at #8 coal seam using downholes.

Figure 2.2.9.14 shows that, without being constrained by the mining abutment stress, the inseam downholes can largely reduce the gas pressure in the target mining level at #8 coal seam. Using downholes to reduce gas-in-place content at the target mining level is much more effective than cross-measure boreholes: the former can reduce gas content by 30% after 2 months of gas drainage while the latter only achieves 10% gas content reduction (Figure 2.2.9.10 and 3.2.9.14).

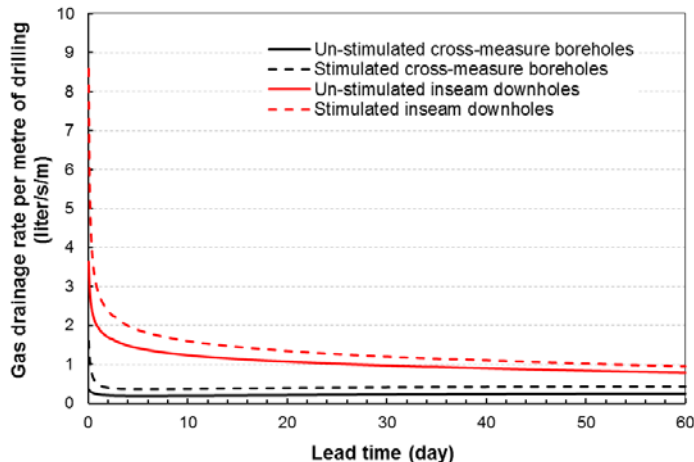
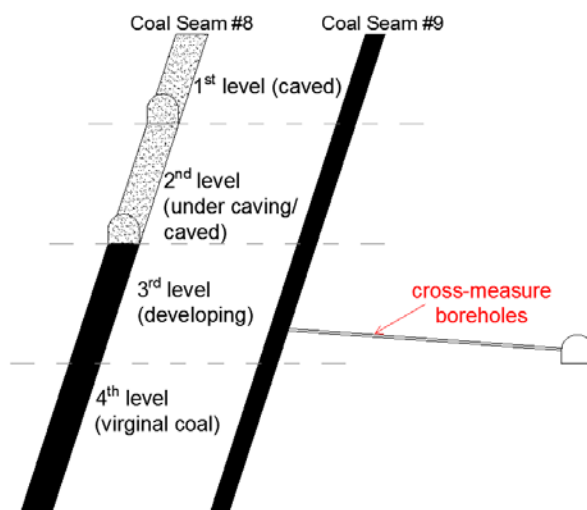


**Figure 2.2.9.15:** Comparison of gas drainage performance between inseam downholes and cross-measure boreholes at Sueros Colliery #8 coal seam.

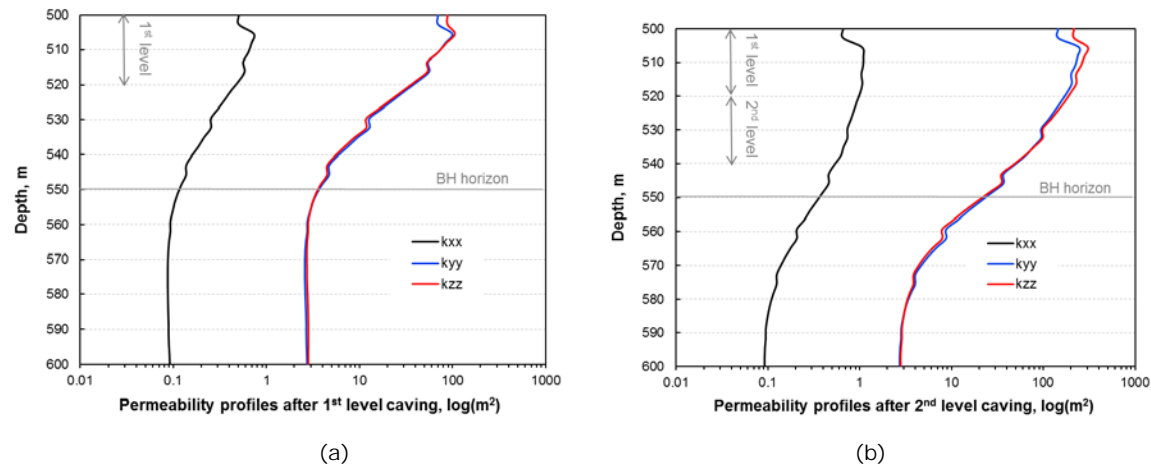
The inseam downholes also have an intrinsic advantage over the cross-measure boreholes: the contact area between the well and coal is not limited by the coal thickness but the length of the well. This suggests gas production increase can be achieved by simply enlarging the length of an inseam downhole. In addition, in terms of gas drainage rate per metre of drilling, inseam downholes are more efficient than cross-measure boreholes as illustrated in Figure 2.2.9.15. Furthermore, due to reduced borehole length as compared to horizontal boreholes through bedrock and #9 seam, the drilling costs would also be reduced.

#### Gas drainage stimulation using slotted boreholes in #9 coal seam

The geomechanical model developed earlier has revealed that #9 coal seam experienced dramatic stress relief during the sub-level caving activities at the #8 coal seam. Gas drainage boreholes target at capturing gas in #9 coal seam were evaluated in this section. These boreholes were also drilled from the gallery at the foot wall, but completed in #9 coal seam, and had no direct contact with #8 coal seam (Figure 2.2.9.16).

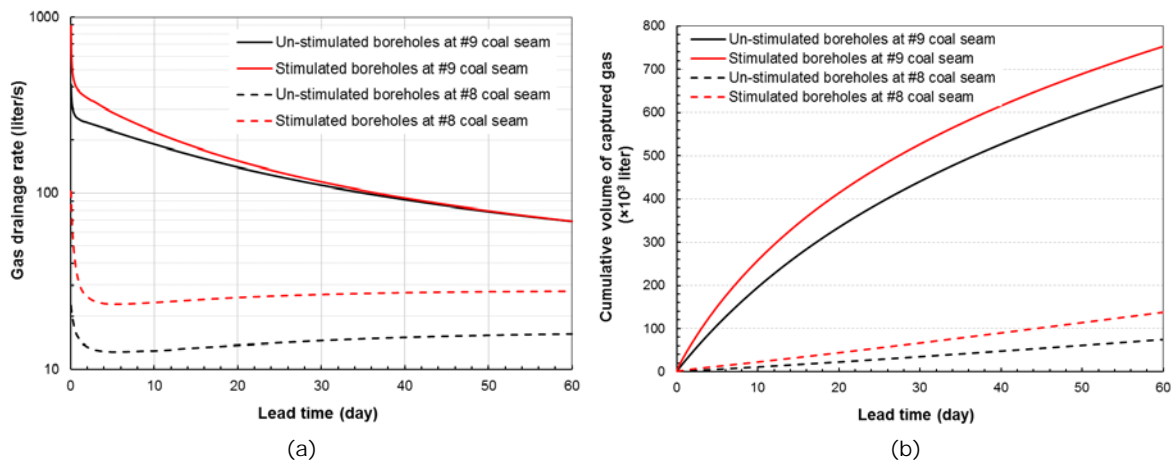


**Figure 2.2.9.16:** Gas drainage using cross-measure boreholes at Sueros Colliery # 9 coal seam.



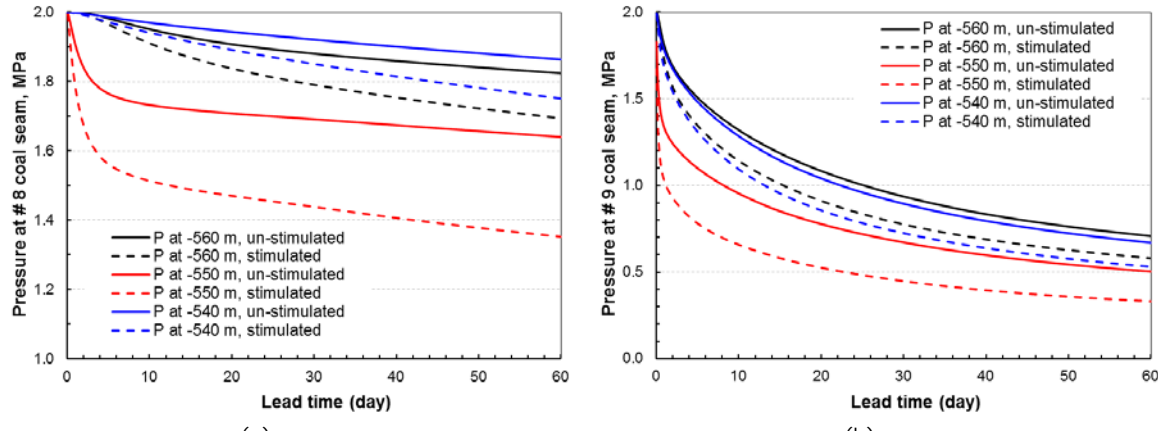
**Figure 2.2.9.17:** Permeability response of #9 coal seam after (a) 1<sup>st</sup> level caving and (b) 2<sup>nd</sup> level caving.

Figure 2.2.9.17 shows the permeability changes in #9 coal seam after the first and second level coal extraction. At the depth of planned boreholes (550 m), nearly one order of permeability enhancement along the y-axis and z-axis was observed after 2<sup>nd</sup> level caving. Consequently, Gas drainage performance of these boreholes are largely boosted and much higher than the boreholes in #8 coal seam (Figure 2.2.9.18). Applying slot cutting stimulation techniques in boreholes at #9 coal seam can further increase gas drainage performance but the stimulation effect can only last a shorter duration compared with that in #8 coal seam.



**Figure 2.2.9.18:** Comparison of gas drainage performance in #8 and #9 coal seams: (a) gas drainage rate, and (b) cumulative volume of captured gas.

Pressure monitoring points at a depth of -540, -550, and -560 m were predefined in both #8 and #9 coal seams. Figure 2.2.9.19 plots the pressure changes at these monitoring points during the gas drainage period. As expected, the degasification process in #9 coal seam is much faster and more significant than that in #8 coal seam. Stimulation is an effective measure to further release adsorbed gas and lower gas pressure in both two seams.



**Figure 2.2.9.19:** Pressure changes at (a) #8 and (b) #9 coal seam during gas drainage period.

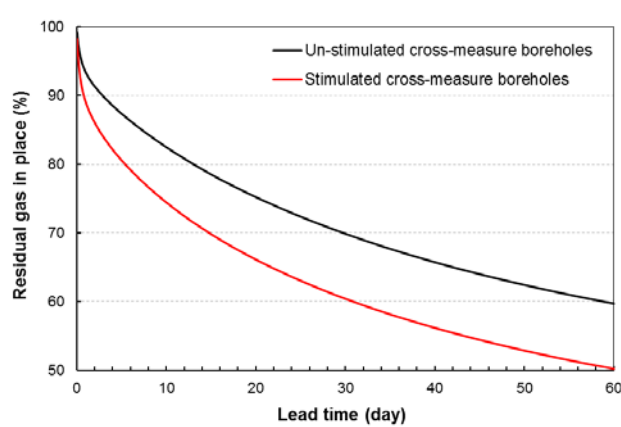


**Figure 2.2.9.20:** The residual gas content within the 3rd caving level at #9 coal seam.

The residual gas content in the 3rd caving level (from 540 to 560 m deep) at #9 coal seam was also continuously monitored during the whole drainage period. Nearly 50% of the gas was captured by the slot stimulated boreholes after two months of gas drainage (Figure 2.2.9.20). It can be expected that the gas emission level during the sub-level caving of #9 coal seam will be much lower than that in #8 coal seam, should this seam also be mined.

### Conclusions

Sub-level caving activities can largely change the stress field around mine openings and thus a dynamic response of permeability can be expected during the coal extraction process. More specifically, for the mining layout of the Sueros Colliery at Hunosa, coal caving in the upper levels creates a notable stress abutment in the next level(s) to be mined. The stress abutment zone created by sublevel caving in the upper zones of a steeply dipping seam can have a negative impact on gas drainage with the cross-measure boreholes targeting to capture the # 8 coal seam's gas in the next mining level. To overcome this, more productive and efficient inseam downholes are proposed, since they have longer open flow sections in coal which are also less constrained by mining abutment stresses.

It was also found that sub-level caving of # 8 seam coal at Sueros Colliery leads to considerable stress relief and permeability enhancement in the neighbouring # 9 coal seam. This can largely promote the gas drainage performance in # 9 coal seam and lowers gas content and pressure prior to the start of mining activities should this seam also be mined.

In summary, the preliminary slot cutting stimulation models applied to the cross-measure boreholes at #8 coal seam nearly doubled gas production rate and lasted over the entire modelling period (two months), while the gas production rate of stimulated cross-measure boreholes at #8 coal seam declined relatively fast and showed no difference to the un-stimulated boreholes after one month.

## 2.2.10. WP4, Task 4.1 In situ testing of the effectiveness and performance range of the newly developed blasting materials and fracturing techniques using explosives (led by GIG, JSW)

### Introduction

Under this task, the researches concerning destruction of coal seam based on the method of directional fracturing of the rock were continued. The tests consisted in trying out new equipment to perform multiple number of initial fractures in single borehole as well as determining effectiveness of fracturing with the use of explosives in the underground conditions of Experimental mine „Barbara” Mikolow.

Rock mass in natural conditions (not disturbed by mining activity) can be characterized by natural grid of discontinuities. In specific it can be e.g. syn-genetic fractures, faults, cracks, etc. Their genesis is connected with natural stress field, which was established during geological processes during development of earth's crust. Mining activities damage this state causing fissures and secondary fractures. Fissuration of the rocks can be recognized then as a structural feature of the rock mass, which is changing together with the intervention into the rock mass (Małkowski, 2004), and has also influence on migration of both: water and gases. Considering above the assessment of the rock mass fissuration is essential – the most favorable if measured in situ. There are several methods aiming at determination of fissuration ratio of the rock mass in the vicinity of mining workings. One of them can be endoscopic method (Frejowski, Merta, 2015; Merta, Myszkowski, 2004; Mlynarczyk, Wierzbicki, 2012; Stasica, Rak, 2012; Stopryra, Stasica, Rak, 1998) or another-one using aerometric probe (Friedland, 1965; Gwiazda, Hładysz, 1973; Niemiec, 2001; Nierobisz, 2014).

### Location of the field test

The research took place in the part of the coal seam 310 at Experimental mine „Barbara” in Mikolow, in the working marked on the seam map – as below (Figure 2.2.10.1).

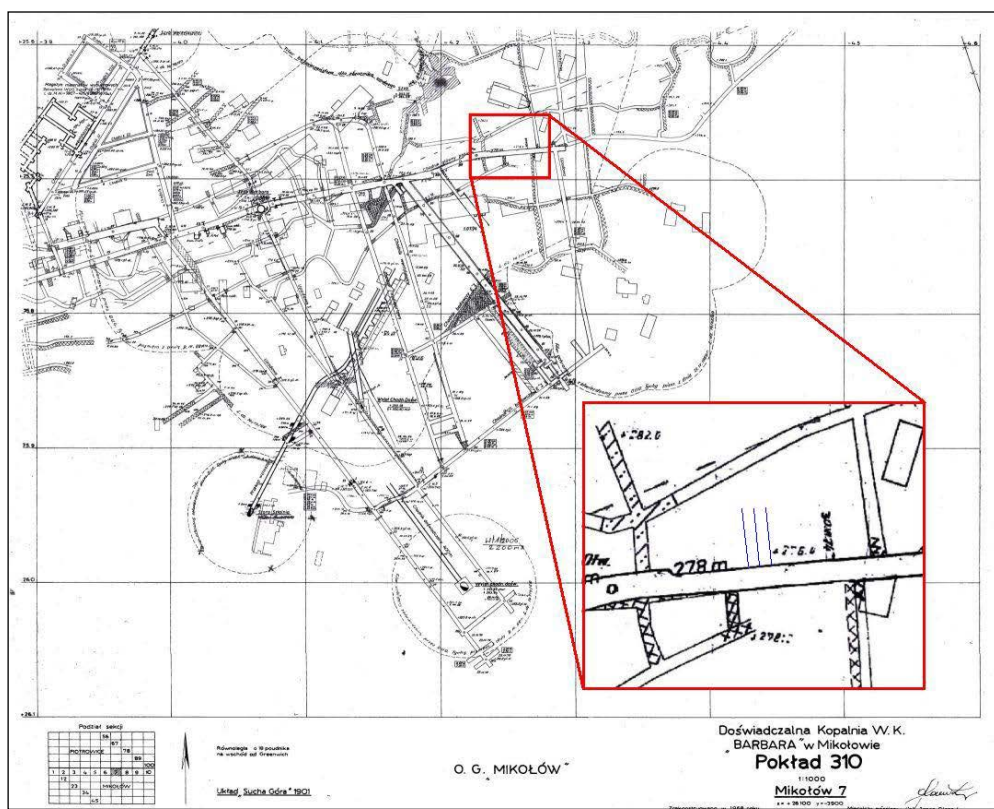


Figure 2.2.10.1: Sector of the coal seam 310 with the location of the field test

### Endoscopic method

The point of the endoscopic tests consists in visual penetration of the borehole interior using miniaturized camera, placed inside metal body with the diameter of 35 mm. Body of the camera is being introduced into borehole using light, bayonet sticks. View of observed wall of the borehole is being transferred to the monitor integrated with digital video recorder. It is possible to enlarge picture of tested object, which enable to test defects of the material with 0.1 mm sizes. Possibility of voice recording

commentary makes the scope of analysed data even wider. Tests using endoscopic camera were performed in 5 test boreholes before and after the blastings. The result of the pictures' analysis are the fissures identified on the side of the borehole. Due to the human's eye disability and resolution of the camera only clearly defined fissures are recognized.

### Aerometric method

Considering above remarks it can be assumed that fissuration measurement performed by the equipment penetrating rock mass in bigger area down deep into the rock mass will be more reliable. Above criteria are fulfilled by aerometric probe under certain conditions of conducting the tests. Measurement performed by aerometric probe in the coal seam of Experimental mine „Barbara” enabled determination of the following parameters:

- Borehole equivalent fissure  $S_0$ , mm<sup>2</sup>,
- Fissuration index  $K_s$ , %,
- Total fissures' opening  $R_s$ , mm.

During testing regime above indexes were determined for the seam 310 in its undisturbed state and after its fracturing using explosives.

Aerometric method consists in the measurement of the pressure drop time of certain compressed air volume flow into the rock mass. Measurements of the rock mass fissures were performed by aerometric probe. Basic elements of the equipment are shown on the figure below.

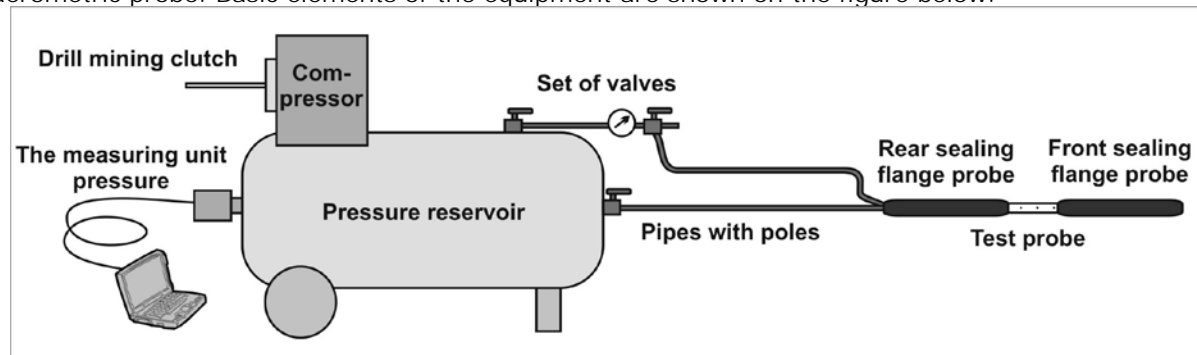


**Figure 2.2.10.2:** Scheme of aerometric probe for testing of rock mass fracturing

Fissuring tests in the coal seam 310 of Experimental mine “Barbara” (Figure 2.2.10.1) were performed by aerometric equipment (Figure 2.2.10.2), which consists of the measurement probe, control and monitoring elements. Basic equipment located in underground working consists of the following elements: pressure tank, with compressed air coming from the compressor driven by mining drill, set of valves meant for air pressure control and equipment enabling recording pressure changes in time (laptop with measurement card and pressure sensor). Digital recording of pressure changes provides high accuracy of measurements.

Measurement probe and pressure hoses are being placed in the borehole using sticks. They are used to pump the air separately down to two sealing collars and to the probe located between them. Measurement of the fissuring and fractures intensity in the space between the collars consists in determining pressure drop in the “closed system” established by the tank, one of the pressure hoses, and space of the borehole. Pressure drop time in above system is proportional to the size and number of fissures located within testing borehole space.

Pressure drop time measurements in above system are made in the range of 0.40÷0.25 MPa, which allow determining following parameters:

- Borehole equivalent fissure  $S_0$  - defined as total value of the fissurings' area located in the borehole side along testing section in [mm<sup>2</sup>],
- Fissuration index  $K_s$  - defined as total value of the fissures' area share in the borehole's side area along testing section in [% or %],
- Total fissures' opening  $R_s$  - defined along borehole testing section in [mm].

Values of above parameters are being calculated based on the following empirical formulas:

- borehole equivalent fissure  $S_0$

$$S_o = \frac{39,866}{0,7169 \cdot t - 1} \frac{39,866}{0,7169 * t - 1}, \text{ mm}^2 \quad (1)$$

where :

39.866; 0.7169 – equipment stamp constants,

$t$  – measured air pressure drop time.

- fissuration index  $K_s$

$$K_s = \frac{1000 \cdot S_o}{37806}, \% \quad (2)$$

where:

$S_o$  – borehole equivalent fissure,  $\text{mm}^2$ ,

1000 – constant used for per mil calculations,

37806 – area of cylinder side with 43 mm diameter along testing section,  $\text{mm}^2$

- total fissures' opening  $R_s$

$$R_s = \frac{S_o}{135}, \text{ mm} \quad (3)$$

where:

135 – circumference of testing borehole with 43 mm diameter.

Based on the experience gained so far when applying aerometric probe, rock mass can be characterized in the following way:

$K_s < 0,2$  – rock mass poorly fissured characterized by total value of the fissurings' area located in the borehole side along testing section not higher than  $7.4 \text{ mm}^2$  or without fissures at all,

$K_s > 0,2$  - rock mass average and highly fissured characterized by total value of the fissurings' area located in the borehole side along testing section higher or equal to  $7.4 \text{ mm}^2$ . Usually these are rock mass areas characteristic for the workings under influence of exploitation.

Scheme of the rock mass fissures' measurement using the aerometric probe is shown on Figure 2.2.10.3.

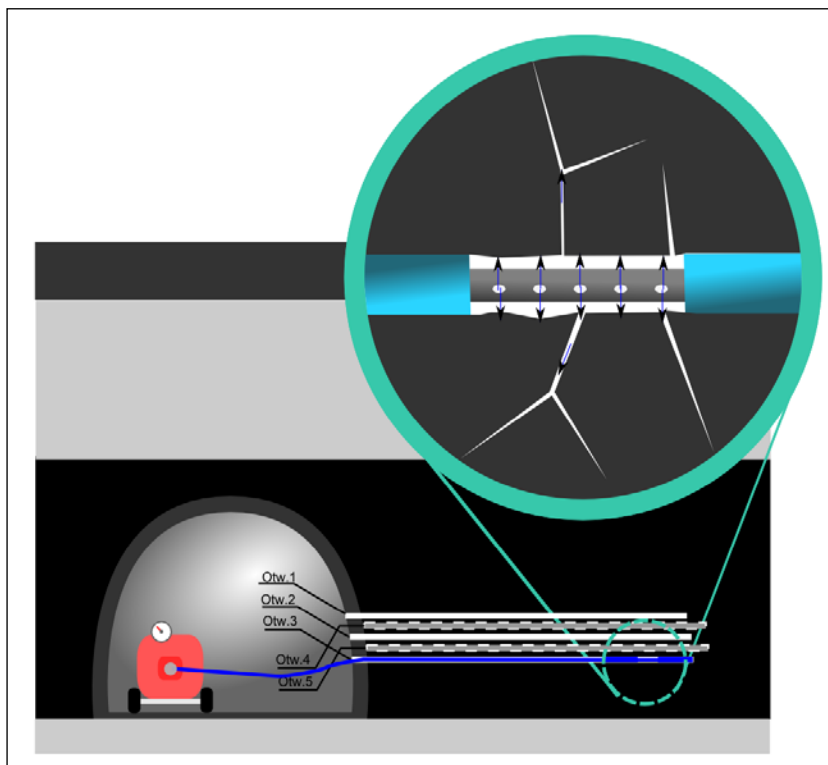


**Figure 2.2.10.3:** Scheme of the rock mass fissures' measurement using the aerometric probe

#### Testing field

According to approved testing program main goal of this test was evaluation of the seam fissuring ratio after applied stimulation by explosives. Test consisted in following stages:

1. Drilling in the main gallery side six boreholes with diameter of 43 mm each. Their space location and picture from the gallery are shown on Figure 2.2.10.4, (red colour means monitoring boreholes, blue colour means the borehole used for inserting the explosives).

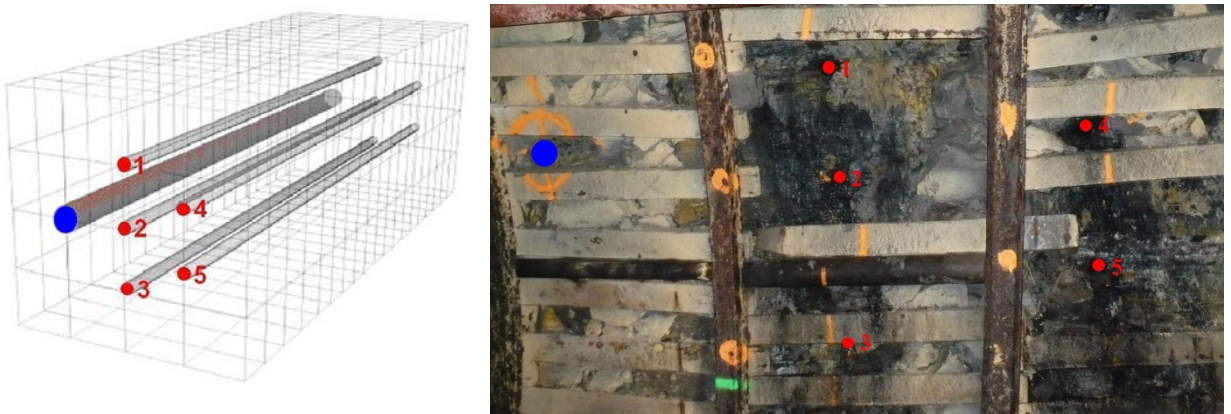


**Figure 2.2.10.4:** Spatial location of the boreholes

2. In the blasting borehole four initial fissures were made perpendicularly to the axis of the borehole [Konopko, 1997; Myszkowski, 1996] using the equipment shown on Figure 2.2.10.5.



**Figure 2.2.10.5** Tools used to perform initial fissuring and view of the initial fissure

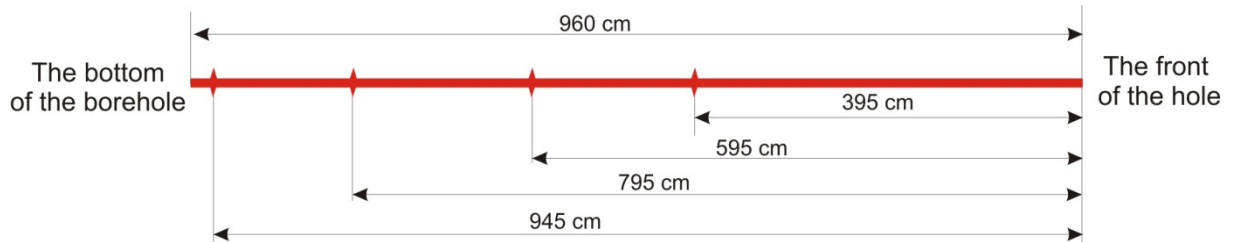


**Figure 2.2.10.6:** Location of the initial fissurings

3. Preparing four explosive charges from the blasting material Emulinit PM by Nitroerg S.A, Table 2.2.10.1, two of 50g and two of 100g – Figure 2.2.10.7.

**Table 2.2.10.1:** Properties of Emulinit PM [<http://www.nitroerg.pl>]

Density)	$1,15 \pm 1,3 \text{ g/cm}^3$
Velocity of detonation	4000 m/s
Lead Block test, average	170 cm <sup>3</sup>
Ballistic pendulum RSW (RSW)	29 % Hx
Sensitivity to impact, min	30J
Sensitivity to friction, min	360 N
Thermal stability in temperature 750C	48 h
Oxygen balance	8,53 %
Specific volume of gaseous products of explosion	767 dm <sup>3</sup> /kg
Heat of explosion	2278 kJ/kg
Concentration of energy	2756 kJ/dm <sup>3</sup>
Proper energy	522 kJ/kg



**Figure 2.2.10.7:** View of prepared explosive charges

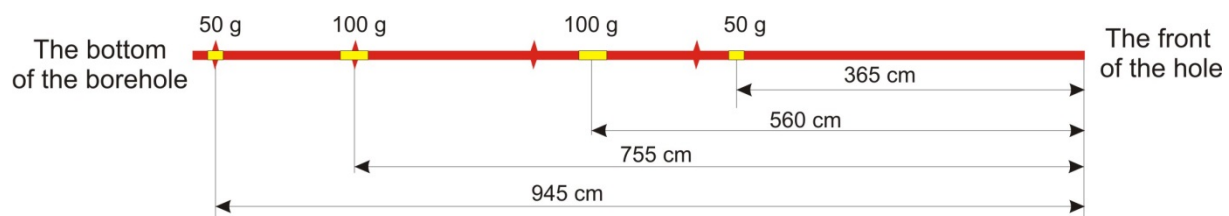


**Figure 2.2.10.8:** Location of explosive charges

4. Preparing of rigid construction stabilizing explosive charges in desired locations of the borehole, (explosive charges were initiated by the detonators, inserted into the explosive material from the boreholes), Figure 2.2.10.9.



**Figure 2.2.10.9:** Rigid pipe construction stabilizing explosive charges in desired locations in the borehole

#### Results of the measurements

As a result of endoscopic tests (using borehole camera) in the control boreholes after performed blastings several fissures and discontinuities were discovered. Example of registered fissures is shown on the figure below.

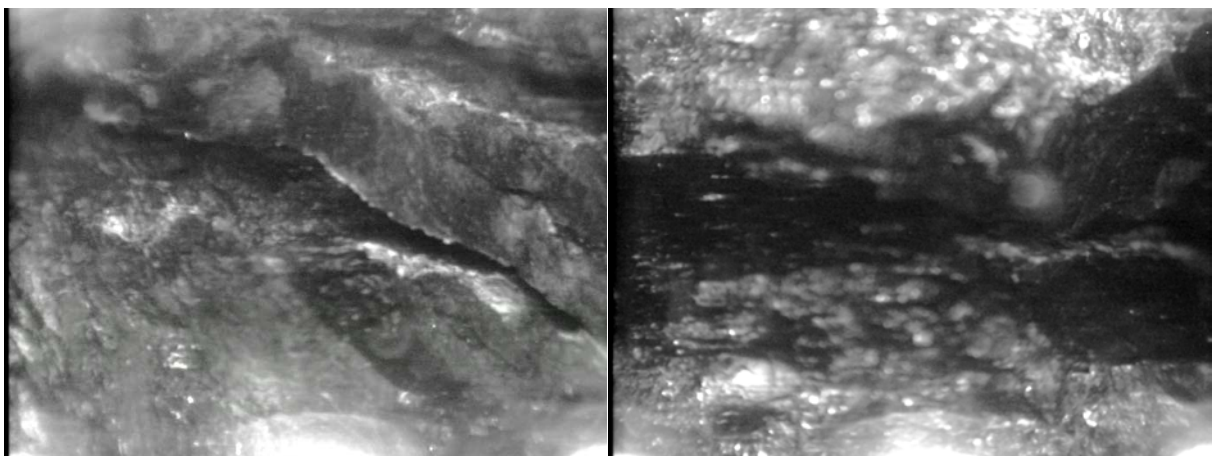


**Figure 2.2.10.10:** View of the fissures in the control boreholes

Measurements by aerometric probe were made in two series. First of them covered pressure drop time  $t_0$  measurement in each control borehole at the distances of 0.3 m. Obtained results were the basis for the coal seam fissuration assessment before its disintegration using explosive material. In the second sequence pressure drop time  $t_1$  measurement in each control borehole were made after firing blasting material. Based on obtained data and formulas 1–3 for each of the boreholes borehole equivalent fissure  $S_0 \text{ mm}^2$ , fissuration index  $K_{s0}$ , %, and total fissures' opening  $R_{s0}$ , mm before and after destruction part of the seam with the explosives were calculated including differences between their values for two above cases. Graphical pictures of the fissuration index  $K_s$  changes' results for the part of the coal seam 310 with the five surrounding control boreholes are shown on the figures Figure 2.2.10.11 - 5.5.1.20

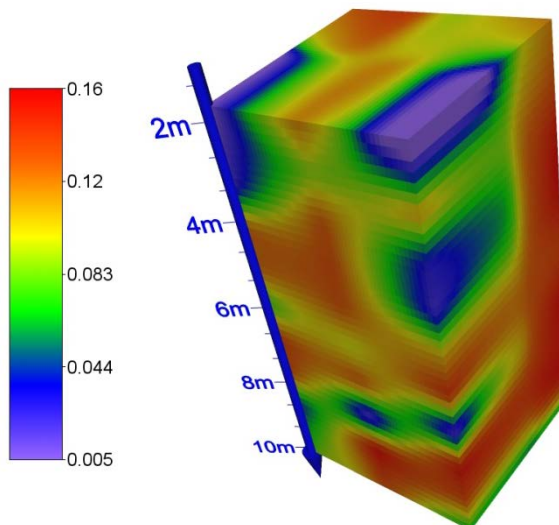


**Figure 2.2.10.11:** Values of fissuration index  $K_s$ , % before blasting

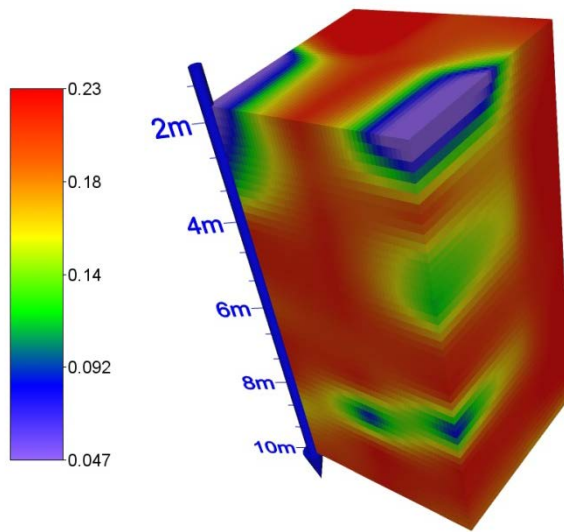


**Figure 2.2.10.12:** Values of fissuration index  $K_{s1}$ , % after blasting

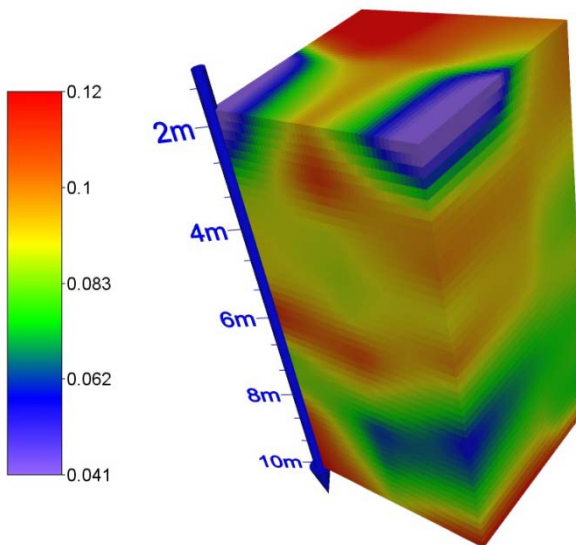


**Figure 2.2.10.13:** Changes of fissuration index  $\Delta K_s$ , % – difference between measurements before and after blasting

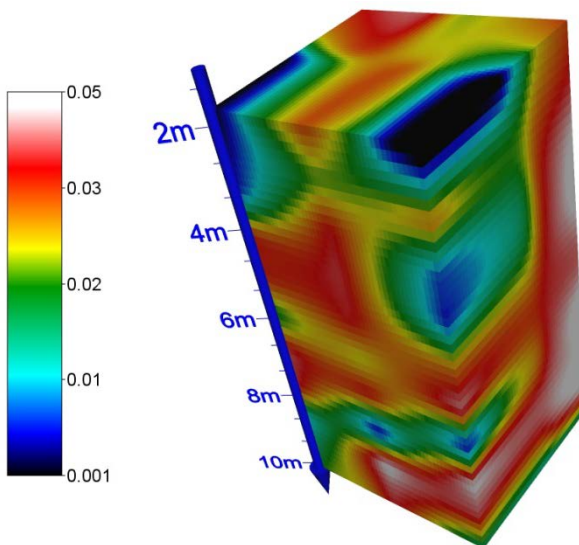


**Figure 2.2.10.14:** Values of the index "total fissures" opening Rs00", mm before blasting

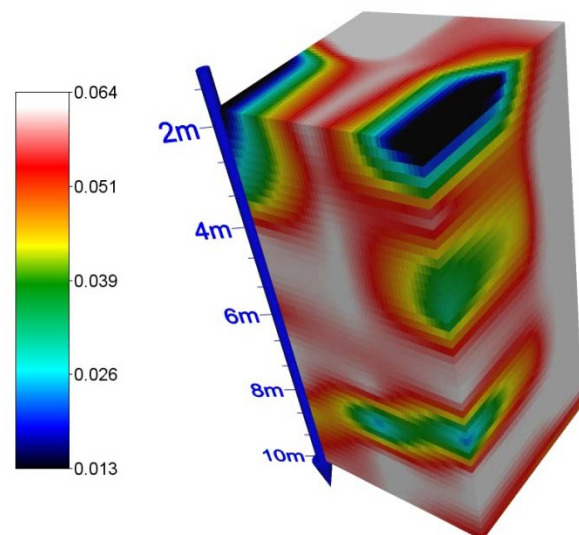


**Figure 2.2.10.15:** Values of the index "total fissures" opening Rs01", mm after blasting

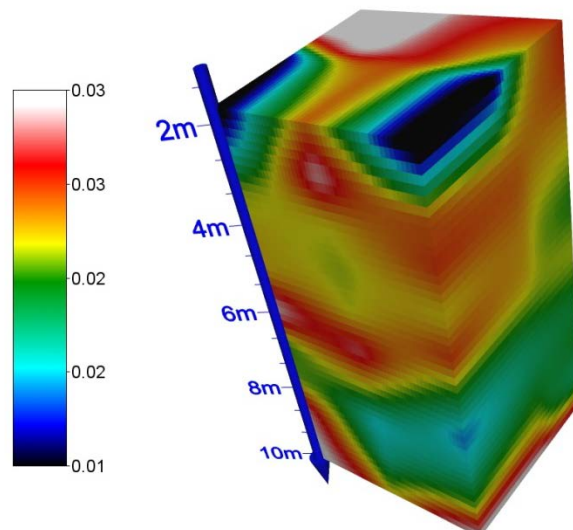


**Figure 2.2.10.16:** Changes of the values of the index "total fissures' opening  $\Delta \triangleleft$  Rs", mm - difference between measurements before and after blasting

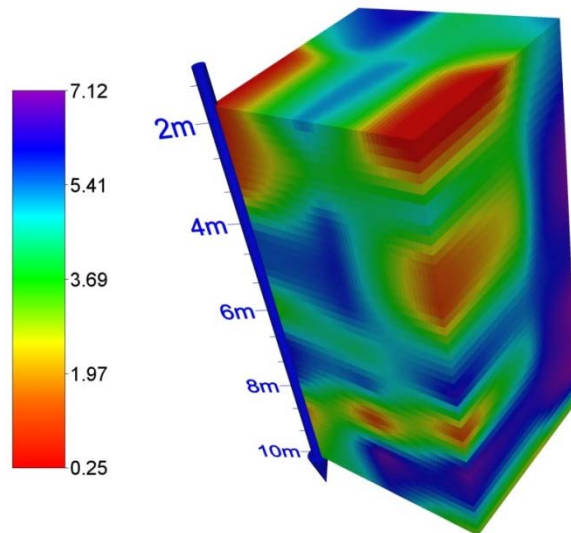


**Figure 2.2.10.17:** Value of the index „borehole equivalent fissure S0” mm<sup>2</sup> before blasting

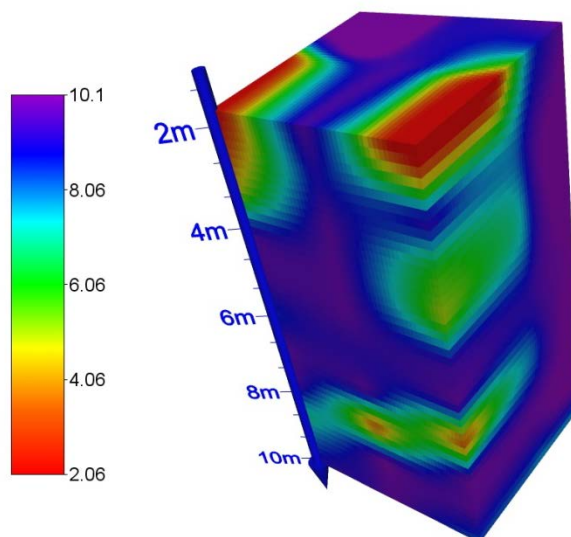


**Figure 2.2.10.18:** Value of the index „borehole equivalent fissure S0” mm<sup>2</sup> after blasting

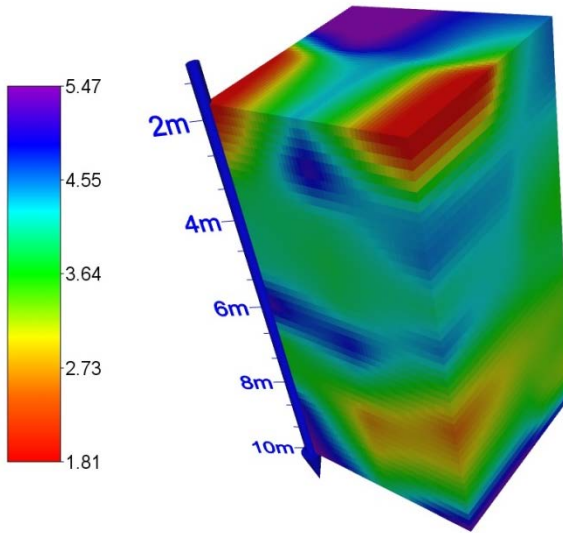


**Figure 2.2.10.19:** Changes of the index „borehole equivalent fissure  $\Delta S$ ”  $\text{mm}^2$  - difference between measurements before and after blasting

#### In situ tests in Zofiówka mine

In situ tests aimed at checking the possibility of performing disintegration blasting were carried out in Zofiówka Mine. The place of research was gate road D-2 in the coal seam 412 (Figure 2.2.10.20).

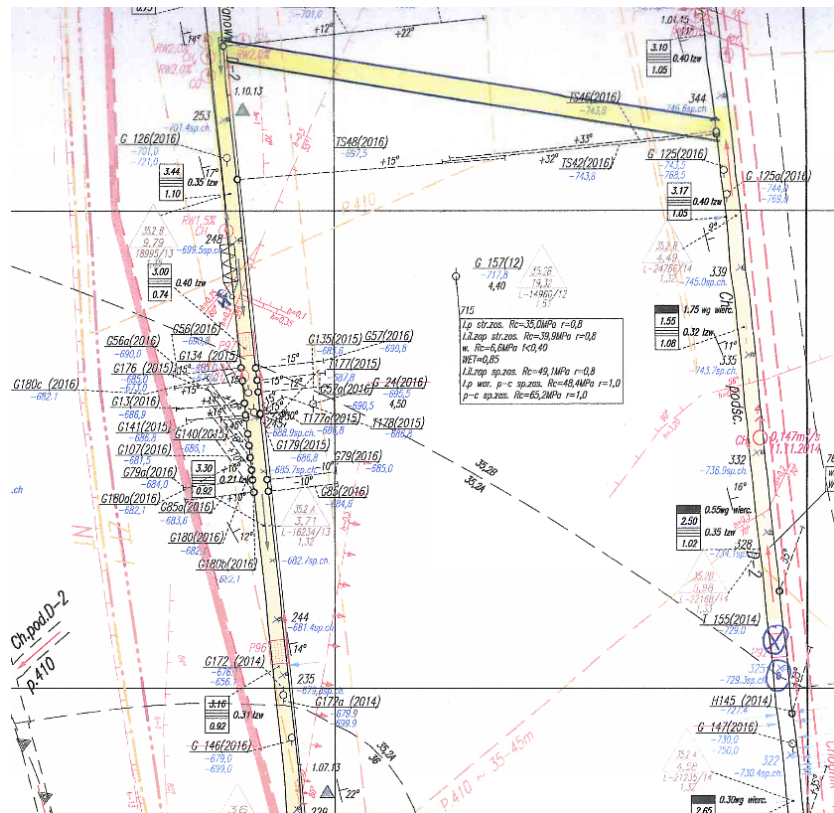


**Figure 2.2.10.20:** Area of underground research in the coal seam 412 in Zofiówka mine

Figure 2.2.10.21 (red rectangles - dust barriers, continuous blue line - dusting zone, broken line – protected zone) presents a diagram of the distribution of explosion-proof firewalls and protection zones against the coal dust in the area of performed shooting tests.

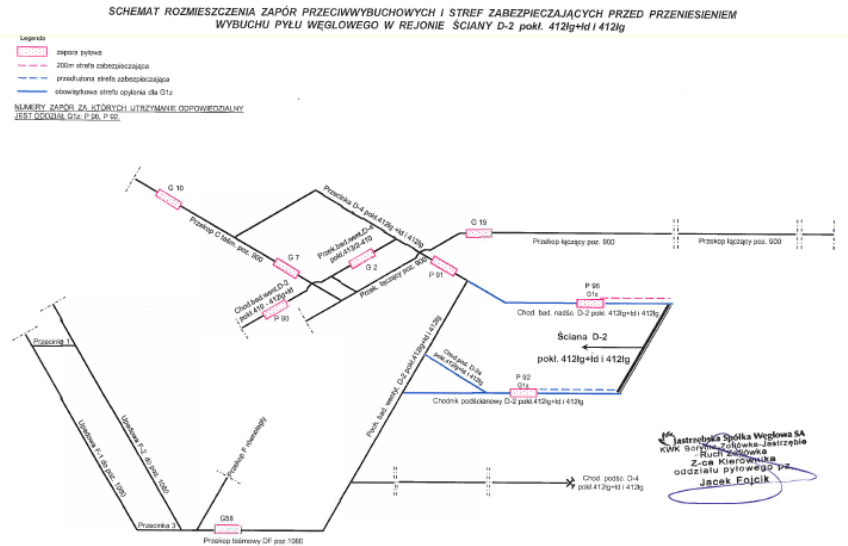


**Figure 2.2.10.21:** Scheme of explosion protection for excavations of the research area

In the mining industry, shooting aimed at destroying the rock/coal structure is commonly used. In this case, the blasting works were made on special rules both as to the construction of the load, the place of its fixing in the borehole and the blasting technique. Shooting was carried out especially for this purpose prepared explosive. The construction of explosive charge is shown in Figure 2.2.10.22 Designed to test the explosive charge is linear, and its elements are:

1. Explosive Emulinit PW produced by Nitroerg (described in charter 2) tested on the surface, and applied to a shooting tests in excavations in Barbara Mine.
2. LD - detonating cord
3. ZE –electric detonator 0.2A millisecond

For the stabilization of the detonating cord an insulating tape was used. The initiation of the explosive followed the electronic exploder ZK-100 of the explosive initiation unit MW, i.e. the triple thread of the detonating cord and two electric detonators surrounded by a clays.

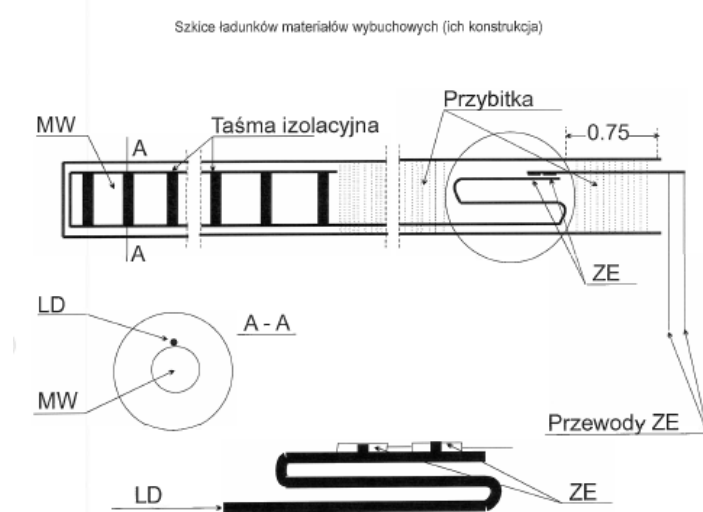


**Figure 2.2.10.22:** Sketch of the elements of the explosive charge



**Figure 2.2.10.23:** Explosive charge ready for use



**Figure 2.2.10.24:** Underground test stand

According to the standard blasting specification, the blast borehole is filled with wadding for a minimum of 30% of its length, while the remaining part fills the explosive. The specificity of blasting in Zofiówka mine conditions resulted from the necessity to blast in the drainage borehole. The length of the borehole with a diameter of 65 mm was 29.5 m. In the borehole, 8 slots with a diameter of about 0.6 m were made by hydraulic method at intervals of approx. 2 m. The borehole in the initial section was equipped with a steel casting pipe with a diameter of 80 mm and 6 m length with a collar for connection to the methane separating network. The blast specification developed for the tests assumed the maximum volume of the explosive in the amount of 900 grams, which gives about 700 dm<sup>3</sup> volumes of gaseous products of explosion. The explosive charge was located at a distance of about 12.5 m from the heading of the excavation, which was tantamount to leaving an empty section 17 m. The total void volume, i.e. the unfilled hole and 8 slots, was approximately 68.2 dm<sup>3</sup>. The specificity of blasting was its execution in such a way that the dynamics of post-blast gases would affect both the coal seam surrounded by the explosive but also, through slots, into its further parts.

### Conclusions

Underground tests in the domain of fracturing 310 coal seam in Experimental mine „Barbara” were performed based on the directional fracturing method using aerometric and endoscopic methods. Obtained results confirmed significant destruction of the seam structure.

Endoscopic method using borehole camera confirmed arising numerous discontinuities (fissures and stratifications) in the monitoring boreholes drilled after blastings.

Based on the tests using aerometric method fracturing of the seam after its destruction with the explosives was recognized. Measurement by aerometric probe performed in the coal seam of Experimental mine „Barbara” enabled determination of the following parameters:

- Borehole equivalent fissure  $S_0$ , [mm<sup>2</sup>],
- Fissuration index  $K_s$ , [% or ‰],
- Total fissures' opening  $R_s$ , [mm].

for the 310 coal seam when undisturbed and after its fracturing using blasting technique/with the explosives [Koniczek, Konecny, Ptacek, 2011]. Obtained results indicate, that applied blasting technique for future borehole stimulation in order to achieve higher methane desorption is effective [Drzewiecki, 2004; Krause, Smoliński, 2013]. Application of explosive charges designed with their directional location according to performed initial fractures resulted in significant increase of fractures zone range after blasting. It can be assumed then, that reproduction of this technique of seam destruction will result in increased intensity and range of seam fracturing and in consequence much bigger volume of coal would be opened for desorption of methane.

Achieved results of observation using endoscopic camera and values of indexes  $K_s$ ,  $S_0$  and  $R_s$  graphically shown on the figures 12÷20 clearly indicate, in what range applied blasting technique caused opening/fracturing tested part of the seam. In order to elaborate coal seam drainage technique significant parameter is  $K_s$  and especially the areas where its value is lower than 0.2 %. As shown on the figures 12÷14 in consequence of applied stimulation technique of the seam with explosives volume of the seam where  $K_s$  exceeded value 0.2 % was significantly increased. It means, that after its application the seam was average and heavily fractured, what was the goal of proposed method.

#### 2.2.11. WP4, Task 4.2 Application of large scale stimulated drainage of methane at multi-seam longwall mining layouts at JSW (led by JSW, GIG, IMPERIAL)

Under task T4.2 sequence of tests were performed. They covered by its scope following activities:

- Drilling of testing boreholes,
- Checking their patency and sides' observation using camera,
- Performing of aerometric tests,
- Performing of the slots using hydraulic cutting method,
- Second testing of boreholes' interior using camera,
- Second aerometric testing in the slots' locations,
- Observations of boreholes' interiors after fracturing using camera,
- Another aerometric tests.

In February 2016 in the testing tail gate D-2, in the coal seam 412g+Id first 4 testing boreholes were drilled: G56(2016), G56a(2016), G57(2016) and G57a(2016).

Boreholes had 105 mm diameter and were about 30m long, they were drilled in couples in the middle of coal seam thickness, on both sides of the testing tail gate D-2. In the boreholes G57(2016) and G57a(2016) inspection by endoscopic camera appeared to be not possible as they were totally filled with mixture of coal cuttings and water. It was assumed that it was result of old gob close vicinity of overlying 410 coal seam, which was filled up with backfilling. Boreholes G56(2016) and G56a(2016) were obstructed due to downfalls. Two trials of cleaning them were not successful at all. Considering above it was decided to move from the edge of 410 coal seam and drilling another 2 boreholes: G85(2016) and G85c(2016) above the dam. They had 65mm diameter and about 30m each. However they also lost their stability after 3 days since they were drilled. Trials to clean them also failed.

Considering above experience it was decided to drill the borehole G107(2016), which was done at the border of 412 coal seam ceiling. Above borehole had 65mm diameter and length of 30m. As it kept its stability, it was decided to drill another 4 boreholes: G180, G180a, G180b, G180c with similar parameters. Their location was shown at Figure 2.2.11.1.

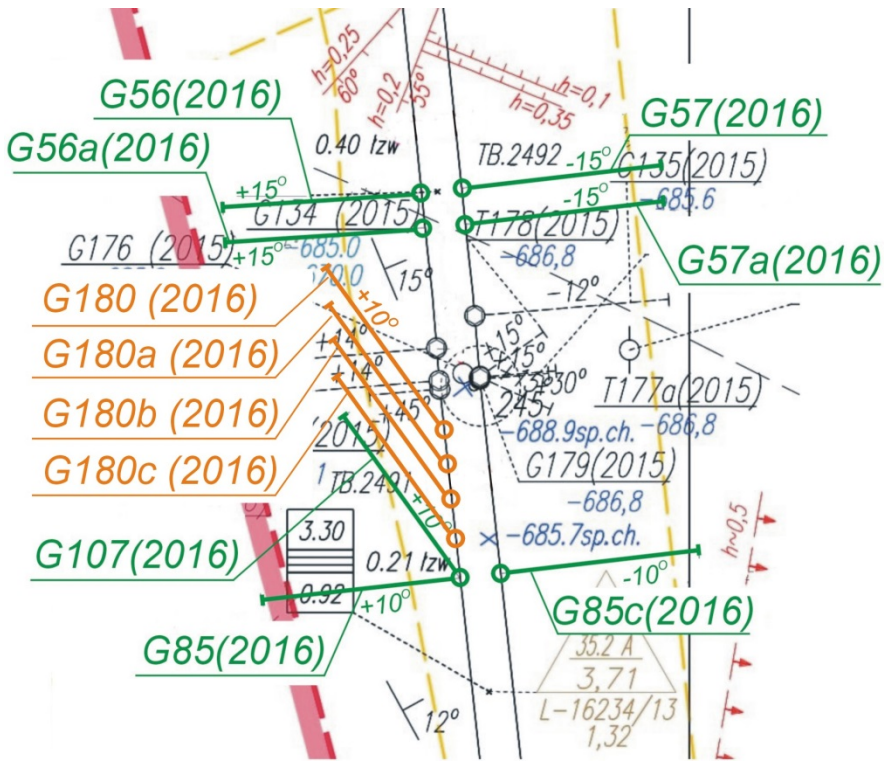


**Figure 2.2.11.1:** Location of test boreholes drilled from the testing tail gate D-2" in the seam 412lg+ld

Layout of boreholes with slots and measurement system was shown below (Figure 2.2.11.2)

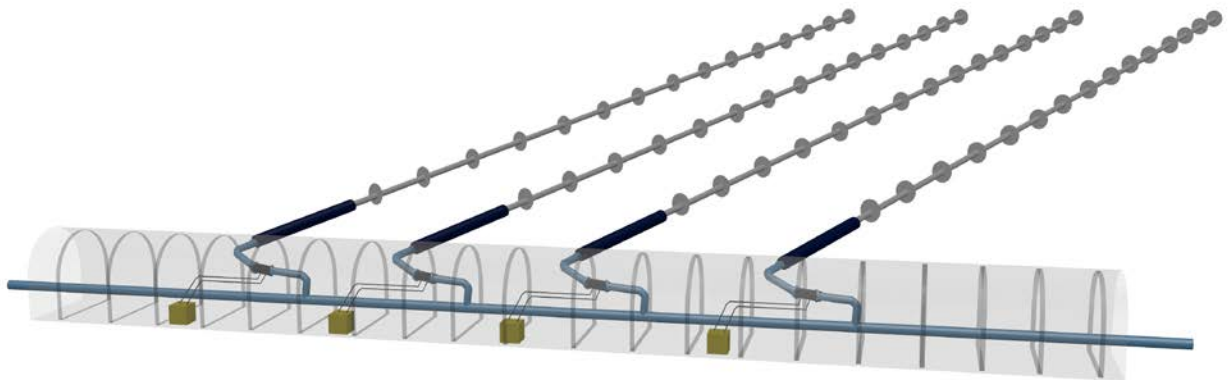


**Figure 2.2.11.2: Layout of boreholes with slots and measurement system**

In these boreholes (G180, G180a, G180b, G180c) patency and endoscopic tests (observations of their sides using camera) were performed. Endoscopic tests were performed directly after drilling (Table 2.2.11.1).

**Table 2.2.11.1:** Results of endoscopic tests performed in the boreholes directly after drilling.

Number of borehole	Commentary
G180(2016)	Total length of the borehole 28.7m, length of conductor pipe 5.2m. Borehole at all its length is located in the ceiling rocks of the seam, occurrence of mudstone and sandstone. Side of the borehole smooth along its length, without cracks and gaps. Borehole was penetrated along its length.
G180a(2016)	Total length of the borehole 29.95m, length of conductor pipe 5.2m. Till its 13m from the inlet occurrence of mudstone and coal by turns. Side of the borehole uneven and heavily cracked. Deeper occurrence of mudstone, side of the borehole heavily cracked, occurrence of significant gaps and has loose rock fragments. Test was performed at the depth of 15m, where the jam in the borehole was recognized.
G180b(2016)	Total length of the borehole 30.2m, length of conductor pipe 5.5m. Till its 10,5m from the inlet occurrence of mudstone and coal by turns. Side of the borehole smooth, sporadically cracked. From depth of 10.5m occurrence of mudstone, side of the borehole smooth. Borehole was penetrated along its length.
G180c(2016)	Total length of the borehole 30.5m, length of conductor pipe 5.3m. Till its 12m from the inlet occurrence of coal and mudstone intrusions. Side of the borehole smooth along its length, without cracks and gaps. From the depth of 12m occurrence of mudstone, side of the borehole smooth, without cracks. Borehole was penetrated along its length.

After endoscopic tests into each of the boreholes ZCO sensor was hooked up, in order to perform measurements and registration of the parameters of collected gas. More detailed description of ZCO sensor is in the point concerning WP5.

Subsequently, the boreholes were connected with methane drainage pipeline depression. Concentration of collected methane from the boreholes (without seam stimulation) was between 1.5-2%. Exemplary results from obtained ZCO sensor parameters' registration were shown on below graph (Figure 2.2.11.3).

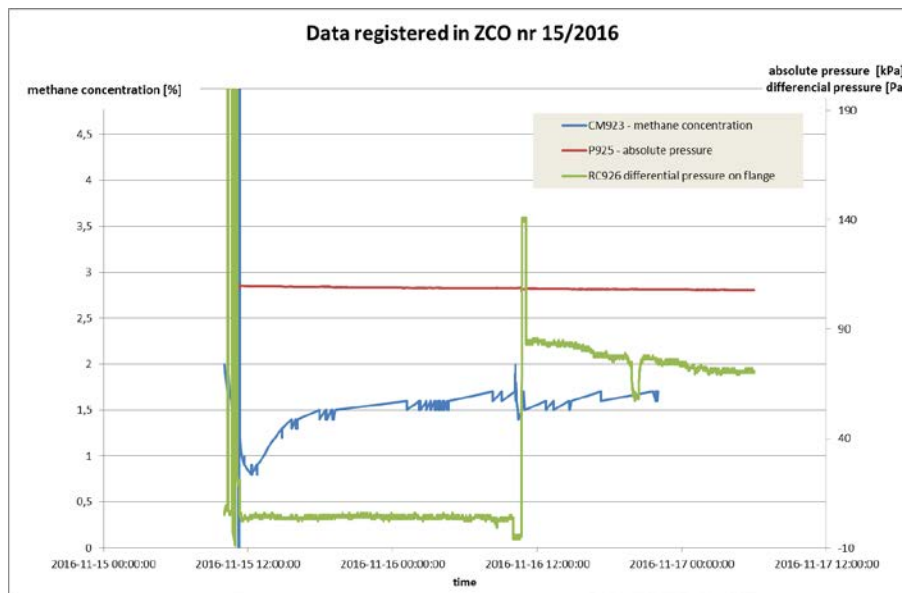


**Figure 2.2.11.3:** Exemplary results from obtained ZCO sensor parameters' registration.

After finishing gas registration ZCO sensors got disconnected, and the preparatory works to boreholes' stimulation (slotting) started. Their scope covered:

- Connecting of the system into hydro slotting (installations: high water pressure, hydraulic and electrical).
- Setting up of USO-1 equipment in the way, to allow axiality of the borehole with portable tool.
- Arranging of the borehole's conductor pipe extension – to cover high pressure rods and to operate them in the pipes at longest possible section.
- Conducting test of the equipment and stabilizing their fixing.

➤ Assembling and introducing set of 34 high pressure rods to the borehole.  
 Technical design of slotting procedure assumed performing sequence of cutting several scores with high pressure water jet in the zone adjacent to the borehole. Below scheme shows method of slotting in the borehole G180b(2016), Figure 2.2.11.4.

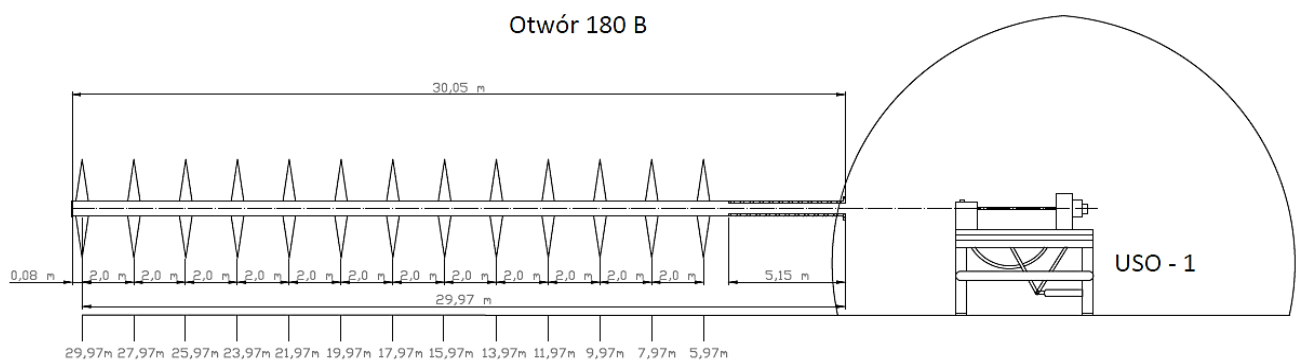


**Figure 2.2.11.4:** Scheme with the method of slotting in the borehole G180b(2016)

Slotting was made in the following way: starting 5cm from the bottom, and each following slot was made 2m closer i.e. after each operation set of the rods was shortened by 2 pcs. After performing four slots set of the rods was taken off in order to check correct operation of the jet nozzle. It was due to its malfunction suspicion (lack of black water outflow with coal partitions from the borehole). Check test confirmed its correct operation. Cutting of one slot (rotating cutting) took about 3 min. Pressure during slot cutting was 1000 bars (100 MPa). To assure most effective hydro slotting range ceramic nozzle with 2.1mm was used (operation time about 40min).

Course of individual slotting stages was without any obstacles.

Before starting stimulation of another borehole (G 180a) the outlet nozzle was replaced into new-one, the same type (ceramic-one) with the same diameter (2.1mm). Individual preparatory works stages were the same as in case of 180b borehole.

Slotting procedure was performed in all 4 boreholes: G180, G180a, G180b, G180c. Before and after conducted procedures aerometric tests were performed in all boreholes and their results were shown on figures below and in the collective Table 2.2.11.2).

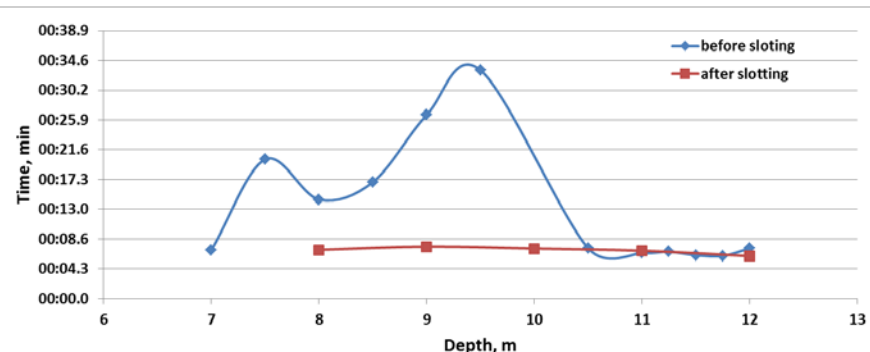


**Figure 2.2.11.5:** Results of aerometric tests in the experimental borehole G180c (2016) before and after slotting.

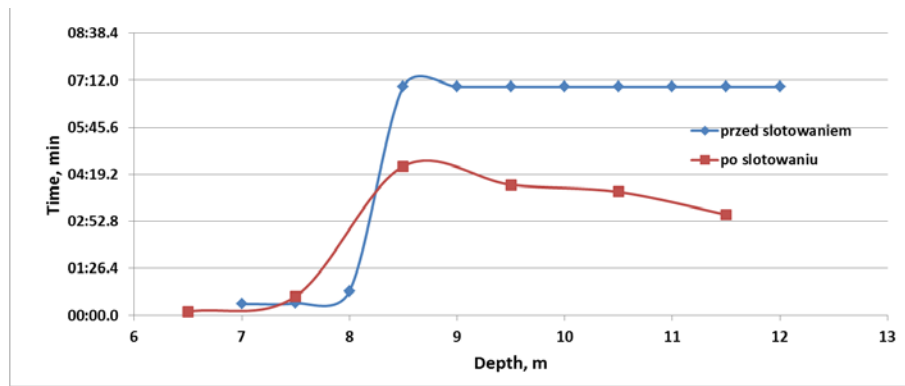


**Figure 2.2.11.6:** Results of aerometric tests in the experimental borehole G180 (2016) before and after slotting.

Collective summary of the aerometric tests results conducted in the experimental boreholes before and after slotting is presented in the table below (Table 2.2.11.2).

**Table 2.2.11.2:** Collective summary of the aerometric tests results conducted in the experimental boreholes before and after slotting.

Borehole #	Commentary
G180(2016)	Borehole was tested using aerometric probe at its length of 5.5m before and after slotting. In case of testing after slotting, measurement points were located based on the reported position of the slots.
G180a(2016)	Borehole not suitable for testing with the use of aerometric probe due to extensive gaps and losses.
G180b(2016)	Borehole in the course of tests using aerometric probe after slotting
G180c(2016)	Borehole was tested using aerometric probe at its length of 5 m before and after slotting. Measurement points were performed based on the tests using borehole camera.

After performing the tests boreholes (G180, G180a, G180b, G180c) were connected with coal mine drainage pipeline, what was shown on below figures: (Figure 2.2.11.7 and 5.5.2.9).



**Figure 2.2.11.7:** View of the cheek with the methane drainage installation connected into 180b borehole



**Figure 2.2.11.8:** View of the collar of conductor pipe of the experimental borehole 180b with its extension

After the slotting procedures, boreholes were locked until renewed connecting integrated ZCO drainage sensors and arranging necessary connections with the mine drainage pipeline. After fulfilling above technical conditions boreholes were connected with depression of the pipeline and ZCO equipment was tested. Technical acceptance protocol was prepared and executed by representatives of GIG, Zofiówka mine and EMAG serwis.

Principal parameters registered by ZCO were: pressure, gas volume and percentage methane content in the place of fixing.

After performing slotting procedures integrated drainage sensors ZCO were again hooked up to the boreholes and the depression of coal mine drainage installation was set. Then operational test of ZCO equipment was performed. Based on above technical acceptance protocol was prepared and executed by representatives of GIG, Zofiówka mine and EMAG serwis.

After hooking up the boreholes to drainage pipeline and starting the registration in ZCO test of installation was started. Principal registered parameters were: pressure, gas volume and percentage methane content in the place of fixing as well as temperature and moisture.

Exemplary results of methane intake from the experimental boreholes: G180, G180a, G180b, G180c were obtained from Zofiówka mine methane measurement system and their results were shown at three collective graphs (Figure 2.2.11.9 - 4.4.11.11). Each graph is based on the results obtained from individual borehole:

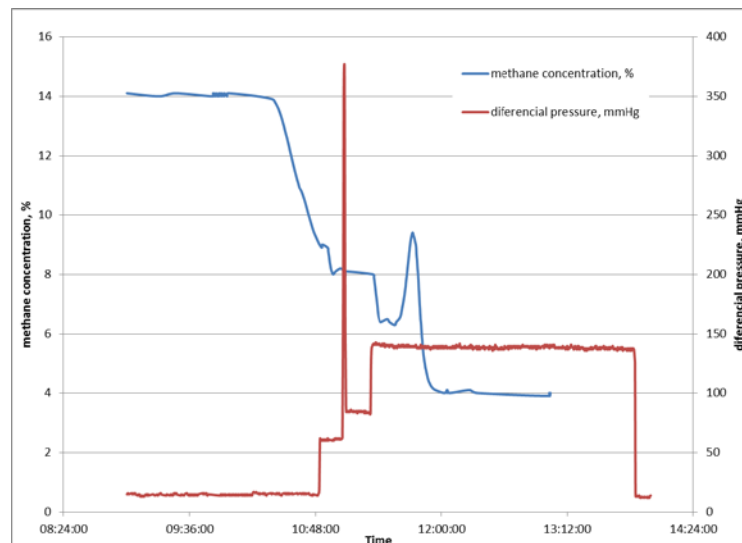


**Figure 2.2.11.9:** Exemplary results of methane intake from borehole G180a

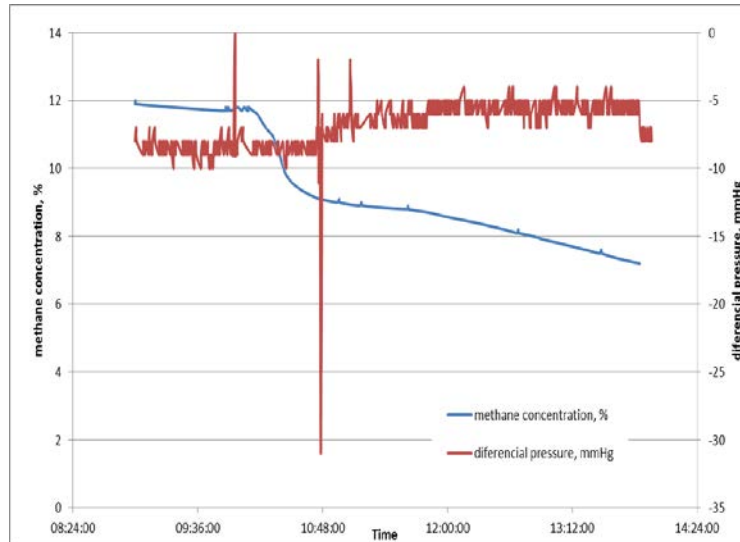


**Figure 2.2.11.10:** Exemplary results of methane intake from borehole G180b

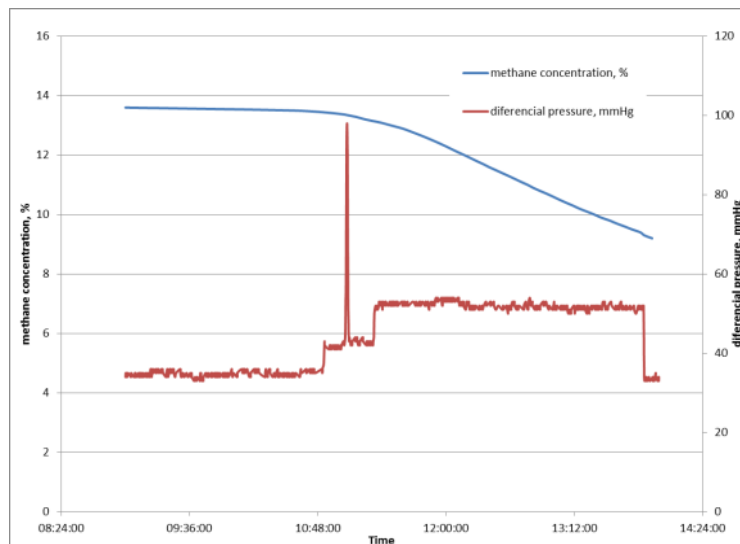


**Figure 2.2.11.11:** Exemplary results of methane intake from borehole G180c

At graph Figure 2.2.11.9 (# G180a) within 3 hours' time methane concentration drops from 14% down to 4%. Due to very low depression of coal mine drainage pipeline, volume of collected gas was relatively low. Using such a low depression resulted from the safety to avoid getting into the system mixture with too low methane concentration. Polish mining regulations prohibit introducing into the collective pipeline gas mixture with methane concentration lower than 20%.

Apart from that, perturbed reading of differential pressure at measurement flange unabled correct reading of collected methane volume.

#### Tests in situ in Zofiówka mine in district G

Tests in test site in main gate D-2 was stopped due to approaching of longwall face and change of ventilation scheme from 'U' to 'Y' scheme, increasing concentration of equipment and impossibility of any active research activity in the area.

Another test site has been established in G district, in opening in neighbourhood of rail drift F and conveyor drift F. Map of the test site location and designed set of boreholes is presented in Figure 2.2.11.12.

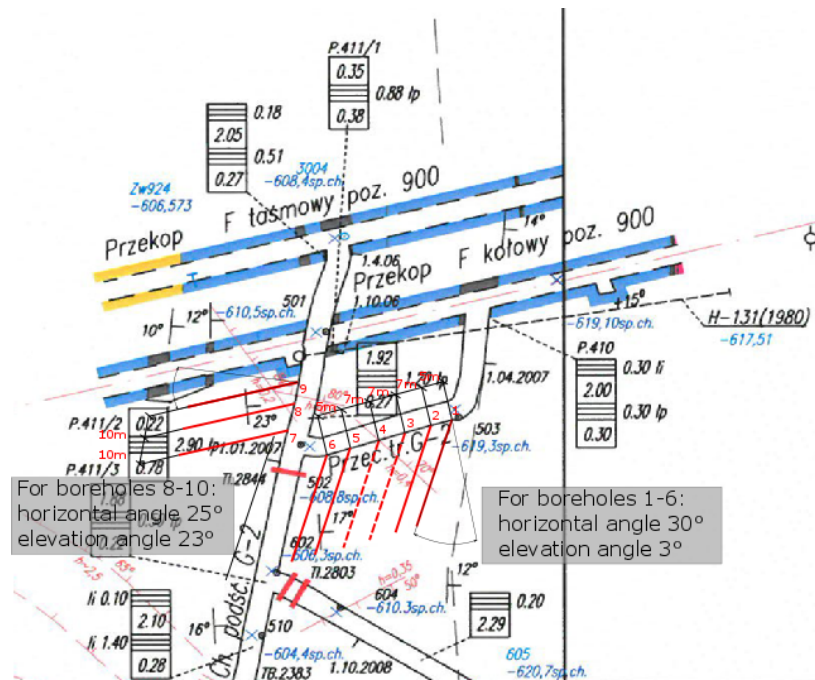


**Figure 2.2.11.12:** Design of the test site in district G - transportation cross cut G-2(seam 410, level 900 m).

This report covers all underground actions and hydro slotting (hydraulic cutting method) tests performed in the boreholes drilled at „Zofiówka” mine in 2017 in the GasDrain project. Under task 4.2 sequence of tests were performed. They covered by its scope following activities:

- Drilling of testing boreholes,
- Checking their patency and sides' observation using camera,
- Performing of aerometric tests,
- Performing of the slots using hydraulic cutting method.

#### Drilling of testing boreholes.

In 2017 for the GasDRAIN purposes twenty (20) boreholes were drilled in “Zofiówka” underground mine in the transportation cross cut G-2. Whole boreholes with parameters are listed below (Table 2.2.11.3).

**Table 2.2.11.3:** List of twenty (20) boreholes drilled in “Zofiówka” mine (cross cut G2).

No	Name	Parameters / direction	Borehole:		length of casing [m]	ø diameter casing [mm]	trail of tightness [Mpa]	date of drilling	
			length [m]	ø diameter [mm]				start	end
1	G115/17	+45° perpendicularly according to design	15.0	65	6.00	80	0.5	13.06.2017	14.06.2017
2	G115a/17	+30° perpendicularly according to design	12.0	65	3.00	80	0.5	29.06.2017	03.07.2017
3	G115b/17	+60° perpendicularly according to design	12.0	65	3.00	80	0.5	28.06.2017	28.06.2017
4	G115c/17	+90° perpendicularly according to design	12.0	65	3.00	80	0.5	28.06.2017	29.06.2017
5	G115d/17	+30° 30° right / perpendicularly	12.0	65	3.00	80	0.5	29.06.2017	03.07.2017
6	G115e/17	+45° 30° right / perpendicularly	12.0	65	3.00	80	0.5	30.06.2017	04.07.2017
7	G115f/17	+60° 30° right / perpendicularly	12.0	65	3.00	80	0.5	30.06.2017	04.07.2017
8	G115g/17	+30° 30° left / perpendicularly	12.0	65	3.00	80	0.5	29.06.2017	05.07.2017
9	G115h/17	+45° 30° left / perpendicularly	12.0	65	3.00	80	0.5	30.06.2017	05.07.2017
10	G115i/17	+60° 30° left / perpendicularly	12.0	65	3.00	80	0.5	03.07.2017	05.07.2017
11	G128/17	-15° 45° left / perpendicularly	10.0	95	3.00	150	0.5	10.07.2017	14.07.2017
12	G150/17	+30° 40° left / perpendicularly	12.0	65	3.00	80	0.5	11.08.2017	16.08.2017
13	G150a/17	+45° 40° left / perpendicularly	12.0	65	3.00	80	0.5	10.08.2017	16.08.2017
14	G150b/17	+60° 40° left / perpendicularly	14.0	65	3.00	80	0.5	10.08.2017	16.08.2017
15	G156/17	+5° 20° right perpendicularly	6.0	rdz. 76	6.00	100	0.5	21.09.2017	21.09.2017
16	G156a/17	+5° 20° right / perpendicularly	6.0	rdz. 76	6.00	100	0.5	22.09.2017	22.09.2017
17	G158/17	+6° 30° right / perpendicularly	36.0	rdz. 76	6.00	100	0.5	28.09.2017	04.10.2017
18	G158a/17	+6° 30° right / perpendicularly	36.0	rdz. 76	6.00	100	0.5	06.10.2017	12.10.2017
19	G158b/17	+3° 30° right / perpendicularly	36.0	rdz. 76	6.00	100	0.5	20.10.2017	24.10.2017
20	G167/17	+3° 30° right / perpendicularly	36	95	6.00	100	0.5	25.10.2017	27.10.2017

#### Checking their patency and sides' observation using camera.

In these (above mentioned) boreholes patency and endoscopic tests (observations of their sides using camera) were performed. Results of endoscopic tests performed in the boreholes directly after drilling are described in WP5. After endoscopic tests into each of the boreholes ZCO sensor was hooked up, in

order to perform measurements and registration of the parameters of collected gas. More detailed description of ZCO sensor is in the point concerning WP5.

#### **Performing of the slots using hydraulic cutting method.**

In the middle of 2017 whole equipment (pump unit, USO-1, rods, etc.) and measurement systems **has been moved from the testing tail gate D-2 (in the coal seam 412lg+ld) to the transportation cross cut G-2 (in seam 410, level 900 m).**

From September till December 2017 in the transportation crosscut **G-2**, in the coal seam 410 first two (2) testing boreholes were drilled: borehole G-167 (lower) and borehole G-158b (upper). Their location is shown below at Figure 2.2.11.13.

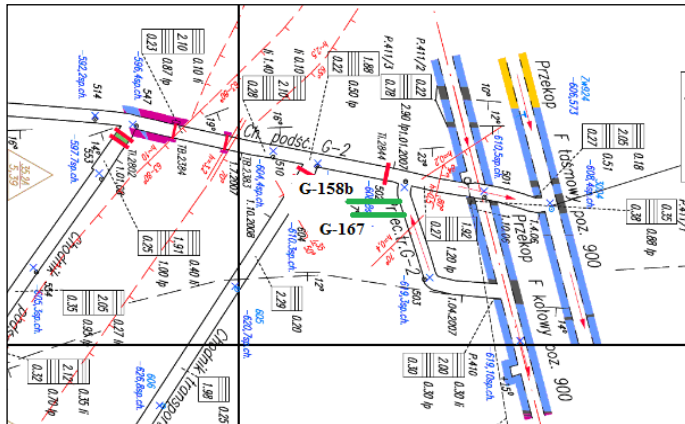


**Figure 2.2.11.13:** Location of testing boreholes: G-167 (lower) and G-158b (upper) drilled in the transportation crosscut G-2, seam 410, level 900 m.

#### **Parameters of the testing boreholes G-167 (lower) and G-158b (upper):**

##### **Borehole G-167 (lower):**

- length 36 m
- diameter 96 mm
- incline 3-5°
- depth of casing 5.20 m

##### **Borehole G-158b (upper):**

- length 35 m
- diameter 96 mm
- incline 3-5°
- depth of casing 5.20 m

In October and November 2017 mining team from GIG Experimental Mine "Barbara" performed the research stage in the **transportation crosscut G-2**. The aim of the work was to stimulate research boreholes: G-167 and G-158b, using hydro-slitting equipment with the use of special rubber hoses protecting the boreholes against downfall. The necessity of using hoses resulted mainly from the earlier tests of the conditions in the boreholes.

#### **Tasks and actions carried out under hydro-slitting operation:**

The inspections and maintenance of test equipment installations were carried out in accordance with the instructions and agreements with Tech-Trading Company.

The measurements of the holes G-167 and G-158b (length and depth) were made.

The boreholes were cleaned - their patency was checked with wooden poles.

After the inspection, the openings were certified to enter the rubber hoses protecting the boreholes.

In the case of the G-158b (upper) borehole at a distance of about 10m from the beginning of the borehole, difficult conditions were found (the borehole was obstructed).

Rubber hoses were installed to secure the boreholes down to the depth of: 22.5 m in case of the G-167 (bottom) and 20m for G-158b (upper).

The stimulation work in the coal seam with the use of hydro-slitting technology was carried out in the hole G-167 (bottom) in a following way:

- installation of hydro-slitting equipment (high water pressure and electricity),
- the USO-1 device has been installed so that the axis of the sliding device is in the line with the borehole axis,
- equipment tests and stabilization were made (foundation was secured),
- column of 36 high-pressure rods were put in into the borehole.

Stimulation of the G-167 borehole was performed in the bare section of the borehole (without casing), starting approx. 2 m from its bottom (34 m), and the next slot 2 m closer (32 m) - see Figure 2.2.11.14.

- Stimulation time (execution of one slot) - 3 min.,
- High Pressure during the slotting: 1000 Bar (100 MPa),

- Outlet nozzle type - ceramic with a diameter of 2.1 mm (new one).

The course of the stimulation operation in a borehole G-167: the first slot at depth of 34m ran initially (about 20-30 seconds) without any problems. After this time, the amount of water outflow from the borehole decreased, which was probably caused by its clogging.

Technical design of slotting procedure assumed performing sequence of cutting several slides with high pressure water jet in the zone adjacent to the borehole. Below scheme shows method of slotting in the boreholes: **G-167 (lower)** and **G-158b (upper)**, Figure 2.2.11.14.

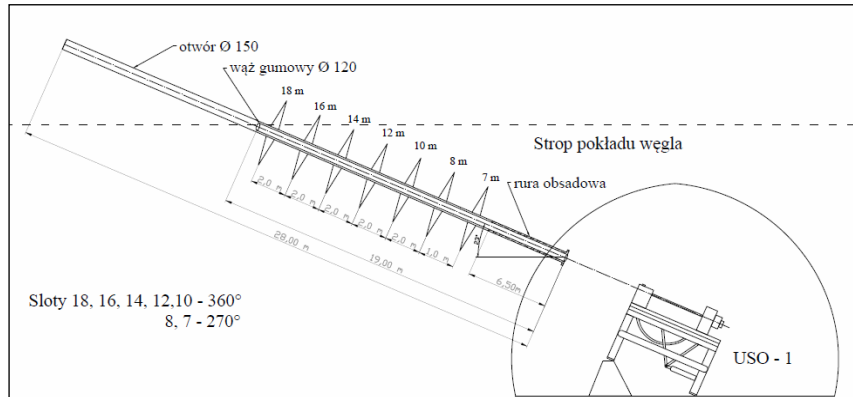


**Figure 2.2.11.14:** Scheme of the slotting method applied in the boreholes G-167 and G-158b

Difficulties with the effortless removal of pieces of coal with water from the borehole caused pressure increase and "clamping" of the rods in the borehole causing resistance during its rotation. The increase in the pressure of the water inside the hole also caused a sealing of the produced "plug". Increase of water pressure inside the borehole resulted in the sealing in of the produced plug consisted of the coal cuttings in the borehole, what made characteristic crack noises coming out of the borehole. In consequence of above the individual connections of the drilling rods were tighten very heavily what resulted in changing the size parameters of the connections. An attempt to withdraw the roads column from the borehole to perform another slots operation (at 32 m) required several strokes of the column to loosen it. Attempts to shorten the rods column (disassembly of two rods) took place with the use of very high force. Also in this case (32m) the hydroslotting operation of coal seam caused the same difficulties and technical hazards - just like for the first slot.

The total amount of water injected into each of the boreholes at a given pump flow (80 l/min) can be estimated at approx. 100 - 120 l. After the slotting operation (32m), due to the problems and risks mentioning earlier, it was decided to make another slot in the protected by "hose" borehole section.

First of all it required shortening column of rods by about 10 – 12m. The attempt to pull out the column of the rods from the borehole was not successful – the force used to pull out the column of rods from the borehole resulted in breaking it apart at one of the threat connections Figure 2.2.11.15. This situation may result from weakening some of the connections due to above factors. Later on the remaining part of the column was pulled out (about 21 m) – using very high force to unscrew each of the individual rods. After installing the jet/nozzle (2.3 mm), the column of rods was screwed again and entered into the borehole to place the outlet of the nozzles at its 20 m length. Unfortunately the course of the process was similar to the previous-one and it can be characterised by clogging the borehole and tightening the column of rods as it happened before.

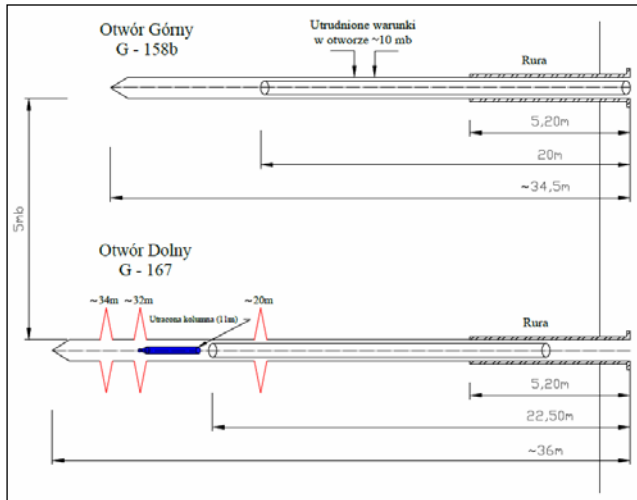


**Figure 2.2.11.15:** Borehole G-158b after completing the slotting.



**Figure 2.2.11.16:** Setting of USO-1 and Limited outflow of water from the borehole

In these boreholes **G-167 (lower)** and **G-158b (upper)** patency and endoscopic tests (observations of their sides using camera) were performed. Endoscopic tests were performed twice: directly after drilling and after hydroslotting.

After endoscopic tests into each of the boreholes ZCO sensor was hooked up, in order to perform measurements and recording of the parameters of collected gas.

Till the end of year 2017 seven (7) out nine (9) boreholes were made and four (4) of them were slotted as presented in Figure 2.2.11.17.

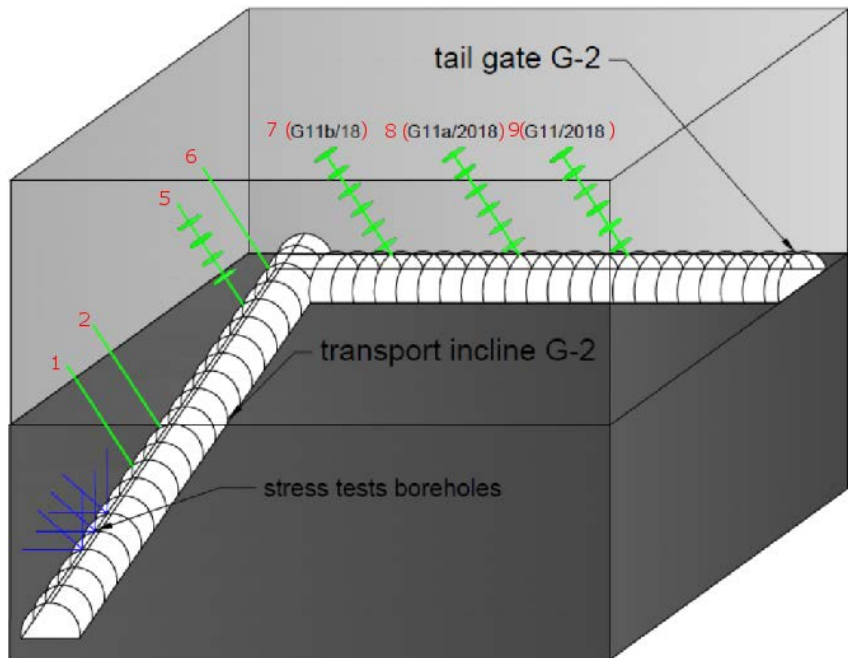


**Figure 2.2.11.17:** The real layout of the boreholes with slots performed in district G - the transportation cross cut G-2 (in the new test site).

Boreholes 1 and 2 were made as explanatory with no any special equipment or treatment except conductor pipes in first 6 meters. Next two boreholes no 5 (G-167 according to internal mine's numeration) and 6 (G-158b) were drilled with diameter of 96 mm, 36 m long with 6 m conductor pipe and then a 30 m long rubber hose (Figure 2.2.11.18 and Figure 2.2.11.19) with internal diameter 63 mm were inserted to preserve its stability and patency.

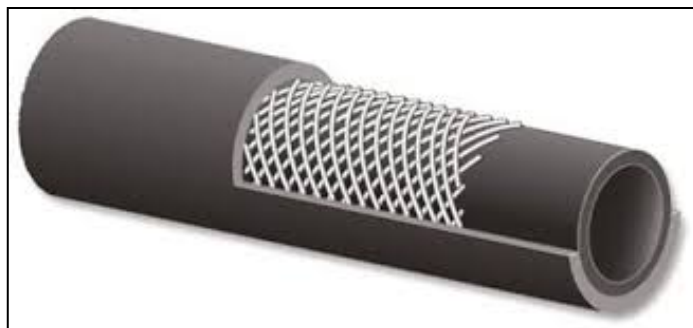


**Figure 2.2.11.18:** Rubber hose used to case slotted borehole



**Figure 2.2.11.19:** Introducing rubber hose to the borehole

First tests of hydroslotting has been performed in the borehole no 5 (G-167) - Figure 2.2.11.17. During hydroslotting process due small space between high pressure rods and rubber hose and small elevation angle 3° generated important problems with water with drilling outflow. As result push rods were occasionally blocked, water pressure was built, producing dynamic water outburst phenomenon. Due to high risk of accidents further works were stopped and another boreholes with different set of parameters has been developed for boreholes 7, 8 and 9 (Figure 2.2.11.17). Parameters of the boreholes were as follows:

- total length: 28 m
- length in coal seam: 14.5 m,
- borehole diameter: 143 mm,
- casing hose internal diameter: 100mm,
- casing hose length: 20 m (starting from heading's rib),
- conductor pipe's length: 6.5m,
- horizontal angle: 18°,
- elevation angle: 33°.

Hydroslotting in the boreholes were performed with no technical problems. Slots were made each 2 m (Figure 2.2.11.20). To preserve casing hose stability the slots were cut on angle ~270°, preparing it to possible future hydrofracturing. Presently the boreholes are connected to the drainage system and drainage efficiency in being monitored.

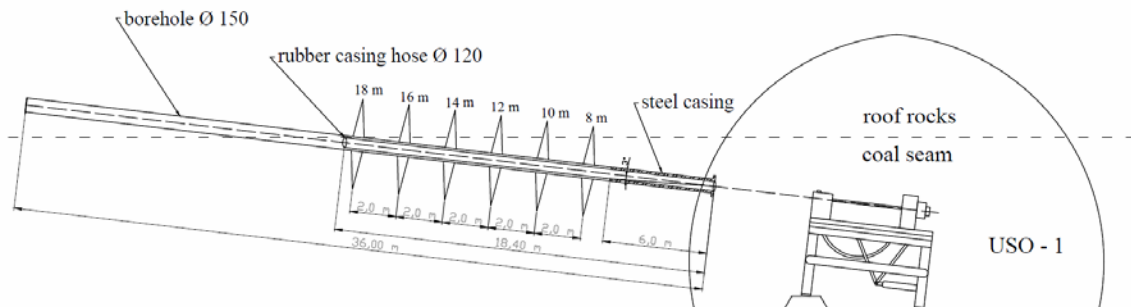


**Figure 2.2.11.20:** Schematic of hydroslotting done in one of the boreholes in tail gate G2

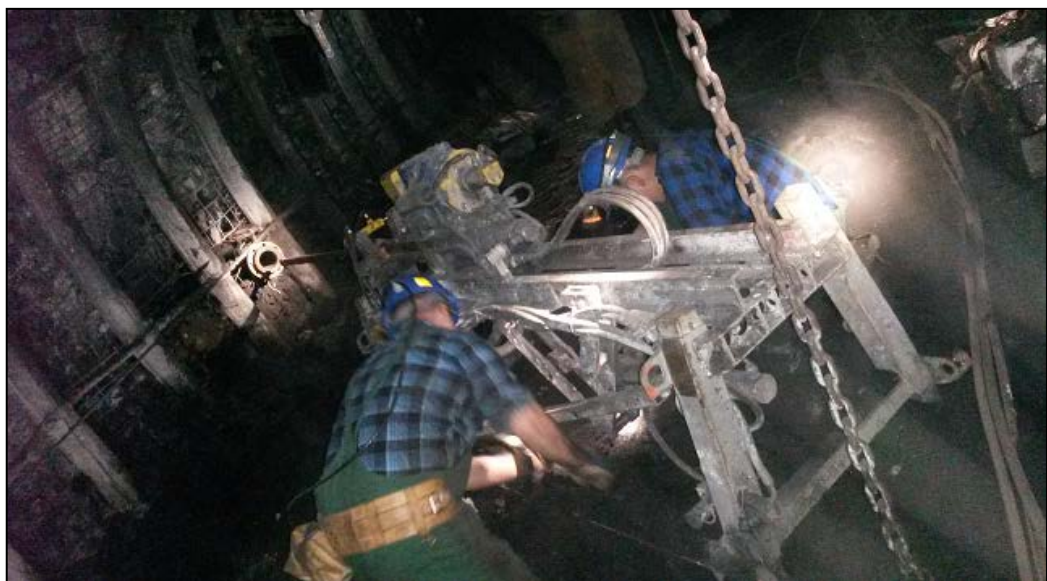


**Figure 2.2.11.21:** Slotting process in one of the borehole

In February nad March 2018 mining team from GIG Experimental Mine "Barbara" performed the another research stage in the **transportation crosscut G-2**. The main goal of the work was to stimulate research boreholes named: G11/2018, G11a/2018 and G11b/2018, using hydroslotting equipment with the use of special rubber hoses protecting

the boreholes against downfall. The necessity of using hoses resulted mainly from the earlier tests of the conditions in the boreholes. The location of three above mentioned boreholes is shown below at Figure 2.2.11.17.

### **Procedure of the tests**

The inspection and maintenance of the research equipment was performed.

The cleaning of the boreholes was done i.e. control of their patency using wooden poles connected by thread. The control confirmed patency of the boreholes allowing to introduce inside rubber hoses protecting the boreholes. In case of G11a/2018 borehole at its depth of about 15 meters some problems were recognized (collapsing of the borehole).

The rubber hoses were introduced at certain depths according to the description of the boreholes' parameters and below figures (Fig. 3, 4 and 5)

The stimulating works of the coal seam were performed using hydro-slitting technology in the following boreholes: **G11/2018, G11a/2018 and G11b/2018**. Each of the slotting was preceded by the following activities:

- the installations of : high water pressure, hydraulic and electrical were connected with hydro-slitting
- the USO -1 tool was installed in the proper way (borehole axis in line with the axis of movable part of the tool).
- tests of the individual equipment were performed including checking their fixing to foundation.

The set of 22-28 high pressure rods was manually assembled and introduced into the borehole.

### **Stimulation in borehole G11/2018**

Stimulation of the G11/2018 borehole was started, starting at a depth of 18 m, and subsequent slots at a distance of 2 m from the previous one in direction of the beginning of the borehole (16 m, 14m, 12 m, etc).

Stimulation time (execution of one slot) - 3 min.

High Pressure during the slotting: 1000 Bar (100 MPa).

Outlet nozzle type - ceramic with a diameter of 2.1 mm (new one).

The borehole was secured by rubber hoses with diameter  $\varnothing=120$  mm on a distance 19,0 m.

The following slots: 18m, 16m, 14m, 12m, 10m were performed in full rotation range ( $360^\circ$ ).

Slots 8m i 7m were performed in part-rotation range  $270^\circ$ .

The course of operation of the individual slots was characterized by the following phenomena:

- constant outflow of water without any stops and symptoms of blocking inside the borehole,
- up to 10 – 20 seconds after starting each slot the outflow of water from the rubber hose was recognized and after this time the water came out from the space between the hose and the internal side of the borehole – what gave evidence that the hose was cut by the water jet. Additionally, the water coming out has black colour and contained cuts of coal what clearly suggested performance of the slotting (cutting the coal) . After about 2.5min from the beginning of the operation the amount of cuttings in the water decreased – what may suggest finishing of the process of effective slotting.

Each slot operation was performed for 3 minutes.

Technical design of slotting procedure assumed performing sequence of cutting several scores with high pressure water jet in the zone adjacent to the borehole. Below scheme shows method of slotting in the borehole Figure 2.2.11.22.

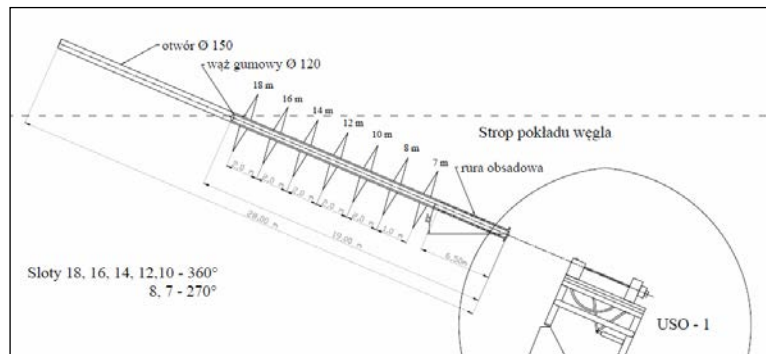


**Figure 2.2.11.22:** Situation in the borehole G11/2018 after hydroslotting

### **Stimulation of the G11a/2018**

Stimulation of the G11a/2018 borehole was started, starting at a depth of 15 m, and subsequent slots at a distance of 2 m from the previous one in direction of the beginning of the borehole (13 m, 11m, 9 m, etc).

Stimulation time (execution of one slot) - 3 min.,

High Pressure during the slotting: 1000 Bar (100 MPa),

Outlet nozzle type - ceramic with a diameter of 2.1 mm (circa 25 minutes of working time),

The borehole was secured by rubber hoses with diameter  $\varnothing=120$  mm on a distance 16m.

Slots were performed in rotation range 270 °.

The course of operations for the execution of individual slots - analogous to the hole G11a/2018, Figure 2.2.11.23.

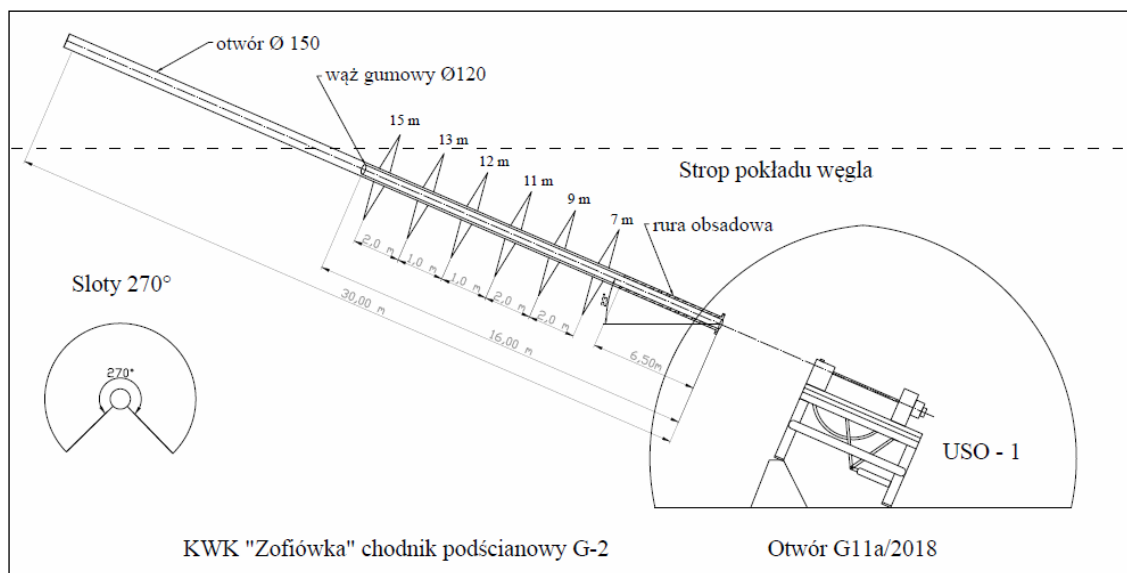


**Figure 2.2.11.23:** Situation in the borehole G11a/2018 after hydro-slotting

### **Stimulation of G11b/2018 borehole.**

Stimulation of the G11b/2018 borehole was started, starting at a depth of 22m, and subsequent slots at a distance of 2 m from the previous one in direction of the beginning of the borehole (20m, 18m, 16, etc).

Stimulation time (execution of one slot) - 3 min.,

High Pressure during the slotting: 1000 Bar (100 MPa),

Outlet nozzle type - ceramic with a diameter of 2.1 mm,

The borehole was secured by rubber hoses with diameter  $\varnothing=78$  mm on a distance 22.5m. Slots were performed in rotation range 270 °.

The course of operation of individual slots was characterized by clear differences in comparison with stimulation in boreholes G11/2018 and G11a/2018.

These differences consisted in the formation of blockages in the borehole, which prevented the free outflow of water. The time duration of gaps in the water outflow was in range from 10 to 70 seconds, followed by the phenomenon of "breakthrough" of the blockage and sudden outflow of a large amount of water with coal particles.

The lack of water outflow in the borehole during these pauses (gaps) caused a significant increase in the temperature of the rods column, which was appeared by the steam coming out of the borehole and a clear change in the operation parameters of the devices.

The observed phenomena were probably caused by using a smaller diameter of the hose securing the borehole.

During the slotting process, the water outflow was characterized by its black color and coal (small pieces) content, but it can be assumed that the slots performed in the borehole G11b/2018 (Figure 2.2.11.24), due to the difficult water outflow from the borehole, and consequently the smaller range of effective slot cutting, have worse geometric parameters (smaller diameter), compared to the holes G11/2018 and G11a/2018.

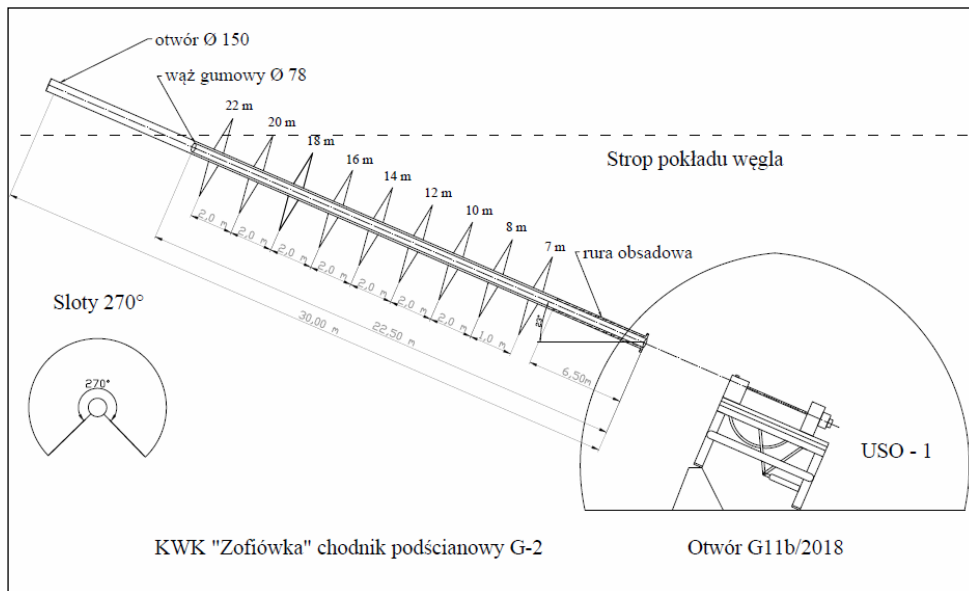


**Figure 2.2.11.24:** Situation in the borehole G11b/2018 after hydro-slutting

#### **Location of G21/2018 borehole.**

The purpose of the works was performing the stimulation of the exploratory borehole G21/2018 using hydro-slitting equipment with special rubber hoses preventing the borehole from collapsing. Location of the boreholes was shown on the figure 1 as below.

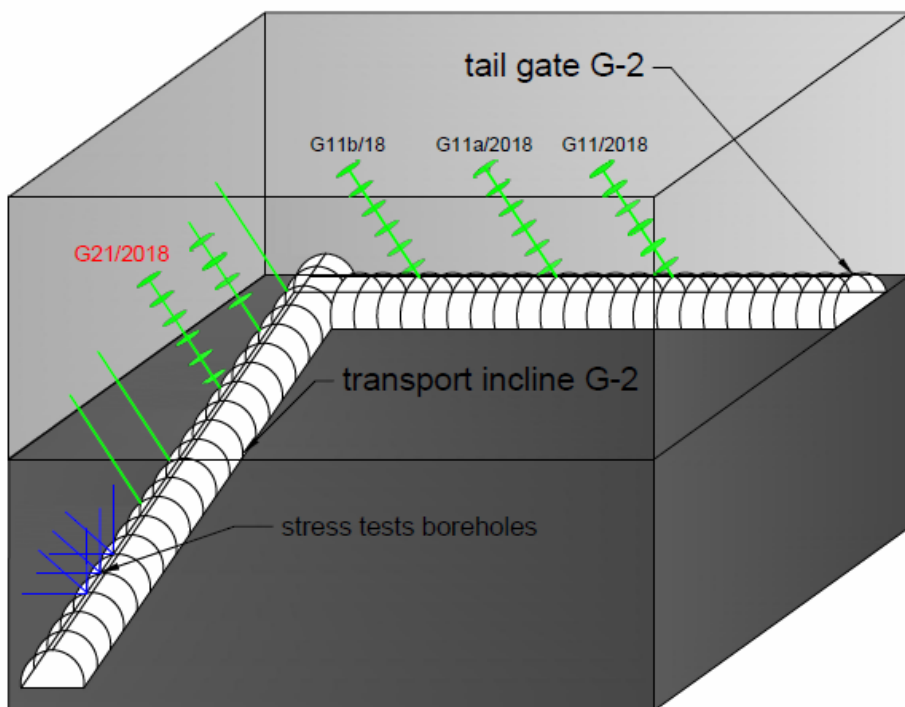


**Figure 2.2.11.25:** Layout of the boreholes with borehole G21/2018

#### **Stimulation of G21/2018 borehole.**

Stimulation of the G21/2018 (Figure 2.2.11.26), borehole was started, starting at a depth of 18m, and subsequent slots at a distance of 2 m from the previous one in direction of the beginning of the borehole (16m, 14m, 12, etc.).

Stimulation time (execution of one slot) - 3 min.,

High Pressure during the slotting: 1000 Bar (100 MPa),

Outlet nozzle type - ceramic with a diameter of 2.1 mm, (60 min. of working time),

The borehole was secured by rubber hoses with diameter  $\varnothing=120$  mm on a distance 18.4 m. The following slots: 18m, 16m, 14m, 12m, 8 m were performed in full rotation range (USO 360 °).

The course of individual slots can be characterised in the following way:

- free outflow of the water for about 1 minute from the beginning of each operation.

After this time certain stops and sudden outflows of increased volume of water can be observed.

- up to 10 – 20 seconds after starting each slot the outflow of water from the rubber hose was recognized and after this time the water came out from the space between the hose and the internal side of the borehole – what gave evidence that the hose was cut by the water jet. Additionally, the water coming out has black colour and contained cuts of coal what clearly suggested performance of the slotting (cutting the coal) . After about 2.5 min from the beginning of the operation the amount of cuttings in the water decreased – what may suggest finishing of the process of effective slotting.

Each slot operation was performed for 3 minutes.

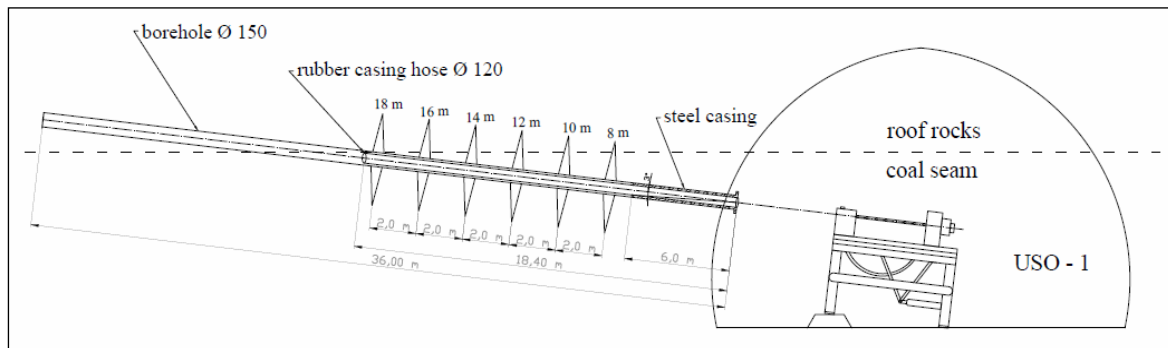


**Figure 2.2.11.26:** Situation in the borehole G21/2018 after hydro-slotting

#### **Conclusions from the hydro-slotting research operations:**

The location of the previous test stand (testing boreholes: G56, G56a, G57 and G57a) drilled in year 216 in the testing tail gate D-2 in the coal seam 412 at "Zofiówka" mine prevented long-term testing operation. Considering the above, for safety reasons in 2017 whole equipment (pump unit, USO-1, rods, etc.) and measurement systems has been moved from the testing tail gate D-2 (in the coal seam 412) to the transportation cross cut G-2 (in seam 410, level 900 m).

The geomechanical parameters of coal seams (410 and 412) at "Zofiówka" mine (low compactness and high friability) caused clogging of the boreholes in time. To assure stability of the boreholes it was applied two approaches: drilling boreholes on a contact of coal and roof rocks and use of rubber hoses inside the boreholes. The latter one, together with large dialemeter and steep angle of borehole elevation permitted to make hydroslotting in whole part of the borehole in coal seam.

#### **2.2.12. WP4, Task 4.3: Application of large scale stimulated drainage of methane at sub-level caving mining layouts at Hunosa (led by HUNOSA, AITEMIN – until 30.09.2016, GIG, IMPERIAL, INIG)**

##### **Gas monitoring and data logging**

RElia AV system is developed specifically for gas monitoring and control applications in underground mining. All signals of the devices, including the control and management of injection and suction pump, are collected by means of the remote control unit (UCR), which is fitted the Relia-AV system. The UCR are equipped with 4 universal inputs/outputs, which can be configured for any type of input and/or output analog/digital. They communicate with the station master Relia-AV by a field bus carrying via serial (RS-485) and master-slave system.

The master station, which has an autonomous operation by using a configuration set, communicates with the control room from the outside through a network of optical fiber with TCP-IP Protocol Ethernet, sending the data of all the inputs and outputs set to a SCADA software, and receiving configurations, where necessary, appropriate orders.

During testing of water injection and suction of gas coal seam 8th, and to detect the influence of the injection in the capture of methane, the following parameters are being monitored:

- Injection pump: pressure input and pressure and output flow. It allows to determine the injection pressure and the volume of water injected into the layer.

- Observation borehole S21: monitors the pressure in the poll during the water injection to detect any significant influence.
- Capturing in the boreholes S12 and S13 is monitoring the pressure in those rods, concentration of CH<sub>4</sub> and of CO. Also controls the flow of aspiration, along with the concentration of CH<sub>4</sub>, determines the volume of methane extracted.

Gas monitoring control. Inside of the mine there are various sensors monitored from outside. In the injection/catchment area and the return of CH<sub>4</sub> and CO sensors have been installed in order to ensure the safety of staff and facilities during the trials.

Water injection pump has automatic disconnection system in case of overpressure or presence of CH<sub>4</sub> in the atmosphere. The vacuum pump has automatic disconnection to prevent sucking methane concentration which is below the upper limit of explosiveness.

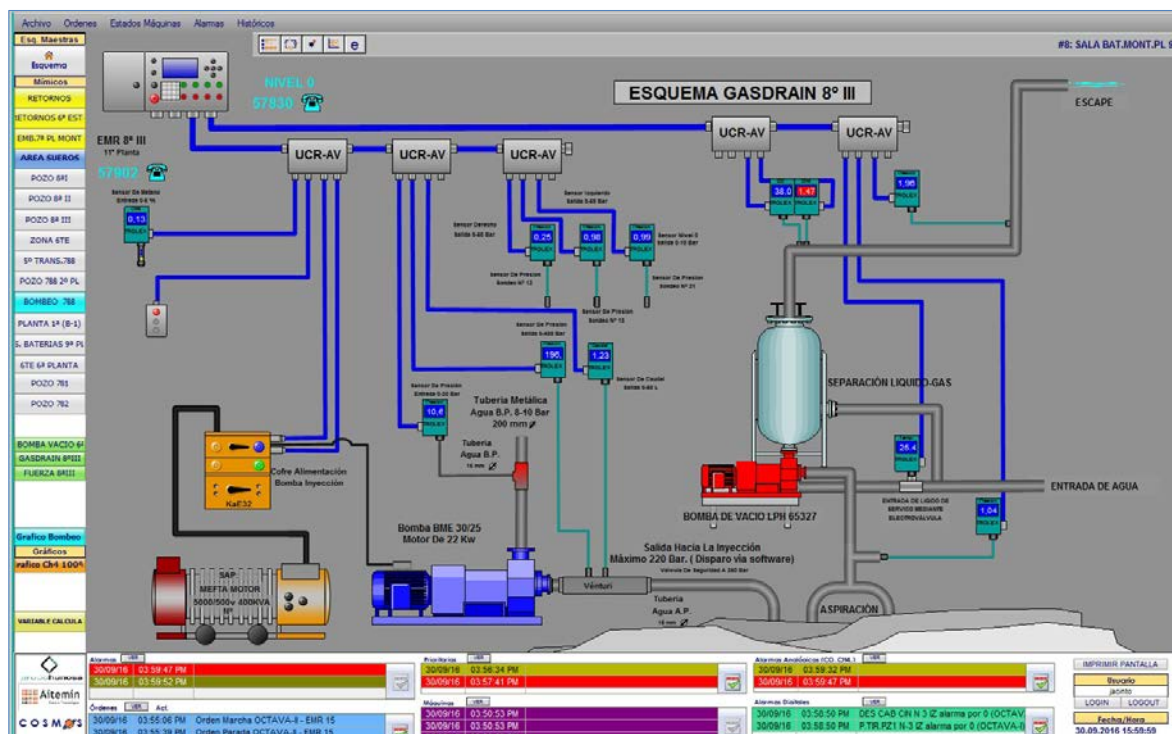


**Figure 2.2.12.1:** Remote gas monitoring and control screen



**Figure 2.2.12.2:** RELIA AV Gas Monitoring and Control System



**Figure 2.2.12.3:** Suction flow measurement



**Figure 2.2.12.4:** Methane and carbon monoxide gas detectors at drainage pipe

#### Combined drainage and stimulation at Location L1

Once the problem detected in the pump regulating valve is repaired, a test combining hydraulic stimulation and methane drainage is carried out. The plan was to continue with the water injection by S14, and extract methane by the boreholes S12 and S13. Figure 2.2.12.5 shows the water injection & gas suction location.

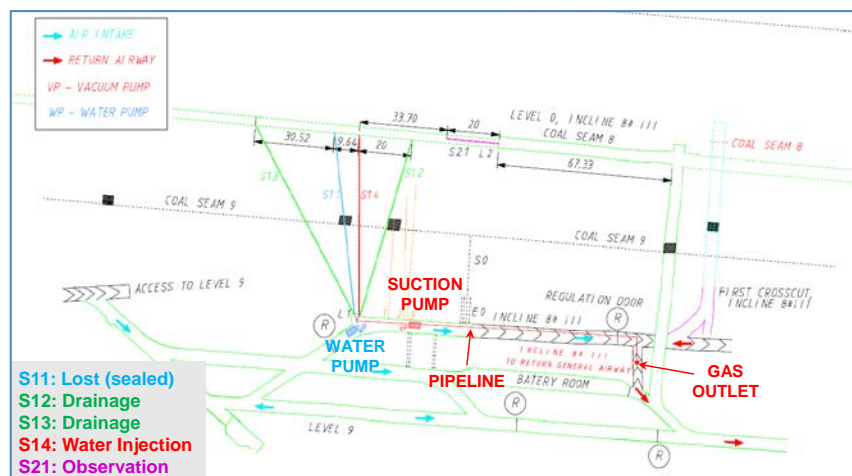


**Figure 2.2.12.5:** Combined drainage and stimulation at Location L1

The plan indicated the location of water (S14) injection pump and the vacuum pump of methane (S12 and S13) at location L1. It also shows the exhaust pipes of suction and injection tests.

**Table 2.2.12.1:** Boreholes features (location L1 & L2)

LOCATION	BOREHOLE	LENGTH		$\varnothing$ (mm)	INCLINE	NOTES
		C/9 <sup>a</sup>	C/8 <sup>a</sup>			
L1	S11	31,0	63,0	56	4°	SEALED
	S12	31,5	63,5	76/56	4°	GAS DRAINAGE
	S13	35,6	71,0	56	4°	GAS DRAINAGE
	S14	31,5	64,0	56	4°	WATER INJECTION
L2	S21		20,0	52	2°	PRESSURE MONITORING

Table above shows the features of the boreholes used to inject of water, capturing of gas and observation from locations L1 and L2.

The vacum pump is located in the gallery for access the incline 8<sup>th</sup> III, close to the injection pump. The exhaust pipe runs along this gallery until it passes the door of ventilation, which separates the area from general return of 11<sup>th</sup> ventilation level. Exaust pipe output was directed on ascending well by which runs the ventilation of returns and which air flow is very high, ensuring dilution of gas to it safe concentration. Near the exit of the pipe some of CH<sub>4</sub> and CO sensors have been installed as well as the anemometer, head of the ventilation well have another CH<sub>4</sub> sensor, which checks that the dilution is really effective.



**Figure 2.2.12.6:** Emplacement of methane drainage system

Two types of tests were carried out during the month of October 2016:

- Water injection through the S14 borehole, at first with an average 170 bar pressure and lowering the pressure at 5 a.m. to 50 bar. The injected volume was low, with a maximum peak of

30.0 l/min down to 2.0 l/min due to automatic disconnection pump maximum pressure. A total of 370 l injection can be estimated as shown in the following chart.

- Methane drainage through boreholes 12 and 13 with several peaks of aspiration and concentrations of methane went quickly down to zero by depletion of volume of methane in the interior of the borehole. The amount of sucked methane was not estimated because the differential pressure, which is used to calculate the vacuum flow had very low values. (there was little methane available in the zone of influence of degassing boreholes and therefore low flow sucked).

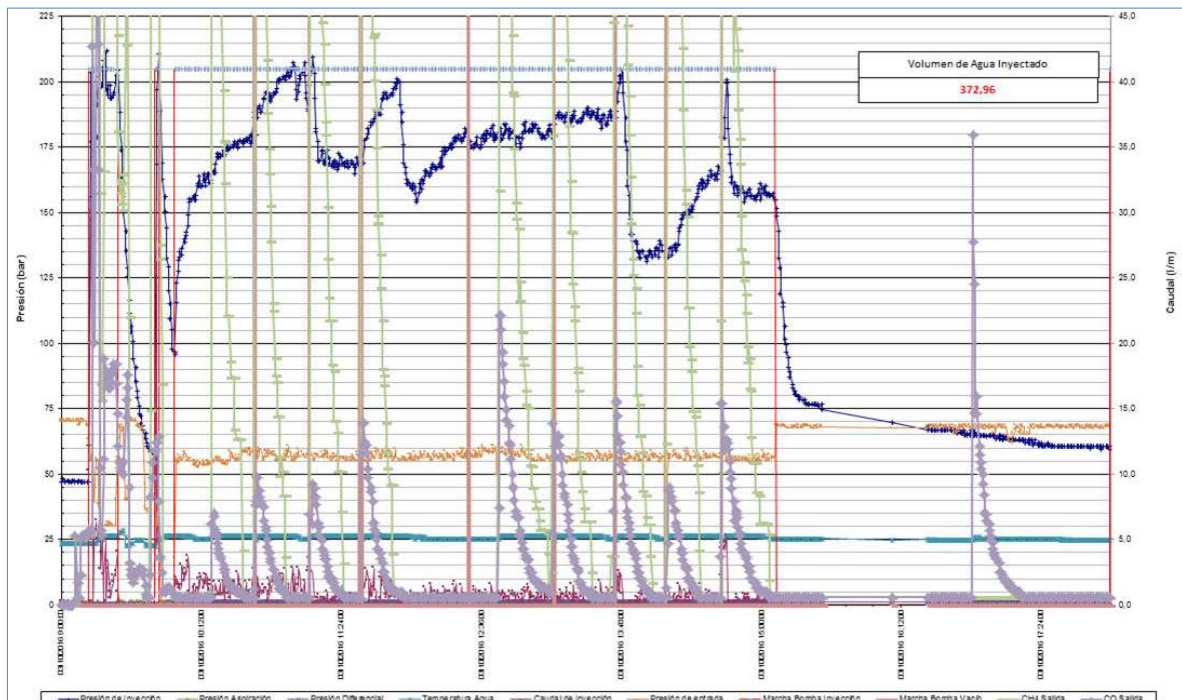


**Figure 2.2.12.7:** Water injection and gas suction on 3 October 2016

In the carbon monoxide sensor located at the outlet of the aspiration several peaks were detected, reaching 50 ppm - the limit value set by the General Regulation of Basic Mining Standards of Spain. Suction works were interrupted due to dysfunction in the CO sensor detection, then suction gas samples were taken to verify the records by using chromatographic analysis. After the analysis of gases, a low oxygen presence was observed, which resulted in erroneous reading of the catalytic sensor of CO, due to its operating system.

After the obtaining results of the analysis, which confirmed absence of CO, it is planned to resume the injection and aspiration work at location L1, while performing the drilling and cementing of the location boreholes L3.

The injection work was resumed trying to maintain a constant pressure between 65 and 75 Bars, obtaining an average injection rate of approximately 70 liters per hour.

On the basis of above average flow rate, the injection frame was established to achieve the marked targets for the increase of the humidity of the 8<sup>th</sup> coal seam.

#### GASDRAIN - S14 WATER INJECTION (m<sup>3</sup>)

Distance between boreholes (m): 20,0

It is assumed that the volume to be injected is a cylinder which radius is half distance between two boreholes  
Increase moisture recommended: 1% - 2 %

WATER INJECTION (m <sup>3</sup> )	Coal Seam Thickness (m)			
	3,0	3,5	4,0	4,5
0,5%	4,71	5,50	6,28	7,07
1,0%	9,42	11,00	12,57	14,14
1,5%	14,14	16,49	18,85	21,21
2,0%	18,85	21,99	25,13	28,27

#### GASDRAIN - INJECTION TIME

Water flow rate (l/h): 70,0

Water pressure: 70 bar

INJECTION TIME (hours)	Coal Seam Thickness (m)			
	3,0	3,5	4,0	4,5
0,5%	67	79	90	101
1,0%	135	157	180	202
1,5%	202	236	269	303
2,0%	269	314	359	404

INJECTION TIME (days)	Coal Seam Thickness (m)			
	3,0	3,5	4,0	4,5
0,5%	2,8	3,3	3,7	4,2
1,0%	5,6	6,5	7,5	8,4
1,5%	8,4	9,8	11,2	12,6
2,0%	11,2	13,1	15,0	16,8

Figure 2.2.12.8: Water injection test targets

#### Planned experimental layout at new location L3

Next experimental test consisted in checking standard methane extraction performance (without hydraulic stimulation) in a virgin area for comparison (Location L3). On the other hand, and in order to measure the influence, that the water stimulation method has on the efficiency of the methane drainage process, it will also be necessary to obtain data on the efficiency of the conventional methane drainage in this area (without stimulation).

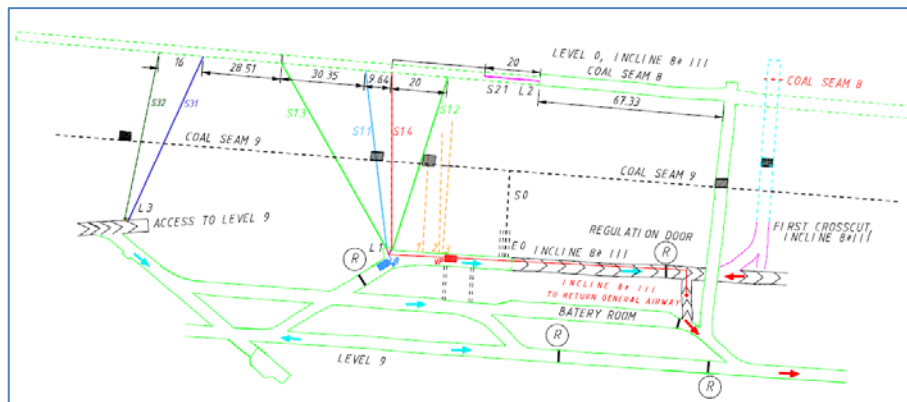
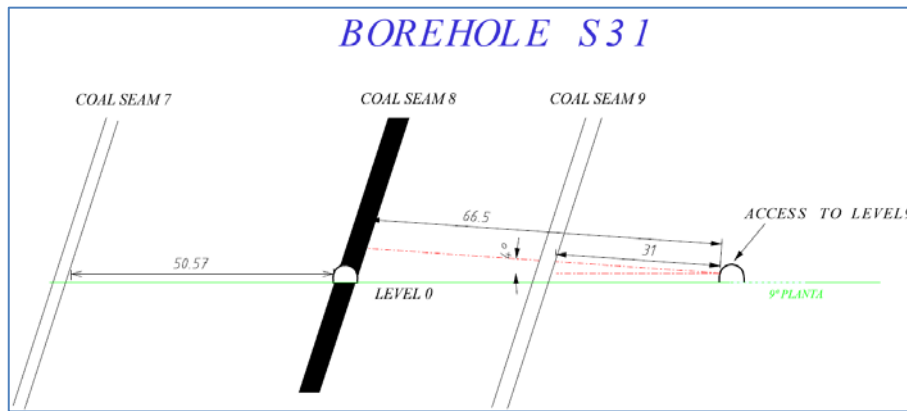
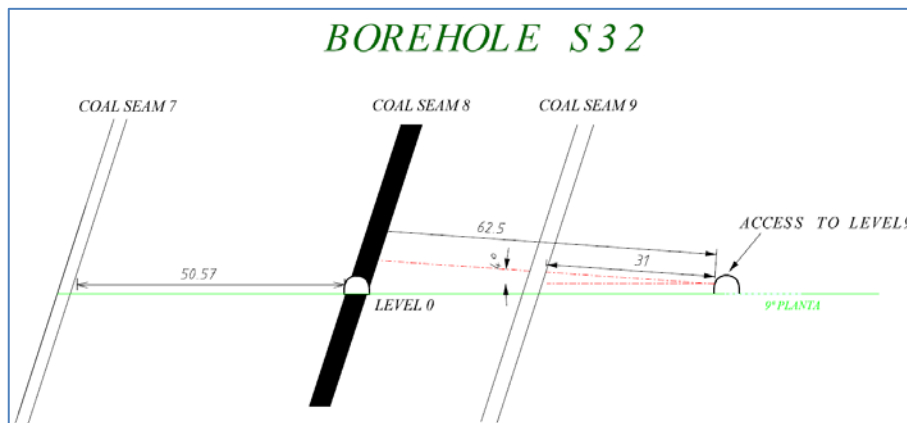


Figure 2.2.12.9: New location L3.



**Figure 2.2.12.10:** Borehole layout at the test site (vertical cross section at S31).



**Figure 2.2.12.11:** Borehole layout at the test site (vertical cross section at S32).

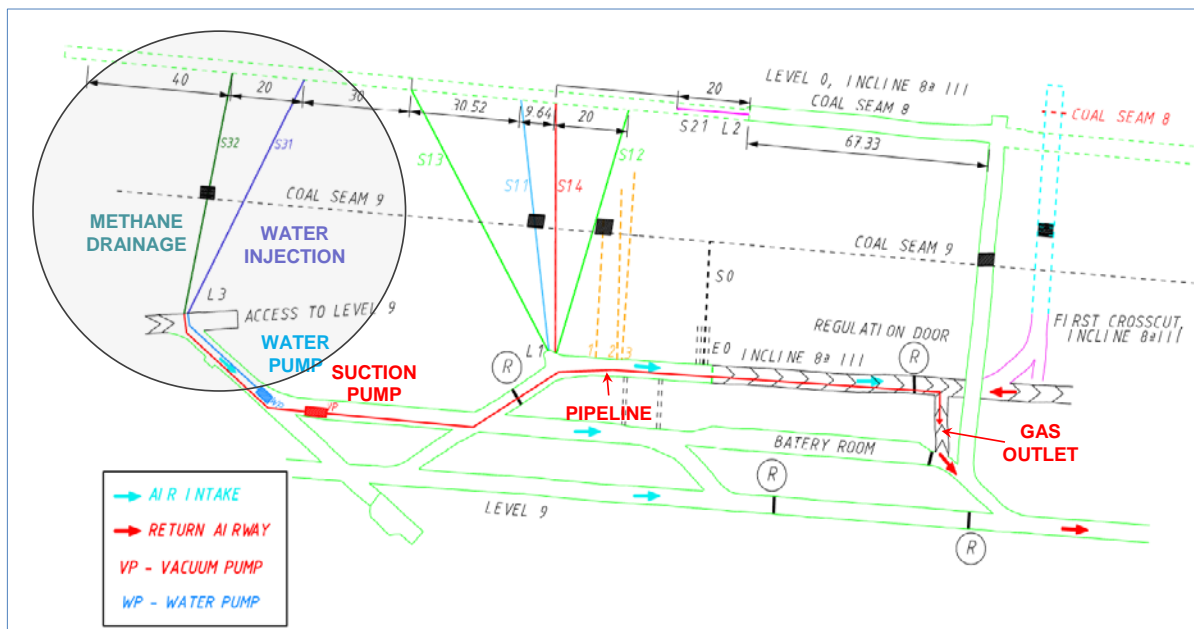


**Figure 2.2.12.12:** Scheme of injection and future aspiration in L3.

### Boreholes analysis of gas

Gas tests taken to date in the locations of L1 and L2 are included in this section. The results of the analysis of the gas composition are presented in the following table.

**Table 2.2.12.2:** Analysis of gas samples

HUNOSA SUEROS COLLIERY - MONTSACRO PIT							
Cod.	Reference	ANALYSIS OF GAS SAMPLES (molar composition in %)					
		Methane	Ethane	Propane	CO <sub>2</sub>	O <sub>2</sub>	N <sub>2</sub>
B1	C/8 – 8th III - LEVEL 0 LEFT	95,2	3,43	0,22	0,41	0,17	0,59
B2	C/8 – 8th III - LEVEL 0 LEFT	95,1	3,47	0,23	0,40	0,17	0,58
B3	Borehole SE1 - 9th LEVEL – 8th III	77,4	0,30	0,03	0,08	4,18	18,01
B01	Borehole S14 - 9th LEVEL – 8th III	88,9	2,90	0,13	0,25	1,07	6,66
G-6	Capa8-MONSACRO-aspiracion 1	78,0	2,04	0,15	0,15	3,22	16,46
G-7	Capa8-MONSACRO-aspiracion 2	35,4	1,25	0,09	0,26	13,07	49,92
							0,00

B1 and B2 samples are samples of gas from the borehole in coal S21, at the L2 position, in the advance of the left Gallery in the 8<sup>th</sup> coal seam.

The sample B3 corresponds to a borehole (SE1) made in rock since the site L1 cut the 9<sup>th</sup> coal seam.

The sample B01 was taken in the borehole used for the injection of water. The probe was made of rock from location L1 to cut the 8<sup>th</sup> coal seam.

Four samples mentioned above were taken prior to the completion of the trials by water injection.

The G6 and G7 were sampled gas suction during the combined testing of injection water and suction of gas, checking in the chromatographic analysis it was 0 ppm of CO content.

The following figure shows the location of outlets carried out gas samples.

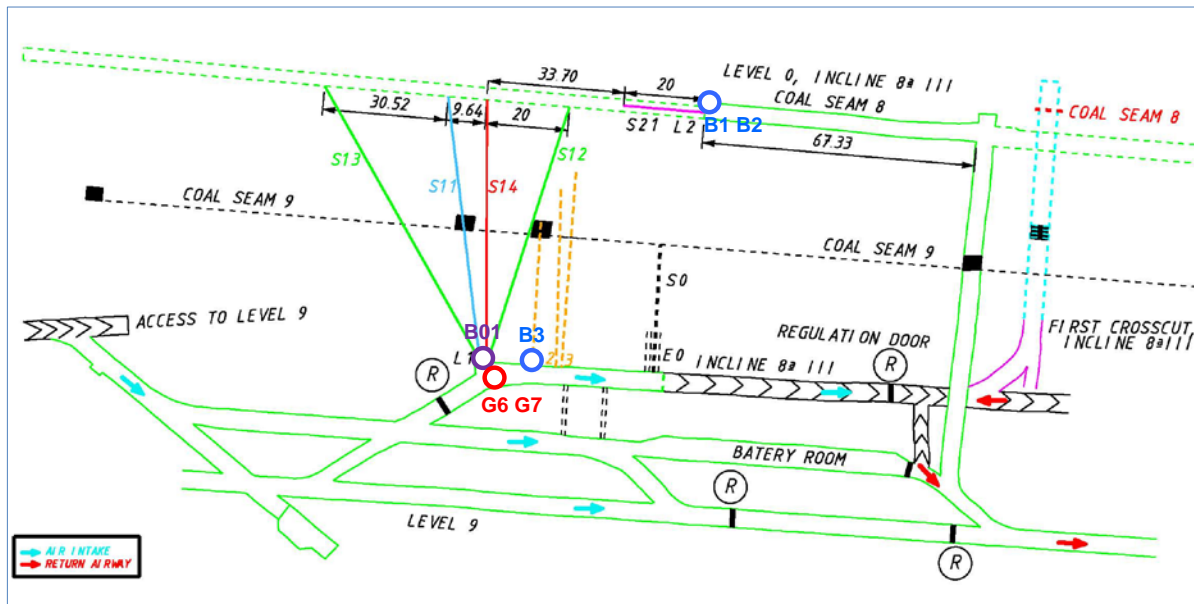


**Figure 2.2.12.13:** Gas samples location

**Development the roadway level 0 incline 8<sup>th</sup> III, coal seam 8<sup>th</sup> and checking the results of water injection & gas suction**

In order to determine the effectiveness of testing hydrofracture test and stimulation of the coal seam through the high-pressure water injection, it was intended to continue advancing work on 8<sup>th</sup> coal seam controlling specific detachment.

It was not possible to continue the advance of the level without the approval of the Mining Authority of Asturias, the decision to check the results of water injection and suction of gas, by means of a horizontal borehole on the front, in front of advance from level 0, the 8<sup>th</sup> coal seam.

Through this borehole the samples of coal were collected for their subsequent analysis. The following figure shows the location of borehole to be performed:

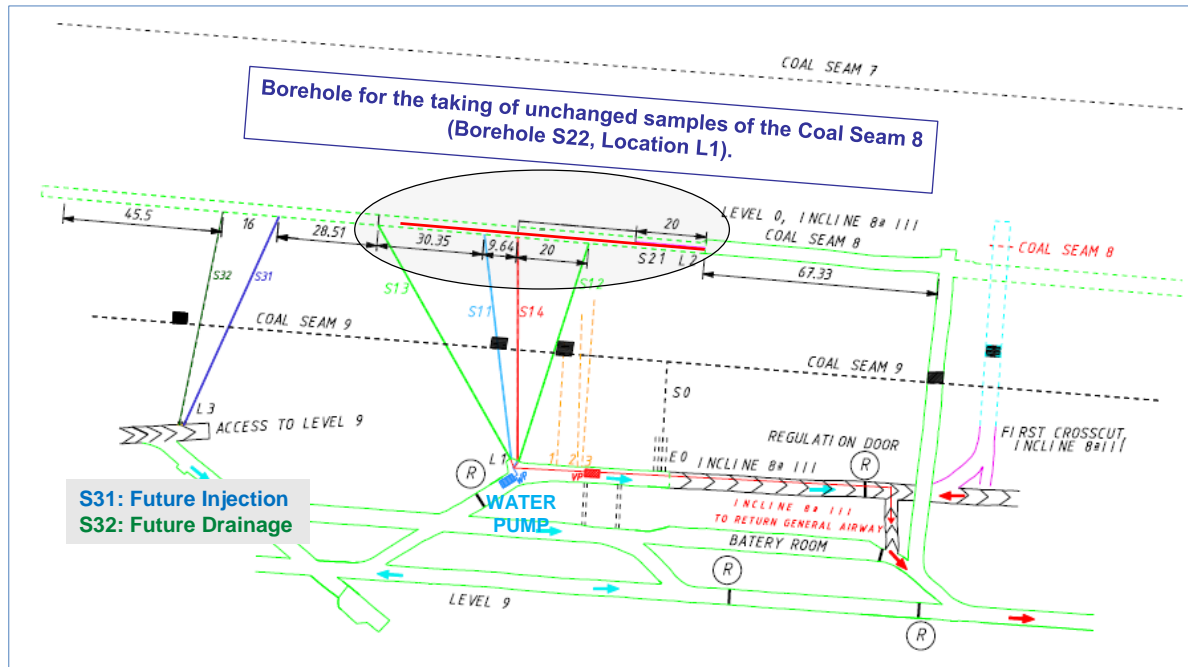


**Figure 2.2.12.14:** Location of the borehole S22 for collecting samples

For drilling of the borehole and obtaining unchanged cores, HUNOSA uses the pneumatic drilling machine Turmag P-100-K. For the drilling of the layered probe and the extraction of unaltered samples, a triple borehole battery has been purchased.

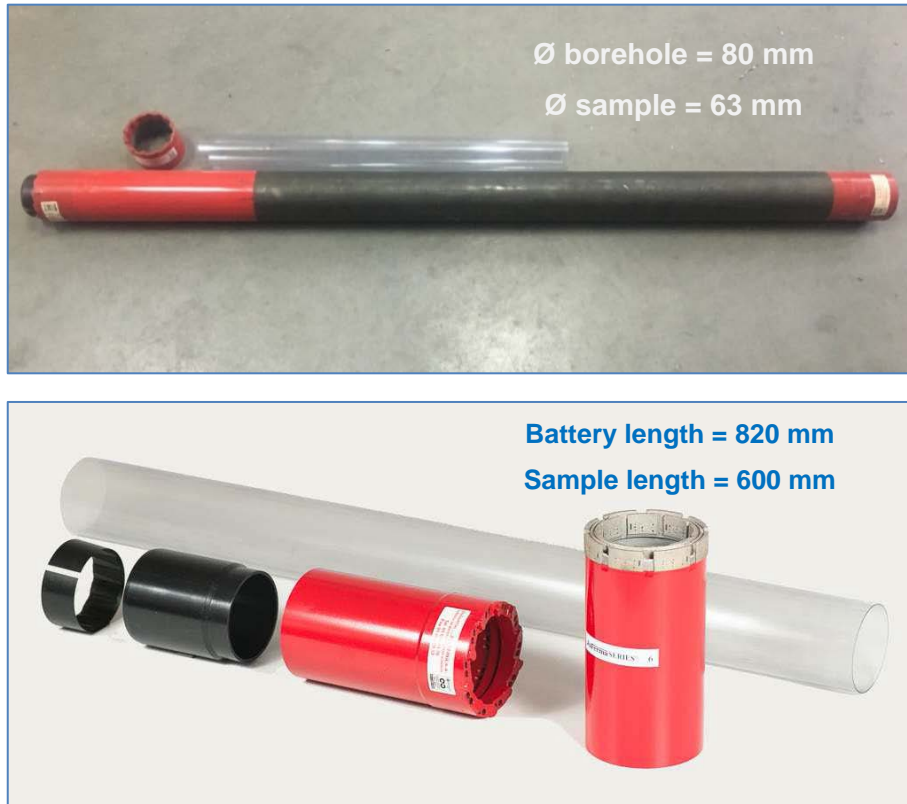


**Figure 2.2.12.15:** Triple borehole battery

The T6 triplex system with plastic tube, allows the control. The standard T6 battery can be transformed into T6 triplex by adding the tube of plastic inside and replacing the standard components by the following:

- Triplex spring
- Spring box
- Crown impregnated or M.D. With frontal discharge

### **Injection/Drainage in 2017**

This part of report contains detailed analysis of the results from the drainage process, which was applied into the boreholes S12 and S13 at location L1.

The map below shows the locations of various injection and drainage boreholes applied in the coal layer C/8 in Montsacro's shaft (Hunosa) at location L1.

Status of individual boreholes was as follows:

- Borehole S11: lost (sealed)
- Borehole S12: used for monitoring
- Borehole S13: used for monitoring
- Borehole S14: used for injection
- Borehole S21: used for monitoring.

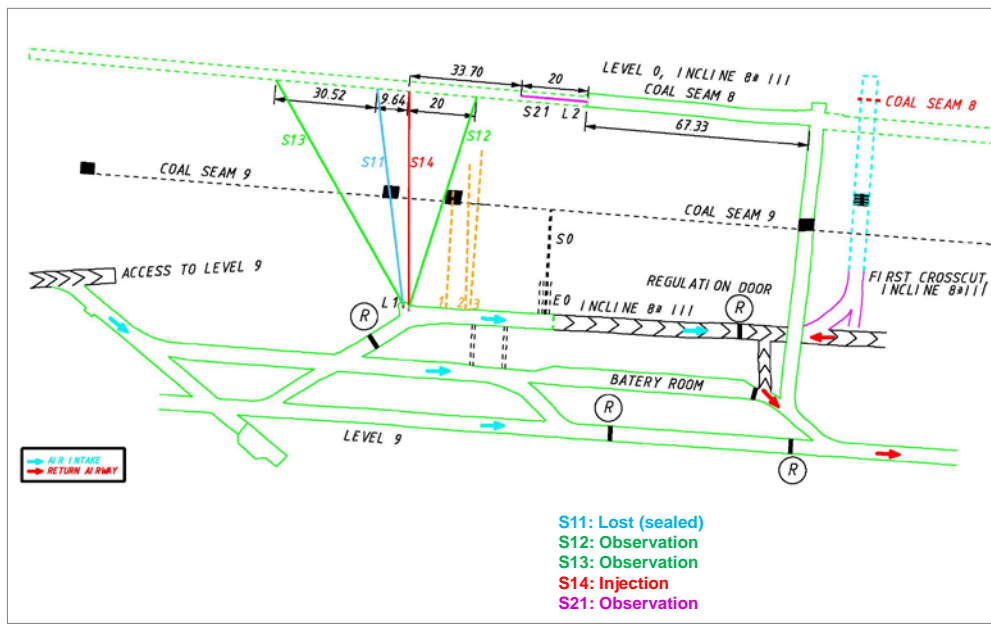


**Figure 2.2.12.16:**The locations of various injection and drainage boreholes applied in the coal layer C/8 in Montsacro's shaft (Hunosa) at location L1

The injection/drainage process was divided into following periods:

- Period 01: from 21-02-2017 to 08-03-2017. Preliminary tests. Pump type BME 30/25.
- Period 02: from 8-03-2017 to 20-03-2017. Breakdown Pump type 30/25
- Period 03: from 22-05-2017 to 31-05-2017. New Pump type BME 30/45.
- Period 04: from 1-06-2017 to 07-06-2017. Pump type BME 30/45.
- Period 05: from 7-06-2017 to 12-06-2017. Pump type BME 30/45.
- Period 06: from 12-06-2017 to 19-06-2017. Pump type BME 30/45.
- Period 07: from 19-06-2017 to 26-06-2017. Pump type BME 30/45.
- Period 08: from 26-06-2017 to 3-07-2017. Pump Type BME 30/45.
- Period 09: from 21-07-2017 to 31-07-2017. New Pump Type BME 30/36.
- Period 10: from 31-07-2017 to 7-08-2017. Pump Type BME 30/36.
- Period 11: from 7-08-2017 to 14-08-2017. Pump Type BME 30/36.
- Period 12: from 14-08-2017 to 21-08-2017. Pump Type BME 30/36.
- Period 13: from 21-08-2017 to 28-08-2017. Pump Type BME 30/36.
- Period 14: from 28-08-2017 to 4-09-2017. Pump Type BME 30/36.

### Water injection

As it was already mentioned above there were three types of pumps used for water injection:

- BME 30/25. Period 01 and 02
- BME 30/45.
- BME 30/36. Used since Period 09.

### Firedamp drainage

The drainage process took place using the same pump (name brand: Sterling Model: SIHI LPH 65327). Its operational characteristics is shown in Deliverable Report 4.3.

### Water injection analysis at location L1

For each period we have done water injection assumptions. The injected volumes (in litres ) are shown in the table below.

**Table 2.2.12.3:** The injected volumes (in litres).

Pump Type	Period		Water Injection
BME 30/25	21/02/2017	07/03/2017	7.280,42
	08/03/2017	19/03/2017	4.786,82
BME 30/45	22/05/2017	31/05/2017	11.856,59
	01/06/2017	06/06/2017	5.524,00
	07/06/2017	11/06/2017	13.286,00
	12/06/2017	18/06/2017	643,00
	19/06/2017	25/06/2017	16.652,86
	26/06/2017	02/07/2017	39.356,37
	21/07/2017	30/07/2017	9.435,29
BME 30/36	31/07/2017	06/08/2017	3.619,00
	07/08/2017	13/08/2017	3.569,00
	14/08/2017	20/08/2017	8.433,00
	21/08/2017	27/08/2017	7.727,00
	28/08/2017	03/09/2017	8.629,00
	<b>TOTAL</b>		<b>140.798,34</b>

#### Firedamp drainage analysis at location L1

The tasks focused on drainage were performed based on the monitoring, which took place in the boreholes S12 and S13, both connected to the system of drainage pump. The map below presents location of the boreholes, the suction pump and the exhaust of the gas drained by the system.

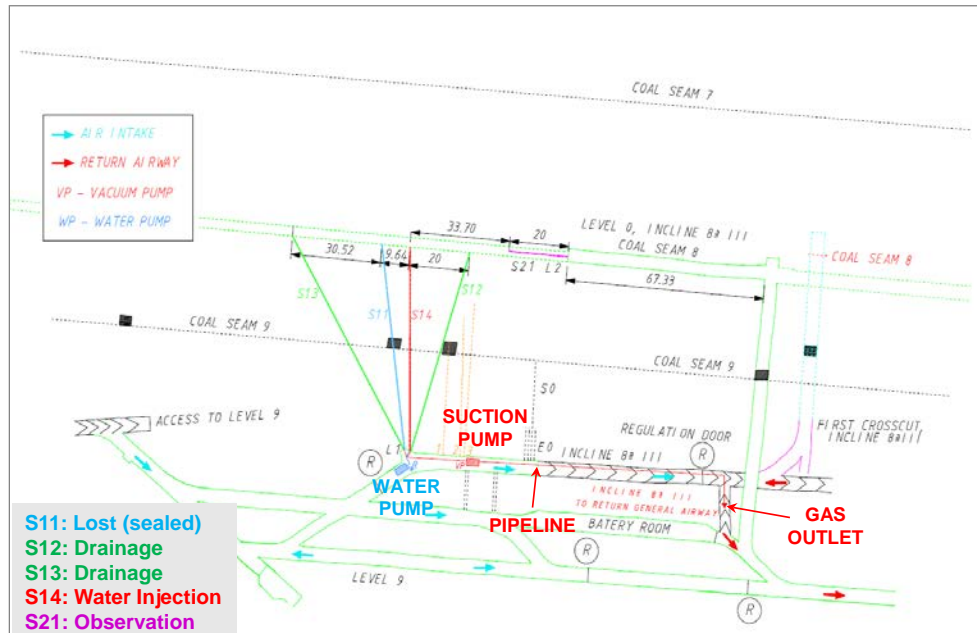


**Figure 2.2.12.17:** Location of drainage boreholes and the equipment.

The regulation/calibration of the drainage system were divided into two periods:

### A. Preliminary tests

These tests of drainage system were performed in the period between 01/06/2017 and 30/06/2017, denominated as the periods 04 to 08. This period covers also: setup of the drainage facilities with the checking of the monitoring sensors.

### B. Drainage tests

These tests took place in the period between 21/07/2017 and 28/08/2017, denominated as the periods 09 to 13.

This period covered monitoring of the automatic drainage with the required security regulations listed below:

- Security regulation on methane percentage contained in the drainage gas. The system stops automatically when the methane percentage in the drained gas is approaching to the superior explosive range. For safety reasons we placed this maximum at 40%.
- Security regulation on drained CO. The system stops automatically when it detects CO levels of 5 ppm
- Security regulations on the pressure of the drainage pump. The system stops automatically when this pressure is below 500 mbar.
- Security regulation on a high concentration of methane in the exhaust zone. The system stops automatically when it detects methane concentration values in the exhaust zone exceeding 1.5%.

The main parameters controlled in the methane drainage of the system were as follow:

Drainage (monitored parameters):

- Methane content at heading
- CO content at heading
- Methane content at the pump location
- Methane content at location L2
- Pump el. current supply (On/off)

We have done the analysis of the drainage for all the periods in which the drainage system has been activated. The periods analysed took place since the start of the drainage (Period 03) to the drainage pump breakdown (Period 13). The working periods of the pump were rather relatively short periods of time.

We have analysed the most remarkable periods to quantify the amount of firedamp drained at location L1. It has been recognized, that the pump makes plenty of stops and starts that are caused by the extraction and depletion of the firedamp available in the boreholes and in its influencing areas. Once the boreholes are refilled, the pump starts again for another short period of time, and so on.

For all periods, we were able to quantify the amount of drained methane, which is shown in table below:

**Table 2.2.12.4:** The amounts of drained methane in individual periods.

Period	Date	Drainage	Time on		Record			CH4 Drained	Observaciones
			min	hh:mm:ss	On	Pdif	CH4		
01	21-02_08-03	NO	0,00	0:00:00	----	----	----	0	Only injection
02	08-03_20-03	NO	0,00	0:00:00	----	----	----	0	Only injection
03	22-05_31-05	SI	59,87	0:59:52	1s	1s	1s	1	Short time of aspiration / low % CH4
04	01-06_07-06	SI	77,88	1:17:53	1s	1s	1s	4	Short time of aspiration
05	07-06_12-06	SI	62,43	1:02:26	1s	1s	1s	273	Short time of aspiration
06	12-06_19-06	SI	50,00	0:50:00	1s	1s	1s	293	Sensor failure
07	19-06_26-06	SI	58,00	0:58:00	1s/1min	1s	1s/1min	508	Short time of aspiration
08	26-06_03-07	SI	48,00	0:48:00	1min	1s	1min	421	Short time of aspiration
09	21-07_31-07	SI	94,77	1:34:46	1s	1s	1min	831	Short time of aspiration
10	31-07_07-08	SI	72,03	1:12:02	1s	1s	1min	631	Short time of aspiration
11	07-08_14-08	SI	86,37	1:26:22	1s	1s	1min	757	----
12	14-08_21-08	SI	134,00	2:14:00	1s	1s	1min	578	----
13	21-08_28-08	SI	195,00	3:15:00	1s	1s	1min	533	----
14	28-08_04-09	SI	----	----	1s	1s	1min	----	Pump failure

Data presented above should be recognized as the evaluations of the quantification of drained methane in the facility - as we believe. The reason for this is that there were plenty of starts and stops of the drainage pump, which could create potential errors and it must be notable.

In the attached document, we include the graphics with the controlled parameters in the main periods of firedamp drainage. The readings from the firedamp as below confirm assumed attitude.

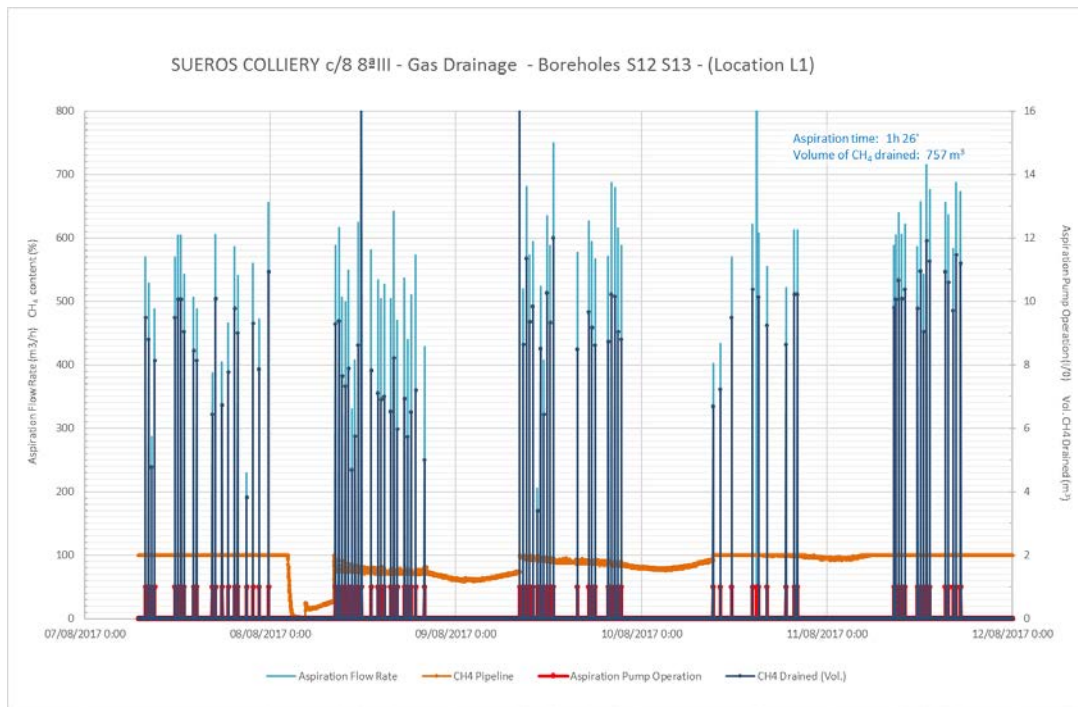


**Figure 2.2.12.18.** The readings from firedamps period from 7/08/17 to 12/08/17

### Boreholes control at location L2

From location L2, we have done a control of the injection effectiveness in the drainage tasks performed in location L1 along the injection/drainage periods.

The starting point for the analysis was characterisation of the borehole from which we have obtained following firedamp data in the coal seam: firedamp concentration, desorption speed, ashes and moisture content in the seam.

From this borehole we have obtained the value of firedamp concentration of  $7.5 \text{ m}^3/\text{t}$ , with a sorption velocity in some points above  $1.5 \text{ cm}^3/35\text{s}/10\text{g}$ .

A total of three characteristic boreholes have been done with this characteristics:

- Borehole S 2-1: with total length of 18 m. We have collected samples for the firedamp concentration, desorption speed, ashes and moisture contents
- Borehole S 2-2: with total length of 30 m. We have collected samples of cores for the lab analysis and for local analysis of the desorption speed and moisture.
- Borehole S 2-3: with total length of 15 m. We have collected samples of cores for the lab analysis and for local analysis of the desorption speed and moisture.
- Borehole S 2-4: with total length of 7 m. We have collected samples of cores for the lab analysis and for local analysis of the desorption speed and moisture.

Below we present data and the graphs of the main, characteristic controlled parameters.

**Table 2.2.12.5:** The main characteristic controlled parameters

S22 LENGTH (m)	S21 Moisture (%)	S22 Moisture (%)	S23 Moisture (%)	S24 Moisture (%)	S21 V1 INDEX	S22 V1 INDEX	S23 V1 INDEX	S24 V1 INDEX
1,0	3,03				0,1			
2,0	3,82				0,2			
2,5				1,20			0,1	0,2
3,0	2,38				0,4			
4,0	2,09				0,3			
5,0	1,98			1,05	0,5	0,0	0,2	0,5
6,0	3,51				0,5			
7,0	1,45				0,5			
7,5					1,6		0,1	
8,0	1,20				2,8			0,0
9,0	1,79				1,4			
10,0	1,85				1,0	1,1	0,3	0,0
11,0	1,71				1,0			
12,0	1,48				1,5			
12,5			0,86			0,3	0,0	
13,0	2,22				1,3			
14,0	0,86				1,0			
15,0	1,17		1,04		1,4	0,0	0,2	
16,0	2,53				1,6			
17,0	2,38				1,3			
17,5					0,0			
18,0	1,70				1,2			
19,0	1,21				1,1			
20,0	1,54				1,1	0,0		
22,5		0,62				0,0		
25,0		1,53				0,0		
27,5		1,73				0,0		
30,0		2,09						

DRILLING DATA: MOISTURE. Boreholes Location L2: S21, S22, S23, S24

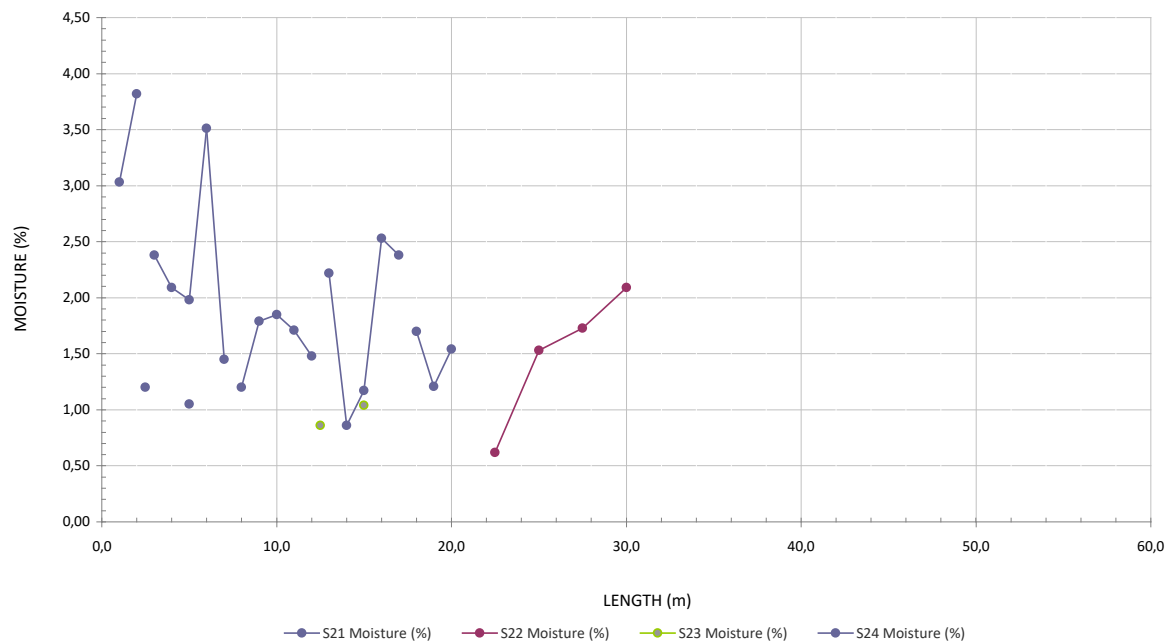


**Figure 2.2.12.19.** Moisture at L2 borehole location

DRILLING DATA: Desorption velocity (V1). Boreholes Location L2: S21, S22, S23, S24

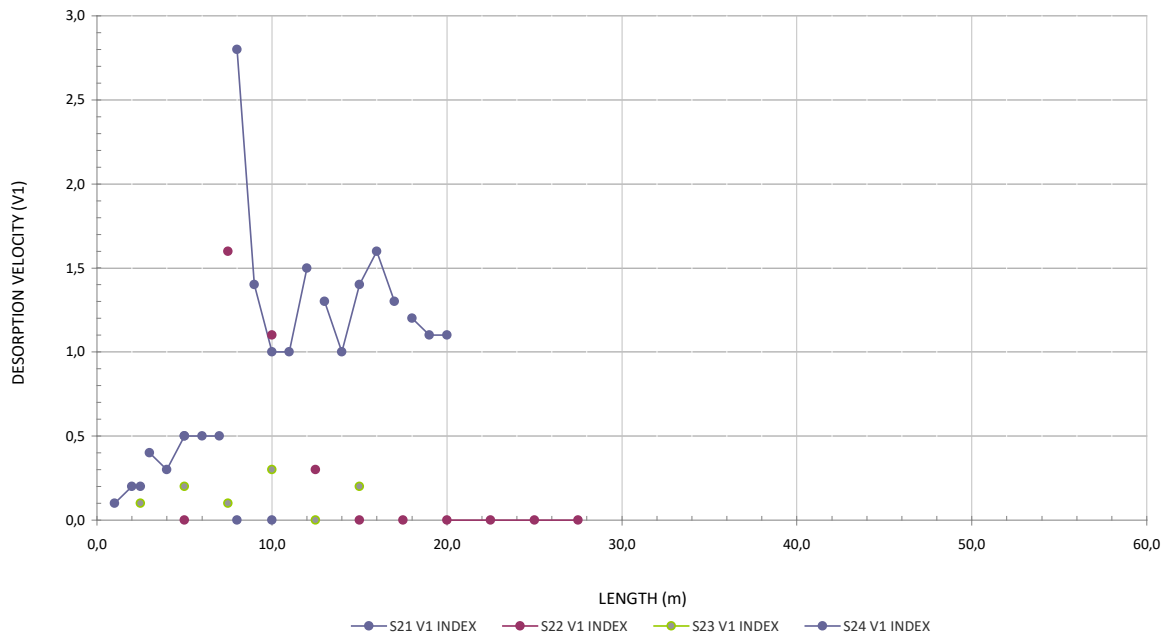


**Figure 2.2.12.20.** Velocity of desorption. Location L2

#### Tracer gas test at location L3

Several possibilities were analysed to do the influence test for the degassing and effectiveness of the influence in the water injection. There were three proposals to do it with:

- HF6 (100% v/v)
- etil-mercaptano , which is detected by its smell
- mix made of H<sub>2</sub>+N<sub>2</sub>. 2% v/v H<sub>2</sub> and 98% v/v N<sub>2</sub>.

Finally it was decided to do it with HF6 by 100% v/v in a 5 litre bottle with 200 bar (1 m<sup>3</sup>).

The tests with the tracer gas (depending on the planning with HUNOSA) were planned according to the following protocol:

- Injection through a borehole and collecting sample from the adjacent-ones.
- The injection pressure of 30 bars.
- Sample taking period in adjacent boreholes: every hour for 8 hours and later on every 2 hours
- Collecting two samples at location L2. First one 4 hours after the beginning of the injection and the second-one, 24 hours after beginning of the injection.

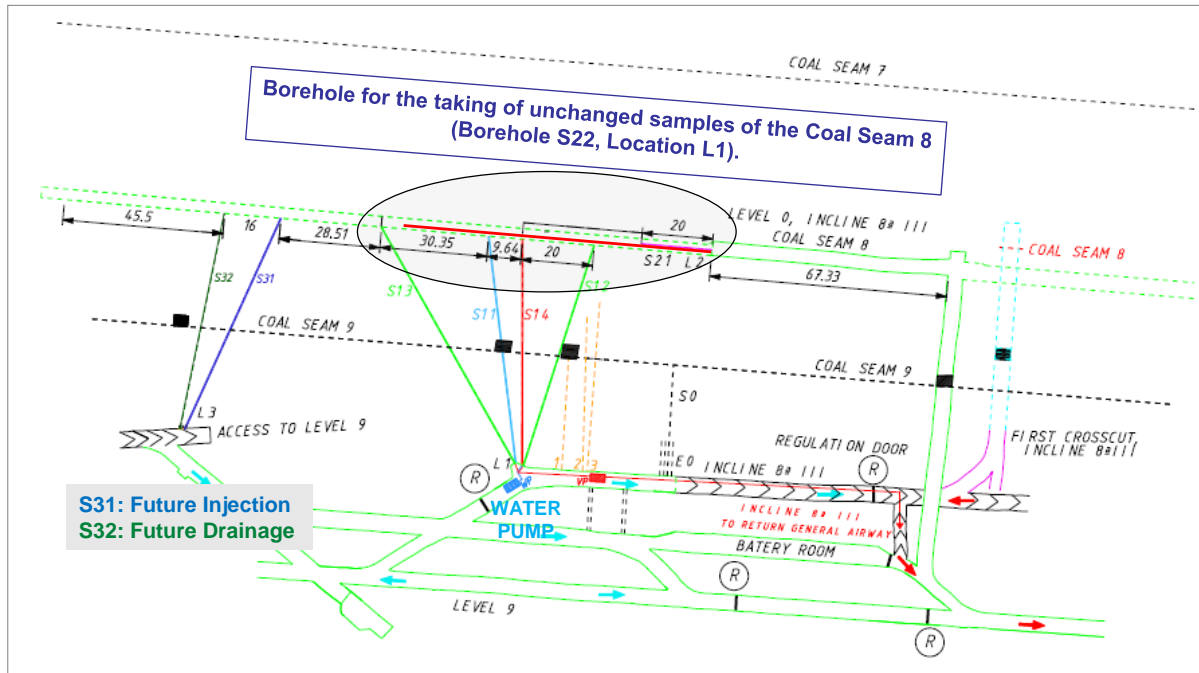


Figure 2.2.12.21. Tracer gas test at location L3

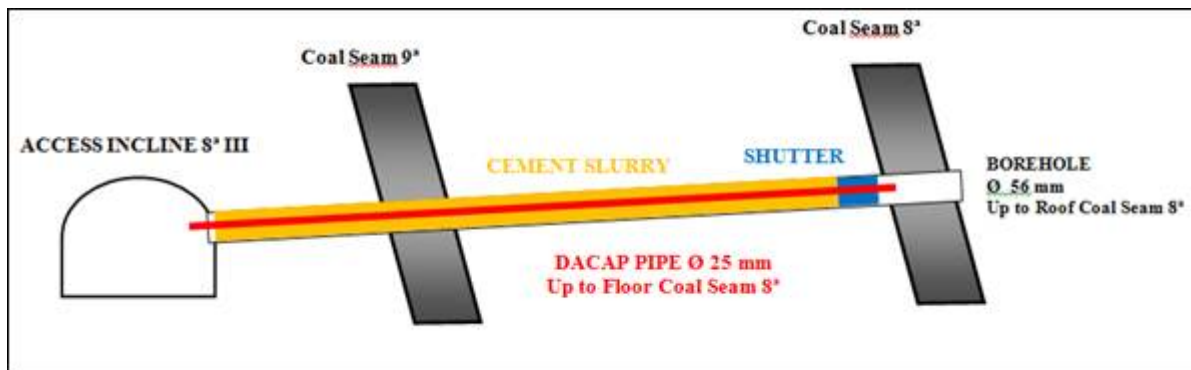


Figure 2.2.12.22. Tracer gas test at location L3. Cross section

On the March 19<sup>th</sup> 2018 the suction to the borehole S31 was changed to check its tightness for the performance of the tracer gas injection test. In view of the results (pump sucks, but CH<sub>4</sub> content decrease) it was suspected, that the borehole S31 is plugged. **Probably the packer placed to retain the cement grout failed, and the cement slid into the coal, clogging the bottom of the borehole and the mouth of the suction pipe** (see the picture above). As confirmed by the graphs recorded by RELIA AV system part of the initial gas pressure was remembered in the borehole S32. **Due to this circumstance, we were forced to suspend the injection of tracer gas injection.**

#### Conclusions:

This report constitutes real evidence of all the efforts, which were undertaken by Hunosa staff in order to verify the "Application of large scale stimulated drainage of methane at sub-level caving mining layouts at location of Hunosa". It covers the following tasks, which were carried out in the period between February 2016 and March 2018:

- Water injection tests performed for hydraulic characterization of seams at location L1.
- Hydrofracture tests
- Final commissioning of the monitoring and control system.
- Installation of vacuum pump for gas extraction.
- Analysis of gases captured by the vacuum pump in order to rule out presence of carbon monoxide.

- Combined water injection with gas suction at the same location: injection by S14, extraction by S13 and S12.
- Drilling boreholes at the location 3
- Results of water injection tests
- Results of methane drainage monitoring after water injection

The report gives also evidence of the difficulties we have encountered during its realisation. Some of them resulted from underground in situ conditions where all of the tests were performed. These caused certain delays and many times lack of continuity of operations due to geological and many times mechanical problems with the equipment. Due to above the research and tests were performed in 14 periods. Some other problems resulted from the safety concern and doubts concerning presence of CO, which were expressed by Regional Mining Authority of Asturias and resulted in refusing to approve progress of LEVEL 0 for security reasons. It made us change the research plans and to decide to drill a borehole allowing to take the unaltered samples and analyse them at the location L 2 - replacing the advance of the LEVEL 0 INCLINE 8<sup>a</sup> III 8th COAL SEAM. Last but not least was bankruptcy and in consequence withdrawal of AITEMIN from the project.

Considering above, obtained results presented in this report are the best possible to achieve –mostly thanks to our Spanish colleagues efforts and their devotion. They did their job very well which allowed us to understand and learn many new things and unfortunately confirmed that in situ mining and geological conditions can verify the best modelling job.

## 2.2.13. WP4, Task 4.4: Risk assessment and mitigation methods (led by INERIS)

### **Overview of stimulation techniques of firedamp drainage boreholes in coal mines**

Because it is not possible to identify a universal stimulation technique that could be applicable to all coal seams and mining conditions, 4 stimulation techniques were investigated in the framework of the GASDRAIN project:

- hydraulic fracturing,
- open or cased hole cavitation,
- high pressure water jet slotting,
- use of explosives.

### **Identification of relevant incidents or accidents**

Concerning the identification of relevant past incidents or accidents related to the stimulation of firedamp drainage boreholes, GASDRAIN partners were asked to share their feedback by answering a questionnaire. This work was afterwards completed through a literature review.

### **Identification of incidents and accidents through a questionnaire sent to GASDRAIN partners.**

The questionnaire written by INERIS was sent to partners by e-mail in mid November 2015. Partners were invited to answer before the end of 2015. The e-mail was sent a second time in mid December 2015 to ensure that partners would remember to answer the questionnaire.

### **Identification of incidents through the literature review**

INERIS completed a literature review to identify relevant incidents related to stimulation of firedamp drainage boreholes. The following hazards have been identified:

- Fluid bypass.
- Cross flow.
- Damage to the integrity of mine openings.
- Spontaneous combustion of coal.
- Gas or coal dust explosion.
- Pollution of groundwater

### **Risk scenarios related to the use of borehole stimulation methods**

A risk scenario is a chain of events that begins with a **specific hazard** (initial cause, e.g. induced seismicity), and ends with the **exposure of a stake at risk** (e.g. effect on human beings) (see Figure 2.2.13.1). The principle is similar for an accidental scenario such as an explosion that causes a human injury after transmission of an overpressure in the air [13, 14]. The collection of all identified risk scenarios defines the “risk model” of the system under study.

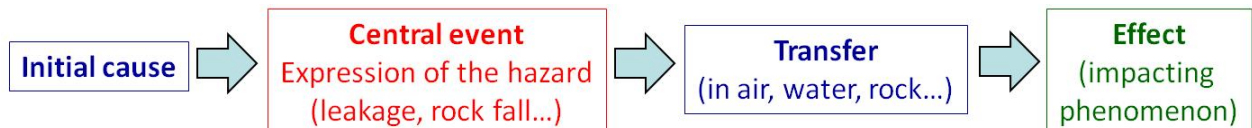


**Figure 2.2.13.1:** A risk scenario

### Identification of risk scenarios

The experience of INERIS in risk analysis on both surface industrial systems and underground operations shows that all methods used for risk analysis or risk assessment are based on a **set of events and scenarios**, either formalized (e.g. in a specific guidance or in a FEPs database: Features, Events, Processes).

The approach we use here is close to systematic approaches such as the "What-If" or the PRA method (Preliminary Risk Analysis) and was already used in the risk analysis of the CO<sub>2</sub> capture and storage (CCS) chain [16]. This approach is completed by an **event tree analysis method**, whose output is a chart that illustrates the cause-consequence relationships between events.

In order to carry out this exhaustive approach and to derive adequate relationships between events, we considered 3 major inputs:

- The learning from experience.
- The scientific literature.
- A series of interactive workshops (brainstorming) with INERIS experts that share experience in different scientific or technical fields. The final objective would be to continue this exercise with other experts and stakeholders, such as industrials, researchers, and NGOs if possible.

The following central events have been identified:

- Rock fall, collapse or coal mass intrusion in mining works.
- Emission of coal dust in mining works.
- Emission of gas in mining works.
- Migration of air along fractures in coal.
- Water migration and water intrusion in mining works.

Then, for each stimulation method, INERIS experts have worked on determining the mechanisms that can lead to the undesired events and on defining their effects/impacts. 4 mechanisms have been identified: rockburst, outburst, seismicity and unattended fracture creation or opening.

The following effects/impacts have been considered:

- Effects on workers: anoxia (i.e. O<sub>2</sub>-deficiency), toxic effects, injuries or death.
- Impacts on the environment: groundwater pollution.
- Impacts on mine productivity: operational problems (e.g. gas detection in mine workings leading to power cuts), damages to equipments.

### Construction of the event tree

All the scenarios with **cause-consequence relationships** have been drawn on a chart or "event tree" (also known as "fault tree" or "bow-tie") to ensure a synthetic vision.

An event tree is read from left (= hazards) to right (= effects). By convention, undesired events are placed in the middle of the event tree. Thus, they are known as "central events". In the graphic representation, each linear pathway is a risk scenario.

Arrows are used on the chart to report cause-consequence relationships between events. Dotted lines or features (e.g. lightning) can be used to point less likely or conditional relationships (refer to the legend of the event tree for further details).

Because there was no need to draw an event tree for each stimulation technique, only one event tree has been drawn.

The event tree highlights strong interactions between mechanisms, central events and effects/impacts, because:

- The same mechanism can lead to several events.
- An impact can be the consequence of different events.

## Safety barriers

### Definition of preventive and corrective safety barriers

Managing risks implies to define **preventive or corrective barriers** to prevent any impact in case a hazard occurs. Those safety barriers can be human (e.g. training), technical (e.g. cement seal) or both human and technical (e.g. manually operated systems).

Preventive barriers are designed to prevent the occurrence of undesired/central events when a hazard occurs. Thus, they are located in the left-hand side of the event tree. Corrective barriers are designed to prevent any impact when a undesired/central event occurs. Thus, they are located in the right-hand side of the event tree (Figure 2.2.13.2).

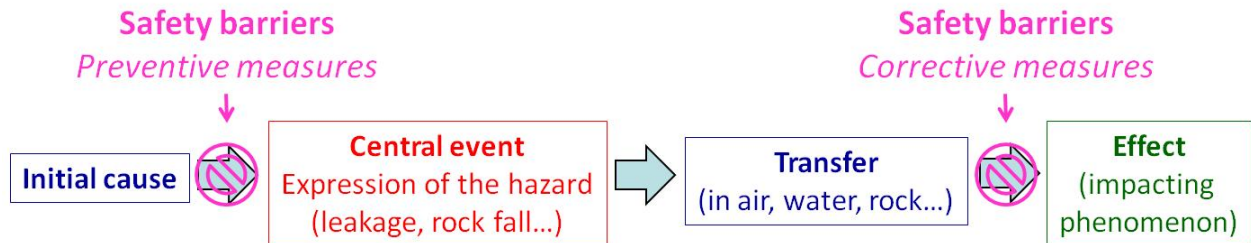


**Figure 2.2.13.2:** Preventive and corrective safety barriers on a risk scenario

As written in [21], prevention and mitigation barriers for underground systems are usually in the following categories:

- A. **Human preventive actions** in operation: they include fire permits or maintenance of the equipment. They can also include the design of the operation and the definition of the operating conditions.
- B. **Technical devices** to prevent failures during operation, such as detection of high temperature or overpressure, safety valves, etc.

After closure, long-term underground prevention barriers may also be relevant, such as plugs in boreholes or reactive barriers to prevent water contamination.

- C. **Corrective measures and intervention measures.**

These measures generally include technical devices (such as closing valves, injection of concrete or inertants), but they also necessitate a human action. They can include works on a borehole/gallery or even depollution works (e.g. correction of the harmful effects after a leakage is detected by monitoring).

- D. **Protection of the assets at stakes** (humans, equipments...) and other **organizational measures**.

- E. **Monitoring measures.**

The categories A and B are preventive barriers.

The categories C to E are corrective barriers.

Monitoring (category E) plays a specific role. Most often, monitoring is part of a corrective strategy, because a corrective action is triggered after a specific problem (e.g. leakage) is detected by monitoring. This means that from a theoretical point of view, **monitoring alone is not an entire safety barrier, because it has to be followed by a correcting action**. More generally, one of the **objectives of monitoring is also to demonstrate that the process behaves as foreseen**.

In what follows, we will assume that monitoring is focused on the milieu (coal, rock, surface environment), whereas the direct control of process/operations (pressure, temperature, etc.) is included in category B: technical prevention devices. Indeed the process control can detect deviations before an accident happens, e.g. by detecting an overpressure before a fracture or a leakage occurs.

The following safety barriers have been identified and placed on the event tree on the Figure 2.2.13.3, see below).

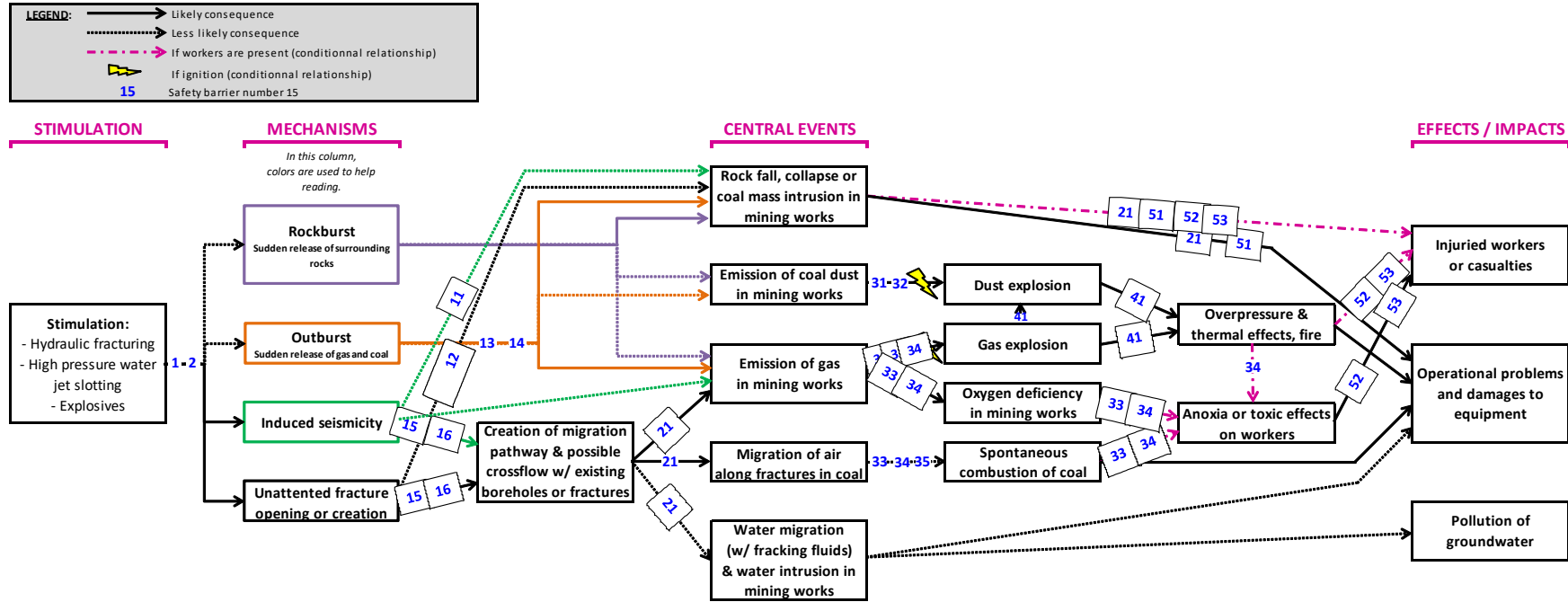


**Figure 2.2.13.3:** Event tree with safety barriers for risk scenarios associated with the use of borehole stimulation methods and mitigation measures underground.



## Description of safety barriers

**Design of a stimulation plan (safety barrier n°1).** Stimulation must be planned prior any operation to:

- Define the operating procedure.
- Identify safety requirements.
- Design the stimulation operations according known geological characteristics and mining conditions. Operations can thus be carried out far enough from known fractures OR pre-existing holes to prevent any unexpected cross flow.
- Inform workers about operations that will be carried out.
- Ensure that stimulation operations will be carried out far enough from active working areas where workers not involved in stimulation operations are present. Operations can also be carried out far enough from any mine opening so that interactions between fractures created during stimulation and mine openings can be avoided.

**Controlling of stimulation pressure (safety barrier n°2).** Stimulation pressure can be increased step by step to allow early detection of any problem during stimulation operations and limit any potential consequence. This is especially relevant in mine areas where coal seams have never been stimulated.

**Convergence monitoring (safety barrier n°11).** Convergence monitoring of mine workings (e.g. with extensometers) can help to detect any rock deformation that could lead to rock fall or roof collapse.

**Resin injection in fractures (safety barrier n°12).** In case stimulation operations create or re-open fractures, operators can inject resin to fill voids and prevent unattended fluid migration.

**Blow-out preventer (safety barrier n°13).** A blow-out preventer is a mechanical device used to close a borehole. It can be used in emergency when there is an uncontrolled flow of gas or coal dust in the borehole to prevent an outburst.

**Cementing borehole head (safety barrier n°14).** Cementing the borehole head helps preventing any emission of gas migrating along the borehole in the mine workings. Indeed, gas can migrate along the borehole axis through the drilling-induced damage zone (i.e. zone of higher permeability caused by drilling).

**Monitoring of stimulation fluid mass balance (safety barrier n°15).** Checking that stimulation fluid inflow equals stimulation fluid outflow helps to detect any leak of stimulation fluid or any production of formation water. Creation of migration pathway (e.g. cracks) or crossflow with existing boreholes or fractures can lead to a difference in mass balance.

**Fractures monitoring (safety barrier n°16).** Microseismic monitoring can help to detect any suspected seismic activity that could lead to rock fall or gallery collapse. Apparent fractures in working areas can be monitored visually.

**Sealing gallery walls with cement or similar material (safety barrier n°21).** Sealing gallery walls with cement or similar material can help to prevent any gas emission from coal seams and surrounding rocks in the mine atmosphere. It also prevents any migration of air (oxygen) from the mine workings to the seams.

**Possession of a fire permit (safety barrier n°31).** Coal mines can be classified ATEX (i.e. explosive atmosphere) area due to risks related to firedamp emission. Possession of a fire permit is compulsory if a hot point work is planned to be performed in order to prevent any ignition of gas or coal dust.

**Rock dusting (safety barrier n°32).** Application of rock dust (limestone, dolomite, gypsum, anhydrite, shale, adobe or other inert material) on floor of mine workings can prevent the propagation of coal dust explosions.

**Regulation of ventilation network and specific ventilation means (safety barrier n°33).** Control of gas releases from the coal seams and surrounding rocks and of gas concentrations in the mine atmosphere can be controlled by regulating the ventilation system and migration of fresh air in the mine workings.

**Gas detection in mine workings (safety barrier n°34).** Gas detectors to monitor O<sub>2</sub>, CO<sub>2</sub>, CO, CH<sub>4</sub>, H<sub>2</sub>, H<sub>2</sub>S, etc. in mine workings can inform about:

- Formation of explosive gas mixtures in case of firedamp emission from coal seams.
- Formation of atmosphere with gas concentrations that reach threshold values below anoxia and toxicity levels.
- Development of self-heating of coal.

**N<sub>2</sub> injection in old mine workings (safety barrier n°35).** Injecting N<sub>2</sub> in old mine workings can help to prevent any spontaneous combustion of coal by decreasing O<sub>2</sub> concentration.

**Gas and dust explosion barriers (safety barrier n°41).** Explosion barriers can be divided into two categories: passive or active barriers. Barriers are sub-divided into stone dust barriers and water barriers depending on the type of inert material (incombustible stone dust or water) used. Compared to stone dust barriers, water barriers are more easily maintained. The inert material is dispersed when the barrier is overturned. Whereas passive barriers are overturned with the blast of the explosion, active barriers are triggered using detection means such as ultraviolet sensors, infrared sensors, pressure sensors, etc. [20].

**Increasing roof and walls support of mine workings (safety barrier n°51).** Increasing support of mine workings in stimulated areas can help to prevent any injuries, casualties or damages to the equipment.

**Staff reduced to minimum and informed of location where stimulation is performed (safety barrier n°52).** Reducing staff to the minimum of people needed during stimulation operations can help to reduce the number of people exposed to potential risks.

**Evacuation equipment and safety procedures (safety barrier n°53).** Staff performing stimulation operations should be equipped with appropriated equipment to face any emergency (e.g. personal respirator and gas detectors) and be aware of safety procedures.

### General comments on safety barriers

Lots of safety barriers refer to techniques which are **common** and whose **efficiency has already been proven** in mining context: those techniques are widely used in mines even without performing stimulation operations (e.g. fire permits, rock dusting, explosion barriers, etc.).

Resin injection in fractures (barrier n°12) and fractures monitoring (barrier n°16) are maybe less common techniques because they appear to be quite specific to stimulations operations even if they may be already used in mines in other contexts. These 2 techniques should be tested during pilot tests to see if they can help to improve safety during stimulation operations. We will have to further discuss this point with the partners involved in work package number 4: "Field scale implementation of improved methane drainage systems at mine sites".

Note that N<sub>2</sub> injection in old mine workings to prevent any spontaneous combustion of coal (barrier n°35) should be implemented carefully in order not to induce oxygen deficiency in active mine workings that can lead to anoxia of workers.

### Conclusion

Task 4.4 of the GASDRAIN research project aimed at **identifying all relevant incidents or accidents** associated with the four stimulation techniques studied in GASDRAIN (hydraulic fracturing, open or cased hole cavitation, high pressure jet slotting, explosives) and at proposing best practice measures to prevent and mitigate these risks.

A questionnaire has first been used to identify relevant incidents known by project partners. The very few number of answers to the questionnaire we have received highlighted the **lack of partners' knowledge concerning past incidents and accidents** or the **lack of partners' feedback related to the use of stimulation techniques**.

Because, the questionnaire was not as useful as expected, INERIS completed a **literature review** to identify relevant incidents related to stimulation of firedamp drainage boreholes. 6 relevant incidents have been identified: fluid bypass, cross flow, damage to the integrity of mine openings, spontaneous combustion of gas or coal dust explosion and pollution of groundwater.

INERIS has then performed a **detailed risk analysis** to help risk management when designing future firedamp drainage projects, by identifying several **risk scenarios** (or chains of events) that begin with a **specific hazard** (initial cause) and end with the **exposure of a stake at risk** (an effect). All the scenarios with **cause-consequence relationships** have been drawn on a chart called an "**event tree**" to ensure a synthetic vision.

Managing risks also implies to define **preventive or corrective barriers** to prevent any impact in case a hazard occurs. Those safety barriers have been defined with all the partners during the second annual meeting held by AITEMIN in February 2016. All the barriers have been chosen among solutions already in use in mines, to ensure that they are operational and that their efficiency is proven. They are reported on an updated version of the event tree.

Because identified central events are typical risks in underground operations and because most of the described safety barriers are commonly used in mining environments, it appears that workers will not face unusual risks when performing stimulation operations. **Managing risks related to the stimulation of firedamp drainage boreholes does not seem to be particularly challenging. Protection of workers, environment and equipments should thus be ensured adequately.**

Next step of this work will be to propose recommendations to assist design of operations, risk prevention measures and monitoring of stimulation of firedamp drainage boreholes. This work will be done in work package number 6.

#### 2.2.14. WP5, Task 5.1 Monitoring and assessment of enhanced methane drainage efficiency of pre-drainage and cross measure boreholes at JSW (JSW, GIG, IMPERIAL).

##### Measurement system

Within preparation to long-term monitoring, JSW specialists elaborated specification of measurement system to measure all parameters necessary of gas obtained during drainage from stimulated boreholes. For the purpose it is necessary to know the following physical parameters: methane concentration, barometric pressure, methane volume flow in given time in galleries adjacent to longwalls and methane drainage pipe-lines. It is important to have continuous results of measurements from measuring devices and the measuring series should be made during mining operations in the longwall.

EMAG Institute developed a sensor for methane drainage parameters of type ZCO designed for measurements of physical properties and gas flow volume in the pipe-lines of the methane drainage system. JSW purchased four ZCO's. They were tested during preliminary measurements and results are shown within Task 4.2 presentation in previous Annual Report and In Delivery Report 4.2. The construction of the sensor is adjusted to operation with a chamber measuring orifice plate installed in the pipe (see Figure 2.2.14.1).

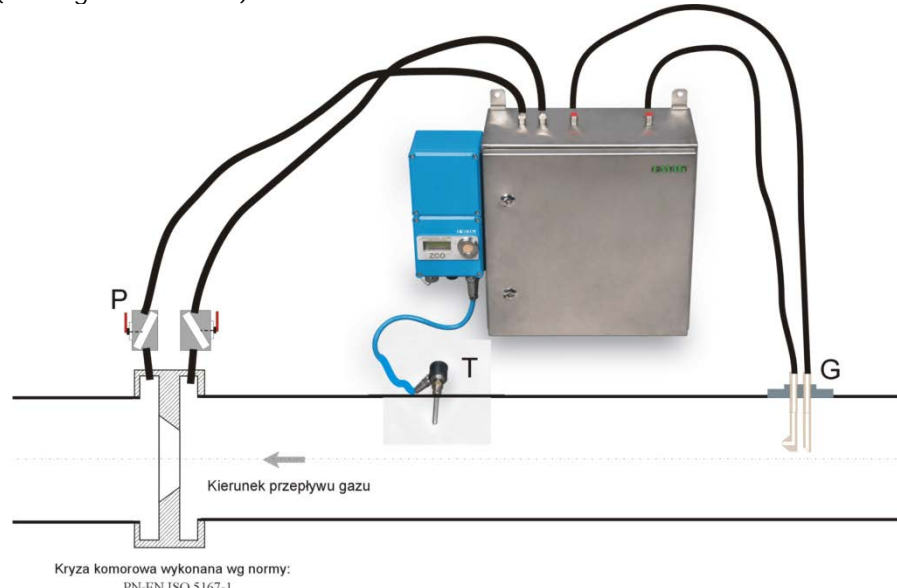


**Figure 2.2.14.1:** ZCO sensor adjusted to operation with a measuring orifice plate

Example of methane drainage system with measuring equipment was shown below (Figure 2.2.14.2).

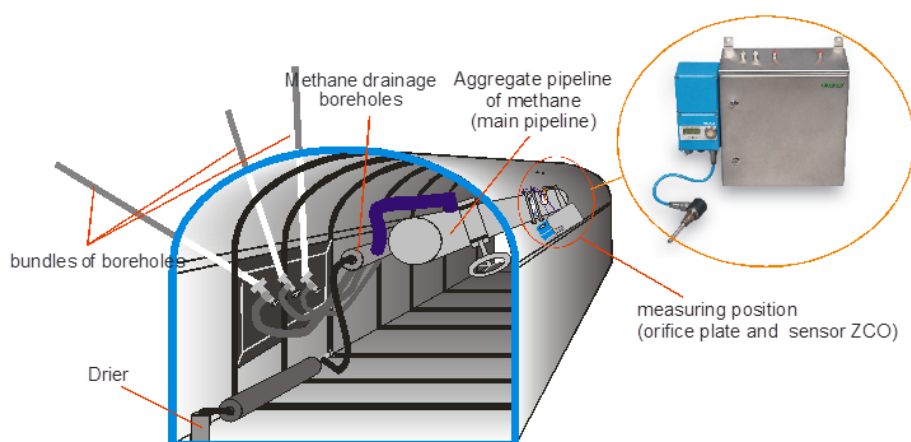


**Figure 2.2.14.2:** Example of methane drainage system with measuring equipment.

A structure of the integrated methane drainage sensor ZCO is presented in the Figure 2.2.14.3 .

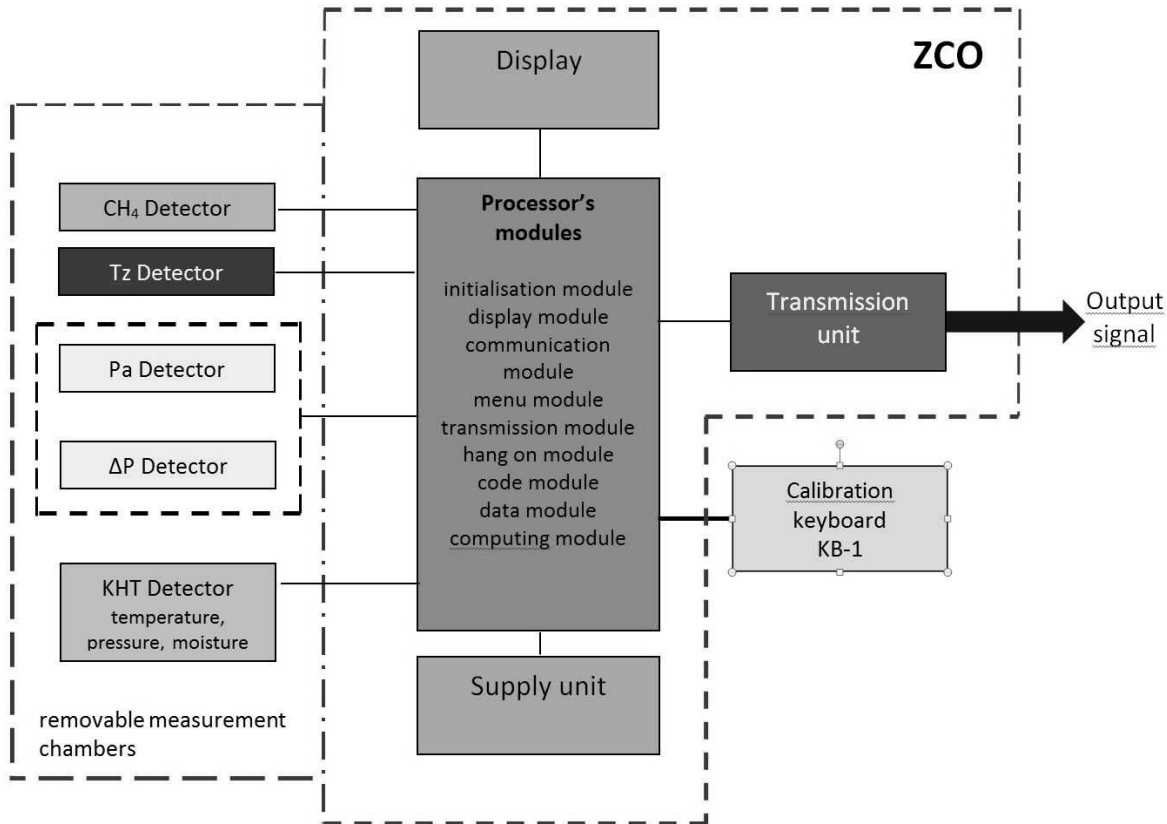


**Figure 2.2.14.3:** Block diagram of the integrated methane drainage sensor ZCO

A task of the integrated methane drainage sensor is to determine a gas flow volume in the pipe-line and to transmit this value to mine officer for methane monitoring in mine. The module of the detectors of the integrated methane drainage sensor ZCO consists of the following components:

- CH<sub>4</sub> - detector of high concentrations of methane (0 ÷ 100 %);
- T - internal or external (mounted at the pipe-line) temperature detector (10 ÷ 40 °C);
- P<sub>b</sub> - detector of the absolute pressure (0 ÷ 110 kPa);
- ΔP - detector of the differential pressure at measuring orifice plate (0 ÷ 200 Pa),

#### Data measured by the ZCO sensor

Methane concentration	0 ÷ 100 % CH <sub>4</sub>
	± 3 % CH <sub>4</sub> for concentrations 0 ÷ 60 % CH <sub>4</sub>
	± 5 % for concentrations 60 ÷ 100 % CH <sub>4</sub>
Temperature	-20 ÷ 80 °C; ±1 °C
Absolute pressure	0 ÷ 110 kPa; ≤ 2 % (2 kPa)
Differential pressure	0 ÷ 2.5 kPa; ≤ 1 % (25 Pa)
Range of atmospheric pressure	800 ÷ 1200 hPa

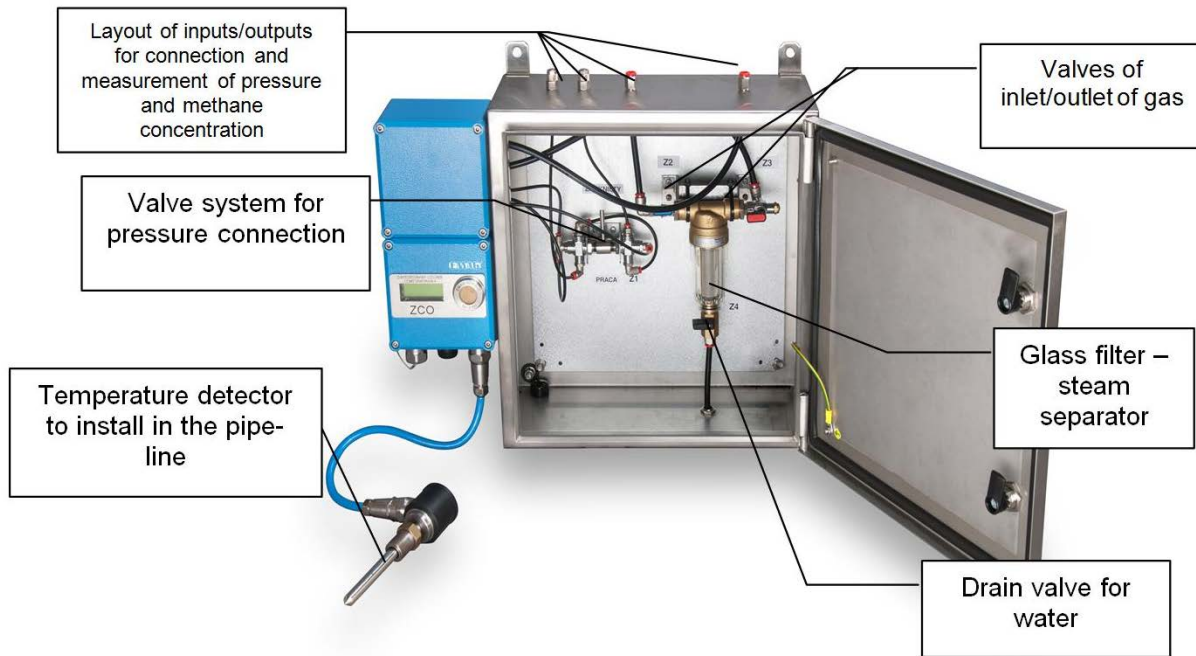


**Figure 2.2.14.4:** Components of integrated methane drainage sensor ZCO

#### Measurements and calculations of the methane drainage parameters

On the basis of the measured parameters there are calculated in the digital part of the sensor: a gas flow volume and a methane flow volume in the pipe-line. The values are transmitted to the central unit of the monitoring system.

The gas flow volume in the pipe-line is calculated by means of the following formula:

$$V_G = 0.11 \cdot a \cdot E \cdot d^2 \sqrt{\frac{P \cdot h}{s \cdot T}} \quad \left[ \frac{m^3}{\text{min}} \right]$$

where:

$V_G$  – gas flow volume in the pipe-line;

0.11 – numerical factor;

$a$  – flow factor;

$E$  – gas expansion factor. The orifices are matched that way to gain  $E=1$ ;

$d$  – diameter of the inlet [cm];

$P$  – absolute pressure in the pipe-line [mmHg];

$h$  – pressure drop at the measuring orifice plate [mmH<sub>2</sub>O];

$T$  – gas absolute temperature in front of the orifice [ $\square\text{K}$ ];

$s$  – relative gas density calculated according the formula or from a diagram:

$$s = \frac{\gamma_{CH_4} \cdot \%CH_4 + \gamma_{pow.} \cdot \%pow.}{\gamma_{pow.}}$$

Methane flow volume is a necessary parameter for the purpose of monitoring the methane drainage system:

$$V_{CH_4} = V_G \cdot \%CH_4$$

where:

$V_{CH_4}$  – methane flow volume in the pipe-line.

The methane drainage system is a subsystem which will be included in the methane-fire monitoring system SMP. This subsystem will allow a complex control of the mining methane drainage

system on the basis of the measurements of physical parameters at the measuring orifice plate and a chemical composition of gas inside the pipe-line.

Boreholes No 1 and 2 (Figure 2.2.11.17) were performed without any stimulations (cross measure boreholes). From this boreholes no gas flow was obtained, so monitoring was not continued.

After performing slots in boreholes: 7(G11b), 8(G11a) and 9(G11), integrated drainage sensors ZCO were connected to the boreholes:

- ZCO 540 (channel: 900, 901...907): registered data first from the borehole 8(G11a) and latter from the borehole 5(G13) - Figure 2.2.14.5,
- ZCO 541 (channel: 910, 911...917): registered data from the borehole 9(G11) - Figure 2.2.14.6,
- ZCO 544 (channel: 930, 931..937): registered data from the borehole 7(G11b) - Figure 2.2.14.7.

### **Preliminary results of drainage and its monitoring**

To prepare test site series of boreholes was prepared in district G as presented at Figure 2.2.11.12, Figure 2.2.11.17 and Figure 2.2.11.25. To preserve its stability and patency for gas drainage they were equipped in rubber hose and then slotted. Whole technique and procedure of test site preparation is described in part concerning actions under Task 4.2 (Chapter 2.2.11).

After connection boreholes to the drainage pipeline, valves at the measuring section line were opened and whole parameters were registered in ZCO sensors and recorded by methanometric system (ZEFIR / SEMP) in control room. Data from the sensors is presented at figures 5.70, 5.71 and 5.72. Before tests 3 ZCO sensors were checked and calibrated. It is visible in Figure 2.2.14.5 and 5.72 between 6:40 and 7:40.

The depression at level 290 mmHg (3942 mm H<sub>2</sub>O) was applied to the borehole.

Principal parameters registered by ZCO were:

- Humidity, % (sensors: MH901, MH911, MH931),
- Methane concentration, % (sensors: CM903, CM913, CM933),
- Absolute pressure in pipe, kPa (sensors: P905, P915, P935),
- Differential pressure at measuring orifice plate, Pa (sensors: RC906, RC916, RC936).

#### **Stage 1.**

The boreholes: 7 (G11b/2018), 8(G11a/2018) and 9(G11/2018) according to the numbering from Figure 2.2.11.17 were connected with the drainage pipeline. After connecting the vacuum there was a gas flow from borehole G11b with differential pressure of 240 Pa, in the boreholes 8(G11a) and 9(G11) the differential pressure (and actually the flow itself) was almost as small as the measurement mistake (about 5 Pa). This stage was visualised at figures 5.70, 5.71 and 5.72 between hours 09:11 and 09:29.

#### **Stage 2**

Due to above the middle borehole 8(G11a) located between 7(G11) and 9(G11b) boreholes was disconnected and stayed opened. The purpose of this was to enable eventual flow of gas through the system of fractures into the boreholes 9(G11) and 7(G11b).

The required effect was not achieved: the differential pressure in the flange of the borehole 9(G11) stayed unchanged, and in the 7(G11b) borehole slightly increased up to 260 Pa. It did not also change after closing the 9(G11) borehole. At figures 5.70, 5.71 and 5.72 it is shown between hours 09:29 and 09:34.

#### **Stage 3**

In these circumstances ZCO with all measurement equipment previously connected to the borehole 8(G11a) was moved and connected with 5(G13) borehole. It can be seen at Figure 2.2.14.6 after 11:50. The flow, which was recorded was again very low - as previously: the differential pressure was between 5 and 10 Pa. Methane content stayed at very low level at about 0.2%. The sensor did not react also for the standard mixture.

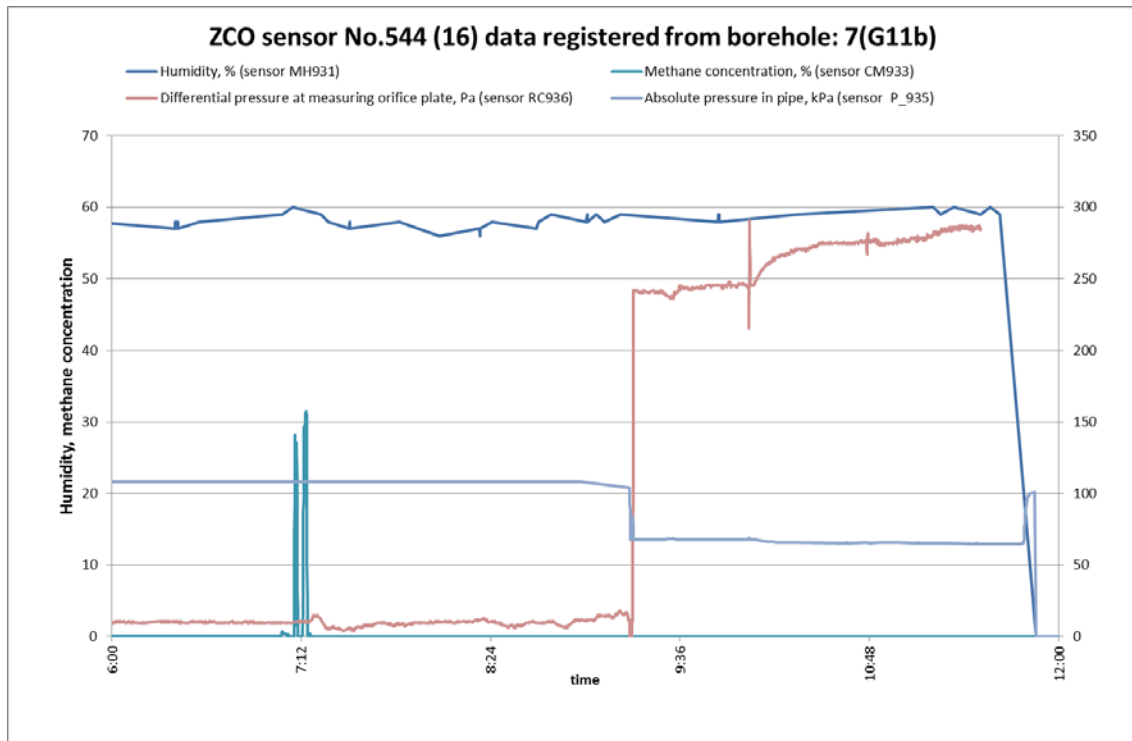


**Figure 2.2.14.5:** Data registered by ZCO sensor 544 on borehole 7(G11b)

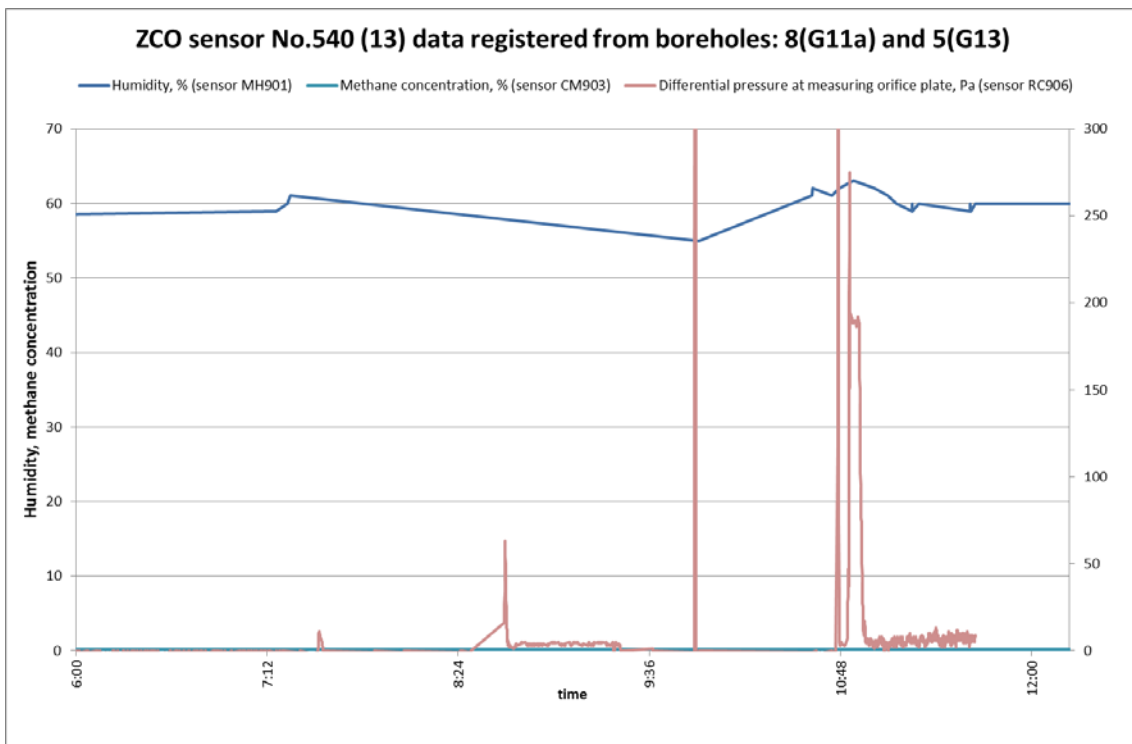


**Figure 2.2.14.6:** Data registered by ZCO sensor 540 on borehole 8(G11a) and 5(G13)

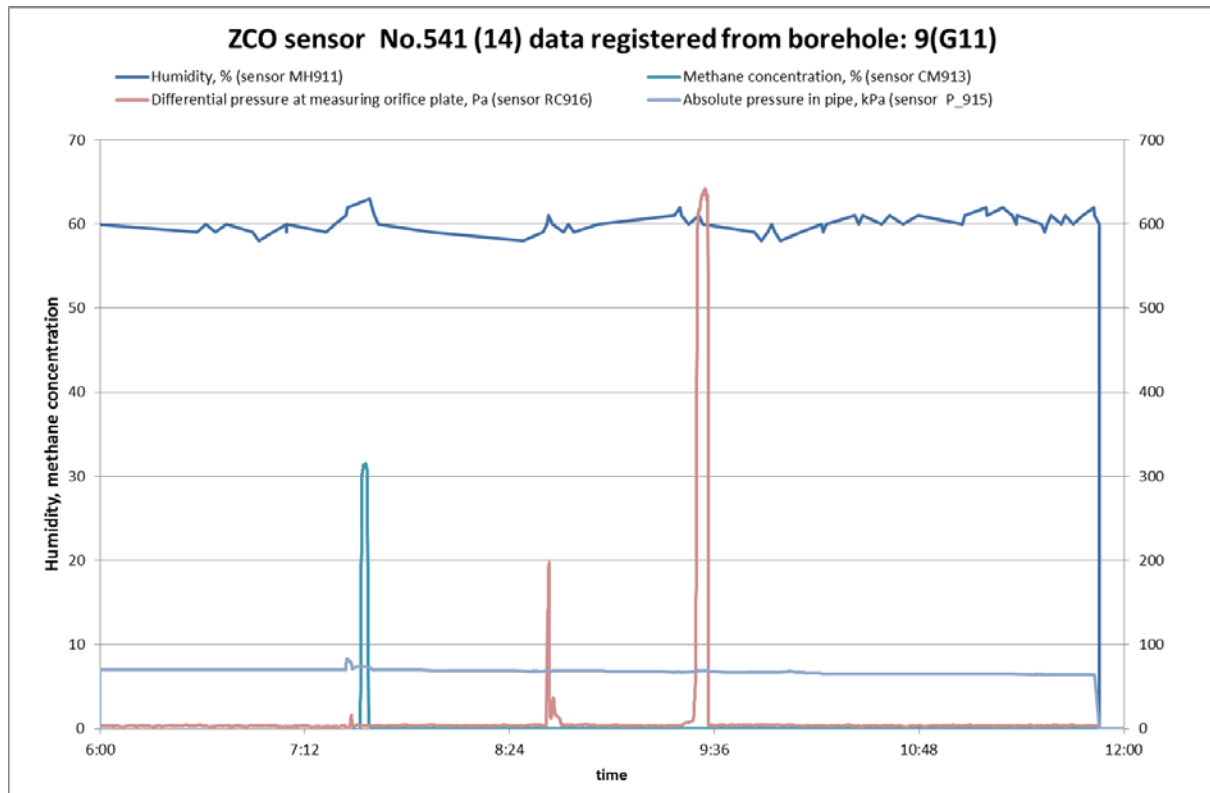


**Figure 2.2.14.7:** Data registered by ZCO sensor 541 on borehole 9(G11)

## 2.2.15. WP5, Task 5.2 Monitoring and assessment of enhanced methane drainage efficiency of pre-drainage and long holes at HUNOSA (HUNOSA, GIG, INIG).

Below you will find description and comments on the water injection test which has been run in Sueros coal mine in location L1. The test consisted in injecting water to S14 well and draining the methane from S12 and S13 wells. The gas drainage wells were connected to the pipeline equipped with a vacuum pump to help evacuation of released gas. Beside the injection and drainage wells the S21 well was drilled for monitoring purposes. The arrangement of test facilities is shown on Figure in Delivery Report Task 4.3, including the position of injection, drainage and monitoring wells as well as location of gas evacuation pipeline and vacuum pump.

Some information on injection and drainage wells is shown in table below.

**Table 2.2.15.1:** Boreholes features (location L1 & L2)

LOCATION	BOREHOLE	LENGTH		$\varnothing$ (mm)	INCLINE	NOTES
		C/9 <sup>a</sup>	C/8 <sup>a</sup>			
L1	S11	31,0	63,0	56	4°	SEALED
	S12	31,5	63,5	76/56	4°	GAS DRAINAGE
	S13	35,6	71,0	56	4°	GAS DRAINAGE
	S14	31,5	64,0	56	4°	WATER INJECTION
L2	S21		20,0	52	2°	PRESSURE MONITORING

The test was run from 21.02.2017 to 04.09.2017. The following injection/drainage periods were distinguished.

- Period 01: since 21-02-2017 to 08-03-2017. Preliminary tests. Pump Type BME 30/25.
- Period 02: since 8-03-2017 to 20-03-2017. Breakdown Pump Type 30/25

- Period 03: since 22-05-2017 to 31-05-2017. New Pump Type BME 30/45.
- Period 04: since 1-06-2017 to 07-06-2017. Pump Type BME 30/45.
- Period 05: since 7-06-2017 to 12-06-2017. Pump Type BME 30/45.
- Period 06: since 12-06-2017 to 19-06-2017. Pump Type BME 30/45.
- Period 07: since 19-06-2017 to 26-06-2017. Pump Type BME 30/45.
- Period 08: since 26-06-2017 to 3-07-2017. Pump Type BME 30/45.
- Period 09: since 21-07-2017 to 31-07-2017. New Pump Type BME 30/36.
- Period 10: since 31-07-2017 to 7-08-2017. Pump Type BME 30/36.
- Period 11: since 7-08-2017 to 14-08-2017. Pump Type BME 30/36.
- Period 12: since 14-08-2017 to 21-08-2017. Pump Type BME 30/36.
- Period 13: since 21-08-2017 to 28-08-2017. Pump Type BME 30/36.
- Period 14: since 28-08-2017 to 4-09-2017. Pump Type BME 30/36.

An estimation of water volume injected has been done for each period. The flow injected is included in table below. The following parameters were recorded during the test:

An estimation of the amount of water injected has been done in each period. The flow injected is included in the next table.

**Table 2.2.15.2:** Water injection volumes

Pump Type	Period		Water Injection
BME 30/25	21/02/2017	07/03/2017	7.280,42
	08/03/2017	19/03/2017	4.786,82
BME 30/45	22/05/2017	31/05/2017	11.856,59
	01/06/2017	06/06/2017	5.524,00
	07/06/2017	11/06/2017	13.286,00
	12/06/2017	18/06/2017	643,00
	19/06/2017	25/06/2017	16.652,86
	26/06/2017	02/07/2017	39.356,37
BME 30/36	21/07/2017	30/07/2017	9.435,29
	31/07/2017	06/08/2017	3.619,00
	07/08/2017	13/08/2017	3.569,00
	14/08/2017	20/08/2017	8.433,00
	21/08/2017	27/08/2017	7.727,00
	28/08/2017	03/09/2017	8.629,00
		<b>TOTAL</b>	<b>140.798,34</b>

The following parameters were recorded during the test:

#### **Water injection**

- Injection pressure at the pump pressure side
- flow rate of water
- pump current
- pump pressure at the suction side

#### **Gas suction**

- Methane content at heading
- CO content at heading
- Methane content at pump side
- Methane content at location L2
- Pump current on/off

The installation required for carrying out the water injection test has been designed to operate in unattended mode and was remotely controlled from the surface control room. The monitoring and control systems has been implemented to collect all the data required for the interpretation of the test. All monitored parameters are connected to the general purpose RELIA control system existing in the mine, which also controls the start/stop function of the injection pump. The injection pressure is regulated manually by a control valve installed at the pump output.

The RELIA system stores data at a frequency of 1 Hz (1 data per second). An example of the data available at the surface control room is shown in the next figure. In addition to this, a portable data logger capable of recording data at 20 Hz was connected in parallel to the RELIA system during the first tests, as it was not clear if 1 Hz would be enough to reconstruct the pressure drop curves with enough accuracy. Finally it was checked that 1 Hz was good enough for the dynamics of this process.

#### **Period 1 and 2: 20.02 – 20.03.2017**

Pump operating time 643 h 49' 30'', water injected 12067 litres

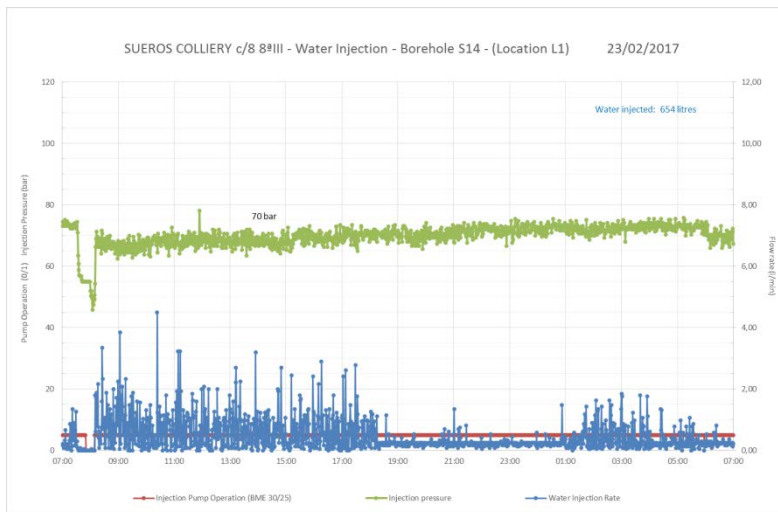


**Figure 2.2.15.1: Water injection, 23-02-2017**

The most meaningful information about coal seam parameters may be gathered by analyzing the detailed behavior of injection pressure vs flow rate record as – for example – shown in a graph for 03.02.2017 for time interval 10:00 - 12:00. The average injection pressure was about 67 bars and water flow rate 1 liter/min.

Please note that each pressure drop is accompanied by momentary increase of water injection rate i.e. increase of volume of water accepted by the coal. For example for 10:20 the four bars pressure drop is accompanied by increase of water injection rate from 1 l/min to 45 l/min. Similar graphs of water injection rate are observed for each of pressure change at 11:10. Such behavior of water injection rate versus injection pressure indicates that the pressure of injected water causes the opening of the micro fracture system and increases the volume into which the water may enter. This is accompanied by the temporary decrease of the injection pressure.

The cycle indicated above is repeated throughout the injection period. The time shift between the pressure drop and flow rate increase is too short to be noted on the graphs of injection pressure versus flow rate. In other words, the pressure of injected water causes the micro fracturing of coal. The similar pressure behavior may be observed for period 2 which lasts from 08.03 do 20.03.2017. The pump operating time was 287 h 22' 00'' and water injected 4787 l.

The pressure jumps are accompanied by sudden changes of flow rate which bears evidence to ongoing process of water pressure impact on coal structure ie. opening of micro fractures or creation of the new ones. This process is particularly evident on graph for 14.03.2017 (10:00 – 12:00 where small deviations from 80 bars injection pressure causes several dozen increases of water flow rate.

#### **Period 3: 22.05 – 31.05.2017**

Water injected 11875 litres, pump operating time 287 h 22' 0''

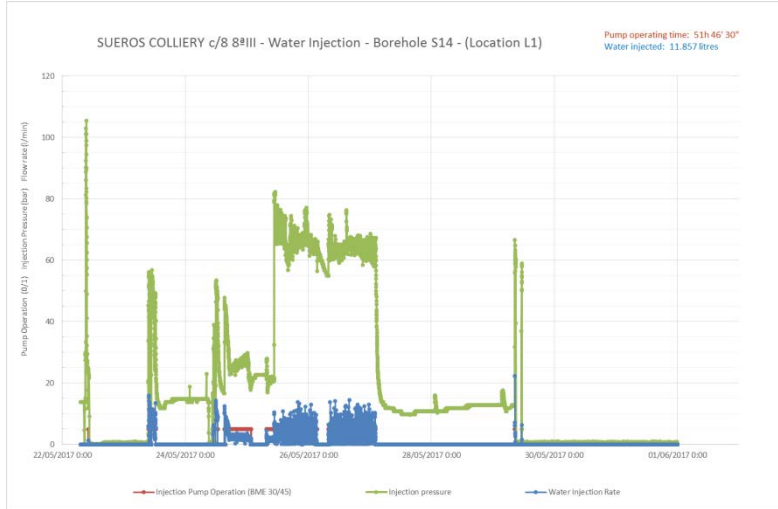


**Figure 2.2.15.2:** Water injection. Period 03: 22-05-2017 to 31-05-2017

Similar behavior of injection pressure versus flow rate may be observed for period 3. Characteristic features are shown in graph for 26.05 (10:00 – 12:00) where small pressure fluctuations are accompanied by large changes of flow rate . This indicate that the water front has reached regions where the coal is less compact and easily fractured by injection pressure (see graph for 26.05.2017 enfolding 24 hours interval from 7:00 am to 7:00 pm).

#### Period 4 01.06-07.06.2017

Water injected 5524 litres, pump operating time 55 h 38' 30"

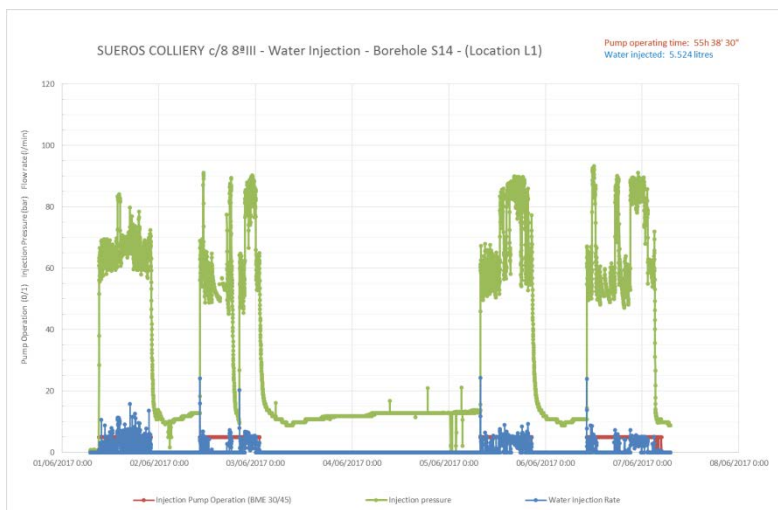


**Figure 2.2.15.3:** Water injection. Period 04: 1-06-2017 to 07-06-2017

The characteristic features of this period are: large pressure fluctuations accompanying small changes of flow rate. This indicate that the water front reached the more compact coal and that the opening of micro fractures system require the higher pressure. The vacuum pump suction pressure versus methane content measured at gas evacuation line from S12 and S13 wells are available for this period. Each engagement of vacuum pump is accompanied by temporary increase of methane content to 50-80% which quickly decay afterwards. The application of vacuum pressure at the suction line causes only temporary increase of methane content. The methane inflow to gas evacuation pipe has a form of single pulses i.e. jumps of CH<sub>4</sub> content. There are also no flow period of methane from S12 and S13 wells in spite of vacuum pump operation (see gas drainage graph for 05.06.2017).

#### Period 5: 07.06 – 12.06.2017

Pump operating time 64 h 41' 30'', water injected 643 litres.

As previously, the behavior of injection pressure versus flow rate indicates the ongoing micro fracturing process. Large fluctuations of water injection rate and small pressure changes indicates that the water front enters the less compact zone (09.06.2017, 10:00-12:00).

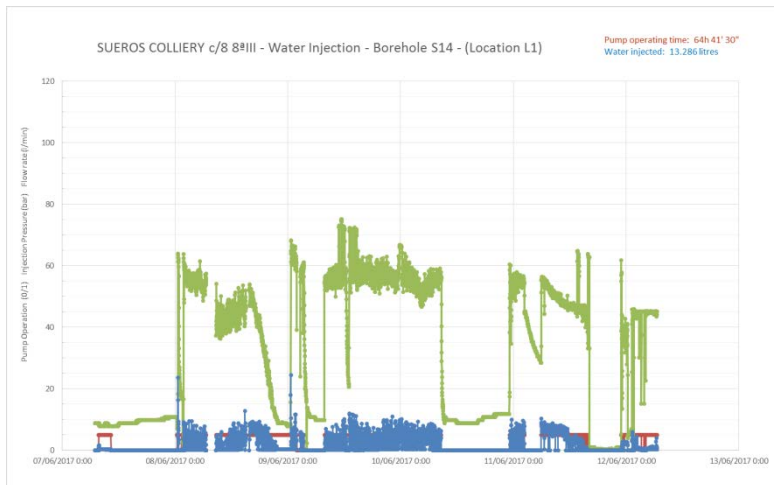


**Figure 2.2.15.4:** Water injection. Period 05: 7-06-2017 to 12-06-2017

#### Period 6: 12.06 – 19.06.2017

Pump operating time 67 h 30' 30"

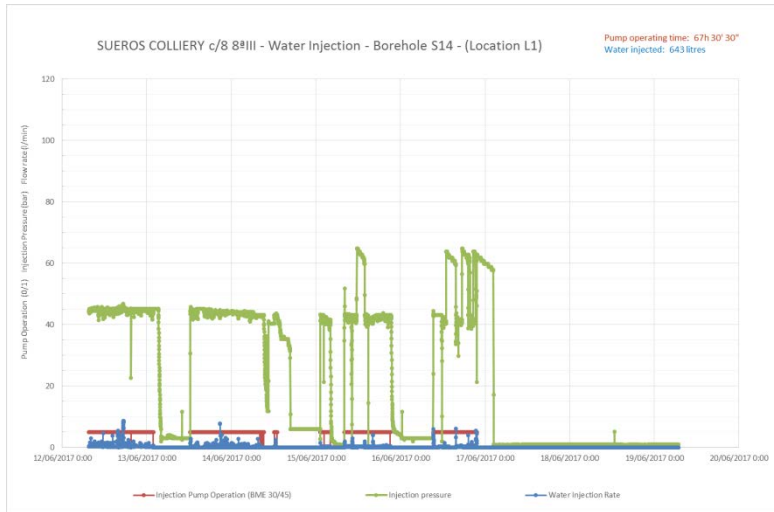


**Figure 2.2.15.5:** Water injection. Period 12-06-2017 to 19-06-2017

At average injection pressure equal to 45 bars the water injection rate is low and basically constant which indicates that the water front has reacted the more compact zone.

#### Period 7: 19.06-26.06.2017

Pump operating time 67 h 30' 30'', water injected 16653 liters.

The nearly constant injection pressure is accompanied by large fluctuation of water injection rate; water is "accepted" by coal matrix in a form of pulses of injection rate (see graph for 22.06 10:00-12:00) which indicates the micro fracturing in coal.

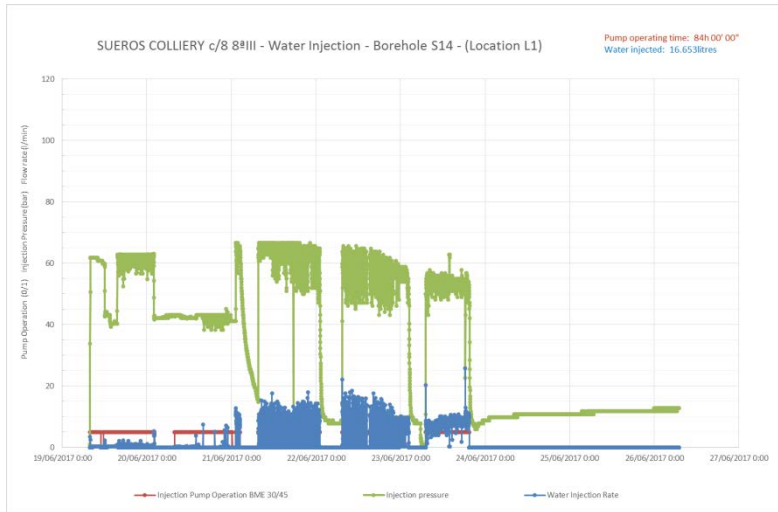


**Figure 2.2.15.6:** Water injection. Period 19-06-2017 to 26-06-2017

#### Period 8: 26.06 – 3.07.2017

Pump operating time 84 h 00', water injected 16653 litres

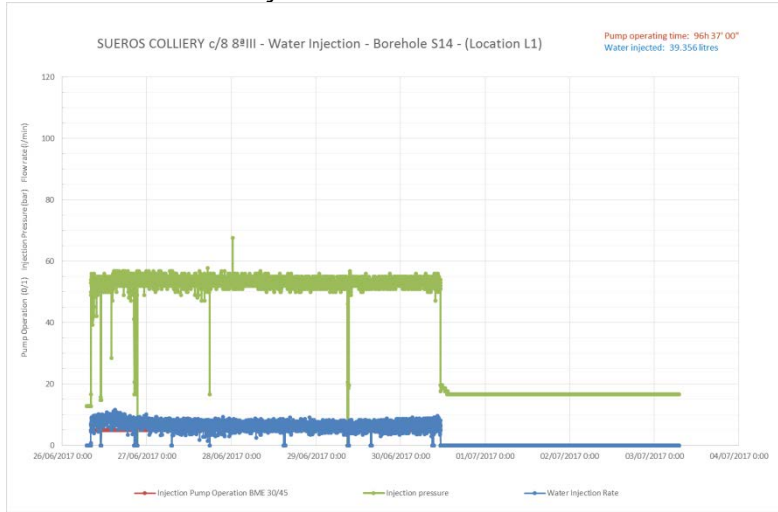


**Figure 2.2.15.7:** Water injection. Period: 26-06-2017 to 3-07-2017

The injection pressure vs. flow rate behavior is very similar as for preceding periods. There are momentary jumps of flow rate for small fluctuations of injection pressure (see 21.07 at the very beginning of next flow period).

#### Period 9-14: 21.07 – 04.09.2017

Pump operating time 374 h 08' 00'', water injected 41412 litres.

The behavior at injection pressure vs. water flow rate for periods 9-14 is commented as a whole. The flow rates and injection pressures are shown in graph provided below. As previously, the increase of injection pressure opens the microfractures system, increase the volume available for water and thus increase of water flow rate which in turn causes of decrease of injection pressure and so on. The time delay between subsequent changes of pressure and flow rate is extremely short and thus cannot be distinguished on the enclosed graphs.

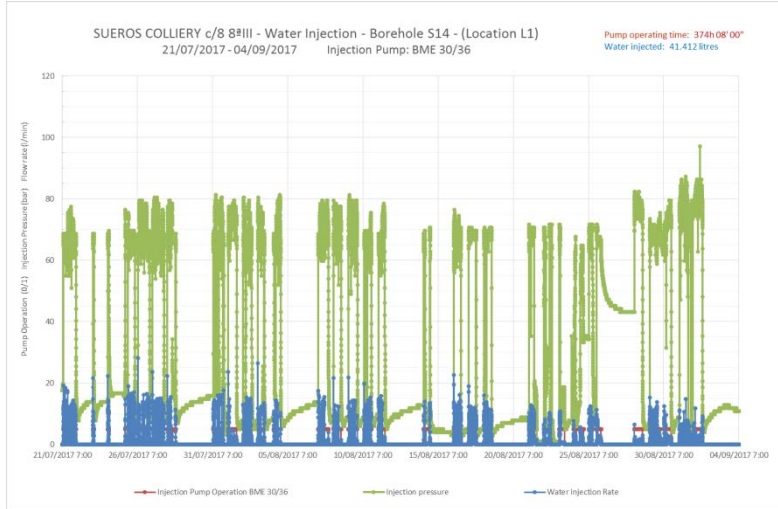


**Figure 2.2.15.8:** Water injection. Periods 09 - 14: 21-07-2017 to 04-09-2017

#### Collection of the methane from drainage wells S12 and S13

The changes of methane content in gas evacuation pipe are shown in graphs provided below (28.08.2017, 10.00-15.00). The constant aspiration pressure causes temporary increase of methane content which concentration amount to 80% (see graphs for 28.08-2.09.2017). Typical behavior of methane content in gas evacuated from S12 and S13 well is shown in graphs for 29.08.2017, 10.00-15.00.

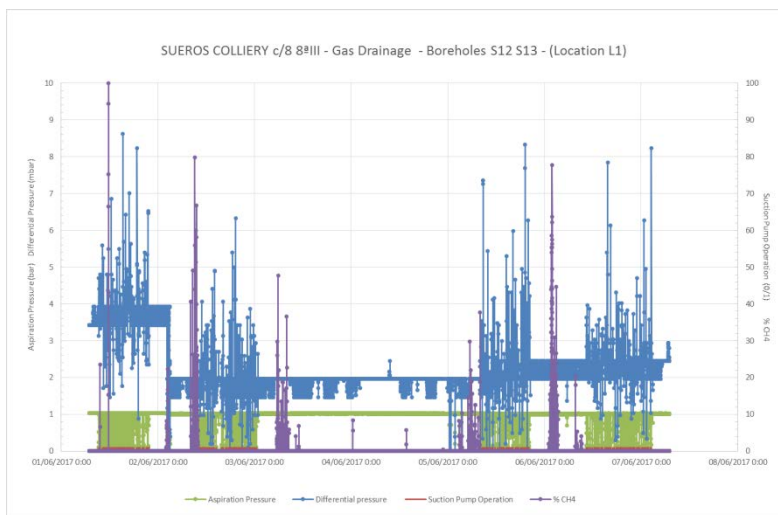


**Figure 2.2.15.9:** Gas drainage (wells S12 and S13). Period 04: 1-06-2017 to 07-06-2017

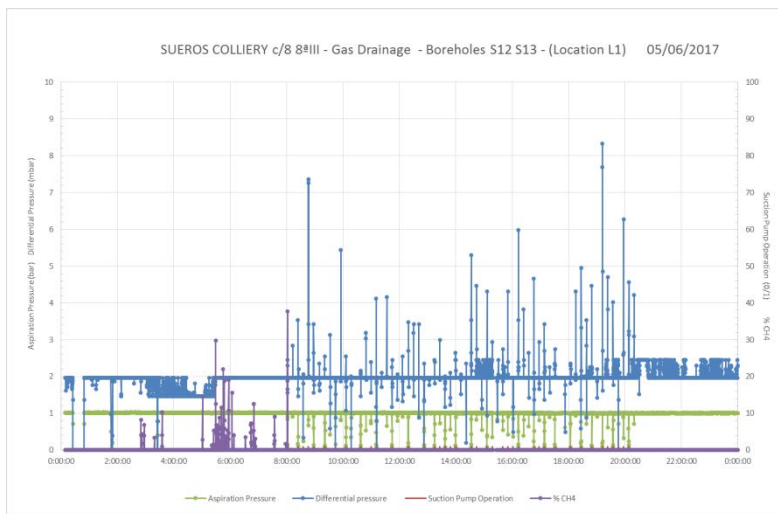


**Figure 2.2.15.10:** Gas drainage (wells S12 and S13), 05-06-2017

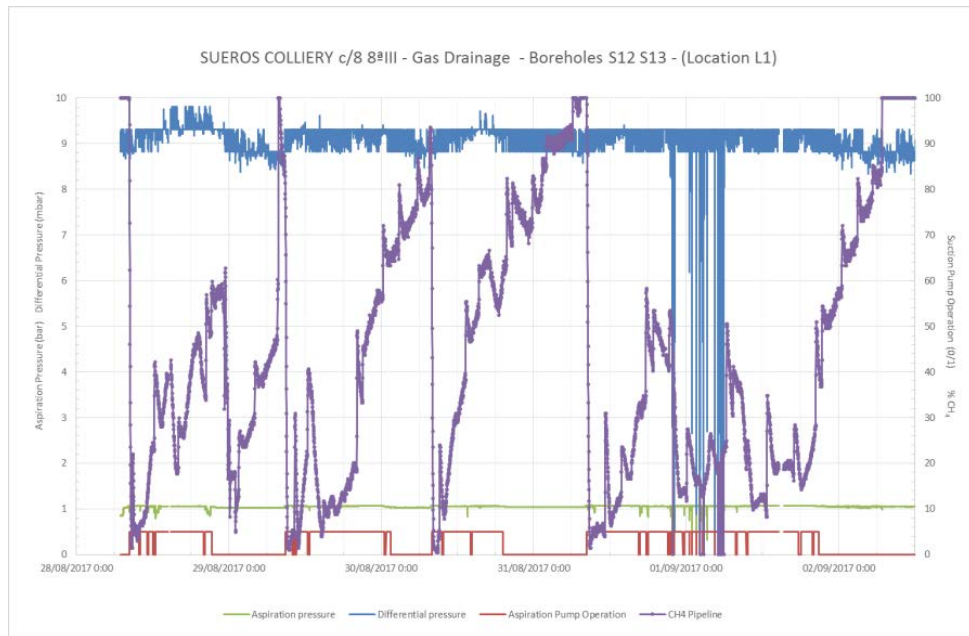


**Figure 2.2.15.11:** Gas drainage (wells S12 and S13). Period 14: 28-08-2017 to 04-09-2017

## Summary

The test being discussed was run in Montsacro coal mine (HUNOSA, Spain). The test duration was subdivided into 14 periods because of frequent failures of equipment. Time between subsequent periods was used for repairs of injection pump, data acquisition system and another facilities.

The test consisted in injecting water into S14 well and monitoring the gas flow on suction pipe which evacuates gas from S12 and S13 wells. The injection pressure and water flow rates in S14 well were recorded. The arrangement of water injection well (S14) and the gas drainage wells (S12 and S13) is shown in Figure 2.2.12.16 provided in chapter concerning Task 4.3. Figure 2.2.12.16 also shows localization of monitoring well S21. The objective of the test was to assess the possibility of producing methane by injecting water of S14 well and displacing the gas contained within the system of micro pores and fractures towards the drainage wells (S12 and S13). The volume of water injected in each period was recorded, as well as volume of produced gas. The gas flow from drainage wells (S12 and S13) was enhanced using the vacuum pump which was installed at gas evacuation pipe.

The analysis of injection pressure versus flow rate behavior allowed us for the following general comments regarding properties of coal in Hunoza coal mine:

- relations between injection pressure and water injection rate indicates that the water flow causes opening of the system of micropores and microfractures. Each increase of injection pressure causes microfracturing of coal, increase of volume available for water accompanied by the increase of flow rate which in turn causes decrease of injection pressure and so on. The whole water injection process is carried on in a cycling mode which can be easily observed on enclosed graphs. Intensity of this phenomenon is not constant but depends on coal compactness (strength parameters) and position of the water injection front. The large pressure fluctuations accompanying with the water minor changes of the flow rate indicates that the water front has entered the highly compacted zone. On the other hand the, the basically constant injection pressure and high fluctuation of water injection rate indicate that the water front has entered the less compacted zone. The afore statements are the "common sense" conclusions because the higher pressure is required for opening the fractures in highly compacted coals which is evident in graphs for all periods. The small amplitude of pressure changes accompanied by possibly large (but not necessarily large) fluctuations of flow rate indicate, in turn, that the water flows through the less compacted zone.
- In a water flooded zone the water can displace only the gas present in a system of micro and macro pores, fractures and crevices. The injected water is displacing the gas towards the drainage wells S12 and S13. On the other hand, the water does not mobilize the gas particles absorbed at the specific surface area of coal matrix. Because the volume of gas absorbed at the coal specific surface is several times greater than volume of micropore system, the water flooding process doesn't seem to be effective method of enhancing the methane production.
- Throughout the test period the injection pressure and water injection rate are fluctuating which is caused by structure of coal matrix. Anyway, one may choose the time period for which injection pressure and flow rate behaves in a predictable manner. On graph for

31.07.2017 (10:45-12:00) the injection pressure trend was approximated using the strength line and the following relations was used for calculation of permeability.

$$p_{inj}(\text{bar}) = p_0(\text{bar}) + 13,54 \frac{Q(l/\text{min})\mu(\text{cp})}{k(\text{mD})h(\text{m})} (\ln(t) + \ln \frac{k(\text{mD})}{\varphi\mu(\text{cp})c(1/\text{MPa})r^2} - 4,818)$$

where:

$Q$  – injection rate

$\mu$  - viscosity of water

$k$  – permeability of coal

$h$  - thickness of coal seam

$p_{inj}$  – injection pressure

$p_0$  – actual pore pressure within the coal

$t$  – time

$\phi$  – porosity of coal

$c$  – compressibility of coal

$r_w$  – well radius

Above relation describe the injection pressure behavior at the borehole wall as the function of time and coal parameters. It is commonly used in oil and gas industry for well testing purposes. It is evident that  $\Delta p = p_{inj} - p_0$  vs  $\ln t$  should plot along the straight line with slope  $m$ , where:

$$m = 13,54 \frac{Q(l/\text{min})\mu(\text{cp})}{k(\text{mD})h(\text{m})}$$

If we record the slope "m" and assume the average flow rate we can assess permeability of coal being analyzed as  $k = 0,05 \text{ mD}$  (details of calculation are omitted). Above calculations – at most – are very approximate assessment of permeability. It only gives us the idea what the value of permeability may be. The permeability of water flooded zone may be higher than permeability of intact coal matrix because of the water pressure impact on micropore system.

The table given below summarizes the results of water injection test in Sueros coal mine. It provides total volume of water injected to S14 well and volume of gas evacuated from S12 and S13 wells. The time of vacuum pump operation are provided for each test period.

**Table 2.2.15.3:** Results of water injection and methane drainage

Period	Date	Vacuum pump operation	Water volume injected	Volume of methane collected at suction pipe	Remarks
1	21.02-08.03	NO	7 280.42	0	Only injection
2	08.03-20.03	NO	4 786.82	0	Only injection
3	22.05-31.05	YES	11 856.59	1	Short time on aspiration/low % CH <sub>4</sub>
4	01.06-07.06	YES	5 524.00	4	Short time on aspiration
5	07.06-12.06	YES	13 286.00	273	Short time on aspiration
6	12.06-19.06	YES	643.00	293	Sensor failure
7	19.06-26.06	YES	16 652.86	508	Short time on aspiration
8	26.06-03.07	YES	39 356.37	421	Short time on aspiration
9	21.07-31.07	YES	9 435.29	831	Short time on aspiration
10	31.07-07.08	YES	3 619.00	631	Short time on aspiration
11	07.08-14.08	YES	3 569.00	757	-
12	14.08-21.08	YES	8 433.00	578	-
13	21.08-28.08	YES	7 727.00	533	-
14	28.08-04.09	YES	8 629.00	-	Pump failure

The table above indicates that, the water injection into S14 well and collection of methane from S12 and S13 wells aided by vacuum pump wasn't a very successful undertaking. Approximate assessment of permeability indicated a very low value ( $k = 0,05 \text{ mD}$ ).

## 2.2.16. WP5, Task 5.3 Assesment of the factors which may affect the performance of developed technique in different coal fields and geological conditions (INERIS, all partners).

Deliverable Report for the task is already finished and uploaded. In the report one can find full analyse done for the purpose of all factors with all references. Here the essencial part of the report is presented.

### **Review of site-specific factors influencing efficiency of stimulation operations**

Site-specific geology can play a key role in influencing fracture behavior and thus stimulation/drainage efficiency. In addition to the effects of the rock type and sometimes even thin layers within strata, natural cleats and fractures also play a role in fracture behavior and fracture propagation.

Factors are cited according alphabetical order.

#### ***Initial coal permeability***

Coal permeability directly affects the time required to sufficiently drain the coal seam. The lower the coal's permeability, the more time is needed to drain gas to reduce coal seam gas content to a targeted average value. Alternately, low permeability coals require a greater number of boreholes to achieve the desired methane content in seams in advance of mining.

#### ***In-situ stress***

Coalbed depth and surrounding rock types have important fundamental influences on fracture dimensions and orientations. The local in-situ stress influence fracture behaviour.

According to Nielsen and Hansen, the direction of least principal stress tends generally to be vertical at depths of less than 300 meters. Thus, at these relatively shallow depths fractures typically have more of a horizontal than a vertical component.

In seams deeper than 300 meters, the least principal stress tends to be horizontal so vertical fractures tend to form. Vertical fractures created in these greater depths can propagate vertically to shallower depths and then develop a horizontal component (Nielsen and Hansen, 1987).

INIG points out that the optimal azimuth of horizontal stimulation boreholes is perpendicular to the direction of the maximum horizontal stress.

#### ***Lithology***

Differences in fracture behaviour may be due to very small layers or irregularities that exist in the seams as part of the sedimentation process that created them.

For example, the presence of a shallow clay layer as thin as 10 millimeters in a coal seam can cause a vertically propagating, shallow hydraulic fracture to "rotate" horizontal and fail to propagate further vertical.

Warpinski et al. (1982) also found that thin ash-enriched beds can influence hydraulic fracture propagation.

#### ***Natural cleat and fracture systems***

Presence of a pre-existing cleat or fracture system leads fracture development as pressure is released into cracks already opened and which will be propagated. Indeed, injected fluid will first migrate through the system of cleats or fractures before creating new cracks.

Performing stimulation by using explosives (blasting) is recommended for formation with limited natural fractures. Indeed, large fracture systems are unfavourable conditions, because explosion energy is dispersed and stimulation is thus less effective.

#### ***Rock mechanical properties***

Naceur and Touboul (1990) state that the primary mechanisms controlling fracture height are contrasts in the mechanical properties of the rock strata within and surrounding the coal zone being fractured. Often, a high stress contrast results in a barrier to fracture propagation.

Coal is generally very weak (with low Young's modulus) and easily fractures. Siltstones, sandstones, and mudstones (other rock types commonly occurring in coal zones) tend to have higher moduli, greater toughness and fracture less easily (Warpinski, 2001). Thick shales, which commonly overlie coalbeds, often act as a barrier to fracture growth.

## **Review of method-specific factors influencing efficiency of stimulation operations**

For each stimulation methods, there are several operator-controlled actions that can play a key role in the efficiency of drainage.

In this paragraph, method-specific factors that can act on the efficiency of drainage are highlighted. Note that only stimulation methods studied in the framework of the RFCS GASDRAIN project are discussed here.

Factors were identified from results obtained and experience gained by partners within the RFCS GASDRAIN project. For this purpose, Ineris reviewed all deliverables published by project partners before the 1<sup>st</sup> of March 2018. Source of each observation is clearly identified by a bibliographical reference. Details on each deliverable can be consulted in bibliography.

When useful, some reference documents published outside the framework of the project are cited to complete lessons learned from project.

### ***Hydraulic fracturing***

Factors are cited according alphabetical order.

#### *Injection rate*

Higher injection rate has a favourable effect on fracture geometry and proppant distribution. Indeed, when injection rate increases, results from modelling performed by IMPERIAL COLLEGE show that:

- The fracture length does not change much, but the fracture height and width keep increasing.
- Proppants tend to accumulate more in the fracture.
- Larger fracture dimensions, larger propped dimensions as well as larger fracture slurry efficiency are induced.

Results from modelling performed by IMPERIAL COLLEGE also concluded that in view of the fracture and proppant dimensions, the proppant concentration and the injection rate upper limit, an injection rate of  $0.05 \text{ m}^3.\text{min}^{-1}$  is suggested for hydraulic stimulation for the two coalfield conditions studied in the project: HUNOSA in Spain and JSW in Poland.

#### *Injection time*

Longer injection time has a favourable effect on fracture geometry and proppant distribution. Indeed, when injection time lasts longer, results from modelling performed by IMPERIAL COLLEGE show that:

- The fracture height, length and width increase and the fracture gradually grows.
- Both the propped dimensions and the average proppant concentration in the fracture increase.

But modelling also shows a detrimental effect of injection time on fracture slurry efficiency.

#### *Nature of fracturing fluids*

The fluids used for fracture development are pumped at high pressure into the well. They may be "clear" (most commonly water, but may include acid, oil, or water with friction-reducer additives) or "gelled" (viscosity-modified water, using guar or other gelling agents).

Increasing fracturing fluid viscosity can increase the pressure due to injection, resulting in greater fracture width, and thus often shorter extension of fractures (Olson, 2001).

IMPERIAL COLLEGE is going to deliver a report on lab experiments designed to test different natures of fracturing fluid (deliverable D2.2B).

#### *Propping agents (proppants)*

Composition of fracturing fluids may vary from simple water and sand to complex polymeric substances with a multitude of additives. Indeed, propping agents (or "proppants") can be used to maintain opening of fractures after the injection (fracturing) pressure is reduced.

IMPERIAL COLLEGE has performed lab tests to highlight role of proppants. It thus appeared that proppant use in fractured coal samples increased the permeability of coal by a factor of 2 to 10 over the range of effective stresses applied.

IMPERIAL COLLEGE noted that lab experiments with large particle size synthetic proppants result in formation damage and clog the fractures by penetrating into the coal matrix. The use of sand as a proppant seems better appropriate. Indeed, sand is used in almost all coalbed methane wells by the industry.

### *Pumping pressure*

Results from modelling performed by IMPERIAL COLLEGE show that the increase of pumping pressure leads to an increase of total crack numbers. Modelling suggested a pumping pressure of less than 40 MPa in field-scale applications in HUNOSA and JSW mines.

### *Volume of fracturing fluids injected*

Large injection volumes also often result in extensive networks of induced fractures.

Generally, the larger the volume of fracturing fluids injected, the larger the potential fracture dimensions. Fluid injection rates and viscosity can also affect fracture dimensions (Olson, 2001 and Diamond and Oyler, 1987).

### **Cavitation**

Concerning stimulation by cavitation, GASDRAIN partners did not identify method-specific factors that can help improving the drainage efficiency.

Partners focused the study on site-specific factors and noticed that a notable improvement in the post-cavitation permeability enhancement is observed when the seam gas pressure is higher and that a lower coal strength (cohesion) leads to a higher failure zone.

Modelling done by IMPERIAL COLLEGE shows opposite results depending the mining context:

- Cavitation failed to lead to any noticeable improvement in seam permeability in the JSW mine context (Poland).

Cavitation led to an increase of the coal permeability by over one-order of magnitude within a region of 0.7 m radius around the borehole in the HUNOSA mine context (Spain).

## **Water-jet slotting**

Factors are cited according alphabetical order.

### *Choice of nozzle*

The nozzle is a key element during water-jet slotting. Early ageing of the nozzle can lead to broaden the water-jet and thus reduce the efficiency of the slotting operation (because energy is no more focused on a small but larger surface).

Water-jet slotting tests performed by GIG in JSW mine highlighted the attention to be paid to the nature of the nozzle. Coal particles might cause damage to the nozzle. Nozzles with ceramic lining has to be preferred to simple metal nozzle; as they appear to be more durable.

### *Slot diameter*

Due to the drilling and the slotting, a stress relief zone forms next to the borehole, surrounded by a stress concentration zone. The stress relief zone would enhance permeability and stimulate gas production, while the high stress zone would hinder gas transport towards the borehole.

Results from modelling performed by IMPERIAL COLLEGE indicate that the simulated failure zone size is comparatively much more sensitive to the change of slot diameter: increasing the slot diameter from 0.50 to 0.75 m would double the failure zone volume.

Compared with slot thickness, increasing slot diameter is more effective in enlarging the stress relief zone and pushing the stress concentration zone further away from the borehole. It means that the size of the enhanced permeability zone is more sensitive to the variation of slot diameter than slot thickness. Larger slot diameter can create a larger pressure relief shadows along the two sides of the slot.

The relationship between slot diameter and failure zone size is non-linear. Modelling shows that the linear increase of slot diameter can exponentially enlarge the failure zone size. Therefore, in engineering practices, slot diameter is recommended to be as large as possible in order to achieve a maximised stimulation zone.

### *Slot plane*

IMPERIAL COLLEGE showed through modelling that a larger stimulated zone can be achieved when the normal of the slot plane is in parallel with one of the principle stresses. The optimal orientation of the normal of the slot plane is found to be parallel to  $\sigma_3$  (see figure 5).

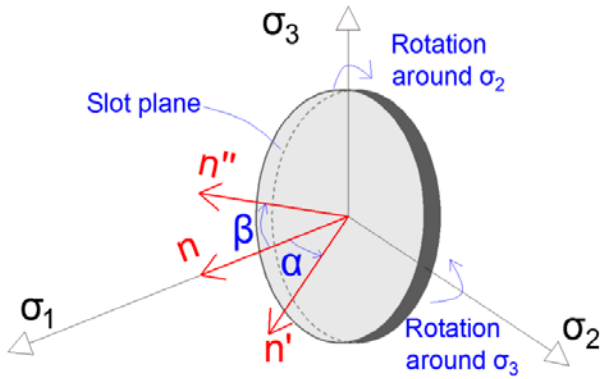


**Figure 2.2.16.1:** Schematic of slot plane rotation with respect to in-situ stresses

#### *Slot shape*

During the field slotting operation, it is rather difficult to accurately control the shape of slots, and consequently, non-circular slots may be created. In general, the elliptical slot yields a smaller failure zone than the circular slot. Modelling demonstrates that the major axis of the ellipse should be placed in parallel with the lower principle stress in the slot plane to produce a larger failure zone.

#### *Slot thickness*

Modelling performed by IMPERIAL COLLEGE showed that increasing the slot thickness fails to effectively enlarge the stress relief zone. Indeed, by enlarging slot thickness (0 m, 0.03 m, 0.06 m, and 0.09 m), only a marginal increase in the percentage of de-stressed failure zone volume can be observed.

In the context of HUNOSA mine, IMPERIAL COLLEGE modelled that a marginal increase in the percentage of failure zone volume can be observed from 8.3% to 9.5% and 11.2% when the thickness of the slot was increased from 0.03 m to 0.06 m and 0.09 m respectively.

In order to maximise the performance of slotting operation, one needs to aim at achieving as large as possible of slot diameter, while increase slot width can be only considered as an additional measure which can only slightly enlarge the stimulated zone.

#### *Slots separation*

According to GIG field experience on JSW mine context, the minimum separation between 2 slots is between 0.5 to 3.0 meters. It is thus possible to ensure an efficient drainage of the coal seams in the JSW mine [14].

This range was confirmed by INIG. INIG performed modelling comparing slot separations of 2, 4 and 6 metres. Better drainage is achieved in JSW mine context when slot separation equals 2 metres.

#### ***Use of explosives***

Factors are cited according alphabetical order.

#### *Combustion time*

The energy of the gases released during the blasting (deflagration) of the explosives is used in order to initiate fractures in the vicinity of the drainage boreholes and to fracture the coal seam. GIG proposes to use explosives with a slow combustion speed i.e. an extended combustion time. These explosives are different from classic mining explosives.

By using explosives with extended combustion time, dissipation of explosion energy favours the penetration of the gases or the compression of the liquid in the borehole, rather than the destruction of the coal structure in the near zone.

#### *Fracture initiation*

Feedback from field experiment helps GIG drawing the conclusion that boreholes to be stimulated using explosives need to be prepared by cutting/creating a number of fractures (so called "initial fractures") to direct the post-explosion gases. Fracture initiation favours gas penetration of the strata rather than destruction of coal structure in the near zone. Thus, fracture initiation aims at extending the area of influence of the stimulation.

Indeed, the use of explosives can create a fine grid of fractures in the coal seam and initiate migration of methane from the seam into the drainage boreholes. However, the use of explosives in boreholes drilled along the coal seam only is not very effective and, an effective drainage can only be achieved

by using a fine grid of blast holes. By creating initial fractures inside the boreholes, it is possible to reduce the number of such boreholes required.

GIG noted that the smaller the distance between these initial fractures the bigger effect they will have.

#### *Nature of the detonator*

Blasting is more effective when borehole is filled with water, but ignition mass and ignition head are usually not moisture resistant/waterproof. Therefore, they have to be equipped with a special cover to protect against moisture and, they must be particularly tight in the vicinity of the initiating combustion unit.

#### *Nature of the explosive*

Explosives shall provide effective fracturing.

The result of the explosives' firing in the heavy gassy coal seam should not be destruction of the coal bed but only establishing in it a fine grid of fractures and dividing it into smaller fractions. Therefore, application of this method in coal seams requires the design and development of charges which lead to minimize the mastication zone and a maximize the crushing and cracks zones.

GIG highlights the fact that using charges made of heterogeneous materials, rather than single explosive charge, can cause the generation of very high toxic gases such as CO and NOx [14]. The risk assessment study achieved by Ineris has pointed out that toxic effects on workers are one of the possible risks encountered when performing stimulation operations. Toxic effects can lead to injured workers or casualties. Toxic effects have several origins such as emissions of gas in mining works after blasting. According GIG experience, not using charges made of heterogeneous materials is a safety measure (or "safety barrier") that prevents excessive emission of toxic gas due to the use of explosives.

### **Conclusion**

Task 5.3 in WP5 of RFCS GASDRAIN project aimed at assessing the factors which may affect the performance of stimulation techniques of firedamp drainage boreholes in different coal fields and geological conditions. The objective was to collect all kind of practical information that may appear useful for the developments planned in the project. The analysis was focused on **positive** as well as **negative experiences** in order to understand the main factors influencing the efficiency of the coal seam drainage process.

This deliverable is a synthetic report proposing recommendations to assist the choice of a technique to stimulate firedamp drainage boreholes and improve pre-drainage efficiency. It summarises all the **experience gained in the RFCS GASDRAIN project** through field testing or modelling. In this purpose, Ineris performed a review of all project deliverables (published by project partners before the 1<sup>st</sup> of March 2018) in order to **highlight factors that have a positive or a negative impact on the performance of a stimulation**.

**Site-specific geology** can play a key role in influencing fracture behavior and thus stimulation/drainage efficiency, as well as **operator-controlled actions**. Site-specific and method-specific factors were identified from a literature review and from results obtained by GASDRAIN partners. The following table lists all key factors that were identified and are detailed in the Delivery Report D5.3.

**Table 2.2.16.1:** Key factors that were identified

Nature of factors	Identified factors
<b>Specific to site where stimulation is performed</b>	Initial coal permeability In-situ stress field Lithology Natural cleat and fracture systems Rock geomechanical properties
<b>Specific to a stimulation method</b>	<b>Hydraulic fracturing</b> Injection rate Injection time Nature of fracturing fluids Propping agents (proppants) Pumping pressure Volume of fracturing fluids injected
	<b>Cavitation</b> <i>No method-specific factors identified</i>
	<b>Water-jet slotting</b> Choice of nozzle Slot diameter Slot plane Slot shape Slot thickness Slots separation
	<b>Use of explosives (blasting)</b> Combustion time Fracture initiation Nature of the detonator Nature of the explosive

## 2.2.17. WP6: Conclusions, Recommendations and Dissemination

Under WP6 GasDrain project progress, its results obtained and encountered problems were presented by GIG during International Workshop on "Best Practices in Methane Drainage & Use in Coal Mines" on March 9th-10th, 2017 in Ranchi (India).

### Dissemination workshop

On June 25, 2018, a workshop disseminating the effects of the GasDrain project was organized at the Central Mining Institute. 35 participants, employees of coal companies, mines and scientific institutions took part in them, including those taking part in the project. The workshops were run according to the following agenda:

9:00 – 9:15      Invitation – Deputy Director of GIG Z. Lubosik, Project Coordinator, J.Makówka  
**Laboratory tests and preparation of in-situ tests**

9:15 – 9:45      Research on the parameters of coal and surrounding rocks - RWTH/ G. Gauss  
9:45 – 10:15      Laboratory research on the fracturing of coal – ICL/ S.Durucan  
10:15 – 10:45      Equipment development and its tests – KD "Barbara"/R.Hildebrandt  
10:45 -11:00      Coffe break

#### **In situ tests in JSW SA, Poland**

11:00 – 11:20      Preparation of the test sites in JSW SA KWK Borynia-Zofiówka-Jastrzębie Ruch Zofiówka in districts D-2 i G-2 – Representative of JSW SA  
11:20 – 11:40      Numerical modeling of pre-mining drainage in conditions of mine „Zofiówka” – dr p. Gołębek/INiG  
11:40 – 12:00      Preliminary tests at the test site of the longwall D-2 - GIG, J.Makówka  
12:00 – 12:30      Tests using improved drainage techniques in the area G-2 – GIG, J.Makówka  
12:30 - 13:30      Lunch

#### **In situ tests in HUNOSA, Spain**

13:30 – 13:50      Test site in Montsacro mine, HUNOSA - F. Fernandez, M. Llamas  
13:50 – 14:10      Numerical modeling of drainage methods in HUNOSA – ICL, S.Durucan  
14:10 – 14:30      Results of injection and drainage tests in the mine Montsacro, HUNOSA - F. Fernandez, M. Llamas  
  
14:30 – 15:00      Risk analyses and 'lessons learned document' - INERIS/ S. Lafortune  
15:00 – 15:30      Conclusions and discussion.

The following photos illustrates the workshops.



**Figure 2.2.17.1:** Dissemination Workshop of the project GasDrain

Relations from the workshop were published in websides of GIG, by Polish Press Agency and by Trybuna Górnica.

**GIG**  
**ULEPSZANIE TECHNIK  
DRENAŻU METANU**

**W GŁÓWNYM INSTYTUCIE GÓRNICTWA 25 CZERWCA ODBYŁO SIĘ SEMINARIUM PODSUMOWUJĄCE PROJEKT O AKRONIME GASDRAIN „OPRACOWANIE ULEPSZONYCH TECHNIK DRENAŻU METANU POPRZEC STYMULACJE POKŁADÓW WĘGŁA W CELU ZAPOBIEGANIA ZAGROŻENIOM I ZWIĘKSZENIA WYDIBIĘCIA WĘGŁA. GŁÓWNYM CELEM PROJEKTU BYŁO OPRAWCOWANIE TECHNIK STYMULACJI OTWORÓW DRENAZOWYCH I ULEPSZONYCH TECHNOLOGII WYPRZEDZAJĄCEGO ODMETANOWANIA POKŁADÓW WĘGŁA.**

Zagrożenie metanem jest jednym z najgroźniejszych zagrożeń naturalnych występujących w kopalniach węgla kamiennego. W ostatnich latach odnotowano wzrost emisji metanu z pokładów wydobytego węgla o ok. 63 proc., co jest spowodowane wzrostem głębokości eksploatacji oraz koncentracji eksploatacji węgla. Zwiększone uwalnianie metanu jest nie tylko poważnym zagrożeniem bezpieczeństwa, ale także stanowi powód ograniczenia intensywności eksploatacji węgla. Wkrótce stanie się też przyczyną wysokich opłat emisyjnych, podobnie jak dwutlenek węgla.

W ramach projektu zbudowany został specjalnie zaprojektowany system do hydroslotingu, czyli techniki odpierania pokładu poprzez wycinanie strug wody pod wysokim ciśnieniem dysków w caliznie węglowej.

– Testy urządzenie przeprowadzone zostały w Zakładzie Badań Doktorskich i Utrzymania Powierzchni Kopalni Dłoniadziałalnej Barbara, gdzie określono m.in. warunki bezpieczeństwa i wykonywanie wszystkich urządzeń systemu, efektywność i wydajność dysz urabiających oraz czas operacji hydrocięcia niezbędny do wykonania stymulacji otworów drenazowych – mówi dr hab. inż. Janusz Makówka, prof. GIG, kierownicą projektu. – Urządzenie pozwala na pracę w otworach do 100 metrów w głęb grotoworu i ciecie węgla struga wody o ciśnieniu 1000 barów.

Pracowany w projekcie system urządzeń do hydroslotingu spełnia swoją podstawową funkcję i jest dostosowany do pracy w warunkach wyrobisk podziemnych kopalni węgla. Prace badawcze z wykorzystaniem urządzenia prowadzone były w nacieku Zofiówka kopalni Borynia-Zofiówka-Jastrzębie, należącej do Jastrzębskiej Spółki Węglowej.

Multimedialny projekt GASDRAIN realizowany był ze środków Funduszu Badań Węgla i Stali, koordynowany przez GIG, a jego partnerami były: Jastrzębska Spółka Węglowa SA oraz Instytut Nafii i Gazu z Polski, Grupa Hunosa i Instytut Aitemin z Hiszpanii, Imperial College London z Wielkiej Brytanii, RWTH z Niemiec oraz instytut INERIS z Francji.

**Figure 2.2.17.2:** Article about the workshop in Trybuna Górnica

### **2.3. Conclusions**

Final summary of the project is presented in Section 2 (starting page 5). Section 2.2 presents in detail the course of the project with all laboratory, model and in situ tests. Great effort was put into conducting laboratory tests on coal from the seams coming from both industrial partners, on their mechanical and deposit parameters, and on laboratory simulations of hydro-fracturing with proppants. In-situ tests were carried out to confirm the values of parameters obtained in the laboratories. The results from these tests were used to develop numerical models and to simulate the planned types of drainage. The simulations allowed to expect good effects of the drainage methods applied, in particular when using hydroslotting combined with hydro-fracturing.

During preparations for in-situ tests, the necessary equipment and measuring installations were developed and made. A unique set of equipment and accessories for making coal cutting with high pressure water in a borehole - for hydroslotting was constructed. This equipment was tested in the conditions of the Experimental Mine Barbara and after correcting the durability of used high pressure nozzles, its very good effectiveness was verified.

In situ research has encountered significant difficulties. In the Zofiowka mine, JSW (Poland), the first set of drilled boreholes has shown significant difficulty in maintaining the stability of the boreholes made in the coal seam. It was solved by drilling them in the contact: plane seam - roof rocks. Drainage tests carried out from these boreholes showed a 7-fold increase in methane concentration in boreholes with hydroslotting compared to the control-ones, but they could not be carried out in the long-term, because the gas mixture had too little methane concentration and could not be introduced into the methane drainage system. The second set of boreholes used casing with rubber pipes. For these boreholes a special hydroslotting technique was developed, which together with piping allowed to maintain their patency. Nevertheless, low methane concentrations at very low gas flow velocities have also been obtained from these boreholes. The hydro-fracturing as well as other stimulation methods, were impossible due to the strong seismic tremor and rock burst that occurred in the vicinity of the testing site. This has stopped for a long time any mining operations, including our research. Subsequent inspection of the boreholes showed their damage.

In the Montsacro mine, HUNOSA (Spain), in the initial stage of the research, methane drainage with water injection was carried out, which was not sufficient to allow the development of the mining opening in the coal seam 8 from which the actual vertical drainage boreholes were supposed to be made. The results of the initial drainage did not allow obtaining mining authority's permission to develop this opening. It resulted in the need to limit testing to drain from the previously drilled boreholes.

**Experience gained in the course of the project indicates that at the current stage of mining and drilling technology development it is not possible to effectively drain methane ahead of exploitation operations in such soft and poorly permeable coal seams as in the HUNOSA deposits and in coking coal deposits in JSW.**

### **2.4. Exploitation and impact of the research results**

#### **Actual applications:**

- Development of the equipment and technology of high pressure water jet cutting in boreholes – hydroslotting – as a drainage stimulation method.
- Drilling, casing and hydroslotting in soft coal seams.
- Elaboration of new blasting materials with lower detonation speed and increased gas production.
- Elaboration of new methodology of testing of detonation processes.
- Elaboration of the complex measurement systems and methodology for methane drainage systems.

#### **Technical and economic potencial:**

Although research within the GasDrain project showed very limited possibilities of using the tested stimulation methods in the conditions of soft coal seams in which the largest methane coal bed resources occur, there is still a potential possibility of using these methods in hard coal deposits, which also occur in Poland.

The developed hydroslotting method can also be used for other purposes, including stress reduction and rock burst hazard. Research on this application has been carried out as a part of the MapROC project.

**Publications:**

- Guangyao Si, Sevket Durucan, Ji-Quan Shi, Anna Korre, Wenzhuo Cao: Key parameters controlling slotting operations to stimulate gas drainage performance in low permeability coal seams
- Wiesław Szott, Małgorzata Ślota-Valim, Andrzej Gołębek, Krzysztof Sowizdżał, Piotr Łętkowski: Numerical Studies of Improved Methane Drainage Technologies by Stimulating Coal Seams in Multi Seam Mining Layouts. Case Study
- Study Of The Impact Of Exploitation Structures On Pressure Distribution And Adsorbed Methane Content In Coal Seams Using Dynamic Flow Models. A Case Study
- Drzewiecki J., 2017. Influence of confining pressure on the combustion dynamics of selected explosives. Procedia Engineering, Volume 191, pp. 225-232.
- Drzewiecki J., Myszkowski J., Pytlak A., Pytlak M. 2017. Testing of confining pressure impaction explosion energy of explosive materials (Badania wpływu ciśnienia okólnego na energię wybuchu materiałów wybuchowych), 2017, Arch. Min. Sci. 62 (2017), 2, 385-396
- Drzewiecki J., Myszkowski J., A. Piernikarczyk 2017. Stimulation of the destruction of coal seam with the use of the device for performing of series of starting notches (Stymulacja destrukcji pokładu węgla z zastosowaniem urządzenia do wykonywania zespołu szczelin zarodnikowych). Przegląd Górniczy, nr. 2, 2017, str.18-23
- Drzewiecki J., Pytlak M. 2017. Impact of circular pressure on the dynamics of burning of selected high-energy materials (Wpływ ciśnienia okólnego na dynamikę spalania wybranych materiałów wysokoenergetycznych). Przegląd Górniczy, nr. 3. 2017, str.36-41
- Drzewiecki J., Myszkowski J., 2015, Research of explosives in an environment of high pressure and temerature using a new test stand, (Stanowisko badawcze dla określania zdolności do wybuchu materiałów wybuchowych w środowisku wysokich wartości ciśnienia i temperatury), Journal of Sustaninable Mining, Issue 4, Volme 14, pp.188-194.

**Patents:**

1. Device for measuring the explosion parameters of the explosive charge and the method of measuring the explosive charge parameters of the explosive with an assessment of its ability to explode, the registration number - P.410384.
  2. Cumulative charge of explosive, the registration number - P.422364
  3. The method of degassing seams, especially coal seams, the registration number - P.422365
- Another 2 patents under preparation.

**Conference presentations:**

Janusz Makówka, Jacek Skiba, Bartłomiej Jura, Jerzy Król, Marian Zmarzły (2017): *New techniques of coal seam panels' pre-drainage – based on „GASDRAIN” project experience*. XXVII School of Underground Mining.

Janusz Makówka, Jacek Skiba, Bartłomiej Jura (2017): *GasDRAIN: Development of Improved Methane Drainage Technologies by Stimulating Coal Seams for Major Risk Prevention and Increased Coal Output*. International Workshop on “Best Practices in Methane Drainage & Use in Coal Mines” on March 9th-10th, 2017 in Ranchi (India).

Janusz Makówka, Jacek Skiba, Bartłomiej Jura (2018): *Methods of capturing methane from underground workings - current practice and new methods in the light of the results of the GasDrain project*. Geopetrol 2018, Kraków

### 3. List of figures

Figure 2.2.1.1: Stress-strain plot for the Zofiowka coal sample plug from seam 412 (butt cleat direction). * Axial load was applied under confined ("isostatic") conditions (confining pressure = axial pressure) .....	17
Figure 2.2.1.2: Gas (N2) permeability coefficients in x- and y-direction (Zofiowka seam #412) .....	18
Figure 2.2.1.3: Permeability data for two coal samples from the Monsacro/Sueros Colliery Seam#8.....	18
Figure 2.2.1.4: Langmuir 3 parameter fitted high pressure isotherms of (a) seam #411 samples, (b) seam #412, (c) seam #413, and (d) from Monsacro/Sueros. All isotherms were measured in dry conditions and at a temperature of 45°C.....	19
Figure 2.2.1.5: (a) Normalised pressure decline curves for gas uptake by different grain sizes of Zofiowka seam #412 coal, (b) normalised pressure decline curves for gas uptake by different grain sizes of Monsacro/Sueros seam #8 coal (semi-logarithmic plots).....	21
Figure 2.2.2.1: The seam section and Longwall D-2 selected as the experimental field site at JSW.....	21
Figure 2.2.2.2: (a) General stratigraphy of the D-2 longwall panel and (b) numerical model geometry.....	22
Figure 2.2.2.3: Vertical stress profiles over D-2 longwall panel: longitudinal section.....	23
Figure 2.2.2.4: Vertical stress evolution at the floor coal seam during the extraction of the D-2 longwall panel (Pa) .....	23
Figure 2.2.2.5: The schematic of the sub-level caving (SLC) mining method applied at HUNOSA (not to scale) .....	24
Figure 2.2.2.6: Model geometry developed for SLC at HUNOSA .....	24
Figure 2.2.2.7: Vertical stress contours for the coal directly above the footwall after each stage excavation (viewed from the footwall side) .....	25
Figure 2.2.2.8: (a) Vertical stress profiles, (b) Maximum horizontal stress profiles at the floor coal being affected by SLC in an upper level .....	26
Figure 2.2.2.9: Location of extracted panels in seam #412 and surrounding seams .....	26
Figure 2.2.2.10: Vertical stress distribution in the longwall panel D-2 and neighbourhood in seam 412 in 31 December 2015.....	27
Figure 2.2.3.1: Simplified schematics of N-UHS measuring system. 1 – mobile pump, 2 – high-pressure hoses, 3 – valves, 4 – manometer, 5 – recorder, 6 – signal cable, 7 – drain hose, 8 – pressure and flow sensors, 9 – cable/high-pressure hose, 10 – packer .....	28
Figure 2.2.3.2: Site of the stress measurements (a) and boreholes to measure characteristic hydrofracturing pressures (b) .....	28
Figure 2.2.3.3: Example of pressure and flow rate record measured in one of the boreholes ..	29
Figure 2.2.3.4: Layout showing many mining plots (edges) in the bundle of seams, a) projection on a plane of analysed seam, b) spatial view .....	30
Figure 2.2.3.5: Vertical stress distribution around longwall panel D-2 isosurfaces of 15 MPa (green), 20 MPa (orange), 25 MPa (grey) and 30 MPa (red) .....	30
Figure 2.2.3.6: Distribution of methane content in D-2 coal panel .....	31
Figure 2.2.3.7: Average methane content along the length of the D-2 coal panel.....	32
Figure 2.2.3.8: Rate of degassing the underlying and overlying layers subject to the length and inclination of the coal panel .....	32
Figure 2.2.3.9: Forecasted absolute methane emission rate along the length of the coal panel D-2 .....	33
Figure 2.2.3.10: Locations and dates of collecting the coal samples in order to perform in situ gas content measurements .....	33
Figure 2.2.3.11: Diagram of the coal permeability measurement A).Hydrostatic pressure balance the reservoir pressure in coal, B) Removal of some fluid volume from the well, C) Monitoring the fluid table behaviour .....	35
Figure 2.2.3.12: Pressure gauge developed by INIG-PIB .....	35
Figure 2.2.3.13: Pressure vs. Time curve .....	36
Figure 2.2.3.14: log pD vs. time curve .....	36
Figure 2.2.3.15: Stratigraphy at the mine test area in Sueros Colliery .....	37
Figure 2.2.3.16: Borehole layout at the Sueros Colliery test site (plan view) .....	38
Figure 2.2.3.17: Borehole layout at the test site (vertical cross section at S14) .....	38
Figure 2.2.3.18: Preliminary cement injection tests .....	39
Figure 2.2.3.19: Test layout .....	40
Figure 2.2.3.20: Total amount of water injected on each pulse test .....	40
Figure 2.2.4.1: (a) Water jet cutting of the coal sample, (b) Cuts in coal after water jet treatment .....	42
Figure 2.2.4.2: (a) Pump unit ZPM HDP 172, (b) Hydraulic pump HDP 172, its drive, filter and control system.....	43

Figure 2.2.4.3: (a) Oil supply unit ZZO-2, (b) Stabilisation-rotation unit USO-1.....	43
Figure 2.2.4.4: A schematic diagram of integrated parts assembled for hydro-fracturing/cutting of coal seams.....	43
Figure 2.2.4.5: (a) The pumping unit ZPM HDP 172 in underground gallery of the hard coal mine, (b) Initial fracture in borehole .....	44
Figure 2.2.4.6: (a) Mechanical head aimed at cutting the initial fractures, (b) Cutting and anchoring module of the head.....	44
Figure 2.2.4.7: Impact zones of the explosive charge .....	45
Figure 2.2.4.8: Column charge (extended charge) .....	45
Figure 2.2.4.9: Distributed charge .....	46
Figure 2.2.4.10: Short column chargé design .....	46
Figure 2.2.4.11: Examples of initiating charges, (a) hammer cartridge 1 – detonator, 2 – explosives; (b) cartridge initiating combustion of heterogenic fuel: 1 – detonator unit, 2 – heterogenic fuel.....	47
Figure 2.2.5.1: (a), (b) Large blocks of coal samples from JSW Zofiówka Seam #412 received at IMPERIAL, (c) 38 mm solid cores, (d) 100 mm hollow cylinder cores. ....	48
Figure 2.2.5.2: Permeability behaviour of Zofiówka coal samples at 2.4 MPa confining pressure .....	48
Figure 2.2.5.3: (a) Schematic of the triaxial testing system configuration, (b) 28 mm core triaxial cell and stress-permeability testing components.....	49
Figure 2.2.5.4: Permeability characteristics of CarboProp ceramic proppants (CarboProp, 2015).....	50
Figure 2.2.5.5: Permeability characteristics of InterProp 30/50 ceramic proppant (InterProp, 2015).....	50
Figure 2.2.5.6: Axial stress-strain-permeability behaviour coal determined through multi-stage triaxial testing (Young's modulus, $E = 3.5 \text{ GPa}$ ; Poisson's Ratio, $\nu = 0.26$ ). ....	51
Figure 2.2.5.7: Fractured coal sample prepared (through multistage triaxial testing) for proppant characterisation experiments.....	51
Figure 2.2.5.8: Fractured coal samples treated with 34-40 Mesh sand proppant (left) and InterProp 30/50 ceramic proppant (right). ....	52
Figure 2.2.5.9: Permeability behaviour of a sand propped fracture in coal comparing baseline (un-propped) and propped N2 permeabilities. ....	52
Figure 2.2.5.10: Permeability behaviour of a CarboProp 20/30 propped fracture in coal comparing baseline (un-propped) and propped N2 permeabilities. ....	53
Figure 2.2.5.11: Permeability behaviour of an InterProp 30/50 propped fracture in coal comparing baseline (un-propped) and propped N2 permeabilities. ....	53
Figure 2.2.5.12: Schematic drawings of the newly constructed 100mm hollow cylinder triaxial cell and coal sample, mechanical stress and pore pressure application principles. ....	54
Figure 2.2.5.13: The newly constructed 100mm hollow cylinder testing triaxial cell during pressure testing. Large cell size and weight requires lifting and stabilising tools. ....	54
Figure 2.2.5.14: The newly constructed 100mm hollow cylinder testing triaxial cell during pressure testing. Large cell size and weight requires lifting and stabilising tools. ....	54
Figure 2.2.5.15: Test chamber for determining the explosive characteristics. ....	55
Figure 2.2.5.16: Characteristics of the pressure changes during explosion of the 10 g EMULINIT PM charge for different values of initial pressure. ....	56
Figure 2.2.5.17: Characteristics of the pressure changes during explosion of the 10 g METANIT SPECJALNY E7H charge (Initial pressure = 1.3 MPa). ....	56
Figure 2.2.5.18: Characteristics of the pressure changes during explosion of the 10 g METANIT SPECJALNY E7H charge (Initial pressure = 1.3 MPa). ....	57
Figure 2.2.5.19: Characteristics of the pressure changes during explosion of the 10 g EMULINIT PM charge (initial pressure = 5 MPa). ....	57
Figure 2.2.5.20: Examples of the fuel.....	59
Figure 2.2.5.21: Pressure path for the charge tested without an inhibitor. ....	60
Figure 2.2.5.22: Pressure path changes for the samples tested without an inhibitor. ....	60
Figure 2.2.5.23: Relationship between combustion rate in the intermediate period of the course, and initial pressure for 50% time of pressure increase. ....	61
Figure 2.2.5.24: Relationship between initial pressure and period of pressure increase. ....	62
Figure 2.2.6.1: Model geometries for (a) Hunosa and (b) JSW. ....	66
Figure 2.2.6.2: Pore pressure and crack evolution in Hunosa model at (a) 1,000 steps, (b) 3,000 steps and (c) 6,000 steps.....	67
Figure 2.2.6.3: Pore pressure and crack distribution in JSW model at pumping pressure of (a) 20 MPa, (b) 30 MPa, and (c) 50 MPa. ....	67
Figure 2.2.6.4: Model geometry and the centre refined area for JSW. ....	68
Figure 2.2.6.5: Vertical stress distribution with different slot thicknesses. ....	69
Figure 2.2.6.6: Vertical stress distribution with different slot diameter. ....	69
Figure 2.2.6.7: Gas drainage performance with varying slot thicknesses: (a) gas drainage rate per metre of borehole length, and (b) cumulative volume of captured gas. ....	70

Figure 2.2.6.8: Gas drainage performance with varying slot diameter: (a) gas drainage rate per metre of borehole length, and (b) cumulative volume of captured gas. ....	70
Figure 2.2.6.9: Borehole drilling plan at Hunosa. ....	70
Figure 2.2.6.10: The effect of varying dip direction and dip angle on failure zone geometry. ....	71
Figure 2.2.6.11: Permeability profiles along the (a) coal seam strike and (b) vertical direction. ....	71
Figure 2.2.6.12: Gas drainage performance after borehole stimulation: (a) gas drainage rate per metre of borehole length, and (b) cumulative volume of captured gas. ....	72
Figure 2.2.6.13: Borehole configurations considered for cavitation modelling. ....	72
Figure 2.2.6.14: Plane-strain model domain and boundary conditions. ....	73
Figure 2.2.6.15: Model mesh (right) and close-up around the borehole (left). ....	73
Figure 2.2.6.16: Performance of cavitation in terms of permeability enhancement around the borehole. ....	74
Figure 2.2.6.17: Plane-strain model domain and boundary conditions. ....	74
Figure 2.2.6.18: Performance of cavitation in terms of permeability enhancement around the borehole at JSW conditions. ....	75
Figure 2.2.6.19: Model geometry and the centre refined area. ....	76
Figure 2.2.6.20: Dynamic loading of the stress wave pulse induced by 10g EMULINIT PM blasting experiment at 10 MPa confining pressure from Task 2.2 (data provided by GIG)....	76
Figure 2.2.6.21: Monitoring point locations near the borehole. ....	77
Figure 2.2.6.22: Velocity response to the applied stress wave pulse. ....	77
Figure 2.2.6.23: Stress respond to the applied stress wave pulse: (a) tangential stress and (b) radial stress. ....	77
Figure 2.2.6.24: Contours showing tangential stress wave propagation during the blast loading period (unit: Pa). ....	78
Figure 2.2.6.25: 3D failure zone distribution 1,000 $\mu$ s after blasting ignition. ....	79
Figure 2.2.6.26: Failure zone propagation during the blasting operation. ....	79
Figure 2.2.6.27: Permeability profiles before and after blasting operation. ....	80
Figure 2.2.7.1: Training of the use of pumping unit ZPM HDP 172. ....	80
Figure 2.2.7.2: Training of the use of stabilization-turning unit USO-1. ....	81
Figure 2.2.7.3: Test boreholes used to investigate hydro cutting and hydro slotting technique. ....	81
Figure 2.2.7.4: Confirmation of hydro slotting range: water and steam flow from the monitoring borehole. ....	82
Figure 2.2.7.5: Hydrofracturing phase 1. ....	83
Figure 2.2.7.6: Hydrofracturing phase 2. ....	83
Figure 2.2.7.7: Pressure at borehole S13. ....	84
Figure 2.2.7.8: Location of the new boreholes S31-S32-S33 planned for the next field tests....	85
Figure 2.2.8.1: Data availability and the development of a structural framework for a 3D geological model of the Zofiówka Colliery. ....	86
Figure 2.2.8.2: Structural model of the interval between #409/3 and #413/2 coal seams.....	86
Figure 2.2.8.3: Structure of the #412 coal seam with polygon of planned methane drainage activity. ....	87
Figure 2.2.8.4: Local model of the methane drainage area compared to the extent of the global model. ....	87
Figure 2.2.8.5: Data sets used for the petrophysical modelling. ....	88
Figure 2.2.8.6: The 3D models of permeability (horizontal - above, vertical - below) for the #412 coal seam.....	89
Figure 2.2.8.7: Distribution of gas in place calculated for a section of the #412 coal seam. ....	89
Figure 2.2.8.8: Structural map of the bottom of the #412 coal seam presenting the modelling object: the model of reservoir scale (orange boundary), model capturing part of D-2 longwall (green boundary) and the D-2 longwall (blue boundary) subjected to coal seam stimulation treatment. ....	90
Figure 2.2.8.9: Distribution of the effective maximum horizontal stresses ( $\sigma_H$ ) acting on the #412 coal seam in Zofiówka Colliery. The polygon coloured in blue marks the boundary of the D-2 longwall. ....	92
Figure 2.2.8.10: 3D distribution of effective vertical stress in the model representing part of the D-2 longwall showing the location of the stimulated horizontal borehole and planes of 2 hydraulic fractures. ....	93
Figure 2.2.8.11: Permeability distribution along a wellbore and in the vicinity of a hydro-fracture – detailed vertical cross section of high resolution model. ....	94
Figure 2.2.8.12: Variation of methane production rate with time in stimulated and unstimulated wellbores. ....	95
Figure 2.2.8.13: Variation of methane production rate with time: effects of longwall face proximity. ....	95
Figure 2.2.9.1: Model geometry for geomechanical simulations (after the 2 <sup>nd</sup> level caving). ....	96
Figure 2.2.9.2: Stress changes in #8 coal seam during sub-level caving. ....	97
Figure 2.2.9.3: Stress changes in #9 coal seam during coal extraction at #8 coal seam. ....	98

Figure 2.2.9.4: Gas drainage using cross-measure boreholes at Sueros Colliery, #8 coal seam. ....	99
Figure 2.2.9.5: Gas drainage model at Sueros Colliery sub-level caving layout developed in ECLIPSE. ....	100
Figure 2.2.9.6: Comparison of gas drainage performance between coupled and uncoupled models: (a) gas drainage rate, and (b) cumulative volume of captured gas. ....	100
Figure 2.2.9.7: Permeability response of # 8 coal seam after (a) 1st level caving and (b) 2nd level caving. ....	100
Figure 2.2.9.8: Comparison of gas drainage performance between un-stimulated and slot stimulated boreholes at # 8 coal seam: (a) gas drainage rate, and (b) cumulative volume of captured gas. ....	101
Figure 2.2.9.9: Pressure contours at # 8 coal seam after two months of gas drainage with: (a) un-stimulated cross-measure boreholes, and (b) slot stimulated cross-measure boreholes. ....	101
Figure 2.2.9.10: The residual gas content within the 3rd caving level at # 8 coal seam using cross-measure boreholes. ....	102
Figure 2.2.9.11: Gas drainage using inseam downholes at Sueros Colliery, #8 coal seam. ....	102
Figure 2.2.9.12: Permeability response of #8 coal seam after 1st level caving and 2nd level roadway development. ....	103
Figure 2.2.9.13: Pressure contours of #8 coal seam after two months of gas drainage with: (a) un-stimulated inseam downholes, and (b) slot stimulated inseam downholes. ....	103
Figure 2.2.9.14: The residual gas content within the 4th caving level at #8 coal seam using downholes. ....	103
Figure 2.2.9.15: Comparison of gas drainage performance between inseam downholes and cross-measure boreholes at Sueros Colliery #8 coal seam. ....	104
Figure 2.2.9.16: Gas drainage using cross-measure boreholes at Sueros Colliery # 9 coal seam. ....	104
Figure 2.2.9.17: Permeability response of #9 coal seam after (a) 1st level caving and (b) 2nd level caving. ....	105
Figure 2.2.9.18: Comparison of gas drainage performance in #8 and #9coal seams: (a) gas drainage rate, and (b) cumulative volume of captured gas. ....	105
Figure 2.2.9.19: Pressure changes at (a) #8 and (b) #9 coal seam during gas drainage period. ....	106
Figure 2.2.9.20: The residual gas content within the 3rd caving level at #9 coal seam. ....	106
Figure 2.2.10.1: Sector of the coal seam 310 with the location of the field test ....	107
Figure 2.2.10.2: Scheme of aerometric probe for testing of rock mass fracturing ....	108
Figure 2.2.10.3: Scheme of the rock mass fissures' measurement using the aerometric probe ....	109
Figure 2.2.10.4: Spatial location of the boreholes ....	110
Figure 2.2.10.5 Tools used to perform initial fissuring and view of the initial fissure ....	110
Figure 2.2.10.6: Location of the initial fissurings ....	110
Figure 2.2.10.7: View of prepared explosive charges ....	111
Figure 2.2.10.8: Location of explosive charges ....	111
Figure 2.2.10.9: Rigid pipe construction stabilizing explosive charges in desired locations in the borehole ....	111
Figure 2.2.10.10: View of the fissures in the control boreholes ....	112
Figure 2.2.10.11: Values of fissuration index $K_s$ , % before blasting ....	112
Figure 2.2.10.12: Values of fissuration index $K_{s1}$ , % after blasting ....	113
Figure 2.2.10.13: Changes of fissuration index $\Delta K_s$ , % – difference between measurements before and after blasting ....	113
Figure 2.2.10.14: Values of the index "total fissures' opening $R_s0$ ", mm before blasting ....	114
Figure 2.2.10.15: Values of the index "total fissures' opening $R_s01$ ", mm after blasting ....	114
Figure 2.2.10.16: Changes of the values of the index "total fissures' opening $\Delta R_s$ ", mm - difference between measurements before and after blasting ....	115
Figure 2.2.10.17: Value of the index „borehole equivalent fissure $S_0$ “ mm <sup>2</sup> before blasting..	115
Figure 2.2.10.18: Value of the index „borehole equivalent fissure $S_0$ “ mm <sup>2</sup> after blasting....	115
Figure 2.2.10.19: Changes of the index „borehole equivalent fissure $\Delta S$ “ mm <sup>2</sup> - difference between measurements before and after blasting .....	116
Figure 2.2.10.20: Area of underground research in the coal seam 412 in Zoflowka mine.....	116
Figure 2.2.10.21: Scheme of explosion protection for excavations of the research area .....	117
Figure 2.2.10.22: Sketch of the elements of the explosive charge .....	117
Figure 2.2.10.23: Explosive charge ready for use.....	118
Figure 2.2.10.24: Underground test stand .....	118
Figure 2.2.11.1: Location of test boreholes drilled from the testing tail gate D-2" in the seam 412lg+hd .....	120
Figure 2.2.11.2: Layout of boreholes with slots and measurement system .....	120
Figure 2.2.11.3: Exemplary results from obtained ZCO sensor parameters' registration.....	121

Figure 2.2.11.4: Scheme with the method of slotting in the borehole G180b(2016).....	122
Figure 2.2.11.5: Results of aerometric tests in the experimental borehole G180c (2016) before and after slotting .....	122
Figure 2.2.11.6: Results of aerometric tests in the experimental borehole G180 (2016) before and after slotting .....	123
Figure 2.2.11.7: View of the cheek with the methane drainage installation connected into 180b borehole.....	123
Figure 2.2.11.8: View of the collar of conductor pipe of the experimental borehole 180b with its extension .....	124
Figure 2.2.11.9: Exemplary results of methane intake from borehole G180a .....	124
Figure 2.2.11.10: Exemplary results of methane intake from borehole G180b.....	125
Figure 2.2.11.11: Exemplary results of methane intake from borehole G180c.....	125
Figure 2.2.11.12: Design of the test site in district G - transportation cross cut G-2(seam 410, level 900 m) .....	126
Figure 2.2.11.13: Location of testing boreholes: G-167 (lower) and G-158b (upper) drilled in the transportation crosscut G-2, seam 410, level 900 m. ....	127
Figure 2.2.11.14: Scheme of the slotting method applied in the boreholes G-167 and G-158b .....	128
Figure 2.2.11.15: Borehole G-158b after completing the slotting.....	129
Figure 2.2.11.16: Setting of USO-1 and Limited outflow of water from the borehole.....	129
Figure 2.2.11.17: The real layout of the boreholes with slots performed in district G - the transportation cross cut G-2 (in the new test site). .....	130
Figure 2.2.11.18: Rubber hose used to case slotted borehole .....	130
Figure 2.2.11.19: Introducing rubber hose to the borehole.....	130
Figure 2.2.11.20: Schematic of hydroslotting done in one of the boreholes in tail gate G2....	131
Figure 2.2.11.21: Slotting process in one of the borehole.....	131
Figure 2.2.11.22: Situation in the borehole G11/2018 after hydroslotting .....	132
Figure 2.2.11.23: Situation in the borehole G11a/2018 after hydro-slotting .....	133
Figure 2.2.11.24: Situation in the borehole G11b/2018 after hydro-slotting .....	134
Figure 2.2.11.25: Layout of the boreholes with borehole G21/2018 .....	134
Figure 2.2.11.26: Situation in the borehole G21/2018 after hydro-slotting.....	135
Figure 2.2.12.1: Remote gas monitoring and control screen .....	136
Figure 2.2.12.2: RELIA AV Gas Monitoring and Control System .....	136
Figure 2.2.12.3: Suction flow measurement .....	137
Figure 2.2.12.4: Methane and carbon monoxide gas detectors at drainage pipe.....	137
Figure 2.2.12.5: Combined drainage and stimulation at Location L1.....	137
Figure 2.2.12.6: Emplacement of methane drainage system.....	138
Figure 2.2.12.7: Water injection and gas suction on 3 October 2016.....	139
Figure 2.2.12.8: Water injection test targets .....	140
Figure 2.2.12.9: New location L3.....	140
Figure 2.2.12.10: Borehole layout at the test site (vertical cross section at S31). .....	141
Figure 2.2.12.11: Borehole layout at the test site (vertical cross section at S32). .....	141
Figure 2.2.12.12: Scheme of injection and future aspiration in L3. .....	141
Figure 2.2.12.13: Gas samples location .....	142
Figure 2.2.12.14: Location of the borehole S22 for collecting samples.....	143
Figure 2.2.12.15: Triple borehole battery.....	144
Figure 2.2.12.16: The locations of various injection and drainage boreholes applied in the coal layer C/8 in Montsacro's shaft (Hunosa) at location L1.....	145
Figure 2.2.12.17: Location of drainage boreholes and the equipment.....	146
Figure 2.2.12.18. The readings from firedamps period from 7/08/17 to 12/08/17 .....	148
Figure 2.2.12.19. Moisture at L2 borehole location .....	149
Figure 2.2.12.20. Velocity of desorption. Location L2.....	150
Figure 2.2.12.21. Tracer gas test at location L3 .....	151
Figure 2.2.12.22. Tracer gas test at location L3. Cross section .....	151
Figure 2.2.13.1: A risk scenario.....	153
Figure 2.2.13.2: Preventive and corrective safety barriers on a risk scenario.....	154
Figure 2.2.13.3: Event tree with safety barriers for risk scenarios associated with the use of borehole stimulation methods and mitigation measures underground. .....	155
Figure 2.2.14.1: ZCO sensor adjusted to operation with a measuring orifice plate.....	159
Figure 2.2.14.2: Example of methane drainage system with measuring equipment. ....	159
Figure 2.2.14.3: Block diagram of the integrated methane drainage sensor ZCO .....	160
Figure 2.2.14.4: Components of integrated methane drainage sensor ZCO .....	161
Figure 2.2.14.5: Data registered by ZCO sensor 544 on borehole 7(G11b).....	163
Figure 2.2.14.6: Data registered by ZCO sensor 540 on borehole 8(G11a) and 5(G13) .....	163
Figure 2.2.14.7: Data registered by ZCO sensor 541 on borehole 9(G11) .....	164
Figure 2.2.15.1: Water injection, 23-02-2017.....	166
Figure 2.2.15.2: Water injection. Period 03: 22-05-2017 to 31-05-2017 .....	167

Figure 2.2.15.3: Water injection. Period 04: 1-06-2017 to 07-06-2017 .....	167
Figure 2.2.15.4: Water injection. Period 05: 7-06-2017 to 12-06-2017 .....	168
Figure 2.2.15.5: Water injection. Period 12-06-2017 to 19-06-2017 .....	168
Figure 2.2.15.6: Water injection. Period 19-06-2017 to 26-06-2017 .....	169
Figure 2.2.15.7: Water injection. Period: 26-06-2017 to 3-07-2017.....	169
Figure 2.2.15.8: Water injection. Periods 09 - 14: 21-07-2017 to 04-09-2017 .....	170
Figure 2.2.15.9: Gas drainage (wells S12 and S13). Period 04: 1-06-2017 to 07-06-2017 ...	170
Figure 2.2.15.10: Gas drainage (wells S12 and S13), 05-06-2017 .....	170
Figure 2.2.15.11: Gas drainage (wells S12 and S13). Period 14: 28-08-2017 to 04-09-2017.	171
Figure 2.2.16.1: Schematic of slot plane rotation with respect to in-situ stresses.....	176
Figure 2.2.17.1: Dissemination Workshopof the project GasDrain.....	179
Figure 2.2.17.2: Article about the workshop in Trybuna Górnica .....	179

#### 4. List of tables

Table 2.2.1.1: Overview of the experimental and analytical measurements conducted by the project partners.....	15
Table 2.2.1.2: Results of petrophysics investigations of samples from G-172 +90° well at Zofiówka Colliery.....	16
Table 2.2.1.3: MIP pore size distribution classes of similarity for coals from ZOFIOWKA (seam 412). .....	17
Table 2.2.2.1: Rock mechanical properties used for JSW longwall model. ....	22
Table 2.2.2.2: Elastic properties used for Hunosa SLC model. ....	25
Table 2.2.3.1: Borehole angles and re-closing pressures. ....	29
Table 2.2.3.2: In situ gas content measurement data for the coal seam 412.....	34
Table 2.2.3.3: Results of slug test method interpretation. ....	37
Table 2.2.3.4: Results from the hydrogeological interpretation.....	41
Table 2.2.5.1: Principal data registered for 50% time of the samples' combustion. ....	61
Table 2.2.6.1: Reservoir parameters representative of Hunosa field. ....	63
Table 2.2.6.2: Design treatment schedule for hydraulic fracture stimulation at Hunosa. ....	64
Table 2.2.6.3: Reservoir parameters representative of the conditions at JSW. ....	64
Table 2.2.6.4: Fracture treatment summaries at Hunosa conditions. ....	64
Table 2.2.6.5: Fracture treatment summaries at JSW conditions .....	65
Table 2.2.6.6: Rock mechanical properties used for Hunosa model. ....	66
Table 2.2.6.7: Microscopic parameters used for Hunosa model.....	66
Table 2.2.6.8: Rock mechanical properties used for JSW model.....	66
Table 2.2.6.9: Microscopic parameters used for JSW model. ....	67
Table 2.2.6.10: Rock mechanical and strength properties of coal in JSW. ....	68
Table 2.2.8.1: The set of parameters of the rock materials occurring in the Zofiówka Colliery necessary in further simulation workflow assigned from available or assumed data.....	91
Table 2.2.8.2: The set of parameters of rock materials representing the Zofiówka Colliery necessary in further simulation workflow assigned from available or assumed data.....	91
Table 2.2.8.3: Parameters describing initial stress conditions in the model.....	92
Table 2.2.9.1: Rock mechanical and strength properties of coal at Sueros Colliery, Hunosa. ....	96
Table 2.2.9.2: Reservoir properties used for gas drainage simulation at Sueros Colliery, Hunosa.....	99
Table 2.2.10.1: Properties of Emunilit PM [ <a href="http://www.nitroerg.pl">http://www.nitroerg.pl</a> ].....	110
Table 2.2.11.1: Results of endoscopic tests performed in the boreholes directly after drilling. ....	121
Table 2.2.11.2: Collective summary of the aerometric tests results conducted in the experimental boreholes before and after slotting. ....	123
Table 2.2.11.3: List of twenty (20) boreholes drilled in "Zofiówka" mine (cross cut G2). ....	126
Table 2.2.12.1: Boreholes features (location L1 & L2).....	138
Table 2.2.12.2: Analysis of gas samples .....	142
Table 2.2.12.3: The injected volumes (in litres). ....	146
Table 2.2.12.4: The amounts of drained methane in individual periods.....	147
Table 2.2.12.5: The main characteristic controlled parameters.....	149
Table 2.2.15.1: Boreholes features (location L1 & L2).....	164
Table 2.2.15.2: Water injection volumes.....	165
Table 2.2.15.3: Results of water injection and methane drainage .....	172
Table 2.2.16.1: Key factors that were identified.....	178

## **5. Acronyms and abbreviations used in the report**

GIG - Główny Instytut Górnictwa  
INIG - Instytut Nafty i Gazu – Państwowy Instytut Badawczy  
JSW - Jastrzębska Spółka Węglowa  
RWTH - Rheinisch-Westfälische Technische Hochschule Aachen  
INERIS - Institut National de l'Environnement et des Risques  
AITEMIN - Asociación para la Investigación y Desarrollo Industrial de los Recursos Naturales  
HUNOSA - Hulleras Del Norte SA  
IMPERIAL - Imperial College Of Science, Technology And Medicine  
CBM - Coalbed Methane  
US - United States  
FTP – File Transfer Protocol  
KOM - Kick-off meeting  
IUPAC - International Union of Pure and Applied Chemistry  
 $m^3$  – cubic meter  
 $m_{CH_4}^{1ads}$  - mass of adsorbed methane in time  
 $m_{CH_4}^{1des}$  - mass of desorbed methane in time  
 $a_{CH_4}$  - sorption capacity with respect to methane  
De - effective diffusion coefficient  
p - pressure  
IGA - Intelligent Gravimetric Analyzer  
MPa – Mega Pascal  
hPa – hecto Pascal  
GPa - Giga Pascal  
FC - face cleat direction  
BC- butt cleat direction  
SLC - sub-level caving  
DAF - Dry Ash Free  
CH<sub>4</sub> - methane  
 $V_1$  - Coal seam gas desorption rate  
 $V_g$  - is the volume of firedamp released ( $m^3$ )  
C - methane concentration in the air  
Q - air flow rate in the ventilation stream.  
t - elapsed time interval between each measurement or record.  
S - Specific emission  
 $V_g$  - Volume of methane released in the district ( $m^3$ ).  
P - coal production during the period methane release is recorded (tons).  
Ce - Ash content of total production (%).  
T<sub>MS</sub> - highest value of the maximum percentages of firedamp in the atmosphere (peak values of the records)  
T<sub>M</sub> - averaged value of the daily mean firedamp content.  
MIP - Mercury Injection Porosimetry  
FLAC3D - is a numerical modeling code for advanced geotechnical analysis of soil, rock, and structural support in three dimensions  
D2 - longwall panel  
SLC - sub-level caving mining method applied at HUNOSA  
E - Young's modulus (GPa)  
 $\nu$  – Poisson's Ratio  
 $P_w$  - Initial Pressure (MPa)  
T - Pressure increase time (s)  
T - Tensile strength (MPa)  
PFC - Particle Flow Code  
E - Elasticity modulus (GPa)  
 $k_n/k_s$  - Stiffness ratio  
SS - Strain Softening (constitutive model)  
J-7B & J-8B – name of wells  
GIP - gas in place,  
CM - coal mass  
G - amount of gas per unit of coal mass  
RG - Reservoir Geomechanics (Petrel platform - Schlumberger)  
UCS - Unconfined Compressive Strength  
f - Friction coefficient  
 $\varphi$  - Friction angle (°)  
 $\nu$  – Poisson's ratio (0-1.0)  
DA - Dilatation Angle (°)

E - Young modulus (GPa)  
 UCS - Unconfined Compressive Strength (MPa)  
 Bd - Bulk density (g/cm<sup>3</sup>)  
 P - Porosity (%)  
 C - cohesion (MPa)  
 Cr - residual cohesion (MPa)  
 $\sigma_H$  - Azimuth (°)  
 $\sigma_H$  - Gradient (MPa/m)  
 $K_i$  = modified permeability in  $i^{th}$  main direction  
 $K_{0i}$  = initial permeability in  $i^{th}$  main direction  
 $c$  = permeability compressibility  
 $\Delta\sigma_j$  = change in effective stress in  $j^{th}$  main direction  
 $\delta_{ij}$  = Kronecker delta

## **6. List of references**

- Myszkowski J. (1996): Ukierunkowane szczelinowanie skał techniką strzelniczą (Directed rock fracturing with blasting technique). Prace Naukowe GIG, Seria Konferencje, Katowice.
- Szymczak K., Gawor T., Wolszakiewicz K.: Metodyka badań liniowej szybkości spalania stałych paliw rakietowych (Research methodology of the linear burning rate of solid rocket fuels), Materiały Wysokoenergetyczne, IPO, Warszawa, tom 1, 2009, pp. 107-116
- CarboProp, 2015, <http://www.carboceramics.com/getattachment/6c1a9d23-33e1-452e-9e11-4bae0d7c7a96/CARBOPROP.aspx>
- InterProp, 2015,  
[http://www.proppants.saint-gobain.com/sites/default/files/InterProp\\_Data%20Sheet.pdf](http://www.proppants.saint-gobain.com/sites/default/files/InterProp_Data%20Sheet.pdf)
- Durucan, S., Ahsan, M., Shi, J-Q., Syed A., Korre, A., 2014. Two phase relative permeabilities for gas and water in selected European coals. Fuel 134, pp. 226–236.
- Bear. J. Dynamics of fluids in porous media. Dover Publications. 1972.
- Shi J., Durucan S., Imperial College London, August 2005 Reservoir Evaluation & Engineering, "A model for changes in coalbed permeability during primary and enhanced methane recovery".
- Eclipse 300 Release 2015.1 GeoQuest, Schlumberger.
- Petrel Release 2015.1, GeoQuest, Schlumberger.
- Visage Release 2015.1, GeoQuest, Schlumberger.
- Drzewiecki J.: Metanowość ścian a postęp eksploatacji [Methane emission from longwalls and its relationship to advance rate]. Archives of Mining Sciences, 49(2), 2004, pp. 271-284
- Frejowski A., Merta G.: Ocena stanu spękania górotworu w rejonie georeaktora podziemnego zgazowania węgla. Wiadomości Górnictwa 2015, nr 5, pp. 281–286.
- Friedland A.M.: Issledovaniye treszzinovatosti parod w Massimie okrujuszczim gornuju wyrabotku. Szchtnoje Stroitelstwo nr 5, 1965.
- Gwiazda J., Hładysz Z.: Badania szczelinowatości skał za pomocą pneumatycznej sondy otworowej. Biuletyn GIG nr 2, Katowice 1973.
- Konicek P., Konecny P. and Ptacek J. (2011).: Destress Rock Blasting as a Rockburst Control Technique, In Proceedings of the 12th International Congress on Rock Mechanics, Bejing, 18-21 October 2011, Taylor & Francis Group, pp. 1221–1226
- Konopko W. i zespół: Ukierunkowane hydroszczelinowanie skał i możliwości jego wykorzystania. Prace naukowe GIG nr 824, Katowice 1997
- Krause E., Smoliński A. (2013).: Analysis and assessment of parameters shaping methane hazard in longwall areas. Journal of Sustainable Mining, Vol. 12 (2013), No. 1, pp. 13–19, Katowice.
- Małkowski P.: Obserwacje stref spękań wokół wyrobisk korytarzowych dla oceny jakości górotworu. Materiały XXVII ZSMG „Geotechnika i budownictwo specjalne”. Zakopane 2004.
- Merta G., Myszkowski J.: Badania introskopowe w otworach wiertniczych, zastosowanie, ocena metody. Materiały XI Międzynarodowej Konferencji Naukowo-Technicznej „Taapania 2004”. Ustroń 2004, pp. 261-269.
- Mlynarczyk M., Wierzbicki M., Badania szczelinowatości górotworu wokół otworu odmetanowania na podstawie analizy zapisów z kamery introskopowej. Prace Instytutu mechaniki Górotworu PAN. Tom 14, nr 1-4, pp. 45-52, 2012

Myszkowski J. (1996).:Ukierunkowane szczelinowanie skał techniką strzelniczą [Directed rock fracturing with blasting technique]. Prace Naukowe GIG, Seria Konferencje, Katowice

Niemiec. B.: Doświadczenia w stosowaniu sondy aerometrycznej w wybranych kopalniach węgla. Miesięcznik WUG nr 2/2001, pp. 19-24.

Nierobisz A.:Sonda aerometryczna jako narzędzie do badania szczelinowatości górotworu, Przegląd Górnictwy 2014/3.

Stasica, J. Rak, Z. Introspective camera to examine rock structure penetrated by drilling operations, AGH Journal of Mining and Geoengineering. 2012, Vol. 36, no. 3 pp. 325—330

Stoprya M., Stasica J., Rak Z.: Introskopowa metoda badania struktury górotworu w otoczeniu wyrobisk górniczych. Bezpieczeństwo Pracy i Ochrona Środowiska w Górnictwie nr 10, 1998, Wydawnictwo WUG, Katowice.

## Getting in touch with the EU

### In person

All over the European Union there are hundreds of Europe Direct information centres. You can find the address of the centre nearest you at:  
[https://europa.eu/european-union/contact\\_en](https://europa.eu/european-union/contact_en)

### On the phone or by email

Europe Direct is a service that answers your questions about the European Union. You can contact this service:

- by freephone: 00 800 6 7 8 9 10 11 (certain operators may charge for these calls),
- at the following standard number: +32 22999696 or
- by email via: [https://europa.eu/european-union/contact\\_en](https://europa.eu/european-union/contact_en)

## Finding information about the EU

### Online

Information about the European Union in all the official languages of the EU is available on the Europa website at: [https://europa.eu/european-union/index\\_en](https://europa.eu/european-union/index_en)

### EU publications

You can download or order free and priced EU publications at: <https://publications.europa.eu/en/publications>. Multiple copies of free publications may be obtained by contacting Europe Direct or your local information centre (see [https://europa.eu/european-union/contact\\_en](https://europa.eu/european-union/contact_en)).

### EU law and related documents

For access to legal information from the EU, including all EU law since 1952 in all the official language versions, go to EUR-Lex at: <https://eur-lex.europa.eu>

### Open data from the EU

The EU Open Data Portal (<https://data.europa.eu/euodp/en/home>) provides access to datasets from the EU. Data can be downloaded and reused for free, for both commercial and non-commercial purposes.

The main objective of this project was to develop new borehole stimulation techniques and develop improved methane drainage technologies.

Project commenced with the laboratory experiments to characterise the baseline reservoir properties of coal and coal measures rock. These data were supplemented by the necessary in situ measurements at JSW Zofiowka and HUNOSA Sueros Collieries.

Parallelly, researches on borehole stimulation technologies and developed tools for use in the field were carried out. Necessary equipment and tools were developed, and performed their preliminary testing for water jet and mechanical cutting and hydrofracturing of coal. Two different explosives were also developed and tested.

Numerical simulations carried out for the Zofiowka Colliery, applying reservoir engineering techniques for assessment of the performance of propped and unpropped hydrofracturing. Similar models, applying a coupled flow-geomechanical model of the seams at Sueros Colliery and modelled the performance of a set of slotted boreholes

In the Zofiowka colliery, in two field testing a trial performed stimulation of the borehole using the slot cutting shown lack of patency in one of the boreholes set and poor permeability of the coal seam in another one. A massive seismic tremor and rockburst made the further works impossible to finish.

In the Sueros Colliery boreholes were drilled and equipped with monitoring devices controlling methane content and its pressure inside. In another boreholes in second testing location, sudden drop in methane concentration was observed. It implied faulty instalment of the packer. Continuation of further tests was stopped due to mining authority's decision.

